NASA SP-41

AMPTIAC

NASA-AEC

55876

LIQUID-METALS CORROSION MEETING

Volume I

LEWIS RESEARCH CENTER
CLEVELAND, OHIO
OCTOBER 2-3
1963

20010913 096

PROCEEDINGS OF THE

NASA-AEC

LIQUID-METALS
CORROSION MEETING

VOLUME I

Lewis Research Center, Cleveland, Ohio
October 2-3, 1963

The classified material presented at this meeting
(Vol. II) is printed separately as SP-42

PREFACE

The fourth in a series of NASA-AEC Liquid-Metals Corrosion Meetings held October 2-3, 1963, was devoted to discussion of the mechanisms of liquid-metal corrosion, the results of compatibility tests with alkali metals, and the problems related to compatibility testing with alkali metals. Previous meetings in this series dealt with a broader range of topics that include mercury corrosion, liquid-metal analytical chemistry, and liquid-metal properties. In the interest of comprehensive coverage, this meeting was restricted in scope. It was felt that topics not covered could be deferred to meetings under other auspices planned for the near future.

The meeting was intended to serve two purposes: It was to provide an opportunity for the exchange and comparison of current test results, and just as important, it was to provide the worker in the field of compatibility testing with information pertinent to conducting and interpreting corrosion tests from experts in allied fields. It has become evident that (1) a well-designed corrosion test, especially under two-phase flow conditions, calls for an understanding of heat-transfer and fluid dynamics; (2) testing of refractory metals, particularly where it is necessary to maintain low impurity levels, requires an insight into the interaction between the environment and the test; (3) furthermore, the ability to interpret and correlate corrosion data is dependent on an understanding of corrosion mechanisms.

Two important subjects, not on the agenda and not discussed in this report, however, were touched on during the course of the meeting and should be mentioned. One subject concerned the lack of suitable instrumentation for corrosion testing, particularly, pressure, temperature, and vapor quality instruments. This deficiency was universally acknowledged and lamented. The other subject was the limitations and significance of the three types of two-phase corrosion tests (reflux capsule, natural-convection loop, and forced-convection loop) currently in use. The cursory nature of the discussion and the heat generated by the participants did not permit a crystallization of conclusions. As a consequence of the wide interest expressed in these two subjects, it is anticipated that they will be placed on the agenda of the next meeting in this series.

It is gratifying to note that, in spite of the short notice given to the participants of the meeting, almost all were able to submit a written copy or a summary of their presentations, which are collected herein. In the interest of rapid dissemination of information, this report has not received technical nor editorial review by either the participants or the sponsors. Consequently, the Government and the participating organizations cannot assume responsibility for the correctness of all details reported.

The Oak Ridge National Laboratory and the Pratt & Whitney, CANEL, presentations (vol. II) are Confidential Restricted Data and therefore are printed separately as Special Publication 42.

<div align="right">

Louis Rosenblum
Corrosion Meeting Chairman

</div>

CONTENTS

E-2492

I. CORROSION MECHANISMS

Leo F. Epstein, Chairman
Valecitos Atomic Laboratory
General Electric Company
Pleasanton, California

A. PANEL PRESENTATION

I. Introductory Remarks

Leo F. Epstein
Valecitos Atomic Laboratory
General Electric Company →2'
Pleasanton, California

Charles F. Bonilla
Columbia University
New York, New York

Eugene E. Hoffman
General Electric Company
Evandale (Cincinnati), Ohio

G. W. Horsley
United Kingdom Atomic Energy Authority
Winfrith Heath
Dorchester (Dorset), England

John R. Weeks
Brookhaven National Laboratory
Upton (L. I.), New York

1. INTRODUCTORY REMARKS

Leo F. Epstein

a. The Liquid Metal Revival

This fourth annual meeting on Liquid Metal Corrosion, sponsored by NASA and the AEC jointly comes as a particularly timely event. These two agencies are largely responsible for a remarkable revival of interest in the subject of liquid metals, and an intensification of effort in this area which corresponds, more or less, with these meetings.

There has been, of course, a science of technology of liquid metals since man first discovered how to extract metals from their ores, and to fuse and shape them into useful objects by casting. Mercury, the only readily obtained metal liquid at room temperature seems to have had a rather special kind of fascination for alchemists and the early workers in chemistry, and over the years many familiar applications of this metal were found — e.g. thermometers, barometers, etc. The modern period, in liquid metals technology, however, dates essentially to the 1920's when the first power plants for the generation of electricity using mercury vapor instead of steam were introduced. This application, although it caused a considerable flurry of excitement for a while ultimately all but vanished from industry and technology, largely due to new developments and innovations which made the mercury cycle less attractive economically than it had initially seemed to be.

Immediately following World War II, many of the scientists who during the years of conflict had been obliged to confine their studies to the use of the nuclear fission process for weapons only, were able to for the first time consider other possible applications. The possibility of utilizing the large energy release of the fission process to produce power had been conceived of very soon after the discovery of the basic phenomenon, and in 1946 active work on the use of nuclear fission for power production began in earnest. The need for a heat transfer fluid with these systems was obvious, and it quickly became clear that because of their resistance to radiation damage, high thermal conductivities and other desirable properties, liquid metals had some outstanding advantages. The interest in liquid metals at this time arose largely under AEC sponsorship, and was carried out at a number of laboratories, Argonne and the Knolls Atomic Power Laboratory, in particular.

For applications, where a fluid is used to remove heat from a heat source, it is easy to show that, all other factors being equal, the amount of power required to circulate the fluid (the pumping horse-power) is roughly proportional to the square of the density. Since the power diverted to pumping the fluid around the system is not available for useful external work, it is desirable to minimize this essentially dissipative quantity, and application of this criterion to the choice of suitable coolants leads rather quickly to liquid metals of minimum density. While the lightest of the known metals is lithium, the use of this material initially was restrained by the unhappy presence of the Li^6 isotope in naturally occurring material. The nuclear behavior of this species, in particular its

6

large absorption cross section for thermal neutrons, made it essential to carry out isotope separation processes to obtain relatively pure Li^7 before this could be seriously considered.*
Thus the earliest work on liquid metals for nuclear applications for the most part concentrated on the next lightest metal, sodium. Initially, it was thought by some workers that the fact that Na was not liquid at room temperature (Melting Point 97.8^oC) would be a serious disadvantage; and for this reason a great deal of attention was devoted to the sodium-potassium alloys, NaK, which have the useful characteristic of being liquid to temperatures as low as -12.3^oC (eutectic, 77.2 weight percent K) although the nuclear absorption cross section of potassium is so much worse than that of sodium that this convenience is not achieved without some penalty.

It was using NaK, then, that the first liquid-metal cooled power plant was built, the Argonne constructed Experimental Breeder Reactor (EBR-I) which achieved criticality at the Idaho Test Site in 1952 and has been operating (except for minor interruptions) ever since. KAPL, which had begun a power plant project at about the same time as Argonne (1946) in about 1950 shifted its attention to the use of a sodium (rather than NaK) cooled nuclear reactor for submarine propulsion, and this work led, in 1955 and 1956, to the operation first of a land-based prototype (West Milton, N.Y.) and then of the submarine Sea Wolf.

_____

* The practical separation of lithium isotopes, and serious consideration of the use of lithium in a nuclear system, was not achieved until the late 1950's.

7

In this first push of effort in the decade from 1946 to 1956, a sound basis for understanding the technology of liquid metals, and of the greatest interest for this meeting, the mechanisms of corrosion of structural materials by liquid metals was developed. In this fast-moving and rather revolutionary era, the progress of the art leaned heavily on the earlier experience with mercury. The explanation of Nerad (General Electric) that corrosion by this liquid was largely a process of physical solution (quite different in kind from the chemical reactions which account for corrosion by water and many other common media), it was found, could be carried over with only slight modification to the behavior of the alkali metals. During this period, there was a great deal of work done with the heavier low-melting, low-cross-section metals Pb and Bi in the U.S. (at Brookhaven in particular) and in Great Britain at Harwell. These studies ultimately led not only to a greater understanding of the corrosion behavior of heavy liquid metals, but also succeeded in clarifying some long-standing puzzles. The mechanism of mercury corrosion inhibition by dissolved Ti or Zr was empirically discovered and patented by Nerad in 1934, but the definitive explanation of how this worked did not appear until the announcement of Gurinsky and his BNL associates at the first Geneva Conference in 1955. In many other areas also, the 1946-1956 period was the Golden Age of Liquid Metals.

How and why it came to a rather dramatic close following Geneva I in 1955 is a fascinating subject for consideration. The problems of the Sea Wolf which were widely and erroneously attributed to its sodium-cooled power plant (rather than to chloride-induced stress

8

corrosion cracking on the water side of the steam generators)

certainly had an effect. The Navy decided to standardize on

pressurized water plants for ship propulsion, and as a result of this

decision, a substantial amount of AEC support of liquid metal studies

disappeared. The liquid bismuth work in both the U.S. and Great Brit-

ain came to a virtual halt, and personnel began to move into other

reactor types that were considered more immediately remunerative. The

new U.S. legislation in 1956 permitting the entrance of private industry

into the nuclear power field also undoubtedly led to a greater con-

centration on the more familiar water systems, and a move away from

liquid metals.

These comments are not to suggest that liquid metal studies

vanished altogether in the period 1955 to 1960. Excellent work was

continued by groups at Oak Ridge, Atomics International, Argonne,

Brookhaven and elsewhere in the U.S., although on a generally reduced

scale. During this period, the hopes for a nuclear-propelled airplane

inspired the development of lithium seven as a reactor coolant. And

isolated zealots, in the U.S. and elsewhere, continued to work in the

liquid metal area, often with little or no support from external

agencies.

Then, with rather dramatic suddenness, there was a new Renaissance

in the field of liquid metals, beginning in about 1959 and 1960. The

nuclear power plant designers who had been concentrating on water

systems became painfully aware of the fact that the best conditions

they could achieve — 1000 psi saturated steam, 545°F, for example —

were rather pathetically poor in comparison with modern fossil fuel

plant practice. The desire for <u>higher temperatures</u>, approaching the 1000°-1100°F range of good modern central station installations quickly led to a consideration of other kinds of system which might lead to these more favorable conditions. In the subsequent race, superheated steam and high temperature inert gases were and are presently being evaluated. But also, the advantages of the liquid metal route, which could lead to elevated temperatures without excessive pressures, were widely recognized.

A second factor, almost simultaneously with the intensified push towards higher temperatures, appeared about 1960 in the thinking of various AEC power plant experts. From the first awareness of the nature of nuclear fission, there had been a widespread recognition that it was unlikely that a vigorous nuclear power industry could be based on the utilization only of the 0.7% U-235 which nature has been so kind as to bestow upon us; and the neglect and wastage of the 99.3% of unfissionable U-238 found in uranium ores. The theoretical concept of <u>breeding</u>, that is the conversion of U-238 (or, also of naturally occurring Th-232) into a fissionable form, had been widely and favorably considered. EBR-I, by direct experiment, established that this could in fact be achieved, that is the burnup of one gram of fissionable U-235 in the right kind of reactor could lead to the production of more than one gram of another fissionable material, Pu-239 for example. There are several types of reactors that can lead to a breeding gain of this kind, but prominent among the systems which look good is the "fast" reactor, that is one in which the average velocity and energy of the neutrons is considerably higher than in

"thermal" systems where the neutrons are essentially in thermal equilibrium with the ambient temperature. To obtain a fast spectrum suitable for breeding, it is necessary to rigorously eliminate hydrogen and other very light elements which tend to slow down the neutrons, and degrade their energy distribution in the direction of thermalization. The use of liquid metals, on the other hand, did not lead to this kind of spectral decay, and seemed ideal for a breeder system. The possibility of combining the high thermal efficiencies possible by the use of liquid metals at elevated temperatures, with the neutron, fuel and raw material economies also conceivable with such a system, were truly exciting. A number of reactors designed to capitalize on this concept suddenly began to take form — the Enrico Fermi plant in Michigan, EBR-II at Idaho Falls, the Dounreay fast breeder in Scotland, the French "Rapsodie" at Cadarache, and others. This acceleration of interest in fast breeders, then, has played an important role in the present revival of effort on liquid metals in AEC and power industry circles.*

Our presence here at Lewis, and the interest of NASA and its associated organizations, arises from still a third factor. Shortly after the opening of the Space Age by the first "Sputniks" in 1957, planning for the extended and accelerated exploration of space underwent a tremendous upward surge. In such a program it was quite clear that the requirements for energy sources in space, in interplanetary exploration, and elsewhere, would be steadily increased as

---

* It is interesting to speculate on how much the revived interest in breeding <u>fission</u> systems is a result of relatively disappointing progress towards power plants utilizing nuclear <u>fusion</u>.

more and more ambitious and sophisticated space programs were under-
taken. For extended periods of extraterrestrial operation, it is clear
that nuclear energy, because of its limited fuel supply requirements,
was about the only practical means of supplying large blocks of
power which was known. This realization then led to the happy
marriage of expediency between NASA and the AEC to combine their
interests and exploit this area together; and this cooperative program
has continued for a number of years now and is undoubtedly responsible
for the free and friendly admixture of people from both agencies in
this room today.

But just to say that the energy source for space is to be nuclear
is only the beginning of the problem. The fission process, as
presently developed, releases its energy largely in the rather
degraded form of heat, and to obtain the work required demands some
kind of a heat engine capable of changing this heat into a more
easily utilized form of energy. So far as I am aware, only two
methods of doing this have been proposed to date, both yielding
electricity as their final products; first, the turbogenerator concept,
which is a simple extension of conventional terrestial power plant
practice; and, as an alternative, thermionic conversion which, in
principle, makes it possible to convert heat into electrical energy
without passing through any intermediate mechanical steps (for example
in the turbine and the generator). This would make it possible to
conceive of a power plant with no moving parts, with the concomitant
advantages in life expectancy and trouble free maintenance to be
expected from such a system. With either of these systems, however,

the engineer quickly comes up against a significant fact which determines how the equipment must be designed and must function. It is a fundamental concept of thermodynamics that any engine which converts heat into another type of energy must operate between two temperatures, one high and the other low. In more familiar earthly surroundings, there is no difficulty at the low temperature end of the cycle — the air, soil and water all around us are quite effective in producing the necessary cooling. But in space the conditions are quite different, and far less favorable. There is no atmosphere to either conduct or convect heat away, and radiation is the only means of removing it. But, unfortunately, as is well known, the rate of radiative heat transfer goes up as the fourth power of the absolute temperature. This large exponent law means that, for the cold zone of a heat engine, the radiator surfaces must be either at a high temperature or of a large area. The large radiator solution to this problem is precluded by the extraordinary high cost of placing each pound of material into space, and there seems to be no practical alternative solution to the problem other than to run the radiator hot enough to achieve good radiative heat transfer rates. This in turn means that the hot zone of the heat engine must also work at quite an elevated temperature.

Thus the special requirements of NASA and the space program lead inexorably to the use of high temperature fluids to cool nuclear reactors. Under these circumstances, the same factors which have lead nuclear engineers to turn to liquid metals for higher temperature

earth-bound power plants, have directed the attentions of the space engineer to liquid metals. There is still a wide gap in the temperatures under examination: the AEC liquid metal program directed towards power production is presently aiming for systems with a maximum liquid metal temperature of about 1300°F. While the NASA-directed work has included systems operating at considerably lower temperatures, here the greatest importance is attached to the achievement of temperatures of 2000°F and higher.* Because of these extreme temperatures, by comparison with power plant requirements, a new class of liquid metal behavior has assumed an enormous new importance in NASA thinking, that is the boiling and condensing properties of liquid metals. Because of this application, there has been renewed interest in the alkali metals more volatile than sodium, potassium and rubidium, as working fluids in a high temperature cycle. Lithium, on the other hand, has the characteristic of having a very low vapor pressure compared with the other alkali metals; and this property can also be used to advantage in some types of high temperature space application. The only remaining member of the alkali metals which occurs on earth is cesium. Although this has a low melting point (28.5°C) and boiling point (705°C), which might make it of interest for use as a high temperature working fluid its very high thermal neutron absorption cross section (31 barns) has discouraged consideration of Cs for this application. But cesium vapor has one other characteristic which is unique: of all the known elements, the least

---

* See Rosenblum, L.: Liquid Metals for Aerospace Electrical-Power Systems J. Metals 15 637 (Sept. 1963).

amount of energy is required to strip an electron from the Cs atom to form the Cs^+ ion. This low ionization potential, only 3.9 volts, makes cesium the material of choice for any application where high temperature ions are required; for example, to neutralize the space charge in a thermionic conversion system, or as the working material in an ion propulsion engine. Used in this way, the nuclear disadvantages of Cs may be avoided, and properties virtually unattainable with other materials can be utilized.

Thus the requirements of the space program have expanded the field of interest in liquid metals markedly, to include all of the alkali metals. The high temperature frontiers of liquid metal technology are being assaulted by this interest, and two phase systems, liquid and vapor, are being vigorously investigated as we shall hear in the subsequent program.

There are then, as I see it, three principal reasons for the revival of liquid metals — high temperatures, breeding, and space applications. I suppose all of us here today should consider ourselves lucky to be involved in this field. Within the unhappy memory of many of the people in this room, there was a period, not so long ago, when liquid metals were treated as something worthy of considerably less interest and support than we have now.

b. The State of the Art

From the review of the history of the liquid metal art above, it will be noted that this is by no means a new field. With mercury, there has been an extensive body of experience and understanding since the early 1930's. Sodium came out of the laboratory and started to

become a useful engineering material after about 1945. A body of experience with lithium began to build up in the period 1955-1960.

The principal change which the recent revival of interest in this field has brought about is the focussing of attention on higher temperatures. Boiling and two-phase behavior which were of importance with mercury but which had no place in earlier liquid metal work has now attained a role of great importance in current thinking.

Although the basis for a rational theory of liquid metal corrosion has long existed, there is still much that is unknown. As will be discussed later, the prediction of corrosion rates depends on a knowledge of such factors as equilibrium solubilities, diffusion coefficients, reaction rates, etc. While theoretical models from which equilibrium solubilities of solids in liquids have been developed, for other types of systems, with solid alloys dissolving in liquid metals these correlations have been so poor as to be virtually useless. For solubilities, as well as the other physical parameters which enter into the analysis of the corrosion process, there is virtually no alternative to direct experimental measurement. The data are largely empirical, and cannot readily be carried over from one solid-liquid pair to another.

This dilemma is, to a considerable extent, a direct consequence of the pathetic lack of understanding of the liquid state, compared with either the solid or the gaseous state. For this reason, physicists have tended to shun this area, and the most important work on heat transfer, fluid flow dynamics, and similar properties has been done by chemical engineers who have often been content to stop with empirical

correlation involving dimensionless quantities (to which they like to give obscure and esoteric names) raised to peculiar decimal powers. These men pride themselves on their "practicality" and are content to leave the analysis of <u>why</u> their correlations work to others — who seldom seem to rise to the challenge.

For these reasons, there has been a rather absurdly small amount of basic work done on the mechanisms of liquid metal corrosion, and the formulation of general relations consistent with these mechanisms. It is even suspected that many workers in this field seriously doubt whether it is possible to formulate general laws of behavior for liquid metal systems. It is the purpose of this session today to call your attention to the amount of work which <u>has been</u> done in this area, and to attempt to explore with you the extent to which such theoretical studies on liquid metal corrosion can be expected to be useful.

c. <u>The Need for Mechanisms and Models</u>

Much of the important corrosion work, in liquid metals as in the more familiar aqueous media, is empirical. Dozens of different techniques of laboratory tests of corrosion resistance have been devised. Some of these have been in static systems, others with flowing liquid. Experiments have been carried out in devices with a ΔT, and others where the system was operated essentially isothermally. Sometimes in the flowing systems the fluid velocities were much lower than those to be expected in a practical operating heat transfer system. In practically no case has liquid metal corrosion proceeded for the length of time which the application being investigated would require.

It is in the correlation of these studies that a theoretical mechanism and a physically sensible model are most required. With such a model, it is possible to predict the behavior of a flowing system from small scale laboratory pot tests. The effect of ΔT and of flow velocity follow from the theory. Extrapolation of test results, obtained over a few thousands of hours at most, to the period of years, tens of thousands of hours, is possible if there is some rational model on which to base this evaluation. Skeptics often question the validity of laboratory experiments on gram quantities of liquid metals for predicting the behavior of full scale systems which may contain tons of the material. As a matter of fact, such predictions based on and guided by a good theory, have been remarkably successful in predicting the corrosion behavior of large assemblies — a situation that is not well known or appreciated.

This remark must not be interpreted to mean that the field has reached the point where a few simple laboratory tests and a few hours on the computer will predict absolutely the corrosion rates of a full size nuclear reactor system years after startup with high precision. It should be recalled that laboratory tests in this field are remarkably difficult to carry out and reproduce, particularly with the alkali metals. A laboratory which can consistently get the same rate on a material which does not undergo a great deal of attack in liquid sodium (and consequently is a reasonable candidate for application), to within a factor of two, say, has reason to be proud of its technique. Having attained this degree of consistency and reproducibility internally, workers at one laboratory often find it a rather shocking

experience to compare their results with those from another installation. The discrepancies often lie far beyond what can be considered reasonable. Basically, this situation seems to arise because corrosion is a <u>rate process</u>, and rate determinations whether they be in chemical kinetics, physical processes, or something else, are notoriously sensitive to small and uncontrolled variations in the test parameters — in general much more susceptible than equilibrium or steady state properties.

But fortunately, as a practical matter, this difficulty is not so horrendous as it may first appear, and in fact is more annoying to the theorist than limiting to the engineer. The man charged with the choice of materials for construction of a system really cares little whether a 0.010 inch thick cladding undergoes 0.0001 or 0.0005 inches of corrosive penetration in its nominal operating lifetime. He might truly be concerned about the difference between 0.001 and 0.005 inches; but then he would not be inclined to use a material that could lose as much as 10% of its initial thickness in the first place, if any alternative solution were available.

It must however be kept in mind that experimental liquid metal corrosion studies are difficult, expensive and time-consuming, especially with the alkali metals. An important reason for pursuing a meaningful theoretical model for the corrosion is not only to permit the kind of extrapolation to large scale systems from laboratory tests which was emphasized above, but in fact to cut down on the amount of laboratory testing as well. This objective will have a considerable appeal to anyone who has gone through the painful process of setting

up a potassium or lithium loop at high temperatures as much as it will to the auditors and cost accountants who undoubtedly maintain a close watch on his expenses!

There has been a widespread tendency in Government-sponsored projects to concentrate on hardware components development rather than on the basic studies of how systems work which has been emphasized above. A more balanced mixture of the two kinds of approach is most desperately needed, and in the liquid metal corrosion field in particular, there is an urgent need for more carefully controlled experiments and analyses, and fewer large scale Edisonian test programs of dubious value.

2. LIQUID-METAL CORROSION AS A SOLUTION PHENOMENON

John R. Weeks, Brookhaven National Laboratory →27

The driving force for liquid metal corrosion is the equilization of chemical potential for dissolution of all solid surfaces in contact with the liquid. In any practical system, this is an impossible goal; therefore, one observes several mass transfer processes. A simple solubility equation is given as:

$$S. M. + L. M. = S. M._{(L.M.)} \tag{1}$$

where $K = S.M._{(L.M.)}$, the concentration of the solid metal dissolved in the liquid.

The dissolution in static systems of pure metals is sketched in Figure 2-1. One should note the following: 1. The rate decreases with time, but does not become zero. 2. In a dynamic loop with a ΔT, we have a steady-state concentration of solute. R, the rate of dissolution, is a function of ΔT, since $S_o - S$ is a function of ΔT. Also, as $S \rightarrow 0$, the free energy of dissolution approaches infinity. Even in isothermal systems mass transfer is not zero, since all surfaces in contact do not have identical chemical potentials for dissolution. An example is shown in

Figure 2-2. Here, Fe was contacted with Fe-saturated Bi for 235 hours at 689°C. Note the grain-boundary etch of polished surface, and the local deposition of Fe crystals.

So far I have discussed pure systems. With an alloy container metal, the situation changes: the solubilities of all components of the alloy are not equal. However, in many liquid metals, the solubilities of the alloy components are in the same sequence, i.e.; Fe, Cr, and Ni are increasingly soluble in that sequence. Also, in Bi and Hg, Cb is more soluble than Ta (in Bi, V is also more soluble than Cb). Data for Fe, Cr, and Ni in several solvents are shown in Table 2-1. Solubilities in the alkali metals are somewhat obscure and controversial, probably because of effects of impurities discussed below. The only exception to the $S_{O_{Ni}} > S_{O_{Cr}} > S_{O_{Fe}}$ sequence is the datum for Cr in Pb; this was extrapolated from data taken above 900°C, and is therefore only a rough approximation. In K, Rb, and Cs, however, selective leaching of Ni has not been observed.

In addition to the higher solubility of Cr than Fe, mutual solubility effects are occasionally observed. In Figure 2-3, we show the concentrations of Fe and Cr in liquid Bi as a function of time during static corrosion of a type 410 steel crucible at 600°C. After the first four hours, isothermal mass transfer

22

similar to that shown in Figure 2-2 continued. The Cr, being
more soluble (see Table 2-1), remained in solution, and reduced the
Fe solubility. Therefore, results of static tests (i.e. selec-
tive leaching of Cr) may not be confirmed by results in dynamic
tests*, in which the Fe and Cr dissolve and mass-transfer in the
same ratio as they are present in the steel (initial slope of the
curve in Figure 2-3).

---

*at temperatures at which the rate of solid state diffusion

$$<< \alpha \frac{A}{V} (S_o - S)$$

Table 2-1

Solubility at 600°C (ppm) of Ni, Cu, and

Fe in Several Liquid Metal Solvents

	Bi	Pb	Hg	Li	Na
Ni	66,000	5,370	~100	660	*
Cr	150	~1.3	6.5	12	*
Fe	50	2.3	0.51	11	*

*Selective leaching suggests $S_{O_{Ni}} > S_{O_{Cr}} > S_{O_{Fe}}$ in Na.

$$S = S_0 \left(1 - \exp^{-\alpha \frac{A}{V} t}\right)$$

$$R = \alpha \frac{A}{V} (S_0 - S)$$

(a) Concentration of solute as a function of time.

(b) Rate of dissolution (slope of a) as a function of time; S is the concentration of solute at any given time; S_0 is the solubility at the temperature of the experiment; α is the solution rate constant; A/V is the surface area to volume ratio.
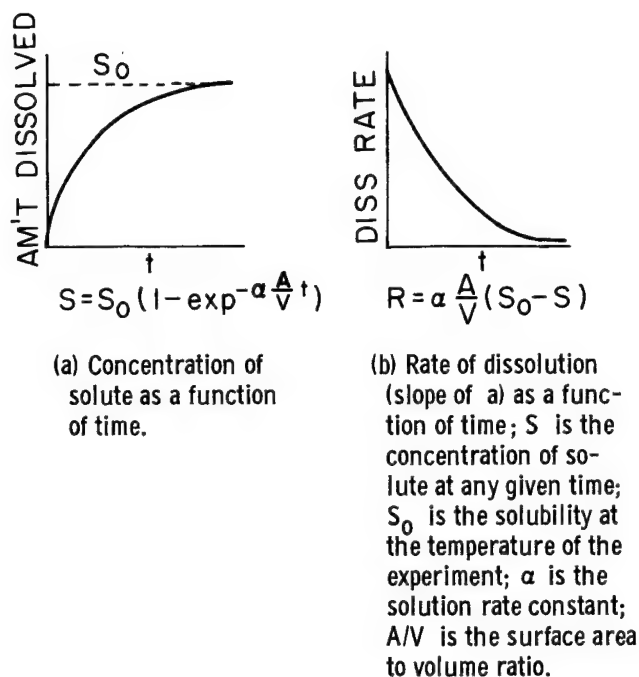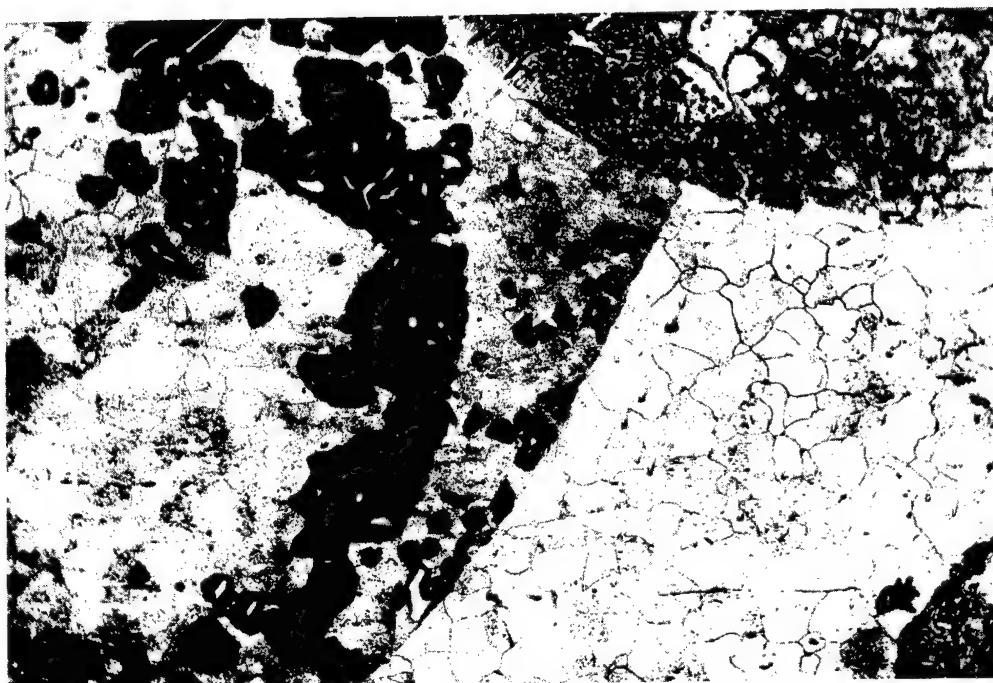
Figure 2-1. - Typical dissolution curves in isothermal systems.

Figure 2-2. - Grain boundary attack and localized crystal growth on a polished surface of pure iron contacted for 235 hours at 689 $\pm 1^0$ C (1270^0 F) with bismuth presaturated with iron (contained in an iron crucible). Original X75. (Unetched.)
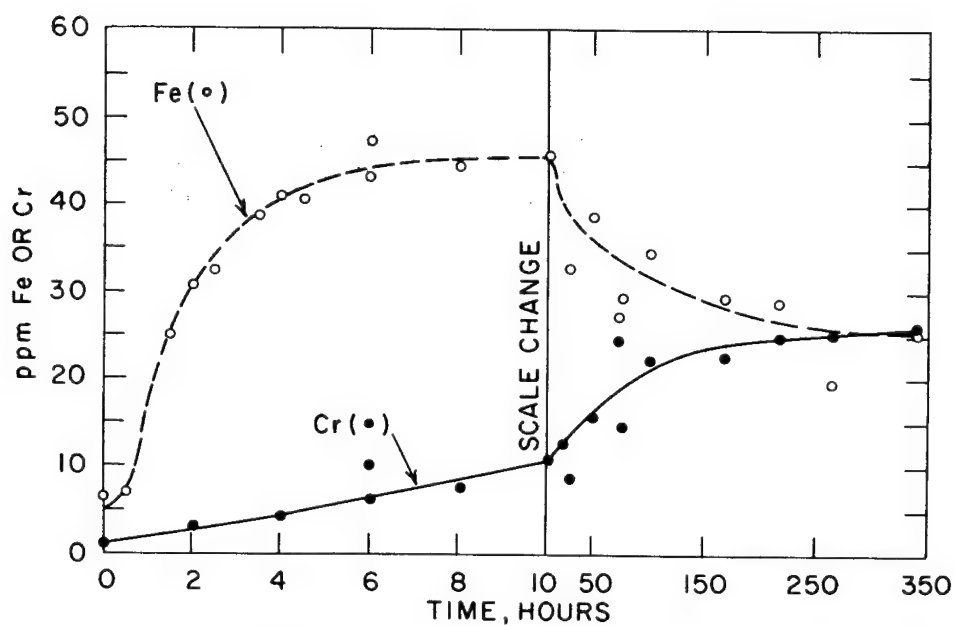
25

Figure 2-3. - Concentration of Fe and Cr in Bi contained in an 410 steel crucible as a function of time at 600° C. Crucible had been filled with Bi at 410° C where solubilities are negligible. Data at zero time are from a sample taken at 410° C immediately before the temperature was raised.

3. CHEMICAL CORROSION PROCESSES

Leo F. Epstein ⟶ 35

a. <u>Chemical Reaction, Formation of Stable Compounds</u>

Mercury is one of the most "noble" of the metals, and it is not really surprising that with this material chemical reactions are of less importance in the corrosion process than physical phenomena, solution and diffusion transport, for example. It is easy to overlook the fact that with alkali metal systems, the formation of new chemical species in the system, by reaction with the fluid or some impurity which it contains may be of considerably greater importance than the solution mechanism.

The reactions of the oxygen-hungry metals Be, Zr, Nb, and Cr, in some steels, are examples of this. In sodium, which ubiquitously contains Na_2O as an impurity, the principal corrosion effect observed is the formation of a film of oxide on the metal surface, e.g.

$$Zr + 2Na_2O = ZrO_2 + 4Na$$
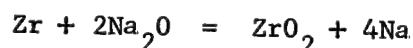
The metallic specimen gains weight, and the correlation between these ΔW's and the metallographically determined film thicknesses is quite good. Occasionally, these films show poor adhesion properties, and are readily spalled off. This is true, for example, of the BeO films formed by exposing beryllium metal to sodium. If the fluid is static and quiescent, the positive weight gains described above are observed. But if the liquid is stirred, or flows past the sample at high velocity, there is a strong tendency of the film to flake off, and the sample may show positive (as above), zero, or even negative

27

weight changes (that is, weight losses). Sometimes these films are rather impermeable to the corrosive medium and are therefore protective — the corrosion process slows down and approaches a zero rate. But as often as not, they are non-protective, and do not seriously inhibit corrosion. It should be noted that with many materials the corrosion film formed by the oxidation process, as noted above, may not be the simple oxide. With zirconium, for example, the formation of stable sodium zirconate by reaction

$$Na_2O + ZrO_2 = Na_2ZrO_3$$
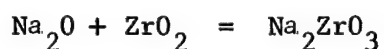
is thermodynamically favored, and may readily occur. The nature of the films actually observed in post-exposure observation is highly dependent on the experimental procedures employed: for example, if the excess alkali metal is removed from the sample with water and alcohol in the case above, some of the sodium salt may be soluble and disappear.

Oxygen is not the only impurity element which contributes to the corrosion process by forming stable compounds. Nitrogen forms a stable nitride with lithium, and this can react with many materials to produce heavy metal nitride films. Attempts to use nitrogen as an inert cover gas over sodium have, in the past, gone awry when the fluid contained calcium (as it frequently does) and was in contact with a strong nitride-forming metal. The dissolved calcium seems to have reacted at the gas-liquid interface to form the stable and soluble nitride. This moves through the liquid and when it encounters the metal, reacts with it to give up the nitrogen.

$$Ca_3N_2 \text{ (in solution in Na)} + 2Zr(solid)$$

$$\downarrow$$

$$3Ca \text{ (in solution in Na)} + 2ZrN(film)$$
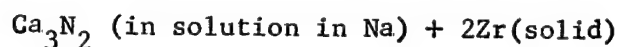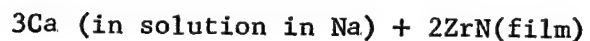
The dissolved calcium metal thus regenerated then is free to pick up another batch of nitrogen at the interface, and the process continues indefinitely.

Another substance occurring quite commonly as an impurity in alkali metal systems is carbon which also plays a significant role in corrosion processes through the formation of stable compounds. Thus stainless steels of the 18-8 type, exposed to sodium or potassium, in the presence of a source of carbon, tend to pick up this element and if the process proceeds far enough characteristic grain boundary precipitation of carbides is observed. It should be noted in passing that the reactions with carbon in alkali metal systems have assumed an enormous importance in recent times. First, nearly every reactor which has had coolant trouble has run into this problem because of carbonaceous material of some kind — the tetralin in SRE, the graphite at Fermi and Dounreay, come to mind immediately. There is a growing feeling that in some kinds of systems, sodium for power plant use in particular, it is carbon and its corrosion behavior which sets an upper limit on the temperatures practically attainable at the present time (not so many years ago it was oxygen, but it is now felt that oxygen can be measured, removed, and controlled, whereas each of these procedures is doubtful in the case of carbon). We shall discuss the problem of carbon again later.

b. Chemical Reaction Without Stable Compound Formation

From the earliest work on liquid sodium corrosion of steels, it was clear that the process was accelerated by the presence of oxygen. Nevertheless, the material which went into solution in the hot zone of a loop, and that which came out in the cold region were both pure iron. How could oxygen act to speed up the reaction

$$Fe(solid) \rightarrow Fe(\text{in solution in Na})$$
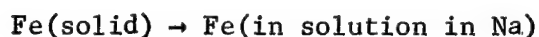
in the presence of huge excesses of the extremely powerful reducing agent Na? All of the familiar oxides of iron, FeO, Fe_2O_3, and Fe_3O_4, are thermodynamically unstable in the presence of liquid sodium at elevated temperatures and should be reduced to the metal at equilibrium. Faced with this perplexing anomaly in the late 1940's it was postulated that a compound of the type

$$FeO \cdot x \ Na_2O$$
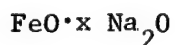
might be stabilized to reduction by Na significantly so that it could participate in the corrosion process and lead to the kinds of relationships observed. This highly speculative and tenuous hypothesis was given a substantial boost in 1954 when our guest, Dr. Geoffrey Horsley of Harwell, was able to prepare a compound of the type considered, with $x = 2$, and to show that it in fact did have the properties needed to explain the behavior of Fe-Na systems. The passage of time has tended to strengthen the hypothesis that in many alkali metal corrosion processes, compounds of only limited stability, whose lifetime or steady state concentration in the system may be extremely small, may nevertheless play an important role in explaining the behavior of the system.

30

c. Comparison with Aqueous Systems

Because of the comparatively greater amount of experience with aqueous corrosion it is instructive to turn to these systems to see whether analogues of what is observed in liquid metals are in fact known. In water, often, the rate of solution of a solid is determined by the diffusion of the resulting solute species in the H_2O, just as has been hypothesized for liquid mercury. Professor Bonilla will discuss this process in some detail shortly. But in a number of cases, it is found that the process is much slower than diffusion control would demand, and a detailed examination indicates that in many of these examples, there is always the possibility of a chemical process occurring to modify the picture. One example is the solution of Fe in strong HNO_3. Here the corrosion rate is slower than it is in other acids, and it is not difficult to believe that the oxidizing characteristics of HNO_3 result in a passivating film on the iron which slows down the process. Similarly, when the reaction of magnesium and acetic acid is studied, using alcohol-water mixtures as a solvent, the process has been shown to depend on something other than the diffusion rate of the Mg^{++} ion in solution, and here the chemical reaction which influences the rate is supposed to be the esterification process where the alcohol as well as the metal compete for the acid present.

d. Liquid Metals

The importance of iron base alloys led to the early study of these materials in liquid metals, and this work has been most

31

illuminating. With Fe in Hg, the corrosion process is quite rapid,
and may be predicted almost quantitatively from information on the
equilibrium solubility of iron in mercury, and the physical properties
of the pure metals. With iron in sodium, the corrosion process is
much slower. This and other aspects of the corrosion process in
this system can be explained in terms of chemical reactions such as
have been discussed above. (In complete fairness and honesty, it
should be pointed out that there is a long-standing controversy on
the value of the equilibrium solubility of Fe in Na, and by choosing
the lower set of solubility values, corrosion rates consistent with
observation can be obtained using the diffusion hypothesis. This
explanation does not however account for the effect of oxygen on
the system.)

The early success of mercury systems industrially was possible
only after it had been discovered, quite empirically, that a few
parts per million of titanium or zirconium dissolved in the Hg had
a profound effect in inhibiting the corrosion process with iron,
that is slowing down the rate of solution. This inhibition was at
an early date attributed to some kind of film formation, which
resulted in the rate of solution rather than the diffusion of the
solvent being the rate-controlling process. The nature of these
films will be discussed later. For the present it is sufficient to
point out that these inhibitors seem to work in other heavy metals —
bismuth and lead, for example — and that the process can most readily
be explained as a shift from diffusion to solution control.

e. Other Examples of Solution Control

The corrosion of Fe by Ti-inhibited mercury has been cited as
an example where the solution rate, as influenced by chemical reaction
processes, rather than diffusion, is the rate-determining step. As
has been indicated, the corrosion of Fe by Na is also believed to be
largely chemically controlled. This arises from the low value of
the rate (although this argument is weakened by the inconclusive
solubility data); and even more importantly, from the strong influence
of oxygen on the system.

As a general rule, it may be assumed that whenever a trace amount
of impurity has a very strong effect on corrosion, a chemical rather
than purely physical process is responsible for the behavior of the
system. The effect of Ti on mercury, the large number of corrosive
systems involving the alkali metals where oxygen markedly accelerates
the process, and the marked increase of corrosion in lithium and
calcium melts by nitrogen contamination are all examples of chemically
controlled corrosion processes, in all probability.

Finally, it should be pointed out for the benefit of our NASA
friends that the refractory metals in which they are becoming so
deeply involved — columbium, zirconium, molybdenum, tantalum, tungsten,
titanium, etc. — all form strongly acidic oxides, which readily combine
with alkali oxides to form rather stable niobates, zirconates,
molybdates, etc. Because of this, it can be quite reasonably pre-
dicted that corrosion in these systems will be chemically controlled,
and that the effect of oxygen present as an impurity will be extremely
large and important in determining the behavior of the system.

33

(4.) MECHANISMS IN LIQUID-PHASE CORROSION

a. Diffusion Controlled

Charles F. Bonilla　Columbia University] ⟶ 45

In aqueous corrosion, the dissolving metal is almost always oxidized to its positive ion, and also frequently undergoes further chemical reaction and precipitation on the metal surface. But the corrosion of solid metals by liquid metals can take place merely by solution of the solid metal at the interface, followed by diffusion into the bulk of the liquid metal phase, without complications from compounds or precipitates. In some cases compounds do form in the liquid metal, but still without altering the diffusion step. In these cases, the diffusion is generally the rate-controlling step, as it is evidently necessary, for such corrosion to proceed, for the solute to leave the area where it dissolved.

The two typical situations, or "geometries", in which diffusion-control can occur are evidently:

a) Pure molecular diffusion of the solute molecules throughout a whole quiescent body of the liquid metal. The diffusivity, D, is here evidently a key factor in the rate and total amount of corrosion, in addition to the solubility of the solid metal and the size of the vessel. However, this situation will not frequently be important, in that seldom would a body of liquid metal be entirely quiescent unless deliberately so intended (as in a test to measure D); and even if it were quiescent in an actual situation, the total corrosion would probably be low due to the low solubility in most practical cases.

b) Transport of the solute away from the corroding area by flowing or stirred solvent (Figure 4A-1). Here the solute only needs to diffuse a short distance (through a "laminar boundary layer" of thickness δ) to get into the

main solvent stream. However, diffusivity is again important, because no matter how short the distance (how thin the boundary layer), the rate of diffusion will be proportional to the diffusivity (as well as to the difference in concentration, etc.).

Diffusivity

Therefore one of the **first** pieces of information one should seek in correlating or predicting diffusion-controlled, or potentially diffusion-controlled, corrosion is the diffusivity of the solute in the solvent.

Unfortunately, this is the most difficult and uncertain of the common physical properties to measure. The Stokes-Einstein formula:

$$D = \frac{RT}{N} \cdot \frac{1}{6\pi\mu r} \qquad (1)$$

where: R = the gas constant

   T = absolute temperature

   N = Avogadro's Number

   μ = solvent viscosity

   r = radius of the diffusing atom (or ion), as calculated from the density of the (molten) solute and the mass of one atom, considering the atom a sphere.

Fortunately, μ is known for the alkali metals to reasonably high temperatures, and the equation is thus readily employed.

Comparison of this equation against available published experimental liquid metal diffusivity data (1,2), shows that the published data are all either:

   a) within an average of $\pm$ 5% of equation 1, or

   b) within an average of $\pm$ 15% of twice equation 1.

Diffusion of the alkali metals in mercury is found to fall under case (a). From a consideration of equimolar counterdiffusion it is expected that the diffusion of mercury in the alkali metals, and thus presumably also of other heavy metals in the alkali metals, will also fall under case (a), which can therefore be used with considerable **confidence** in corrosion. However, if it is desired to be conservative, case (a) should be used for desirable phenomena (e.g., dissolving of a fuel in a homogeneous liquid metal reactor) and case (b) for undesirable phenomena (e.g., container or pipe corrosion).

Mass Transfer Coefficients

Knowing the diffusivity of the metal pair and the "geometry" and flow conditions, one can proceed to estimate the mass transfer coefficient for a corrosion situation, or correlate it as obtained from a corrosion test. The usual units are moles/(sec $\times$ cm^2 $\times$ $\frac{mole}{cm^3}$) = $\frac{cm}{sec}$, and the symbol in corrosion work is α.

This coefficient is used in the equation for the mass transfer or corrosion rate N per unit time θ over area A:

$$\frac{N}{A} = \frac{dn}{d\theta} = \alpha \ (S_0 - S). \tag{2}$$

As shown in Figure 4A-1, S_0 is the solubility of the dissolving metal in the liquid metal and S is the appropriate concentration in the liquid phase. Actually, non-ideality of the solution may be significant; it can be determined in various ways and taken into account (2), if desired.

One way that α can be predicted is from correlations of dimensionless ratios obtained in other diffusion-controlled corrosion or dissolution tests in the same geometry (i.e., to exact scale). For instance, in forced convection, it can be presumed, and has been verified, that:

$$\left(\frac{\alpha}{u}\right) = \phi\left(\frac{\mu}{\rho D}\right), \left(\frac{du\rho}{\mu}\right) \tag{3}$$

Sherwood No. $= \phi$(Schmidt No., Reynolds No.)

where u is an appropriate velocity in the stream, d an appropriate dimension, such as a length or diameter, and ρ is the stream density. The function ϕ is identical for any one shape or "geometry", regardless of the size or materials involved.

However, few mass transfer tests have been carried out under sufficient control to establish the correlation with reasonable accuracy. Fortunately, it has been established (2, 3) for three key geometries (forced flow through packed beds, forced flow in tubes, and **natural** convection outside of horizontal cylinders) that liquid metal mass transfer follows the same **correlations** as mass transfer of non-metals in the same geometry, and much more importantly, is analogous to non-metal heat transfer in the same geometries.

Mass Transfer from Heat Transfer Correlations

In translating the heat transfer correlations into mass transfer correlations, the following substitutions are employed: replace the heat transfer coefficient h by ($\alpha C\rho$), where C is the specific heat of the liquid; replace the thermal conductivity k of the liquid by ($DC\rho$); replace the rate of heat transfer q by N; replace the driving force Δt by ΔS; and (in natural convection) replace the fractional thermal expansion ($\beta\Delta t$) by the fractional expansion (or contraction) due to change in concentration, $\left(\frac{d\rho}{dS} \cdot \frac{\Delta S}{\rho}\right)$. Of course, in a non-symmetrical geometry, if the dissolving metal decreases the density of the liquid metal, that element must be the heated element in the heat transfer analog, and vice versa.

If these conclusions hold closely for such different geometries, it is evident that they can be presumed to hold for all other geometries, although

38

no liquid metal tests, and even maybe no mass transfer tests, have ever been carried out on those geometries. These would include such situations as forced flow across one tube or a bank of tubes, forced flow along a short tube, natural convection inside a vertical or horizontal tube, impingement of a jet on a wall, and many other for which heat transfer correlations are available for non-metals (4). However, it is important to recognize that only non-metal heat transfer correlations may be used, since heat transfer in liquid metals follows a different mechanism than that of mass transfer, i.e., electron flow is the main mechanism of heat conduction in metals, but does not contribute to diffusion.

As an example of profitable or potential carry-over from heat transfer (or fluid flow) knowledge to diffusion, the short tube or L/D effect may be cited. Established laminar flow pressure drop theory (4) shows that the velocity distribution across a tube containing laminar flow does not reach the asymptotic value until a downstream length L, expressed in tube diameters as (L/D), of 6% of the Reynolds Number. Between parallel plates the corresponding (L/equivalent D) is 1.5% of the Reynolds Number. For turbulent flow heat transfer several complicated expressions are available, but the simple generalization that some 6 to 10 diameters is sufficient for the local coefficient of heat transfer (thus mass transfer) to become substantially constant is frequently adequate. If total corrosion is to be measured or predicted from the inlet, rather than local corrosion, the test specimen should be some 20 to 50 diameters in length to approach the asymptotic corrosion fairly closely. This L/D effect is no doubt the cause, or at least the principle cause, of the "down-stream" effect, recently identified independently for corrosion by Epstein, and covered in Section (10 A) of this discussion. From the theoretically or experimentally known effect of L/D on pressure gradient or on heat

transfer, the corrosion test specimen length to approach within any desired percentage of the asymptotic or long specimen corrosion rate can be predicted with confidence for either laminar or turbulent flow.

Prediction of Rate and Amount of Corrosion

Assuming we know, measure, or predict D, then α, we still have a question as to how much corrosion will occur, in view of variations in the driving force $(S_0 - S)$ and other factors. This will be important in predicting corrosion, but also in interpreting tests.

The equation can be set up, and integrated if pertinent, according to the geometry and circulation in the system. Two principal cases in testing will be described.

1) Capsule tests, or the saturating of a pool kept uniform by natural circulation or by strong agitation. At each instant:

$$N = \alpha A (S_0 - S) \tag{4}$$

However, also
$$N = V \frac{dS}{d\Theta} \tag{5}$$

where V is the volume of the pool or system. Eliminating N and integrating from S_1 (frequently zero) to S_2:

$$\ln \frac{S_0 - S_1}{S_0 - S_2} = \frac{\alpha A}{V} \Theta \tag{6}$$

Thus, a semilog plot of $S_0 - S$ vs. Θ for an experiment gives a straight line if diffusion-controlled, and yields α from the slope. Or knowing α for a situation, S can be predicted as a function of time, and $V\Delta S$ = total weight lost by corrosion. When the pool is saturated (assuming it is isothermal) the corrosion stops.

2) In a natural circulation or forced circulation loop the circulating metal goes from subsaturated towards saturation in the hot region, and in turn

40

gives up the metal recently dissolved when it gets back into the cold region, where it again approaches saturation, but from the supersaturated direction. This thermal corrosion can keep on indefinitely until the hot spot corrodes through and/or the cold spot fills up with crystals, thus is much worse. The concentration map is as shown in Figure 4A-2. It is seen that both curves follow logarithmic approaches, the one with the larger conductance αA approaching its S_0 more closely.

By setting up and solving the simultaneous equations of dissolving and precipitating and flow transport, we get (5):

$$N = \frac{Q(S_{0,h} - S_{0,c})(1-e^{-(\alpha A)_h/Q})(1-e^{-(\alpha A)_c/Q})}{\left[1-e^{(-\frac{(\alpha A)_h - (\alpha A)_c}{Q})}\right]} \tag{7}$$

where Q is the flow rate in the same mass units as S, N and α, and the subscripts h and c refer to the hot and cold sections, respectively. $(S_{0,h} - S_{0,c})$ can be obtained from the slope of the solubility curve $\frac{dS}{dt}_0 \times (t_{hot} - t_{cold})$. Clearly, if all of the other quantities in the equation are known N can be predicted, and thus the life of the loop. Or in a test, knowing N and (say) everything but $(S_{0,h} - S_{0,c})$, this can be calculated, and thus the temperature coefficient of the solubility.

Evidently theory is available to predict or interpret most cases of diffusion-controlled liquid metal corrosion. The main problem is setting up and doing good experiments so as to be able to identify the diffusion-controlled systems, and so as to obtain the solubility data to permit designing around, or containing, such corrosion.

Bibliography

(1) Bonilla, C. F. et al. AEC report NYO-3088 (1952).

(2) Bonilla, C. F. "Mass Transfer in Molten Metal and Molten Salt Systems".
     Proceedings of the Geneva Conference on Peaceful Uses of Atomic Energy
     $\underline{9}$, 331 (1955).

(3) Dunn, W. E., Bonilla, C. F., Ferstenberg, C., and Gross, B. "Mass Trans-
     fer in Liquid Metals". A.I.Ch.E. Journal $\underline{2}$, 184-189 (1956).

(4) Bonilla, C. F., Ed. "Nuclear Engineering", p. 294. McGraw-Hill, New
     York (1957).

(5) Ibid., p. 494.

E-2492

42
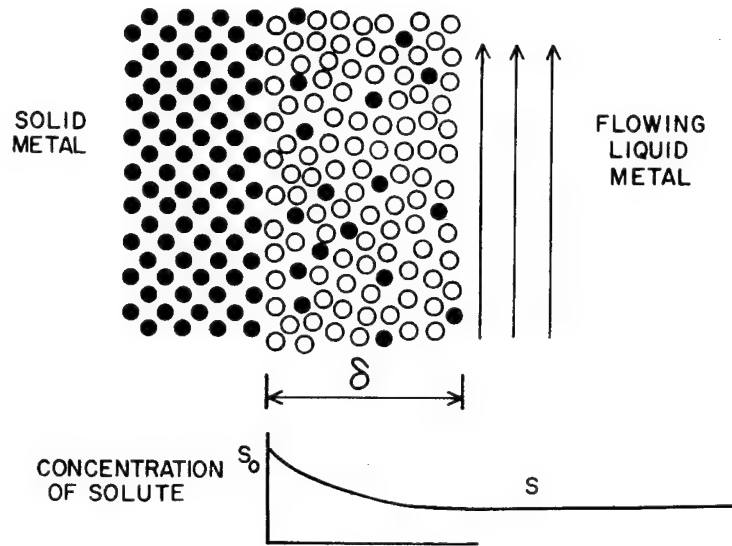
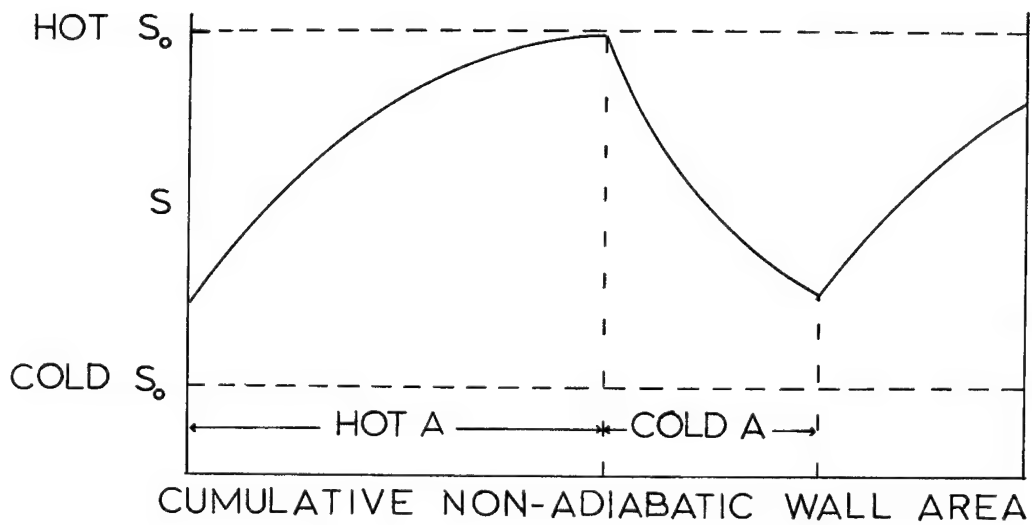Figure 4A-1. - Dissolution of a solid metal into a liquid metal.

Figure 4A-2. - Concentration of solute around a thermal loop.

In previous sections, corrosion processes determined by solution rates, rather than the diffusion rates which Professor Bonilla has just discussed, have been considered from a phenomenological point of view. It is possible to formulate quantitative relations for these various kinds of corrosion which are equally applicable to either of these models.

Thus if a solid sample of surface area A (cm^2) is immersed in V (cm^3) of a liquid metal at constant temperature for a time t sec., the concentration of solute in solution S (g/cm^3) is given by the equation

$$S = S^o \left[1 - e^{-\alpha (A/V) t} \right]$$

where S^o is the equilibrium solubility of the solid, and α is the specific solution rate constant of the pair, with the units of a velocity, cm/sec. The mechanism of the process in this case, whether it is diffusion or solution-controlled, how oxygen and other impurities influence the system, etc., enter into this equation only insofar as they influence α.

The simple physical concepts which lead to the equation for an isothermal system above can also be applied to the more important case where the fluid is flowing in a system where there is a temperature gradient. In such a system, the corrosion rate at each point R (g/cm^2-sec) is given by

$$R = \alpha(S - S^o)$$

where all of the quantities appearing in this equation refer to a specific point in the flow pattern at which the temperature is $T(^oK)$ and α, S, S^o and R all refer to this temperature. Specifically, if the corrosion process is diffusion limited, the rate equation may be written in another form

$$R = - D \, (\partial S/\partial y)_{y=0}$$

where $\partial S/\partial y$ is the solute concentration gradient, passing from the wall into the solution, and this value at y=0 represents the concentration gradient at the solid-liquid interface. D is the diffusion coefficient of the solute in the fluid ($cm^2/sec.$). Those who are familiar with heat transfer relations will note the similarity of α to a heat transfer coefficient, and the parallelism between D and the thermal conductivity, and other provocative relations. For a closed loop of diameter D (cm) operated with two temperature regions, a hot (symbol H) and a cold zone (symbol C) and with the fluid flowing around the system at a constant velocity v cm/sec., the corrosion rate at a distance x cm. from the beginning of the hot zone $R_H(x)$ is given by

$$R_H(x) = - \frac{S_H^o - S_C^o}{\left(1/\alpha_H + 1/\alpha_C\right)} \exp\left(- \frac{4\alpha_H}{D \, v}\right) x$$

While the model here, with sharp discontinuities between the hot and cold regions is rather unrealistic, this oversimplified system brings out many important points on the corrosion pattern in dynamic loops with a ΔT.

In sodium systems, and presumably with other alkali metals as well, the effect of oxygen on the corrosion process is to a first approximation described by taking α as directly proportional to p, the oxygen content of the sodium (generally expressed in parts per million by weight), i.e.

$$\alpha \;=\; kp + \;.....$$

While this relation is not well-confirmed experimentally, and further observations are required, it should be pointed out that this equation leads to quantitative predictions in the Fe-Na system that are in excellent agreement with the observations made at the General Electric Company in San Jose, California, by R. W. Lockhart and his co-workers on the AEC-sponsored Sodium Mass Transfer Program.

In solution-controlled corrosion, one of the important problems is to identify the exact step which determines the overall rate for the process. In the case of the sodium-iron system, recent developments have suggested that the rate-determining step is the diffusion of the $(Na_2O)_2 \cdot FeO$ the stabilized oxide species, in solution (rather than dissolved metallic iron). This conclusion was arrived at largely from an analysis of the "down-stream" effect which will be discussed later, again from the data obtained in the G.E.-AEC Sodium Mass Transfer Program. One fragment of evidence that may be cited in support of this model is the dependence of the corrosion rate on the fluid flow velocity. Based on the explanation above, this should vary as $v^{0.8}$. The results of approximately 2000 tests on iron base alloys in Na, has on statistical analysis led to a value for the exponent of v of 0.76 ± 0.18, quite excellent agreement with the predictions of the theory.

47

5. EFFECTS OF IMPURITIES

a. Oxygen

John R. Weeks

John R. Weeks 59

In the alkali metals, O, N, H, C, and inhibitors all have
an important and often dominating influence on corrosion processes,
both individually, and in combination.

In the alkali metals oxygen may have either or both
of two effects: it may accelerate corrosion by catalyzing
dissolution of the solid metal atoms, or oxygen itself may be
the major migrating constituent. Either process is a direct
result of simple thermodynamics.

A mechanism for O-catalyzed mass transfer is sketched
schematically in Figure 5-1. The reaction is presumed to reverse
in the colder portion of the flowing system. The predicted first
order dependence has been experimentally demonstrated, Oxygen-
catalyzed mass transfer through Na was observed at KAPL with
Ni, Cr, Co, Mn, Ta, from stainless steels; however, J. De Van
has found Ni to be less sensitive than the other metals to
O-catalyzed mass transfer; perhaps a result of the higher solu-
bility of Ni.

When the solid metal oxide is insoluble in the liquid
metal, we observe oxygen exchange ÷ oxygen from the alkali metal
reacts with the solid metal surface, where it either forms
surface oxides or dissolves in and embrittles the solid metal.

49

Alternatively, oxygen in the solid metal may be leached out by the liquid metal, resulting in severe intergranular attack. In either case, the important consideration is the exchange thermodynamics of O. Evans and Thorley calculated the maximum embrittlement of Cb at 700°C to be less than 10 ppm, in agreement with experiment. We shall review their method and apply it to several systems.

The activity of O in the liquid metal at any given temperature, from Henry's law, can be assumed equal to the fraction of solubility of the dissolved phase present:

$$[a_{O\ in\ L.M.}]_T = [(ppm\ O\ in\ L.M.)/(ppm\ O\ soluble)]_T. \tag{2}$$

The free energy of O in solution $\Delta F^{\circ\prime}$ then is

$$\Delta F^{\circ\prime} = \Delta F^\circ + RT\ \log\ a_{O\ in\ L.M.}, \tag{3}$$

where ΔF° is the standard free energy of formation of the oxide at temperature T when the solubility and standard free energy data are known. The Henry's law approximation is probably good in the dilute solutions we are considering here. Figure 5-3 shows the results obtained for the Na-Cb-O and the Na-Ta-O systems using the Na-Na$_2$O solubility data of Salmon and Cashman and the ΔF° curves of Coughlin. Inouye has shown that high temperature oxidation of Cb at low O pressures (analogous to the low O activities here) proceeds by internal migration of O in the Cb

and precipitation of CbO in the grain boundaries. For prevention of precipitation of CbO by O exchange and the resultant embrittlement of the Cb, the free energy of O in Na must be more negative than that for unit activity of CbO. The required O level at 700°C is <25 ppm and at 600°C <20 ppm from Figure 5-3, in agreement with the observation that cold-trapped Na (20 to 50 ppm O) embrittles Cb at 600°C while Na hot- "gettered" with Ti (assumed <1 ppm O) does not. Free energy calculations above the melting point of Na_2O (915°C) are questionable, since the change in the solubility function is not known, and thus are dashed in Fig. 5-3.

Figure 5-4 shows the results of similar calculations for the systems $Li-Li_2O$ and $K-K_2O$, using the solubility data of Hoffman for Li_2O and Williams, et al. for K_2O. Hot-gettering of K (or Na) with Ti or Zr (but not Ta) will prevent oxidation of Cb, while Li itself will take O from Cb or Ta. Indeed, only Y of the solid "getters" shown or Ca as a soluble getter would be expected to deoxidize Li significantly at ~800°C. Hoffman showed slight O reduction of Li contacted with Y at 816°C; work in our laboratory showed the addition of 1 wt. % Ca to raw (~1000 ppm O) Li reduced the O content ~400-fold.

Extremely pure Ti has been shown by Hoffman and DiStefano to deoxidize Li, whereas Ti containing >1000 ppm O did not. The

51

free energy function for TiO in Figure 5-4 is for unit activity of TiO; the activity of O in solid solution in Ti is considerably more negative. By using the data of Schofield and Bacon for the solubility of O in α-Ti and a Henry's law approximation analogous to equations (2) and (3), one can estimate the free energy functions for O in Ti as a function of temperature:

$$\Delta F^{\circ}{}'_{O \text{ in } Ti} = \Delta F^{\circ}_{TiO} + RT \log [(O \text{ in } Ti)/(O \text{ solubility})]_T. \qquad (4)$$

The results are compared in Figure 5-5 with the calculated activities of O in Li. At 800°C one estimates the O content of Li could be reduced to <10 ppm by Ti. For this purpose the Ti/Li ratio must be sufficiently great that the O content of the Ti is not increased above 200 to 300 ppm, and sufficient time must be allowed for the reacted O to diffuse into the Ti and away from the Ti-Li interface. Thus deoxidation of Li by pure Ti is limited in the amount of O that could be absorbed in the Ti; the rate of deoxidation is probably controlled by the rate of diffusion of O in Ti. Similarly, Cb would probably pick up small amounts of O even from Na very low in O but not in sufficient quantity to produce the embrittling oxide phase. We must emphasize, however, that the major problem in corrosion of Cb by Li is not the activity of O in the Li, but rather the activity of O in the Cb; Figure 5-4 shows the potential, and a mass of experimental

data shows the experience that Li will go after O in the Cb, resulting in serious penetration of the Cb.

MoO_2 on a plot such as Figure 5-4 lies well above the Na_2O line; Na may well behave towards O-contaminated Mo in a manner similar to the way Li behaves towards O-contaminated Cb; use of $Mo\frac{1}{2}Ti$ or TZM alloys should reduce this possible problem by lowering the O-activity in the Mo. The oxides of Rb and Cs lie above the K_2O line on the figure, in that sequence.

There are two important effects not considered in these calculations. Gibbs adsorption equation is given as

$$\Gamma_2^{(1)} = \frac{-c_2}{RT} \frac{\partial \gamma}{\partial c_2}. \tag{5}$$

Since O lowers the surface free energy, γ, of most liquid metals; one anticipates a higher O concentration at the surface of the liquid, $(\Gamma_2^{(1)})$, and therefore more O pickup than otherwise would be observed. (C_2 is the concentration of O in the liquid metal in this case.)

Also, alkali metals tend to form spinels with many transition metals - analagous to the ferrite shown in Figure 5-1. The importance of these spinels appears to increase with atomic weight of alkali metals: O in Li does not effect dissolution rates, whereas O in Na has the above-noted effect on Fe (Figure 5-2)

53

which appears to be increasingly important in K, Rb, and Cs,
particularly with the refractory metals. The stability of
these spinels may add an important (and unknown) free energy
term in the above calculations.

In addition, the oxygen solubility is higher in the heavier
alkali metals, as seen in Table 5-1. This solubility increase
and equations (2) and (3) suggest that, although ΔF_o is lower
for Rb and Cs, traces of oxygen may be more difficult to remove
from these metals than might be anticipated.

Table-5-1
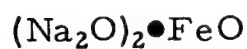
Solubility of O at 300°C

	wt (ppm)	at. (ppm)
Li	200	86
Na	126	180
K	6000	15,000
Rb	?	?
Cs	~31,000	~260,000

$$Na_2O + Fe = 2Na + FeO$$
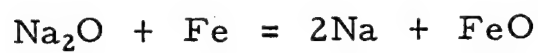
$$\Delta H = + 36,000 \text{ cal.}$$

FeO presumed soluble as

$$(Na_2O)_2 \bullet FeO$$

Corrosion rate can be written

$$\frac{d(FeO)}{dt} = kA(Na_2O)$$

Figure 5-1. - Model for catalytic effect of O on Fe dissolution into Na.
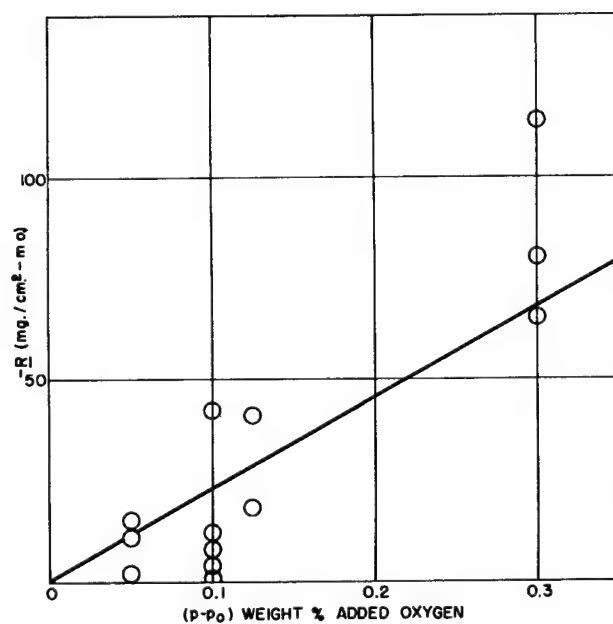

Figure 5-2. - Effect of O on rate of mass transfer of Fe through Na.
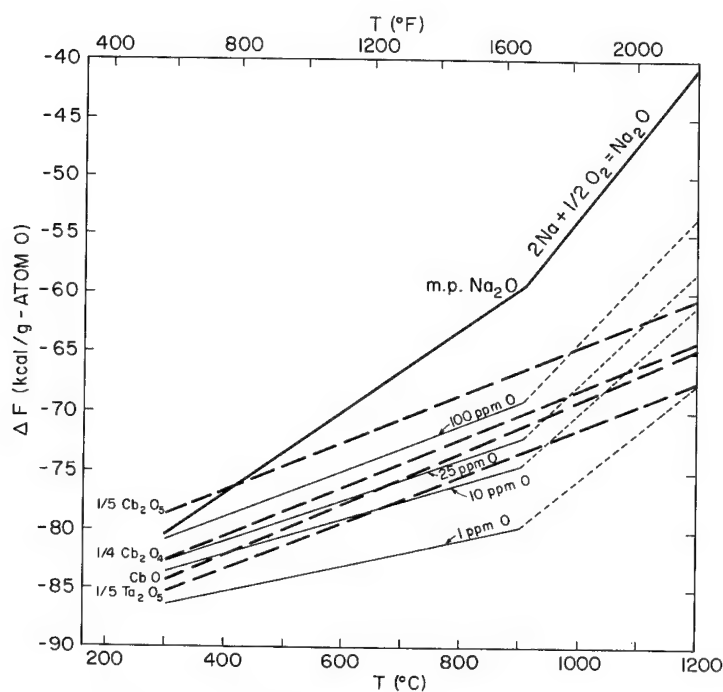
Figure 5-3. - Free energy of O in Na as a function of O concentration compared with the free energy of formation of the oxides of Cb and Ta.
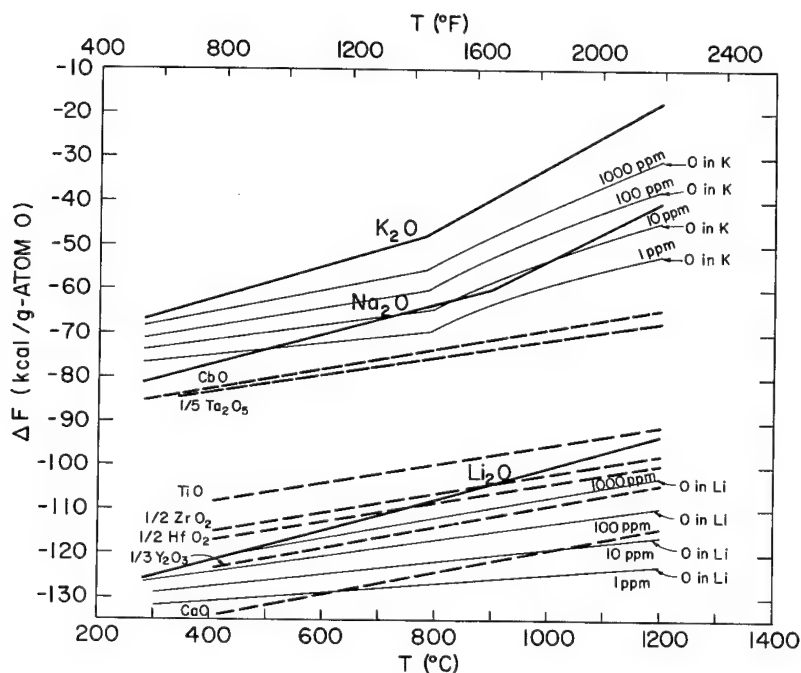

Figure 5-4. - Free energy of O in Li and K as a function of O concentration compared with the free energy of formation of the oxides of Na, Cb, Ta, Zr, Hf, Y, and Ca.
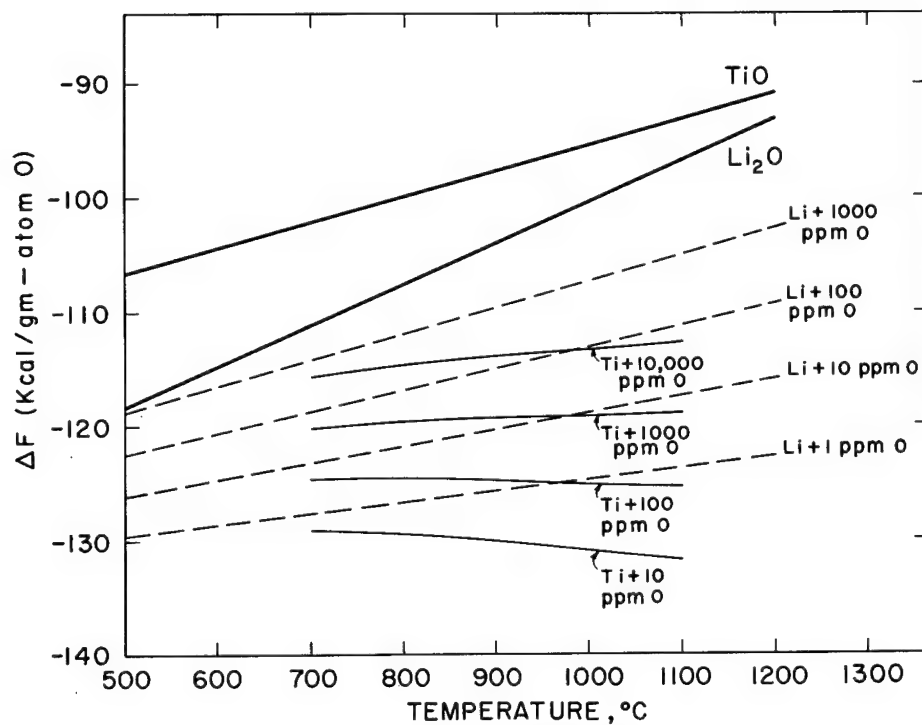
56

Figure 5-5. - Free energy of O dissolved in liquid Li and solid Ti.

57

b. Nitrogen and Hydrogen

John R. Weeks

John R. Weeks
61

In the alkali metals, N like O may also have either or both of two effects. N in Li may accelerate dissolution in a manner analagous to the above mentioned behavior of O in Na. Solubilities in Li of Fe, Cr, Ni, Cb, Ti, and Mo appear to be a function of the N content; therefore N makes Li much more aggressive by catalyzing dissolution. In Li, N in solution is a much more active dissolution catalyst than O.

Nitrogen may migrate through Na from impurities in the cover gas to nitride steel or Cb or Zr surfaces. Alan Thorley of the Culcheth Laboratory observed nitriding of Cb only when the Cb extended through the surface of quiet bath, suggesting that N_2 migration is due to surface rather than to bulk liquid diffusion. Ca in Na increases the N solubility and often introduces N and N transfer problems. This effect may override any benefit from the lowering of O activity by Ca. The large loop at Cadarache, France has recently been shut down due to N embrittlement catalyzed by Ca in the Na.

H embrittlement of the fuel elements occurred at T<300°C in Dounreay from H_2O in cover gas. H may react in conjunction with O in accelerating corrosion of Fe by Na: the NRL work on Fe solubilities in Na showed ~10 x increase in Fe solubility with O additions, and ~100 x increase in Fe solubility with O + H (added as NaOH).

59

c. Carbon

Leo F. Epstein⌡ 67

In the study of materials for high temperature service in sodium the role of carbon as an impurity has come to assume an extraordinarily high importance. It is now thought by some workers that the upper limit in the temperatures that can be practically attained in such systems may very well be determined by the behavior of carbon — rather than by the oxygen impurity which was thought to be limiting no more than a few years ago. There has been a growing realization that carbon is a rather ubiquitous impurity in Na - after all, the metal is manufactured by fused salt electrolysis with graphite electrodes. Thus effects due to carbon are observed even when no external source of this element may be present.

Austenitic stainless steels, the familiar 18-8's for example, which are among the most corrosion resistant iron base alloys known for Na service, in the presence of carbon show a voracious appetite for this element, and rather hungrily remove it from the system. In so doing, the carbon deposits on the surface layer of the steel, and a significant amount of embrittlement and other deterioration of mechanical properties results. This carbon seems to readily combine with the chromium and the stabilizing elements (i.e. Mo, Nb, Ti, etc.) present in some steels of this type to form quite stable carbides. These austenitic alloys are thermodynamically unstable at room temperature, and can exist only because the delicately poised Cr-Ni-Fe

balance inhibits the kinetics of transformation. When this ratio
is changed by the carburization process described above, it is not
surprising that the transition to the ferrite phase is observed.
This transformation also is accompanied by a change in the volume
of the metal, heat effects, and other processes which may result in
degradation of the useful life of the metal.

Ferritic alloys, on the other hand, seem to show just the opposite
behavior, as a general rule. Materials like low carbon steel,
or the common alloys like $2\frac{1}{4}$ Cr - 1 Mo are quickly decarburized by
hot Na. Since a significant part of the strength of these materials
arises from the presence of carbon, it is not surprising that the
loss of this element results in a metal that is considerably
weaker and more limited in its usefulness than the original alloy.

These observations on the importance of carburization-
decarburization reactions have been developed principally from the
AEC's power reactor program, with iron alloys and sodium. The extent
to which carbon will be a source of difficulty with the other alkali
metals and the refractory alloys of principal interest in the NASA
space program still remains to be determined. Evidence to date is
limited and conflicting.

Because of the great importance which carbon in Na systems has
assumed, there has been a renewed and vigorous effort to develop
good analytical methods, as a step towards understanding the nature
and mechanism of the carburization-decarburization reactions. For
many years the standard technique for determining carbon in sodium
was by wet combustion in a strongly oxidizing chromic acid medium.

62

The technique was to dissolve the Na sample in water, acidify, then add the oxidant (Van Slyke reagent) and collect and determine the CO_2 thus produced. Recently, some rather surprising results have turned up with this technique. Using gas chromatography, it has been found that carbon-containing gases are released from an Na sample (along with large amounts of hydrogen, of course) when pure water is reacted with the metal. The resulting alkaline solution releases more C-containing gas when it is acidified. In a great deal of earlier work, the carbon bearing gases evolved during these water and acid steps were not collected, and as a consequence of this, only about half the total carbon content of the sample accurately determined.

Dry combustion as a means of determining carbon in Na and the other alkali metals has also been revived recently. This method is quite similar to that used to analyze for C in steel and other heavy metals, and has many attractive advantages. Early in the history of sodium work, however, it was found that there was a grave problem in using this technique: while Na readily burned to Na_2O and the carbon present to CO_2, the latter was not released as a gas in the system but ended up as stable, non-volatile Na_2CO_3. The addition of SiO_2, Al_2O_3 and similar acidic solids to promote carbonate dissociation through reactions like

$$Na_2CO_3 + SiO_2 = Na_2SiO_3 + CO_2 \uparrow$$

seemed to work to some extent, but did not give quantitative results. Within the last year, reports from both Great Britain (Aldermaston) and the U.S. (Ethyl Corporation) have claimed that if the combustion

is carried out in quartz boats at a temperature of about $1100^{\circ}C$

(some 300°-400° higher than the usual combustion) the CO_2 is com-

pletely and readily released. Since sodium carbonate is one of the

most stable materials known, the simple dissociation reaction

$$Na_2CO_3 \;=\; Na_2O + CO_2 \uparrow$$
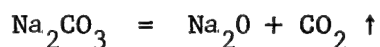
is not considered to be responsible for these recoveries — at $1100^{\circ}C$

this reaction has a ΔF of $+$ 33 kilocalories. It seems much more

likely that the reaction of Na_2CO_3 with the SiO_2 of the container

results in the release of the CO_2: at $1100^{\circ}C$, the free energy change

for the reaction is $-$ 11.5 kilocalories. One of the most important

aspects of the use of the higher temperatures however probably arises

from the fact that at $1100^{\circ}C$ all of the reactants and products are

fluid: sodium metasilicate has a melting point of $1088^{\circ}C$. Work

has recently been reported on dry combustion in which materials other

than SiO_2 have been used to promote carbonate dissociation. Also,

a dry-wet process has been suggested: dry combustion at 600°-$800^{\circ}C$,

followed by treatment with H_2SO_4 to break down the carbonate formed.

This revival of interest in dry combustion methods is an extremely

interesting and important new development in recent times, and a

continued vigorous exploration of this method should be encouraged.

In this work, careful attention should be paid to the problem of Na_2O

or other oxide smoke being deposited on the system walls outside of

the reaction zone, and picking up CO_2 produced in the high temperature

region.

Recently the AEC has been most anxious to develop dependable methods of analysis for carbon in Na, and in an attempt to evaluate the success achieved to date has sponsored two "round robins" in which supposedly identical Na samples were analyzed for C by a score or more laboratories, by a number of different techniques. The results up until now have been grossly disappointing and both the sample preparation and handling and the analytical methods are open to some suspicion.

The purpose of all of this analytical work of course is to attempt to correlate the carbon content and form with the carburization-decarburization reactions observed. To date, this effort has been almost completely frustrated. It is now known that CO, methane and other hydrocarbons, and some CO_2 are evolved on reaction of Na with water and acid. The assumption that the bulk of the carbon present in sodium loop samples (that is, sodium which had been maintained at high temperatures for an extended period, with vigorous agitation) is present as free C, either in solution or suspension, is a rather oversimplified picture, even though the naive application of themodynamic calculations seems to lead to this postulate. Few workers experienced in this field are likely to argue with the statement that the nature of carbon in alkali metals and its reactions with other parts of the system are essentially still unknown, and need extensive further exploration.

d. Inhibitors and Accelerators

Leo F. Epstein

The use of dissolved titanium and zirconium to inhibit the corrosion of ferrous alloys in liquid mercury has been mentioned previously. The mechanism of this inhibition behavior was obscure for many years. It was known that the use of these additives resulted in a change over from the diffusion-controlled corrosion previously discussed by Professor Bonilla, to the solution-controlled process. The production of Ti or Zr-containing films on the steel surfaces was long suspected, and there were some interesting studies on intermetallic compounds of Fe and these elements. It was, rather early in the AEC's sponsorship of liquid metal studies, found that these inhibitors seemed to work with other heavy metals, lead and bismuth, about as they did with mercury.

An important breakthrough on how these additives worked came from the work at Brookhaven by Gurinsky, Weeks, et al on Bi systems. At the first Geneva convention in 1955, these workers were able to announce that the inhibiting films had been identified as largely ZrN and ZrC. This immediately raised the question as to where the nitrogen and carbon needed to form these compounds came from, and it came as somewhat of a surprise to many metallurgists to learn that ordinary steels contain very large amounts of nitrogen. (The extensive development of vacuum fusion techniques, and a widespread application to the study of gases in metals since 1955 has tended to support this concept.) Gurinsky, et al claimed that there was more than enough N_2 present to form the products necessary to obtain inhibition.

67

The proof of this position came about from a further study of

the time dependence of the action of Zr as an inhibitor in Bi.

The initial effectiveness of this procedure, it was found, was

decreased by prolonged exposures. The explanation offered for this

phenomenon was that the ZrN or ZrC films formed by reaction of the

dissolved Zr and the non-metallic elements in the steel were not

perfectly adherent. After a while they tended to spall off, to be

worn away by the action of the flowing liquid metal. This resulted

in a depletion of the nitrogen and the carbon in the steel, and the

inhibiting films could not readily be re-formed on the surface because

virtually all of the N and C capable of participating in the film

producing process were gone. It was at this point that Geoffrey

Horsley, our guest here, conceived of a brilliant solution to this

problem of extending the useful life of a Zr inhibited system, which

simultaneously offered strong support to the Brookhaven hypothesis

on the importance of nitrogen. What Horsley did, at Harwell, was

to operate a high temperature Zr-inhibited bismuth loop at high tem-

perature, not in air, vacuum or an inert atmosphere as is customary,

but in ammonia gas. NH_3 at high temperatures is one of the best

materials known for producing nitriding in heavy metals — nitrogen

goes into steel much more readily from ammonia than it does from air.

It was found that under these conditions, the fall-off of the

inhibiting action of the Zr with time did not occur — so long as

both nitrogen and zirconium were supplied to the system, the corrosion

rate continued to be acceptably low.

The acceleration of corrosion processes in the alkali metals by certain trace impurities in many ways appears to be parallel to the inhibition process described above for the heavy metals. Oxygen, at very low levels, appears to speed up the corrosion process with many materials, principally by increasing the solution-rate constant which has previously been called α. (As was suggested earlier, so far as can be determined from the relatively meager data available, α is roughly linear in the oxygen content of the liquid.) Nitrogen in lithium, the only alkali metal which forms a nitride stable at elevated temperatures, seems to act in the same way, essentially.

It should be pointed out that the liquid metal itself is not always the sole source of the oxygen and nitrogen impurities which bring about accelerated corrosion. Some metals, including both Zr and Nb, which are of such great interest in space work, have the ability to dissolve considerable amounts of oxygen. When a sample of such a metal is brought into contact with an oxygen-free or oxygen-deficient alkali metal, a partition or redistribution of the oxygen between the liquid and the solid phases takes place, and the solution rapidly contains the amount of oxygen needed to explain accelerated corrosion. This redistribution phenomenon will be the subject of a paper by Thurber of ORNL at this afternoon's session.

The similarities in the corrosion mechanism between inhibited mercury and sodium systems led to an early hope that corrosion by alkali metals could be slowed down by addition of a few parts per million of an appropriate material. This concept is still a valid one — there is no reason to dismiss the possibility of inhibition of

69

corrosion in liquid alkali metal systems as inconceivable on the basis of anything known at present. But in spite of vigorous search, no such specific inhibitor (parallel with Ti or Zr in Hg systems) has ever been reported for the alkali metals. For a while the decrease in the corrosion rate of certain types of iron-base alloys in Na on the addition of the alkaline earth metals (particularly Ca and Ba) to the fluid was thought to be evidence for this phenomenon. Subsequently, it became clear that the mode of action in these systems was largely to grab oxygen from the Na_2O in solution

$$Na_2O + Ca = 2Na + CaO$$
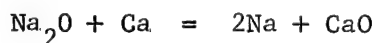
producing the more insoluble alkaline earth oxide.* Essentially then these so-called "soluble getters" act simply by reducing the concentration of available (i.e. dissolved) oxygen in the system rather than through the sought-for specific inhibiting action.

Another class of materials which have been examined as possible corrosion inhibitors with the alkali metals are the so-called "insoluble getters". These are metals like Zr and Ti which (1) have the ability to react with Na_2O and extract oxygen from it

$$2Na_2O + Zr = 4Na + ZrO_2$$

---
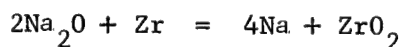
*It should not be forgotten that the use of soluble getters of this type inevitably leaves material in solution which may be highly deleterious to some systems. Thus, as has been discussed elsewhere, the use of Ca as a getter, while quite effective in removing oxygen, leaves calcium metal in the fluid which reacts with nitrogen, nickel in some alloys, and has other disadvantageous properties.

and (2) in which the oxygen (or metal oxide) is significantly soluble. This combination of properties makes it possible to obtain very low oxygen levels in solution by "cooking" the alkali metal with the solid material for some time. In this application, a large surface area is desirable for the getter, so that foils, turnings or gauze is frequently employed.* Note that with these materials, as with the soluble getters discussed above, the behavior of the additive is to remove oxygen from the system rather than a specific inhibiting action.

Although the search for specific inhibitors in the alkali metals has to date been singularly unsuccessful it will no doubt continue, and it should perhaps be encouraged. Unfortunately there is no credible rationale to guide such a search that is readily discernible, and the effort must be largely Edisonian (as was the original discovery of the mercury inhibitors). At the present time, THE BEST TECHNIQUE FOR INHIBITING ALKALI METAL CORROSION IS ELIMINATION OF OXYGEN IN THE SYSTEM.

---

*Some of the metals used as insoluble getters for oxygen in alkali metals also have a strong attraction for carbon and can remove this element simultaneously with oxygen.

6. HETEROMETALLIC PHENOMENA

John R. Weeks | ⟶ 1₅

From the equal – chemical – potential postulate it is immediately apparent that mixing materials can be dangerous since the surfaces of both would strive to become a common alloy between the two metals. An example of this is shown in Figure 6-1, where Ni migrated through Na to a Mo surface at 1000°C. The more soluble constituent usually migrates through the liquid to form layers on the surface of the less soluble constituent. The compound MoNi is stable up to 1300°C. Even without intermetallic compounds in the system, alloying to make both surfaces equivalent alloys is likely when solubilities of one or both are finite. When both metals or alloys are essentially insoluble, migration of non-metallics is the major concern. Gettering O, N, and C in Na with Ti or Zr is a classic example. Non-metallic exchange was previously discussed; in its more subtle forms we see O migration through Na from Cb to Cb-1Zr at 1200°C, C from one steel to another at 500°C. Gettering all solid metals with Ti or Zr seems advisable to avoid exchange of C, N, and O.

The safest way to minimize problems from heterometallic phenomena is to avoid mixing alloys in a liquid metal system unless the major metallic constituents of all alloys are known to be essentially insoluble, and the activities of all possible non-metallic transferring species (O, N, C, H) are equalized in all alloys by gettering.
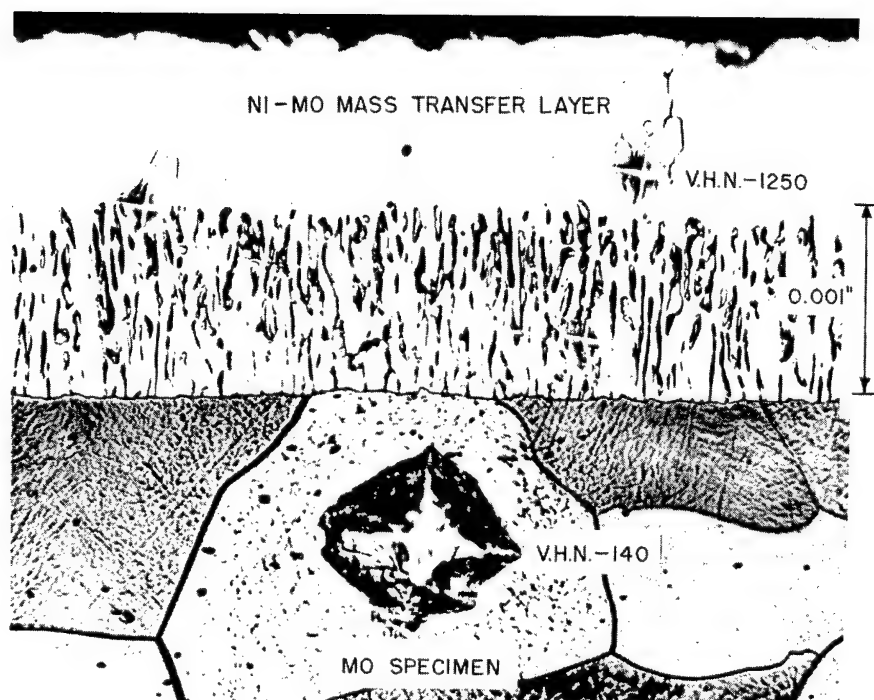
73

E-2492

Figure 6-1. - Mo specimen - Ni container - contacted with Na for 100 hours at 1000° C (ORNL).

7. NONMETALLIC SOLIDS

a. Ceramics (Thermodynamics)

Leo F. Epstein[19]

While metals are the principal structural materials which come into contact with liquid metals, there are many applications where the high electrical and thermal conductivity of the metallic state is undesirable. For this reason, there has always been an interest in the behavior of liquid metals and non-metallic solids. In this section, a few of the common classes of materials will be discussed with respect to their resistance to attack by liquid metals, particularly the alkali metals.

The most important group of substances of this type examined to date are the oxidic ceramics. These materials are often used as insulators, thermal or electrical. They may be represented by the formula M_aO_b in general. The best guide to the probable stability of an oxide in the liquid metal is the thermodynamics of the reaction, like

$$M_aO_b + 2b\ Na = a\ M + b\ Na_2O$$
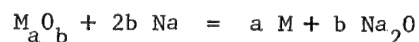
which in many cases (but unfortunately not all of importance) can be derived from available tables of free energy data. Along with the main reactions of the type described by this equation, secondary interactions to form salts, like

$$M_aO_b + x\ Na_2O = M_aO_b \cdot x\ Na_2O$$
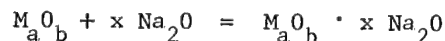
can occur, and reactions of this type can be very important in some systems. Compounds like silicates, zirconates, and aluminates, are extremely stable, as is evident from their frequent occurrence in

75

minerals and ores in the earth's crust. Unfortunately, the amount of information available on these double oxides or salts, with the alkali metals, is quite limited and much more extensive data on their properties would be desirable.

Impurity levels in ceramics tend to be much higher than those in metals, and constant care must be taken to avoid problems which arise as a consequence of their presence. An interesting example of this is the early history of work on ZrO_2. Thermodynamically this material should be stable in Na, according to all of the tabulated ΔF data. But experimentally, zirconia ceramics, most puzzlingly, fell apart, crumbled to dust, when exposed to the alkali metal. The answer eventually turned out to be silica: ceramists love to use a little bit of SiO_2 or silicaceous clay to produce improved forming and firing characteristics in ceramics. For many materials this is advantageous — but if the material is to come in contact with sodium or other alkalis, it can be disastrous. The reaction of SiO_2 with Na is rapid and extensive: the reaction products include sodium silicate (due to salt formation with the Na_2O present), sodium silicide, it has been reported, and even some free elementary Si. When ZrO_2 was pure, and no silica-containing binder was used in the preparation of the ceramic, it behaved in liquid sodium just as the thermodynamic tables predicted it would.

With insulating ceramics, perhaps the most extensive work has been done with alumina, Al_2O_3. This compound in its purest form, corundum or synthetic sapphire, is quite resistant to Na, again in agreement with the thermodynamic data which suggests that reduction by Na to form Al metal should not occur. With sapphire, there is

usually a slight weight gain on exposure to hot Na, due to interaction with Na_2O to form sodium aluminate. Passing to other forms of alumina, generally speaking the purer the material (FeO and SiO_2, both of which are readily reduced by Na are particularly harmful contaminants), the higher the firing temperature (or what is equivalent, the higher the density), the better is the corrosion resistance of the ceramic. Porosity seems to promote reaction since the alkali metal penetrates cracks and produces changes by both chemical and mechanical actions (see discussion on graphite, below).

Having discussed the generally harmful character of silica in crystalline ceramics, it should not be surprising, on turning to glasses, to learn that these have only poor corrosion resistance with Na and the other alkali metals. The higher the SiO_2 content, generally speaking, the worse the misbehavior. Thus Vycor and silica glass are much less resistant than the lowly soda-lime glasses or common laboratory Pyrex. This, perhaps the most familiar of the glasses, is most gratifyingly one of the best for alkali metal service, possibly because of its high B_2O_3 and consequently lowered SiO_2 content. This is not to recommend any glasses for sodium service: at best, the differences are small. The corrosion behavior takes the form of a browning, or in the case of extensive reaction, blackening of the glass and this is highly dependent on time, temperature, surface area, etc. It should not be forgotten that exposure of any glass to hot alkali metal for more than a few minutes will inevitably introduce oxygen into the material. Few glasses should ever be used above $200^{\circ}C$; in the case of Pyrex this figure may be as high as $250^{\circ}C$, and for quartz or Vycor it might be well to stay below $150^{\circ}C$.

There have been a few studies on the development of alkali metal resistant glasses that have been concerned with vapor, rather than liquid, attack. The not-uncommon sodium vapor lamps contain a coating on the glass envelope which improves their lifetime and performance. It should be noted that, generally speaking, alkali vapors are much less destructive on glasses than the liquids, due to nothing more or less than the fact that the concentration (atoms per cubic centimeter) is less in the vapor state. Thus lithium, which in the molten state reacts vigorously and rather spectacularly with Pyrex, can under proper conditions actually be distilled in glass to produce bright shiny mirrors.* The secret lies in keeping the liquid phase away from the glass.

Finally, among glasses, attention should be directed to the newer developments in recent years. The phosphate glasses, the high alumina types, the use of rare earths and other new heavy metals, have resulted in a very large number of products. Some of these are reputed to be better in their resistance to liquid metals than the older more familiar types, and the research worker faced with a problem involving a glass and a liquid metal should not ignore these possibilities, although really long life at high temperatures should not be expected.**

---

* Epstein, L. F. and Howland, W. H., SCIENCE 114 443 (1951).

**Ceramics other than metallic oxides are becoming increasingly important in nuclear and space technology, but their behavior with liquid metals is largely unexplored. In the section which follows there is a short discussion of carbides, but the behavior of nitrides, sulfides, phosphides, silicides, etc., with high temperature liquid metals is virtually virgin territory.

b. Graphite

Leo F. Epstein ⌋ 83

Metallurgists and ceramists love to argue over whether graphite is a metal or a ceramic, and its inclusion here is rather arbitrary and for convenience only rather than an indication of a strong partisan stand on this rather trivial question. Graphite has been used in many sodium-containing systems — in fact it is <u>the</u> moderating medium in liquid metal cooled thermal neutron systems such as Atomics International's SRE or Hallam plants. It has also been used in and around sodium-cooled fast reactors — the Fermi plant and Dounreay for example. For this reason, and because all too frequently, unfortunately, the graphite has been a source of difficulty, it is considered worthwhile to spend a little time discussing its behavior in liquid sodium and other metallic fluids.

It should be recalled that no stable carbides of sodium have ever been prepared by direct action of the elements at low temperatures. In fact the only clear-cut sodium-carbon compound that is well known is the acetylide

$$Na - C \equiv C - Na$$

In view of this, it is, at first, somewhat surprising to some workers to learn of the tendency towards instability of graphite on exposure to Na — many forms of this material simply disintegrate and fall to powder.

Lithium does form a carbide, Li_2C_2, quite readily. Also the heavier alkali metals potassium, rubidium, and cesium form well characterized compounds with graphite, KC_8, for example.*

---

*For an excellent review on this subject see the paper "Graphite Intercalation Compounds" by W. Rüdorff, pp 223-266 in <u>Advances in Inorganic Chemistry and Radiochemistry</u>, H. J. Emeléus and A. G. Sharpe, Editors. Volume 1. Academic Press (New York, 1959).

In these very interesting compounds, the alkali metal atom is located between the plane sheets of carbon atoms which make up the graphite structure. The interplanar spacing is such that the heavier alkali metals can readily fit in, but the sodium atom is too large to be accommodated comfortably. Nevertheless, Na seems to be able to penetrate the solid and to become lodged between the graphite planes. In so doing, however, it distorts the graphite, because of its large size, and the resulting stresses are what cause the material to disintegrate, it is believed. How the atoms manage to get into the interplanar region is another question: it is believed that this is possible only because of the presence of defects and fissures in the lattice. Thus the resistance of graphite to Na will depend largely on the elimination of these flaws. This can be influenced by the method of preparation of the graphite*, by various kinds of impregnation which tend to clog up the holes and similar procedures. Such tactics result in improved resistance to the alkali metal, but graphite is still a material whose corrosion resistance in Na can hardly be characterized as anything but poor; and in using it in a liquid metal system, jacketing is virtually mandatory.

In this discussion, the emphasis has been on Na where there is the most extensive body of experience. Data on graphite in the presence of the other alkali metals is however quite meager. From the nature of the compounds which can be found, it is to be expected that corrosion resistance of graphite in these materials should be much worse than that in Na.

---

*The dense "pyrolytic" graphites which have become popular in recent years are markedly superior to older types.

No discussion of the use of graphite in liquid alkali metal systems would be complete without an admonitory comment about the volatile impurities which occur in graphite. In a surprisingly large number of cases, these materials have come out of the solid (as CO, H_2O vapor, etc.) and ended up by reacting with the alkali metals with in some cases rather horrifying consequences. Some important nuclear reactor projects have been delayed for months, and perhaps even years, by this phenomenon, and the rectification of this oversight has involved millions of dollars. This is particularly regrettable since methods of preparing graphite which is not gassy are well known, and such material can be obtained without major difficulty if only the engineer and his associates are aware of the problem.

This discussion of graphite leads quite naturally to another class of ceramic materials which are beginning to attain a great deal of importance, the carbides. A little is known about the behavior of the fissionable metal carbides (UC, PuC) and the refractory metal carbides (of Mo, Zr, Nb, etc) in sodium, but not nearly enough. Among other factors, the stoichiometry, that is the carbon to metal ratio, is important in determining corrosion resistance. With alkali metals other than Na, the dearth of experimental data is even more painful.*

---

*Note that one of the more promising combinations for thermionic conversion and space application involves a UC-ZrC mixture exposed to hot Cs vapor.

8. VAPOR PHASE PHENOMENA (Metallic Vapors)

Leo F. Epstein 87 ⟶

Most of the discussion of corrosion phenomena here this morning has been concerned with reactions with <u>liquid</u> metals. In the last three or four years there has been a growing interest in the behavior of materials, in particular metals, in the presence of metallic <u>vapors</u> at high temperatures. This phase of corrosion has come into prominence largely because of the growing interest in the use of metallic vapors in turbo-electric power conversion systems. This field is by no means new. As has been pointed out elsewhere, the first large scale industrial utilization of liquid metals came about in the use of mercury vapor as the working fluid in a turbogenerator system. The work with sodium in the late 1940's and early 1950's was in some cases carried out at temperatures high enough so that the vapor pressures were significant, but observations of effects due to the metal in gaseous form were generally incidental to rather than a direct object of the research.

Corrosion by liquid metals in many systems has been explained previously as a solution phenomenon. If this is so, it is to be expected that vapor phase attack should be much less than that of solids in contact with the liquid, because materials do not "dissolve" in gases, in the usual sense. Also, in some cases, it has been pointed out that liquid metal corrosion is due largely to dissolved oxygen, present as an impurity in the liquid. Recognizing that in the systems where this is most important, i.e. the alkali metals, the common oxides are (1) extremely non-volatile and (2) stable to very high temperatures, far beyond those of current interest, it is not surprising that for these materials as well vapor phase corrosion is much less severe than attack by the liquids. These predictions are in fact verified by observation.

Sometimes there is the possibility of direct reaction between the metallic vapor and an impurity in the solid. An example of this might be pure potassium vapor reacting with oxygen dissolved in a columbium or zirconium alloy. Similarly reactions with carbon are conceivable. When corrosion involves intermetallic compound formation, it should make little basic difference if one of the constituents of the pair is in the vapor rather than the liquid state. Ca or Li, which form intermetallic compounds with nickel, for example, would be expected to severely attack Ni-bearing alloys at temperatures where the concentration in the vapor is high enough.

Most so-called vapor phase corrosion is, in fact, due to liquid condensed from the vapor. Such a material is extremely pure, free of solute, and consequently tends to dissolve fresh metal quite rapidly. For this reason, in Hg systems, a large amount of corrosive attack is ordinarily observed in the condensing vapor region.

Another important source of apparent rather than real vapor phase attack arises from the carry-over of liquid droplets with the vapor. At the very high heat fluxes in the two-phase heat transfer systems which are currently attracting so much interest, it is not easy to prevent "bumping" and boiling instabilities that result in a significant number of liquid droplets being carried along with the vapor, depositing on solid surfaces some distance removed from the liquid-gas interface, and exerting a strong corrosive influence. Note that in this mode of action, the non-volatile impurities dissolved in the liquid (Na_2O in Na, for example) are not only available to exert their pernicious effect, but their action may in fact actually be intensified. This could come about in the following way:

1. Droplets of liquid Na, containing dissolved Na_2O, are thrown into the vapor phase, and carried along by the flowing gas stream.

2. At some "superheat" region farther downstream, enough energy may be pumped into the system, so that the liquid metal in the drops evaporates. This leaves a dust or fog of the Na_2O and any other non-volatile impurities to float around in the metal vapor.

3. At some point in the system, these Na_2O particles impinge on the walls. This may come about through some hydrodynamic or geometric peculiarities or otherwise.

4. In any case, the walls are then subjected to attack by the hot oxide in a very concentrated form, which may be much worse than anything normally observed with the comparatively dilute solutions of the oxide in the liquid metal. Such reaction, microscopically, should be characterized by pinhole-like corrosion sites, corresponding to the tiny particles of solid oxide whose deposition was the source of the trouble.

These considerations on the behavior of vapor systems are based on a relatively small amount of observation, and a great deal more work is required in the field and will no doubt be forthcoming as more and more NASA-inspired boiling-condensing studies come to fruition. The importance of minimizing boiling instabilities and liquid carry-over in order to eliminate corresponding errors in the interpretation of vapor phase corrosion cannot be over-emphasized. How to achieve this kind of

stability, which has significance over and beyond the corrosion question considered here, will be the subject of other papers today and tomorrow. Suffice it to say that this objective is not easy to attain, and good vapor phase corrosion data is still very scarce as a result of this unhappy state of affairs.

9. TWO-PHASE MECHANISMS

John R. Weeks⌋ →91

A schematic boiling loop is shown in Figure 9-1. Dissolution occurs primarily where the solute-free condensate contacts the metal surface. Precipitation may occur at the coldest spot in the metal circuit, or where the solute is concentrated by flow at the boiler interface. With useful boiling rates, back diffusion of the solute is too slow to prevent concentration to the saturation point of most solutes in the boiler.

Slugging may cause corrosion in the superheater by carrying liquid against the hot surfaces there. Bumping may carry saturated droplets into the superheater, which vaporize there, leaving their dissolved metal behind as fine deposits on the superheater wall.

Adsorption on metal surfaces may occur even in dry vapor when liquid wets solid. A simple calculation, assuming complete (γ_{SL}=0) wetting of the solid by the liquid at the superheater temperature, suggests that with ~50% saturation vapor, one has ~.99999 of a complete monolayer of adsorbed liquid atoms on the superheater surface, which amount is quite sufficient to initiate non-metallic exchange attack. Therefore, the requirements for selecting materials for liquid metal use also must be followed in selecting materials for use in dry vapor.

At the liquid-vapor interface in static reflux capsules, Gibbs adsorption isotherm predicts concentration or depletion of solute. As a possible example, Cb-1Zr-Na-5000 hour 1200°C reflux capsules at BNL have shown slight intergranular attack in both the liquid and the vapor regions and none at the interface, suggesting that whatever was being leached in the attacked regions may have concentrated at the interface and locally reduced the attack.
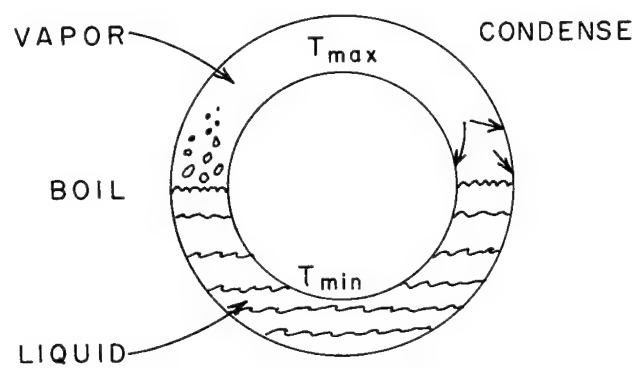
Figure 9-1. - Schematic boiling loop.

10. SPECIAL TOPICS

a. Downstream Effect

Leo F. Epstein

Comparatively few new types of phenomena have been uncovered in liquid metal corrosion work in the last few years. It is therefore of very great interest when an altogether unexpected and surprising relation is found. This seems to be the case with the so-called "downstream" effect.

This has been brought to the attention of workers in this field by R. W. Lockhart and his associates working on the AEC's Sodium Mass Transfer Program at the General Electric Company installation in San Jose, California. In this study, a series of pumped loops, of various steel alloys considered suitable for power plant application have been extensively studied over the last few years. Over 100,000 hours of operating experience has been accumulated and of the order of 2500 samples examined, from the point of view of corrosion and the associated mass transfer phenomena.

In theory, heat exchange systems and loops of this type should have temperature distributions which are continuous and smooth, from the hot to the cold zone. In reality, of course, this is a difficult if not impossible state of affairs to achieve. With this particular

set of loops, at various points in the flow pattern there were regions
of considerable length which were at the same temperature. In these
isothermal regions, the corrosion rate was highest near the beginning
of the constant temperature zone, and decreased downstream from this
point. This briefly is the downstream effect. It seems to have
escaped detection for many years because few other systems have
been operated with isothermal regions* in which corrosion samples
could be taken.

The exact nature of this downstream effect is still obscure.
Professor Bonilla (see elsewhere) feels that it is simply related
to the familiar entrance condition relations of heat transfer. The
phenomenon would then be associated largely with the establishment
of a hydrodynamic steady state, and this would be dependent, more
than anything else, on the ratio x/a, where

> x = distance downstream from beginning of isothermal
> region at which corrosion measurements are made
>
> a = tube radius

While this hypothesis is plausible, and entrance condition relations
certainly play some part in the phenomenon, there appear to be other
important factors as well. Quite reasonably good quantitative agree-
ment with observation can for example be obtained ignoring this aspect

---

*This is probably a very poor way to operate a heat transfer system, and in
principle, a smoothly varying temperature distribution around the loop should
be the design objective, with no plateaus or discontinuities. In power
plant systems, as in laboratory set-ups, this ideal configuration is much
easier to describe than it is to attain.

entirely and approaching the problem from a completely different point of view. Such an analysis has been quite revealing, and has yielded new insights into the nature of liquid metal corrosion phenomena which may be much more important than the application to the downstream effect. The details of this analysis are too lengthy for this audience, and will be issued shortly in AEC reports, it is expected, and consequently only the briefest mention of the results can be made here, those which are most important to the subject of this discussion, <u>Mechanisms of Corrosion by Liquid Metals.</u>

The simplest (and most fashionable!) way to describe the corrosion process in a constant temperature hot region of a loop has been with an equation like

(1) $$R = -(D/\delta)(S^o - S)$$

where

> R = corrosion rate (g/cm^2-sec.). The minus sign indicates that this is a weight <u>loss</u>, in the hot zone.

> S^o = equilibrium solubility of the loop wall material in the liquid metal at the temperature under consideration (g/cm^3).

> S = actual concentration of solute in solution (g/cm^3).

> D = diffusion coefficient of dissolved species in the liquid (cm^2/sec).

> δ = boundary layer thickness (cm). In a turbulently flowing stream, moving at a high velocity v (cm/sec) on the average, the fluid velocity adjacent to the wall is taken to be zero. Moving into the stream a distance δ, the fluid has attained its mean velocity $\underline{v}$.

Applied to an extended isothermal region, this formulation leads

to an expression for the corrosion rate R(x) at any point x cm.

downstream from the beginning of the constant temperature zone.

(2) $R(x) = - (D/\delta)(S^o - S_e) \exp (- 2D/\delta a)(x/v)$

All the symbols here have been defined except S_e; this is the con-

centration of the solute in the liquid (g/cm^3) at the entrance of

the region under examination.

Long usage and familiarity have caused many workers to forget

or ignore the fact that equation (1) above is only an approximation,

and one of rather dubious physical significance at that. This is no

place to argue over the validity of the whole boundary layer concept

— most hydrodynamicists, if pressed, will immediately concede it to

be a useful model for some applications, but will be equally quick

to acknowledge its approximate nature.

If, as has been assumed here, liquid phase diffusion of some

dissolved species determines the rate of corrosion, then an exact

expression can be written down for R, derived from Fick's first

law of diffusion. In place of the approximation (1), the exact

relation is

(3) $R = - D(\partial S/\partial y)_{y=0}$

Here y is the distance into the stream, measured from the wall, so

that the term $(\partial S/\partial y)_{y=0}$ represents the concentration gradient at the

wall-fluid interface. Applying (3) rather than (1), the expression

for the local corrosion rate comes out very different in form

(4) $R(x) = - (D/\pi \cdot x/v)^{\frac{1}{2}} (S^o - S_e)$

94

Careful analysis suggests that the approximate technique results above should be valid only for long residence times, i.e. high x/v values. For the conditions observed in the SMT loops, on the other hand (high velocities, short residence times), J. M. Mottley, who was largely responsible for the theoretical analysis of this effect, found that the exact relation (4) rather than the result of the approximate treatment (2) gave substantially better agreement with observation.

Obviously, this is an intriguing problem, with implications far beyond those to which it can be immediately applied. The downstream effect is mentioned here as an interesting example of a new discovery in what was long considered a thoroughly explored and well-understood field. The theorists as well as the experimentalists may derive some encouragement from this case — there is still a great deal that they can do in liquid metal corrosion. It is to be hoped that there will be an appreciation of the importance of the new insights which this problem has given into the nature of liquid metal corrosion phenomena, and that further encouragement and support for this kind of study will continue to be available in the future.

b. Physical Properties (Embrittlement)

John R. Weeks

Except for the embrittlement under stress of AISI 4130 when wetted with Li, no instances of liquid metal embrittlement of useful containers by the alkali metals are known to me*. All other changes in mechanical properties can be directly attributed to mass transfer during the contact period: carburized steels become harder and stronger, O and H pickup make Cb more brittle, etc. However, there is still a remote possibility of liquid metal embrittlement in some unknown system, especially when high-strength age-hardening alloys are used under stress, so the phenomenon should be briefly described here.

Embrittlement occurs in specific systems. These have no intermetallic compounds and low solubility of the solid in the liquid. Embrittlement is related to properties at the liquid-solid interface. A high adsorption energy of the liquid on the solid results in a low interfacial energy. The liquid atoms, being strongly adsorbed on the solid atoms, reduce the inter-facial surface energy, and therefore reduce the stress required to separate atoms of the solid metal, as sketched in Figure 10-B-1.

Failure by liquid embrittlement may be intergranular at

---

*Embrittlement by alkali metals of Al and Mg - base alloys has been observed.

97

twin boundaries, or trans-granular; in all cases external or internal stresses are required. The phenomenon is similar in many ways to stress corrosion cracking by aqueous solutions.

General References

No attempt has been made to provide a detailed bibliography for this discussion. The majority of the material has been discussed previously in three survey papers by the writer:

1. J. R. Weeks and D. H. Gurinsky, "Solid Metal-Liquid Reactions in Bismuth and Sodium", chapter 5 of the Book Liquid Metals and Solidification pg. 106. American Society for Metals, Cleveland, 1958.

2. J. R. Weeks and C. J. Klamut, "Liquid Metal Corrosion Mechanisms" chapter 8 of the book Corrosion of Reactor Materials Vol. 1 p 105, International Atomic Energy Agency, Vienna, 1962.

3. J. R. Weeks, "Corrosion in Liquid Metal Cooled Reactors" in book High Temperature Materials for Nuclear Applications (edited by M. T. Simnad and L. Zumwalt) MIT Press 1963.
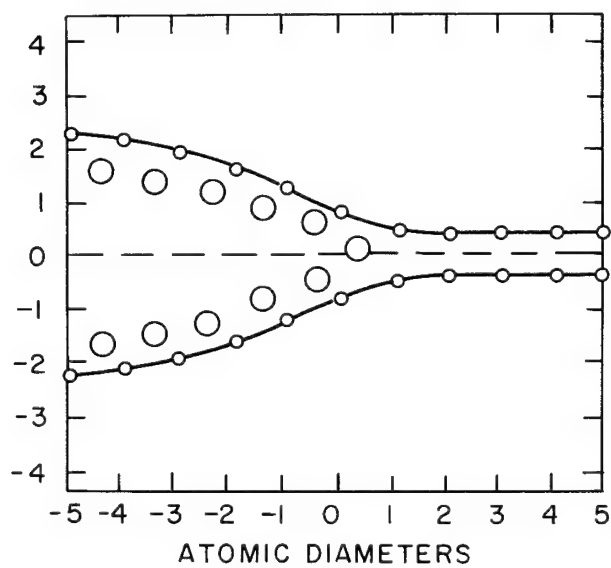
Figure 10B-1. - Schematic diagram of relations between solid and liquid atoms at crack tip. The energy of attraction between the solid (small circles) and liquid (large circles) atoms reduces the energy required to separate the solid atoms. The presence of liquid atoms at the crack tip is therefore a requirement for crack propagation by this mechanism.

c. Radiation Effects

Leo F. Epstein

Since the important applications of liquid metals in recent years have involved their use in and with nuclear reactors, it is not surprising that a great deal of effort and thought has been devoted to the question of the influence of radiation on the corrosion characteristics of these materials. Although, theoretically, there are cases where radiation acceleration of corrosion could readily be imagined, as a matter of fact no such serious and detrimental behavior associated with the radiation environment have been observed.

If the corrosion process is controlled by the diffusion of a dissolved species in a liquid metal, radiation would not be expected to influence the process. First, because with monatomic fluids (i.e. liquid metals) there are no compounds to be damaged by radiation (this is in marked contrast to water systems, for example, where the radiation-induced dissociation to form H_2 and O_2 is one of the basic facts of life which can never be ignored). Secondly, in liquid systems there is enough disorder so that the effect of radiation in bringing about structural damage is quite negligible. This is in marked contrast to crystalline solids, whose properties depend significantly on the existence of an orderly patterned array of atoms or molecules. Here, even with a monatomic material, a violent disruption of the lattice, producing a significant number of displacements, defects, dislocations, etc., in the solid structure can certainly affect many of its properties, including its solution

101

behavior. Specifically, it is difficult to imagine how the diffusion
coefficient of a solute species in a liquid could be altered by a
radiation environment.

In solution-controlled rather than diffusion-controlled liquid
metal corrosion, on the other hand, radiation could and should be
expected to have an affect on the corrosion rate. This could come
about because the species participating in the rate-determining step
in the corrosion process may be polyatomic (e.g., the $FeO \cdot 2\ Na_2O$,
which is believed to be responsible for the behavior of iron in Na)
and consequently vulnerable to attack by the energetic particles
present in the radiation field. It will be recalled, also, that
in some very important cases, the rate of corrosion is markedly
influenced by the presence of adherent films on the corroding sur-
faces. If these protective layers are exposed to the bombardment
of radioactive particles, they may spall off or slough off or suffer
cracks and flaws, all effects which should accelerate the corrosion
process.

Quantitative evaluation of these conceivable radiation damage
effects, however, indicates that for radioactive environments normally
encountered in power plant and space applications, or likely to be
encountered in the near future, radiation acceleration of corrosion
by liquid metals should be only a small effect, of quite negligible
importance. There is to date, so far as I am aware, no experimental
evidence for such radiation enhanced corrosion. People have looked

102

for it in the sodium-cooled nuclear submarine program; an attempt
was made to detect differences in corrosion behavior in the West
Milton prototype and in the Sea Wolf, compared with the observations
on non-radioactive corrosion loops. These attempts failed — if any-
thing the large operating systems showed less rather than more corrosion
than the laboratory tests. (The decrease, rather than the looked-for
increase due to radiation, was attributed to the better control of
liquid metal purity possible with the larger system.) Also, in the
work with bismuth at Brookhaven, Gurinsky and his associates* built
and operated an in-pile corrosion test loop specifically "...to
determine the effect of in-pile irradiation on the corrosion of
various materials by a uranium-bismuth solution." This, it might
be noted, should show an effect on corrosion if anything does, for
the fission process takes place right in the corroding liquid.
Nevertheless the authors concluded that "Results indicate that
in-pile and out-of-pile experimental results are similar and that
fission fragment recoils did not contribute materially to either
wetting or corrosion under the conditions imposed in this test."
Similar conclusions have been reached in all other tests of this
point that I know of.

*Waide, C. H., Kukacka, L. E., Meyer, R. A., Milau, J., Klein, J. H., Chow, J. G . Y,
Klamut, C. J. and Gurinsky, D. H.: Uranium-Bismuth In-Pile Corrosion Test Loop.
Radiation Loop No. 1. Report No. BNL 736(T-365), Brookhaven National
Laboratory (Upton, New York, May, 1961).

In spite of this lack of confirmatory experimental data on radiation enhanced liquid metal corrosion, it seems certain that under sufficiently severe conditions, this will sooner or later be seen in some kinds of systems. Solids where corrosion results in films with weak adhesion characteristics (BeO on Be in Na is an example which comes to mind) should be particularly vulnerable. The effect should be greater at higher fluxes (nv — neutrons/cm^2-sec.). Also, it should depend on the neutron and fission product energy spectrum — the larger the fast (more energetic) component, the greater the expected damage should be. It would not be surprising if some minimum energy was required for this phenomenon, that is that there was an energy threshold for this radiation process as there seems to be for so many others. If these considerations (or perhaps they are best called speculations) are correct, the fast liquid-metal cooled reactors just now beginning to function should be the first to show radiation enhanced corrosion. Workers at Fermi, the EBR's, Dounreay, Cadarache, Obninsk (BR-5), and elsewhere who are in the vanguard of the effort on fast reactor systems should be urged to be particularly watchful for any signs of this effect.

11. SUMMARY AND CONCLUSIONS

Leo F. Epstein

From the information presented and the subsequent discussion, the following conclusions can be reached on the state of knowledge of the mechanism of corrosion by liquid metals:

1. So far as the basic phenomena of liquid metal corrosion are concerned, the physical and chemical origins of the effects are probably well understood.

2. Quantitative predictions of corrosion rates, and extrapolation to working systems, is presently possible in only a very few cases. Although the basic concepts and formulations required for this are available, there is a lack of observational data required for the equations. Information on equilibrium solubilities, diffusion coefficients, and rate constants, for example, is available for only a limited number of liquid metal-solid pairs. Even in the cases where such measurements have been attempted, some glaring discrepancies and inconsistencies exist.

3. While the gross phenomena of liquid metal corrosion appear to be adequately described by relations which have been developed, many details are still obscure. The nature of the downstream effect (the change in local corrosion rate in a flowing stream in an isothermal region) is one example. The transport of carbon in liquid alkali metal systems is another phenomenon which is unclear.

4. The lack of precise experimental and analytical data has in many cases inhibited the progress of development of theories of liquid metal corrosion. The poor reproducibility of corrosion observations from one laboratory to another, and the lack of dependable techniques for the analysis of oxygen and carbon in the alkali metals are typical examples of this.

5. While sodium and bismuth have been extensively and intensively studied, there are still many aspects of these liquid metals which require clarification and further study. The situation with the other alkali metals — lithium, potassium, rubidium and cesium — is even worse, and the information on the physical and chemical behavior of these metals necessary for a meaningful analysis of the mechanism of corrosion is only just beginning to be accumulated. Similarly, while data on the behavior of iron base alloys in these fluids is available, much more information on the interactions of the refractory metals — columbium, zirconium, tantalum, molybdenum, tungsten, etc. — which are of great interest in high temperature applications, particularly for space systems, is urgently needed for intelligent design. $\longrightarrow$

105

6. There is a widespread and growing interest in two phase liquid-vapor, systems using the alkali metals. A great deal of experimental work on these systems is still required before they can be adequately understood. The problem of attaining reproducible steady-state conditions in boiling metals is a severe one, and there is widespread disagreement even among experts on the state of the art with these systems.

7. As in previous periods of liquid metal history, the present revival of interest in the use of these materials is characterized by a concentration of effort on component fabrication ("hardware") and empirical testing. The support being given to basic studies on the behavior of these systems, which is most desirable, if not essential, to the development of dependable equipment, is relatively minor. An expansion of this program, to fill in the gaps noted above, and others, would seem to be urgently required.

E-2492

B. SURFACE ENERGY PHENOMENA AND CORROSION

Robert J. Good
General Dynamics/Astronautics
San Diego, California

127

SURFACE ENERGY PHENOMENA AND CORROSION

Robert J. Good

A. Theory

For two substances, having the same type of cohesive forces (e.g., two metallic phases) the free energy of adhesion, ΔF^a_{12}, should be approximately the geometric mean of the free energies of cohesion of the separate phases, ΔF^c_1 and ΔF^c_2:

$$\frac{-\Delta F^a}{\left(\Delta F^c_1 \cdot \Delta F^c_2\right)^{1/2}} = \Phi \simeq 1 \tag{1}$$

The theoretical basis for this equation was given in Ref. 1. It was shown [1] that if the intermolecular forces are of the same type, and if the molecular radii are appreciably different, that

$$\Phi = \frac{4(V_1 V_2)^{1/3}}{\left(\sqrt[3]{V_1} + \sqrt[3]{V_2}\right)^2} \tag{2}$$

where the V's are the molar volumes of the two substances. Unless the molar volumes are extremely different, the expression for Φ, equation 2, yields a value quite close to unity. (If the forces are of unlike type, and if the force laws are sufficiently well known, then it is possible to compute Φ from the physical properties — dipole moments, polarizabilities, etc., — that determine the force laws. This was done with good success for organic liquids vs. water, as will be reported in a forthcoming paper[2]).

Since $\Delta F_{12}^a = \gamma_{12} - \gamma_1 - \gamma_2$, where γ is surface free energy*, and $\Delta F_1^c = -2 \gamma_1$, $\Delta F_2^c = -2 \gamma_2$, equation 1 may be put in the form

$$\gamma_{12} = \gamma_1 + \gamma_2 - 2\Phi \sqrt{\gamma_1 \gamma_2} \qquad (3)$$

If $\Phi = 1$, then

$$\gamma_{12} = \left(\gamma_1^{1/2} - \gamma_2^{1/2}\right)^2 \qquad (4)$$

(Equation (4) bears a striking resemblance to the Hildebrand-Scatchard equation [3] for the energy of mixing, ΔE^m, of two substances that form a regular solution:

$$\frac{\Delta E^m}{N_1 V_1 + N_2 V_2} = \left[\left(\frac{\Delta E_1^V}{V_1}\right)^{1/2} - \left(\frac{\Delta E_2^V}{V_2}\right)\right]^2 \varphi_1 \varphi_2 \qquad (5)$$

where E^V is the energy of vaporization, the V's are molar volumes, the N's are mole fractions, and φ_1 and φ_2

---

* We will discuss only the surface free energy, γ, usually referring to it as the "surface energy". The total surface energy, ϵ, and the surface entropy, σ, are related to γ by
$$\gamma = \epsilon - T\sigma$$
The total surface energy can be treated by the same theoretical methods, resulting in equations resembling those given here. However, the theory should, in principle, be less accurate in predicting ϵ's than γ's (cf. ref. 3); and also the necessary data to determine ϵ's are less often available. The relationship between surface free energy and surface tension (which are dimensionally the same) is discussed by McLean[4] and by Yates[5].

are the volume fractions in the mixture. The resemblance between
(4) and (5) is no coincidence, for the derivation of the inter-
facial energy theory is closely related to the derivation of the
Hildebrand-Scatchard solubility theory).

For substances that have appreciable mutual solubility, it
was shown[6] that γ_1 and γ_2, in equation (3), should be replaced
by the terms g_1 and g_2, defined as follows*;

$$g_1 = \gamma_1 - N_2 \, \Delta\gamma$$
$$g_2 = \gamma_2 - N_1 \, \Delta\gamma \tag{6}$$
$$\Delta\gamma = \gamma_1 - \gamma_2 > 0$$

Thus,

$$\gamma_{12} = g_1 + g_2 - 2\Phi' \sqrt{g_1 g_2} \tag{7}$$

or

$$\gamma_{12} = \gamma_1 + \gamma_2 + (N_1 - N_2)\Delta\gamma - 2\Phi'\sqrt{(\gamma_1 - N_2 \, \Delta\gamma)(\gamma_2 + N_1 \, \Delta\gamma)} \tag{8}$$

Here N_1 is the concentration of substances 1 in phase 2 at saturation,
and N_2 is that of substance 2 in phase 1. Φ' is given by

$$\Phi' = \frac{4(V_1' V_2')^{1/3}}{\left(\sqrt[3]{V_1'} + \sqrt[3]{V_2'}\right)^2} \tag{9}$$

---

*g_1 and g_2 are the concentration-weighted average surface tensions of
the two phases, and correspond to the <u>hypothetical</u> surface tensions
of the solutions, that would obtain if there were no adsorption. They
are used, rather than the <u>actual</u> surface tensions of the solutions,
because the latter in general represent surfaces containing an adsorbed
film (surface excess) of one component at the liquid-gas interface.
Adsorption at a liquid-gas interface clearly has little bearing on
the adsorption at a <u>liquid</u>-<u>solid</u> or <u>liquid</u>-<u>liquid</u> interface.

where

$$V_1' \equiv V_1 - N_2 \, \Delta V$$

$$V_2' \equiv V_2 + N_1 \, \Delta V$$

$$\Delta V = V_1 - V_2 > 0$$

If N_1 and N_2 are small, then equation 7 or 8 reduce to equation 3. For practical purposes, "small" N_1 and N_2 usually means less than about 2 to 5 mole %.

B. Tests of theory, not involving solid metals.

Equations 1 and 2 have been tested successfully[1] for fluoro-carbons vs. hydrocarbons. Their general application to liquid-solid interfaces have been developed for the interpretation of heat immersion[7] and contact angle[8] data, for solids such as Teflon[7,8], graphite[7], and adsorbed films[8] such as octadecylamine, perfluorolauric acid, etc.

For metallic systems, data obtained in this laboratory[2,9] are in accord with this theory, for gallium vs. mercury; and Russian data[10] show fair agreement for the Pb-Zn system.

TABLE I

System	Temperature	γ_{12} Expt.	Φ (calcul.)	Φ expt.	γ_{12} (calcul.)	Method
Hg-Ga	30°	39.7	0.997	0.989	30	Drop Weight
Pb-Zn	420	128	0.985	0.926	65	Frozen Sessile Drop*

---

* The method used by Geld and Chuchmarev[10] is open to challenge because of (a) their use of an approximate equation to treat their data, and (b) possible distortions of drop shape or freezing. The application of the theory, eq. 1 etc., to Pb vs. Zn is open to challenge, because the failure of this system to obey the predictions of solubility based on Hildebrand's[3] theory is, to date, an unexplained anomaly.
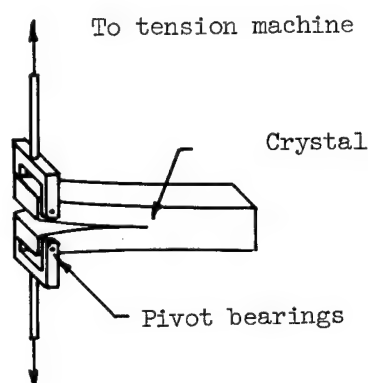
While these data constitute a very far from sufficient proof of the interfacial tension theory, for metals, still they are encouraging enough that an application of this theory to liquid-solid metallic systems may be essayed.

C. Applications

Two applications of this treatment can be made to corrosion phenomenon. The first is to stress-corrosion cracking; the second is to the prediction of grain boundary penetration in corrosion by solution mechanisms.

(1) Stress corrosion cracking.

The cracking of a metal, under stress, in a corrosive environment such as a liquid metal, can be studied quantitatively by the Obriemov-Gilman method[11], and by the effect of grain size on fracture stress[12,13,14]. In the former method, the energy of fracture is measured by first initiating a crack, in the desired crystallographic direction, with the crystal clamped so that cleavage does not propagate through the crystal. The sample is then placed in a tensile machine, as shown in Figure 1, and pulled until the crack propagation starts. The energy necessary to cause the crack to increase by unit area is then a measure of the surface energy of the cleavage plane. In the second method, a theory due to Petch and Stroh[12,13,14] predicts a relation between the applied tensile stress at failure, σ_m , the surface free energy, γ , the shear modulus, G, Poisson's ratio, ν , and the average grain diameter, d:

To tension machine

Crystal

Pivot bearings

FIGURE 1

$$\sigma_m = \sigma_o + \sqrt{\frac{6\pi\gamma G}{(1 - \nu)d}} \tag{10}$$

113

A comparison was made by Stroh[14] of the slope of the line
obtained, when σ_m is plotted vs. $d^{1/2}$ vs. the theoretical
slope, for several metals, with agreement in the range of
10 to 40%. This method has been used by Rostoker et al[15]
to estimate the interfacial energies in certain solid metal/liquid
metal systems.

In addition, the Cottrell-Petch condition[16,17] for
ductile-to-brittle transitions employs the surface free energy
of the solid as a parameter; and results for the Cu-liquid Bi
system were reported by Rostoker, et al[15] using this method.

Table II shows the liquid-solid interfacial tensions cal-
culated by equation 3, (or in the Cu-Bi case, where solubility
is appreciable, equation 7) compared with the experimental
values obtained by the three methods. Also included are the
calculated interfacial tensions for Fe vs. molten Na, K and Cs.

TABLE II

System Solid metal-Liquid metal	Temperature	Surface Tension Solid Metal	Surface Tension Liquid Metal	Interfacial free energy Calculated	Interfacial free energy Experimental	Experimental Method for Fracture study	References Liquid Surface Tension	References Fracture Data
Fe-Li	200°	1800*	400	500	730	a	18,19	15
Cu-Li	200°	2000*	400	600	1010	a	18,19	15
Cu-Bi	350	2000	373	450	160	b	20	15
Zn-Hg	25	940**	485	70	54	c	21	25,26
Zn-Ga	30	940	735	14	42	c	22	27
Fe-Na	100	1800	205	850	(see note d)	d	23	15
Fe-K	100	1800	97	1150	"	d	18,19	15
Fe-Cs	60	1800	68	1200	"	d	24	15

Methods for fracture studies:

(a) Fracture stress as function of grain size

(b) Ductile-brittle transition temperature

(c) Fracture energy, Obrienov-Gilman technique (Stress corrosion cracking is also observed. See Ref. 26).

(d) Stress-corrosion cracking of Fe by Na, K and Cs is not observed[15].

* Surface free energy of solid Fe and Cu from high temperature creep data, extrapolated to temperature indicated.

** Estimated value of γ_S for a high-index plane, from extrapolated liquid surface tension plus a small increment for solidification.

115

(2) Discussion of stress corrosion cracking.

The qualitative agreement between values of γ_{sl} calculated by equation 3 and the experimental values is quite notable. The behavior of the series of alkali metals on iron is now explainable, as due to the fact that lithium has a high enough cohesive energy density (and hence surface tension) that the liquid-solid interfacial tension vs. iron is relatively low. Hence the energy required to form a crack is relatively small. But Na, K and Cs have much lower liquid surface tensions than does Li; hence the predicted γ_{sl} is higher than that of the Li-Fe interface, and the energy of crack formation is also higher. Apparently the critical interfacial tension for stress corrosion cracking of iron is between 500 and 850 ergs/cm^2.

The calculated value of γ_{sl} cannot be used alone, for the prediction of stress corrosion cracking (in particular, it cannot as yet be so used for alloys) because the deformation behavior of the solid metal must be taken into account, and also the occurrence of intermetallic compounds. But at this stage, it is evident that the theory presented above yields a qualitative explanation of the surface energy aspect of stress corrosion cracking; and it gives a good explanation of the trend in stress corrosion cracking in a series such as the alkali metals on steel. Thus for a given series of liquid metals, all having surface tension lower than that of a given solid metal, the embrittling power of the liquid metal will increase with increasing surface tension.

(3) Grain boundary grooving and penetration.

When a metal surface which is intersected by a grain boundary is heated at a temperature within a few hundred degrees of the melting point, surface diffusion (or some other transport mechanism) enables the surface to attain its equilibrium shape.

116

The contour then exhibits a groove at the grain boundary, shown
schematically in Figure 2*. (Thermal grooving is reviewed
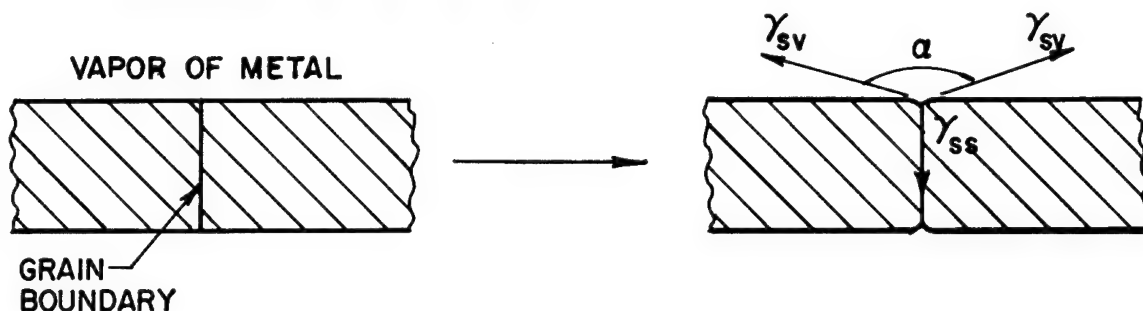extensively by Gjostein and by others, in Ref. 28).

VAPOR OF METAL

FIG. 2

GRAIN
BOUNDARY

The angle α is determined by the equilibrium of the three
surface tensions, indicated in fig. 2, and by Smith's
equation[29]

$$\cos \frac{\alpha}{2} = \frac{\gamma_{ss}}{2\gamma_{sv}}$$

(11)

or

$$\cos \frac{\alpha}{2} = \frac{\gamma_{ss}}{2\gamma_{sl}}$$

When a similar metal surface exposed to a liquid metal is
heated, a similar grooving phenomenon may occur, except that
the groove angle is in general more acute, and may be zero.
(In practice, the grooves may be somewhat obscured by surface
faceting effects, which are ignored here). See figures 3 and 4.

---

* The fine-structure of a thermal groove, which may include a slight
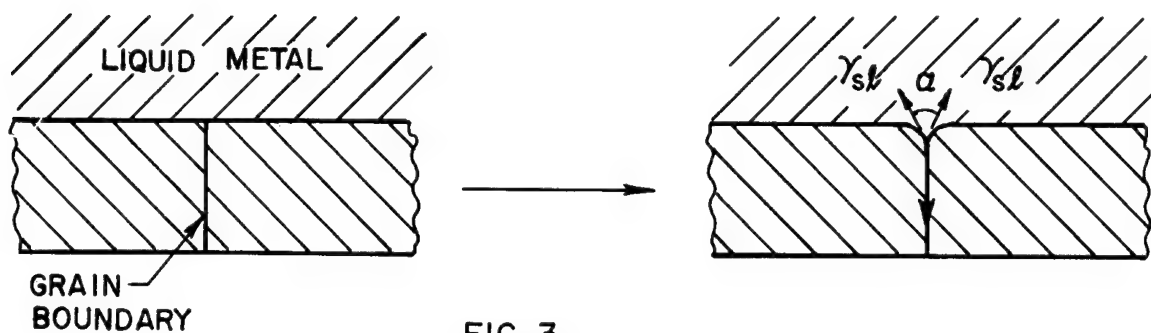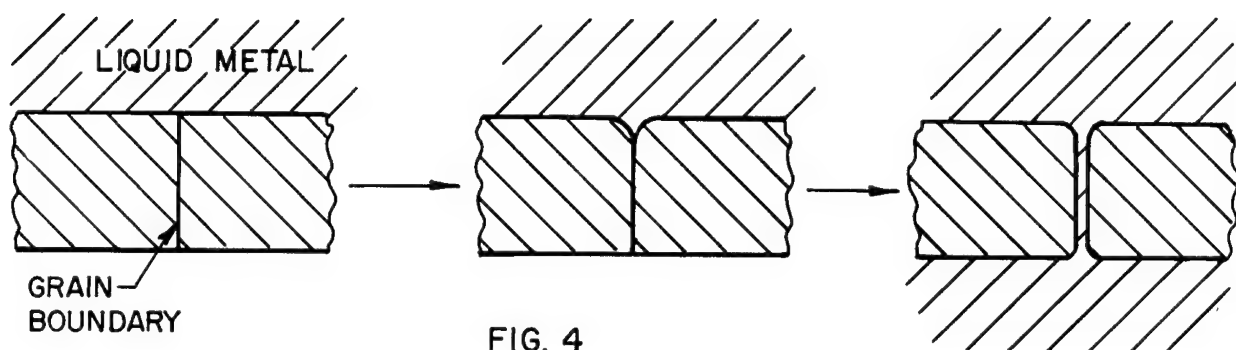hump on one side, is ignored in Figures 2 and 3. See ref. 28.

FIG. 3

FIG. 4

In the case illustrated in fig. 3, $|\vec{r}_{ss}| < 2\,|\vec{r}_{sl}|$ and $\alpha > 0$; the groove angle is stable. In the case illustrated in fig. 4, $|\vec{r}_{ss}| > 2\,|\vec{r}_{sl}|$, and the groove angle is zero. Hence no stable location for the triple-interface-line exists, and the liquid penetrates the grain boundary without limit, destroying the adhesion between the grains. The behavior is as if the grain boundary tension had "pulled" the two liquid-solid interfaces "down" in between the two grains. The actual mechanism of the grain boundary penetration, of course, is the transport of solid metal from the region of the grain boundary to some other part of the system, e.g., into solution, or if the liquid is saturated, redeposition on some other crystal faces.

118

The two types of behavior just indicated in figs. 3 and 4 are actually observed in the Cu-Pb and Cu-Bi systems respectively. At 900°, molten lead does not embrittle copper, but molten bismuth (even bismuth saturated with copper) rapidly destroys the mechanical strength of copper. Figures 5a and b are drawn from photomicrographs of C. S. Smith[29] showing that for Cu + Pb, a stable groove angle is formed, about 60°; but for
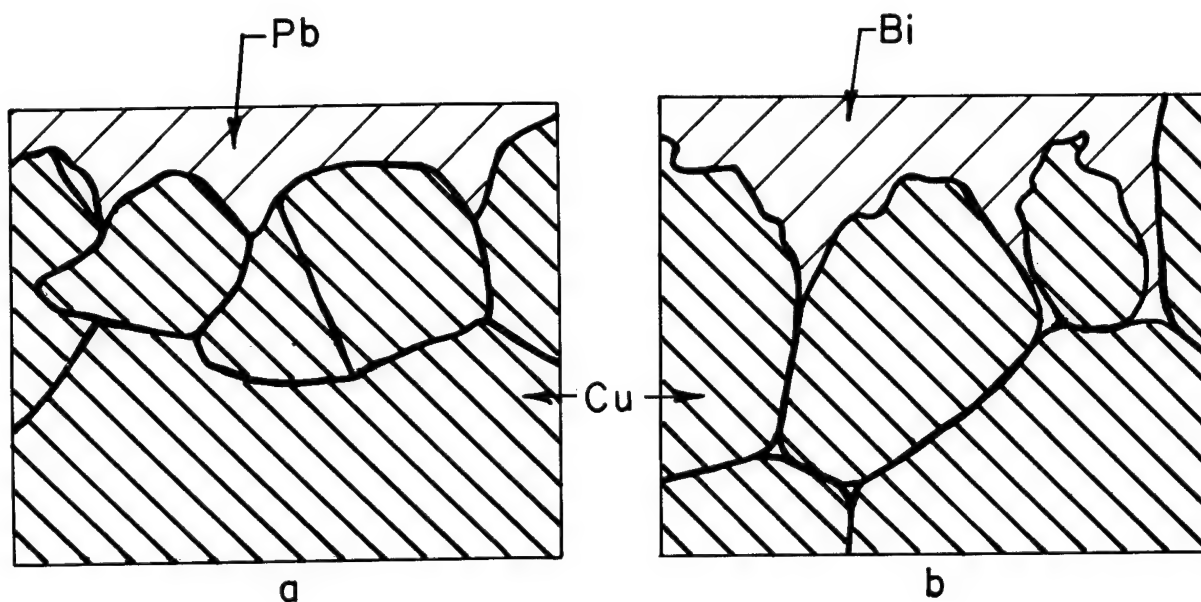

FIG. 5

Cu + Bi, the groove angle is zero, and grain boundary corrosion occurs.

The behavior of these two systems can be explained quantitatively by means of equations 6 to 8 and equation 11. Table III shows the comparison of theory with experiment. The grain boundary tension is taken to be 550 ergs/cm^2 [30].

TABLE III

GRAIN BOUNDARY CORROSION OF Cu BY Pb AND BY Bi

System	Temperature,°C	Dihedral Angle	Solubility of Cu, mole %*	γ_{sv} Extrapolated) ergs/cm^2	γ_{ss} ergs/cm^2	γ_{sl} Calcul. ergs/cm^2	γ_{sl} Exper. ergs/cm^2
Cu-Pb	900°	50°	21	1740	550	290	305
Cu-Bi	900°	0	74	1740	550	100	275

For the Cu-Pb system, the agreement is well within the experimental error. For Cu vs. Bi the dihedral angle data lead to the conclusion that γ_{sl} is less than 275, but give no further information; the calculated γ_{sl} of 100 is in full agreement with this experimental result.

(4) Discussion and speculations regarding liquid metal corrosion.

For systems such as alkali metals on refractory metals, it is reasonable to expect that equation 3, together with equation 11, should lead to a good accuracy of prediction of mode of grain boundary attack. (Since solubility is very small, there is no need to employ equation 8). The theory is in accord with the observed lack of grain boundary penetration of the pure refractory metals by the alkali metals. The depth of grain boundary grooving should decrease with increasing atomic weight of the alkali metal.

The theory as presented applies only to two-component systems. The effect of a third component, such as oxygen, on grain boundary attack would depend on the adsorption. (This discussion is not concerned with the rate and mechanism of dissolution of the solid metal, which may involve oxygen complexes, nor with the effect of third components on the equilibrium solubility of the solid metal. It is recognized of course that such rate, mechanism and solubility effects may very often be the dominant influences in the corrosion behavior).

* Solubility data from references 31, 32, 33.

There are three loci where the adsorption of oxygen (or nitrogen, carbon or hydrogen) may influence corrosion behavior. These are: the liquid-vapor interface, the liquid-solid-vapor interfacial line, and the liquid-solid interface. Oxygen is known to lower the surface tension of liquid alkali metals [34]. By the Gibbs equation, we know that this means adsorption of oxygen. (Much less is known about the surface behavior of C, N and H in liquid alkali metals). The adsorption of oxygen at the liquid-vapor surface means a concentration of oxygen at the liquid-vapor-solid interfacial line. Hence enhanced corrosion at that line, over the corrosion underneath the liquid surface, is to be expected.

The adsorption of oxygen (or N, H or C) at the liquid-solid interface is at present a completely unexplored field. It must be emphasized that the adsorption at the liquid-gas interface does not lead to any prediction of adsorption at the liquid-solid metal interface*. On the basis of chemical affinities, no very great adsorption (either positive or negative) would be predicted. In the very different case of an alkali metal on a metal oxide, or on glass, chemical considerations lead to the confident prediction of strong oxygen (or metal oxide) adsorption. The wetting behavior of liquid potassium on stainless steel or glass is in accord with these prediction.

---

* See also ref. 35, on the modification of the Gibbs equation that must be used for a 3-component system.

Finally, it must be pointed out that caution must be used in applying this theory to the corrosion of alloys. No generalizations can be made, as yet, but it is evident that marked differences in the solubility of the components of an alloy in a corroding liquid metal could overwhelm interface and grain boundary energy effects. Cf. Harrison and Wagner, ref. 36. Besides, the presence of precipitates at grain boundaries may so drastically modify grain boundary energies as to render predictions of the type described above quite difficult.

E-2492

122

REFERENCES

1. L. A. Girifalco and R. J. Good, *J. Phys. Chem.* 61, 904 (1957).

2. R. J. Good, *J. Phys. Chem* (to be published). See Annual Report to AEC, 1962, Contract AT(04-3)297.

3. J. H. Hildebrand and R. L. Scott, "Solubility of Non-Electrolytes", Reinhold, 1950.

4. D. McLean, "Grain Boundaries in Metals", Oxford, 1957.

5. D. J. C. Yates, "Advances in Catalysis", vol 12, 1960, pp 265-312, D. D. Eley, P. W. Selwood, P. B. Weiss, eds., Academic Press, N.Y., 1960.

6. R. J. Good, *J. Phys. Chem.* (to be published). See Annual Report to AEC, 1961, Contract AT(04-3)-297.

7. R. J. Good, L. A. Girifalco, G. K. Kraus, *J. Phys. Chem.*, 62, 1418 (1958).

8. R. J. Good and L. A. Girifalco, *ibid*, 64, 561 (1960).

9. R. J. Good, J. D. Opdycke and C. S. Tucek, Annual Report to AEC, 1961, Contract AT(04-3)-297.

10. P. V. Geld and S. K. Chuchmarev, *Doklady Adad. Nauk. S.S.S.R.*, 83, 887 (1952)

11. J. J. Gilman, *J. Appl. Phys.* 31, 208 (1960).

12. N. J. Petch, *Phil. Mag.* (8) 1, 186 (1956): *ibid*, (8) 3, 1089 (1958).

13. N. J. Petch, in "Fracture", Proceedings of the International Conference on Fracture, Swampscott, Mass., 1959. B. L. Averbach, D. K. Felbeck, G. T. Hahn and D. T. Thomas, eds., Wiley, 1959.

14. A. N. Stroh, _Advances in Physics_, 6, 418 (1957).

15. "Embrittlement by Liquid Metals" by W. Rostoker, J. M. McCaughey and H. Markus, Reinhold, N.Y., 1960.

16. A. H. Cottrell, _Trans. AIME_, 212, 192 (1958).

17. N. J. Petch, _J. Brit. Iron & Steel Inst._ 174, 25 (1953).

18. J. W. Taylor, _J. Inst. Met._ 83, 143 (1954).

19. J. W. Taylor, _Phil. Mag._ 46, 867 (1955).

20. "Liquids Metals Handbook", AEC, Washington, D.C., 1952

21. C. Kemball, _Trans. Faraday Soc._ 48, 1 (1946).

22. G. L. Mack, J. K. Davis & F. E. Bartell, _J. Phys. Chem._ 45, 846 (1941).

23. C. C. Addison, W. E. Addison, D. H. Kerridge & J. Lewis, _J. Chem. Soc._ (1955) 2262.

24. O. A. Timofeevicheva & V. B. Lazarev, Izv. _Adad. Nauk. S.S.S.R._, _Odt. Khim. Nauk._ 1962, 358.

25. A.R.C. Westwood, Fall meeting, 1962, New York, of Metallurgical Society of AIME.

26. P. A. Rehbinder & V. I. Lichtman, in Proceedings of the Second International Conference on Surface Activity, London, 1957, Vol. 3, pp 563-582. Academic Press, Inc., N.Y., 1957.

27. A.R.C Westwood, personal communication.

28. "Metal Surfaces", ASM Seminar, New York, October, 1962. American Society for Metals, Cleveland, Ohio, 1963.

29. C. S. Smith, Trans. AIME, 175, 15 (1948).

30. J. C. Fisher & C. G. Dunn, in "Imperfections in Nearly Perfect Crystals", pp 317-351, Shockley, Holomon, Maurer & Seitz, eds., Wiley & Sons, Inc., N.Y., 1952.

31. M. Hansen, "Constitution of Binary Alloys", 2nd ed., McGraw-Hill, N. Y., 1958.

32. O. J. Kleppa, J. Am. Chem. Soc. 74, 6047 (1952)

33. M. W. Nathans and M. Leider, J. Phys. Chem. 66, 2012 (1962).

34. C. C. Addison, W. E. Addison & D. H. Kerridge, J. Chem Soc. (1955), 3047.

35. T. J. Whalen, S. M. Kaufman & M. Humenik, Trans. ASM, 55, 778 (1962).

36. J. D. Harrison & C. Wagner, Acta Met., 7, 722 (1959).

II. COMPATIBILITY TESTS WITH ALKALI METALS

David Gurinsky, Chairman
Brookhaven National Laboratory
Upton (L. I.), New York

The time allotted for this session permitted only
a limited discussion of current compatibility test
results, under the headings of (1) test type (i. e.,
capsule or loop) and (2) fluid.   However, detailed
questionnaires (designed by C. A. Barrett, NASA
Lewis) completed by those participating in this
session are presented herein. The purpose of
the questionnaires was to ensure completeness
and uniformity in reporting of corrosion test in-
formation.

A. CAPSULE TESTS

MSA RESEARCH CORPORATION $\longrightarrow$ 135
Callery, Pennsylvania

Liquid Metal Corrosion Capsule Questionnaire

1. Purpose of Test and Sponsor - Evaluate mechanisms of attack
      of structural metals by liquid and vapor cesium, AF
      (ASD) sponsored.

2. Fluid - cesium.

3. Type - All liquid to date. Dissimilar metal and "solubility"
      capsules. Future tests to include boiling-reflux capsules.

4. Alloys -   Cb-1 Zr recrystallized rod
             Mo-1/2 Ti recrystallized rod
             Haynes-25 annealed tubing

   After machining, capsule components are lightly abraided
   and degreased with acetone.

5. Test Specimens - Dissimilar metal couples that have been studied
      to date are:

               Haynes-25   vs   Cb-1 Zr (tab)

               Mo-1/2 Ti   vs   Zr (tab)

               Cb-1 Zr   vs   Mo-1/2 Ti (tab)

   Solubility capsules of Haynes-25, Mo-1/2 Ti and Cb-1 Zr have
   been fabricated with an inverted sampling crucible of either
   high purity alumina or refractory alloy. Solubility capsules
   are inverted at temperature.

6. Dimensions of Capsule - 3/4 in. O.D. x 1/2-5/8 in. I.D. x 4 in.
      long. Approximately 10 grams of cesium covering tabs that
      are ∼1 in. x 1/2 in. x 1/8 in. thick. Solubility capsules
      include an inverted crucible.

7. Controlled Variables Studied - Time, oxygen and carbon content of
      cesium.

8. Purity of Alkali Metal - The cesium was hot-trapped with zirconium
      turnings at 1400°F for at least 15 hours. Negative oxygen
      values were obtained by the amalgamation and butyl bromide
      techniques. A modified amalgamation method resulted in higher
      oxygen levels. Evaluation of freezing point depression of
      cesium by oxygen has indicated a reliable and precise method
      for oxygen in cesium.

   Carbon is analyzed by dissolution in water, acidification,
   boiling to dryness and dry oxidation of the salt with O_2

at $\sim 1400°F$. The CO_2 produced is analyzed by infra-red.

9. Method of Loading and Sealing Capsules - Capsules are charged with cesium in argon filled vacuum dry-box, and are TIG-welded shut.

10. Test Environment - Haynes-25 capsules are heated in air, refractory capsules in vacuo ($< 10^{-4}$ mm Hg). Getter turnings and foil are included in the furnace hot-zone.

11. Fluid Flow Rate - Negligible - both the dissimilar metal and solubility capsules have been maintained isothermal ($\pm 2°F$).

12. Flow Stability - not applicable.

13. Method of Heating and Control - Manually controlled continuous electrical power input to SiC element furnace with overnight variation less than $\pm$ 10°F. Temperatures are measured with L&N, K-3 potentiometer.

14. Instrumentation - Capsule exposures are relatively uninstrumented. Argon cover gas analysis (for dry-box) includes Minoxo indicater for oxygen (sensivity = 0.5 ppm).

15. Post-Test Procedure - Sectioning of capsules in a dry-box under argon.

16. Method of Measuring Corrosion - Includes metallography, x-ray diffraction, weight change, E.B. microprobe analysis, microhardness, analysis of refractory components for oxygen, carbon and nitrogen.

17. Reproducibility - Too few capsules are run under identical conditions to permit an adequate description of reproducibility.

18. Number of Premature Failures due to Causes Other than Corrosion - Early in the program, four capsules failures resulting from cracked welds - 3 Cb-1 Zr and 1 Mo -1/2 Ti capsule. Two Cb-1 Zr solubility capsules have plastically failed in the region of the sampling crucible.

19. Manpower - Level of effort - 1-1/2 technical men + 1 technician.

20. Summary of Results -

Dissimilar Metal Tests - The transfer of oxygen, carbon and nitrogen between two components of a dissimilar metal capsule is being evaluated as a function of time. Considerable isothermal mass transfer in all couples has been indicated by microprobe analysis.

Solubility Tests - Necessary variations in technique have not permitted quantitative solubility relationships to be derived at this writing. Low solubility values ($\sim$10 ppm at 2500°F) and possible interaction of "catch" crucible with the charge have been responsible for the variations.

DIVISION OF NORTH AMERICAN AVIATION, INC.

Liquid-Metal Corrosion Capsule Questionnaire

1. Purpose of Test and Sponsor: The purpose of this investigation was to define and develop a better understanding of the modes of attack of various structural metals by as-received cesium under both static and refluxing conditions. This program was sponsored by the Aeronautical Systems Division under USAF Contract No. AF 33(616)-8435.

2. Fluid: Cesium (as-received)

3. Type: Two-phase static and refluxing capsule tests.

4. Alloys or Materials: The metals investigated were Inconel-X, 310 stainless steel, zirconium, hafnium, columbium, columbium + 1 percent zirconium, molybdenum, tantalum, and tungsten.

   Inconel-X was purchased in the hot-rolled condition, 310 stainless steel in the annealed condition, and the remaining metals in the recrystallized condition. The recrystallization heat treatments are given in Table I.

TABLE I

RECRYSTALLIZATION HEAT TREATMENTS FOR CAPSULE MATERIALS*

Metal	Time, hours	Temperature, F
Zirconium	1-1/4	1450
Hafnium	1	1750
Columbium	1	2200
Columbium-1 percent Zirconium	1	2200
Molybdenum	1	2100
Tantalum	1	2200
Tungsten	1/4	3100

*Performed by suppliers.

E-2492

4. (cont.) The hafnium, columbium, and tantalum were electron-beam melted, and the zirconium, molybdenum, and tungsten were vacuum-arc cast. The columbium-1 percent zirconium alloy was vacuum-arc cast starting with electron-beam melted columbium. All capsule materials were purchased as 1/2- and 1-inch diameter bars.

Conventional methods were used in machining the capsules of all materials except tungsten. The tungsten capsules were produced by the Elox method.

After machining, the capsules were cleaned, first with acetone and then with alcohol.

The Inconel-X capsules were given the following heat treatment in argon: 2100 F for 4 hours followed by a flowing argon quench to room temperature, plus 1550 F for 24 hours, followed by a flowing argon quench to room temperature, plus 1300 F for 20 hours, followed by furnace cooling in argon.

All capsules were degassed by heat treating in a vacuum of 10^{-5} torr or less for the times and temperatures given in Table II.

TABLE II

CAPSULE DEGASSING HEAT TREATMENTS, HEAT TREATED IN
VACUA OF 1 X 10^{-5} TO 3 X 10^{-6} TORR

Metal	Static Capsules		Boiling-Refluxing Capsules	
	Time, hours	Temperature, F	Time, hours	Temperature, F
Inconel-X	1-1/3	1490		
Zirconium	1-1/3	1490		
310 Stainless Steel	1	1975 - 1700		
Hafnium	1	1975 - 1700		
Columbium	1	2150	1	2200
Columbium-1% Zirconium	1	2150	1	2200
Tantalum	1	2150	1	2200
Molybdenum	1	2150	1	2200
Tungsten	1	2150	1	2200

4. (cont.) As can be seen, the degassing heat treatments were carried out at essentially the same times and temperatures as had been used for the recrystallization heat treatments. Thus, the degassing heat treatments also served to eliminate the surface cold work produced by machining. The Elox process used on tungsten does not produce cold work.

5. Test Specimens: The containers were the test specimens.

6. Dimensions and Sketch of Capsule: The capsules for the static tests were 2 inches long with an outside diameter of 1/2 inch and an inside diameter of 1/4 inch. The capsules for the boiling-refluxing tests were 6 inches long with an inside diameter of 1 inch and an inside diameter of 1/2 inch. The capsules were closed at one end by welding in a cap, in which a 0.030-inch hole had been drilled at a 30-degree angle.

    A sketch of the capsules for all materials other than tungsten is shown in Figure 1. The only difference for tungsten was that the lip was not machined into the caps.

7. Controlled Variables Studied: Time, temperature, variation between static and refluxing conditions, and fluid phase environment (i.e., pure vapor, pure melt, or the two phase exposure) were the controlled variables. The static tests were for 1000 hours at 1600 F. The refluxing tests target conditions were 1800 F for 1000 hours and 2500 F for 1000 hours if possible. The 2500 F tests were discontinued after 54-1/2 hours when the next to the last of the molybdenum capsules corroded through.

8. Purity of Alkali Metal: The purity specifications to which the cesium was bought are given in Table III along with the analyses. No purification method was used as the purpose of the test was to study corrosion modes with as-received cesium. The oxygen content was analyzed independently by two laboratories by the mercury amalgamation method. The data obtained by this method of oxygen analysis are of relative value only and probably do not represent the actual oxygen content. Refractory metal determinations in cesium were made on converted chloride or sulfate of the cesium utilizing colorimetric and emission spectrographic methods.

TABLE III

SPECIFICATION AND ANALYSIS OF AS-RECEIVED CESIUM

Impurity	Specification Maximum Content, ppm	Analysis, ppm
Lithium	50	39
Sodium	100	69
Potassium	500	192
Rubidium	2000	626
Oxygen	500	9*
Calcium	100	**
Silica	50	**
Iron	10	**
Aluminum	10	**

*All oxygen considered present as Cs_2O. Mass spectrometer tests proved other oxides are actually present. However, the value can be used for comparison purposes. The reported result is the average of three tests carried out independently in two laboratories.

**Not determined.

138

9. Method of Loading & Sealing Capsules: The caps were TIG welded into the capsule bodies (see Fig. 1).

In a purified argon filled glove box, cesium was loaded into the capsules through the 0.030-inch holes, using a plastic syringe fitted with a stainless steel capillary.

The fill holes of the static capsules were closed in the glove box by TIG welding.

The fill holes of the refluxing capsules were closed by electron-beam welding. For transfer from the glove box to the electron-beam welder, each capsule was placed in an airtight fitting so that purified argon was maintained over the cesium during transfer. This fitting was then opened in the electron-beam welder.

10. Test Environment: Both the static and refluxing capsule tests were run in vacuum at pressures of 3×10^{-6} torr or lower.

Pressures were determined by ionization gages (Consolidated Vacuum Corp.).

11. Fluid Flow Rate: Refluxing conditions were originally assumed to be predominating in the reflux tests and calculations were made before running the refluxing tests on vapor velocity at pool surface (V_v), velocity of condensate returning to pool (V_c) and the seconds per inventory change (t). For the 2500 F tests, these values were roughly as follows:

$$V_v \ 2500 = 0.6 \text{ ft/sec}$$
$$\text{Mean } V_v \ 2500 = 0.5 \text{ ft/sec}$$
$$t_{2500} = 6.5 \text{ seconds/inventory change}$$

11. (cont.) The lower furnace setting and the higher latent heat of vaporization for cesium in the 1800 F tests resulted in a calculated approximate t_{1800}/t_{2500} of   1.5.

Examination of the capsule interiors after test and observations during tests indicated that splashing of liquid cesium predominated over refluxing conditions in the actual tests.

12. Flow Stability: The flow was not very stable. Constant monitoring of capsule base temperatures revealed sudden steady temperature rises occurring, followed by audible clicks and abrupt lowering of the capsule base temperature. The temperature rise is attributed to formation of a bubble between the capsule base and the molten pool. The noise is attributed to the bubble bursting after dislodging from the capsule base and rising to the top of the pool. The abrupt lowering of the temperature was due to quenching of the hot capsule base by the pool coming into contact with the capsule metal again.

13. Method of Heating and Control: For the static tests, the capsules were placed in an Inconel tube vacuum chamber which was heated with a clam-shell-type furnace. The furnace had a heating zone 18 inches long. The capsules were held in a stainless steel fixture in three rows and all capsules fit within the central 10 inches of the heating zone. A number of radiation shields were placed at each end of the rows of capsules. Chromel-alumel thermocouples were used for capsule temperature read-out and control. The temperature recorder indicated a temperature of 1600 F $\pm$ 5 over the 1000 hour run at the center of the group of capsules. The temperature gradient

140

13. (cont.) from one end of the rows of capsules to the other was not measured but is estimated to have been about 20 F.

The refluxing capsule tests were conducted in a furnace designed for this program. It is of the cold wall tank type. Thirteen cylindrical tantalum heating elements, each with molybdenum radiation shields, are arranged on a 12-1/2-inch reference circle. The heating elements are connected in series. The capsules are supported in the heating elements on pedestals. Approximately the lower 1 inch of each capsule is in the heating zone. The capsule support is vertically adjustable over a total distance of about 1 inch.

A cold-wall heat barrier separates the lower (heating) portion of the furnace tank from the upper (cooling) portion. A cooling cell, each with its own water inlet and outlet, is provided for each capsule.

A tantalum-sheathed platinum-6 percent rhodium/platinum-30 percent rhodium thermocouple is brought up through each capsule support and fits into a small cavity drilled in the bottom of the capsule. A tungsten/tungsten-26 percent rhenium control thermocouple extended in through the side of the furnace to within about 1/8 inch of one of the heating elements.

Although individual capsule temperatures could be controlled over 200 to 300 degree ranges by changing the capsule positions within heating elements, it was not possible to maintain all of the capsules at the same temperature.

The temperature measured at the bottom of the capsules during the 1800 F refluxing run are shown in Table IV. The temperature ranges indicated for

141

13. (cont.)   some capsules represent short-term temperature cycles believed
    due to nonnucleate boiling of the cesium. It is believed that the top
    of each capsule was about 50 F cooler than the bottom.

    Premature failures during the 2500 F refluxing run, which are discussed
    below, make difficult an estimation of temperature gradients and stability
    for that run.

TABLE IV

CAPSULE TEMPERATURES DURING 1800 F BOILING-REFLUXING RUN

	Temperature, F
Tungsten No. 3 No. 2	1820 1820
Tantalum No. 4 No. 5	1698 to 1755 1718
Molybdenum No. 6 No. 5 No. 2	1825 to 1762 1800 1728
Columbium No. 3 No. 5 No. 6	1675 to 1680 1725 to 1786 1705
Columbium-1% Zirconium No. 3 No. 4 No. 1	1635 to 1650 1630 to 1700 1750 to 1820

14. Instrumentation: The instrumentation on the static tests included chromel-
    alumel thermocouples, ion gages, and a controller recorder which controlled
    to $\pm$ 5 F. Temperature sensing devices also served to actuate liquid nitrogen

142

14. (cont.)   valves serving the cold traps. Three thermocouples were inserted along the furnace.

The refluxing capsule tests utilized platinum-6 percent rhodium/platinum-30 percent rhodium thermocouples (see item 18) for recording temperatures and a tungsten/tungsten-rhenium thermocouple for controlling* the temperature. Thermocouples in each capsule base were monitored separately.

Thirteen thermometers were used to measure the temperatures of the water coming from the cooling coils around each of the 13 capsules and one upstream thermometer indicated the original water temperature. The water from each cooling coil was ejected through individual fountains into a basin in a manner that allowed measurement of the flow. Thus by measuring the ΔT and water flow, the heat taken out from the top portion of each capsule was individually monitored.

---

*The special Rocketdyne reflux capsule furnace utilizes a saturable core reactor device in its controlling mechanism to minimize temperature excursions and fluctuations. The parts and description of the controller are given below:

(a) Wheelco Model 8000-2517-XX MMC Potentiometer Strip Chart Recorder-Controller; 11" calibrated scale; dual range, a manual switch operated; #1 Range: 0 to 3000 F. Calibrated for platinum-platinum 13%. #2 Range: 2500-4500 F. Calibrated for tungsten-tungsten 26% rhenium; measuring accuracy 1/4 of 1% of scale span, chart speed 1, 2 and 4 inches per hour; Zener diode constant voltage standardization; MMC current controller with three function control; proportional band, automatic reset, and rate action; 115 volt, 60 cycle, one phase.

(b) Fidelity Saturable Core Reactor, Model FE6-7, 440 volt, one phase 60 cycle input, 396 volt, one phase, 60 cycle output, 40 KVA; current limit device provided.

(c) Stepdown Transformer, 396 volt, one phase, 60 cycle, 30 KVA output.

143

15. Post-Test Procedure: After the test runs were completed, the capsules were quenched. They were then photographed, a section was thinned down on a lathe, and the capsules were then opened with a tube cutter and the contents, which up to this time had been kept cold, were warmed up to about 85 F and transferred by means of a hypodermic needle to glass vials. The neck of each glass vial was attached to a vacuum line inside the glove box and radiant heating was applied around the vial neck until closure occurred. The sealed glass vials and the empty capsules were then removed from the glove box. The capsules were measured for I.D. changes and then longitudinally sectioned and photographed. Sections from the vapor zone, melt zone and interface zones were removed and prepared for metallurgical examinations. A thin layer of alloy (0.040 in.) was machined away from the I. D. of other sections and these layers were subjected to chemical analyses.

16. Method of Measuring Corrosion and Material Change: The methods of measuring corrosion and material change included metallographic examination, microhardness surveys, changes in capsule specimen I.D., visual inspection, and chemical analysis. The metallographic examination served as the main diagnostic tool.

17. Reproducibility of Results: The reproducibility of results can be seen in the similarity in photomicrographs between duplicate and triplicate specimens exposed to nearly identical conditions.

18. Number of Premature Failures Due to Causes Other than Corrosion: Failures due to causes other than corrosion did occur. All the vacuum-arc cast

18. (cont.) tungsten "pressure vessel" capsules cracked through the welds as did a few of the vacuum-arc cast molybdenum capsules. In the static tests, nitrogen cooling of cold traps occasionally gave trouble when valves would freeze and cold traps would heat up. The most troublesome failures were the EMF decay of the platinum-6 percent rhodium, platinum-30 percent rhodium temperature recording thermocouples during the refluxing tests.

The cesium released into the furnace cavities by failure of some of the capsules caused considerable trouble. The platinum collectors of the vacuum measuring devices (ion gages) on the static tests were visibly attacked by the cesium vapor to the extent that these ion gages had life-times of approximately two days. The reflux tests avoided this problem by trapping cesium vapor, but no other vapors, prior to admission into the ion gage. The temporary high transient cesium pressures caused drastic sputtering and arcing of tantalum heating elements within the furnace cavity in the refluxing tests. The arcing and sputtering resulted in destruction of these heating elements which caused shutdown for element replacement or rewiring to allow for omission of damaged elements in the series heating circuit.

19. Manpower Involved: No significant hardware design time.

2/3 man year for Engineer in preparation and operation.

2/3 man year for Technician in preparation and operation.

1/3 man year for Engineer in analyses

1/3 man year for Technician in analyses

1/3 man year for Shop time

20. Summary of Results to Date: All the results indicated below obviously
    apply only to the unpurified cesium used in this program. The following
    materials appear adequate for structural applications in stagnant cesium
    liquid or vapor at 1600 F.

      310 Stainless Steel

      Inconel-X

      Hafnium

      Columbium

      Columbium-1 Percent Zirconium Alloy

      Molybdenum

      Tantalum

      Tungsten

Zirconium is not adequate for structural applications at 1600 F because a
phase change occurs near that temperature. Almost no zirconium was found
in the cesium from these capsules.

Columbium, columbium-1 percent zirconium alloy, molybdenum, and tantalum
do not appear corrosion resistant to boiling, splashing, and refluxing
cesium at 1800 F. Molybdenum is the least compatible. Columbium-1 percent
zirconium alloy suffers grain boundary attack, associated with preferential
leaching of zirconium from this alloy at 1800 F.

Columbium-1 percent zirconium alloy was the best material tested in boiling,
splashing, and refluxing cesium at 2500 F. The grain boundary attack
noticed in the 1800 F tests did not appear at 2500 F. Molybdenum dissolves

20. (cont.) rapidly in boiling cesium at 2500 F. The dissolution of molybdenum into cesium melt, under these conditions, leaves the molybdenum with a mirror smooth surface finish.

These compatibility conclusions do not apply to stress corrosion phenomenon which were not studied.

Interstitials enter into the compatibility problem. Both 310 and Inconel-X are decarburized by cesium of the purity used in these tests. Oxygen content may be one of the most important variables in compatibility studies.

The mode of corrosion included intergranular attack and general dissolution. No prediction can be made as to which mode would be operative as a function of chemical composition of the material used. The mode of attack can change under different exposure conditions.

Fluxing of oxides may contribute to dissolution. The columbium-1 percent zirconium alloy, with coherent precipitate particles of ZrO, preferentially loses zirconium to cesium. A possible reaction to explain this is

$$2 \ Cs_2O + ZrO \longrightarrow Cs_2O.ZrO_2 + Cs$$
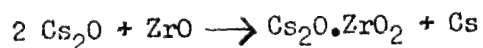
Oxygen carrying compounds, other than Cs_2O, occur in molten cesium, hence all analytical methods, other than vacuum fusion, mass spectrometry, or neutron activation, can give only relative results.

Pertinent photomicrographs and figures are shown below (Figs. 2 to 4).

STATIC TEST CAPSULE　　　　REFLUXING TEST CAPSULE
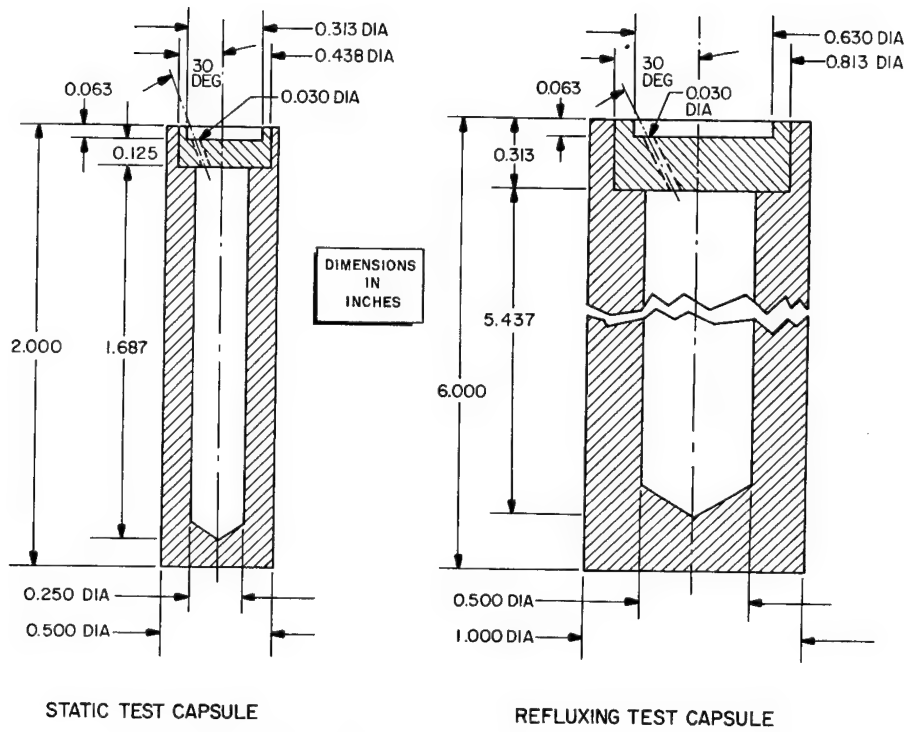
Figure 1. - Capsule design for materials other than tungsten.
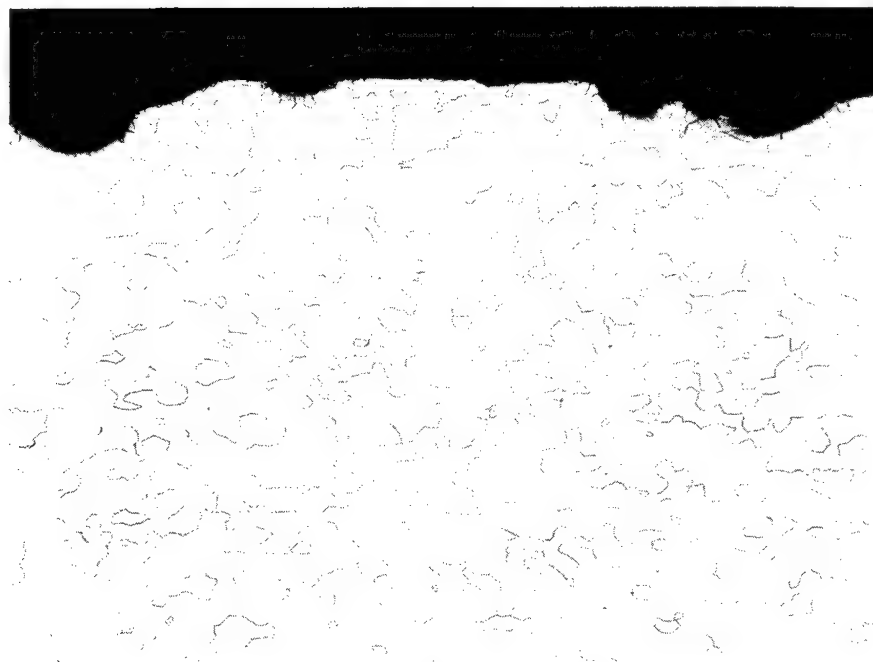
(a) Magnification, 100X.
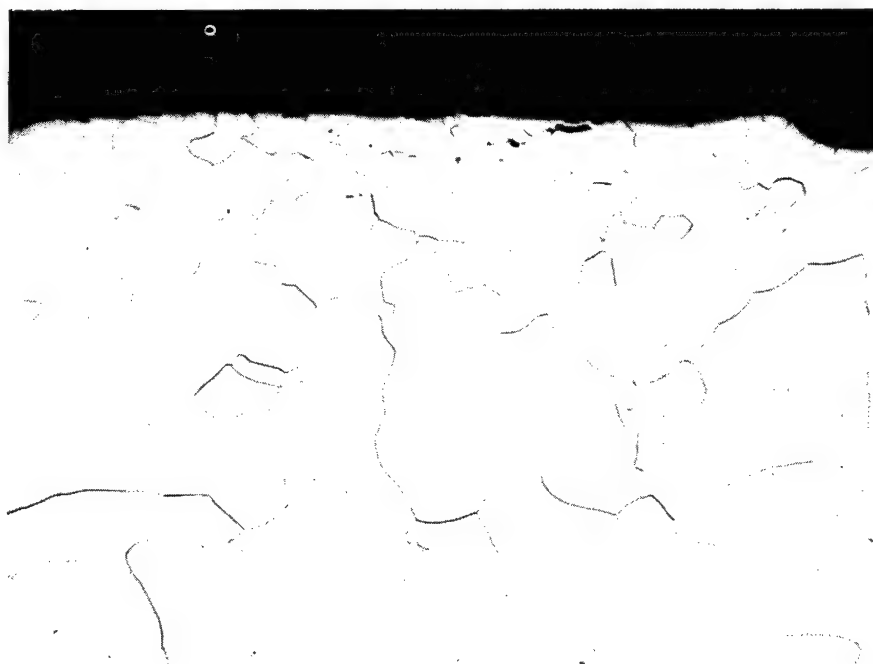
(b) Magnification, 500X.

Figure 2. – Columbium capsule from 1800 F reflux test run. Surface shown exposed to 1800 F condensing cesium vapor for 720 hours. The scooped-out appearance of the surface is difficult to explain. One possible hypothesis would be that an intergranular precipitate was attacked by cesium fluids. The higher magnification photomicrograph may be showing this phenomenon in its initial stages. Etchant: 30 lactic/ $2HNO_3/10HF$.

(a) 1800 F for 720 hours.
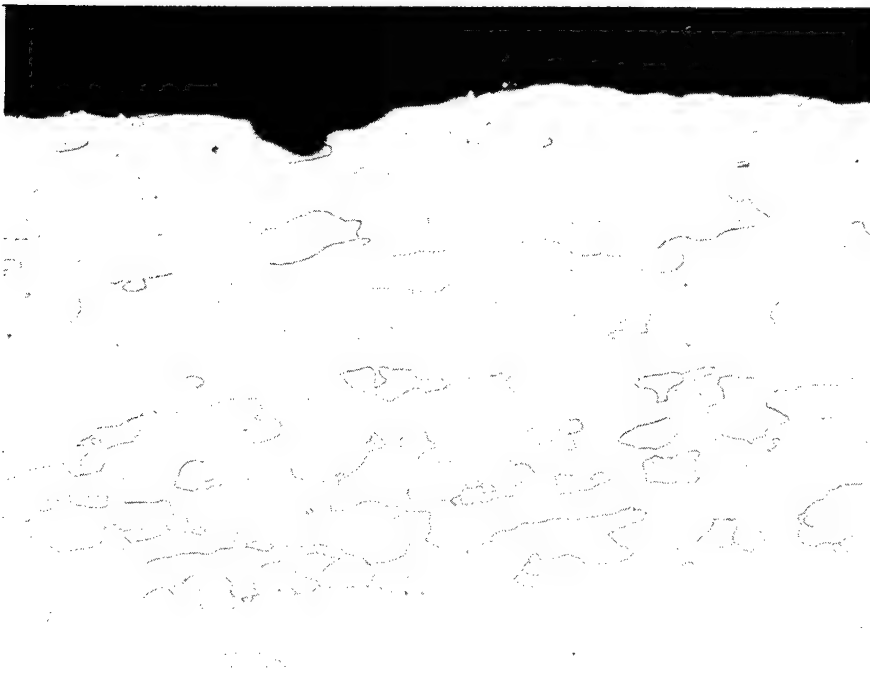
(b) 2500 F for $54\frac{1}{2}$ hours.

Figure 3. – Columbium-1% zirconium capsules exposed to boiling cesium melt. Note intergranular nature of attack at 1800 F as compared to braod attack at 2500 F.

Figure 4. - Section through molybdenum reflux capsule exposed to boiling, splashing cesium at 2500 F for $54\frac{1}{2}$ hours. Effect may be due to Redox reaction involving a volatile molybdenum oxide or merely to hot cesium solution splashing against a cooler wall and precipitating dissolved molybdenum.

Evandale (Cincinnati) Ohio
Space Power and Propulsion Section

Liquid-Metal Corrosion Capsule Questionnaire

E-2492

1. Purpose: To examine the corrosion resistance of Cb-1Zr, AS-55,
    and D-43 (X-110) in refluxing potassium environments.

    Sponsor: NASA Contract NAS 3-2140, AS-55 Program.

2. Fluid: Potassium.

3. Type: Reflux capsule.

4. Materials: Cb-1Zr: 1 hr at 2200°F, weld, 1 hr at 2200°F
    AS-55: 1 hr at 2800°F, weld, 1 hr at 2400°F
    D-43: 1 hr at 2200°F, weld, 1 hr at 2400°F
    All 80-mil thick sheet pickled in 20% HF, 20% HNO_3,
    60% H_2O and degreased in acetone and ethyl alcohol.
    Heat treatments were conducted in vacuum environments,
    10^{-5} torr.

5. Test Specimens: Monometallic capsules with tab inserts in the
    liquid and vapor regions.

6. Capsule Dimensions: See Figure 1.

7. Range of Variables: Temperature - 2000°F to 2200°F; time - 245
    to 10,000 hrs.

8. Potassium Purity: Oxygen - 22 to 760 ppm by zirconium gettering
    in an auxiliary Cb-1Zr capsule; 7 to 72 ppm by the
    amalgamation method.

9. Loading and Sealing: Refer to report GE62FPD365 for initial pro-
    cedures. The current procedure involves filling and
    sealing under a 10^{-5} torr vacuum in an electron beam
    welding chamber (Figures 2 and 3). This is a modifica-
    tion of the procedure used at the NASA-Lewis Laboratory.

10. Test Environment: Vacuum - 10^{-7} to 10^{-9} torr at test conditions
    (Figure 4).

11. Fluid Refluxing Rate: 0.5 lb/hr at 2000°F and 1.0 lb/hr at
    2200°F under stable conditions.

12. Refluxing Stability: Some of the first capsules bumped, up to 5,000
    times in 1,000 hrs with 50°F temperature surges. More
    recently tested capsules appear stable at the test
    conditions, as indicated by the absence of temperature
    surges (limit of detection approximately 5°F).

13. Method of Heating and Control: Tantalum resistance heater with
    constant voltage control (Figures 1, 5, and 6).
    Thermocouples are used to record the temperature, and
    optical pyrometer measurements are used to correct
    for drift and to set the tantalum heater voltage.
    Theoretical estimates indicate that the temperature
    gradients must be small, less than $25^{o}F$.

14. Instrumentation: Tantalum-clad, Al_2O_3-insulated, Pt **vs.** Pt + 13%
    Rh thermocouples attached to the outside of the capsule
    by tantalum straps. Using a similar MgO-insulated
    thermocouple at $2200^{o}F$ led to a reaction with the AS-55
    and a capsule failure after 245 hrs of testing.

15. Post-Test Procedure: Capsules are opened and drained under an
    inert gas cover and then cleaned with a hexane – ethyl
    alcohol solution.

16. Methods of Measuring Corrosion: Weight change and bend testing
    of tab specimens; light and electron microscopy;
    hardness measurements; chemical analysis and stress
    rupture testing of sections from the capsule wall.

17. Reproducibility of Results: Duplicate tests have not been con-
    ducted. However, results from somewhat similar tests
    indicate a generally consistent behavior with respect
    to weight change, hardness, chemistry, stress rupture
    properties, and the amount of general corrosion. The
    selective attack of some of the weld grain boundaries
    of one Cb-1Zr capsule does not appear reproducible, as
    will be described presently.

18. Premature Failures: One capsule was discarded after it was acci-
    dentally overheated during start-up. Another capsule
    failued after 245 hrs at $2200^{o}F$ as a result of a reaction
    with the thermocouple and penetration of the capsule
    wall. No weld, heater, or corrosion failures have
    occurred.

19. Manpower: Approximately one engineer and one technician with
    support for design, chemical analyses, and fabrication.

20. Summary of Results: Detailed results are presented in GE62FPD365,
    an interim report which describes the work conducted
    under NASA Contract NAS 3-2140.

    In summary, 1000-hr exposures of Cb-1Zr and AS-55
    capsules to potassium at $2000^{o}F$ resulted in a small

amount of general corrosion, as evidenced by solution-
ing, stains visible at the liquid-vapor interface and
other locations, a slight increase in hardness in the
vapor region of the capsule, and small changes in the
weights of specimens enclosed in the capsules. The
selective attack of some, but not all, of the grain
boundaries in weldments exposed to liquid is considered
one of the more serious aspects of the observed corro-
sion effects, since it is not understood and it can
extend to a considerable depth (approximately 10 mils
in Cb-1Zr, Figures 7, 8, and 9). Possibly, this non-
reproducible attack is associated with vapor nucleation.

Of major significance from the alloy strengthening
standpoint is the fact that the carbides in AS-55 were
apparently stable for long times in a high vacuum and
in potassium environments at temperatures on the order
of 2000°F to 2200°F. Chemical analyses revealed no
significant mass transfer of carbon, and metallographic
examination showed no significant coalescence of the
carbides. As additional evidence of the carbide
stability, stress rupture tests, conducted at 2200°F on
specimens which were machined from the wall of the AS-55
capsule exposed for 1,000 hrs at 2000°F, showed that the
elevated temperature strength was not appreciably
affected by the exposure to potassium and high vacuum.
Presumably, the carbide strengthened D-43 alloy will
behave similarly. Exposures of Cb-1Zr, AS-55, and D-43
alloys for 5,000 and 10,000 hrs at 2000°F are in progress.
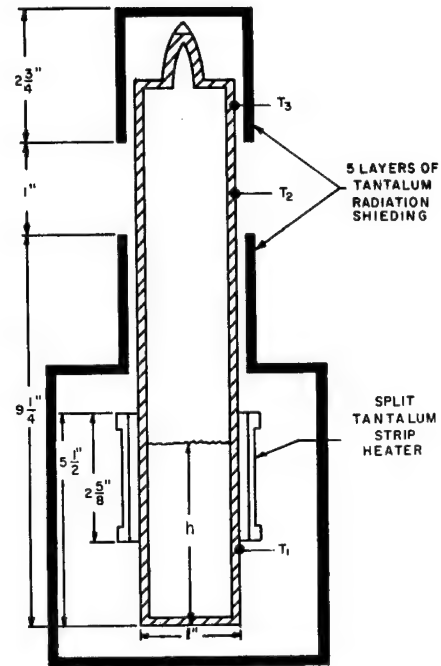
Figure 1. - Reflux capsule illustrating the location of radiation shielding, radiation zone, tantalum heating element, and height of potassium at temperature.
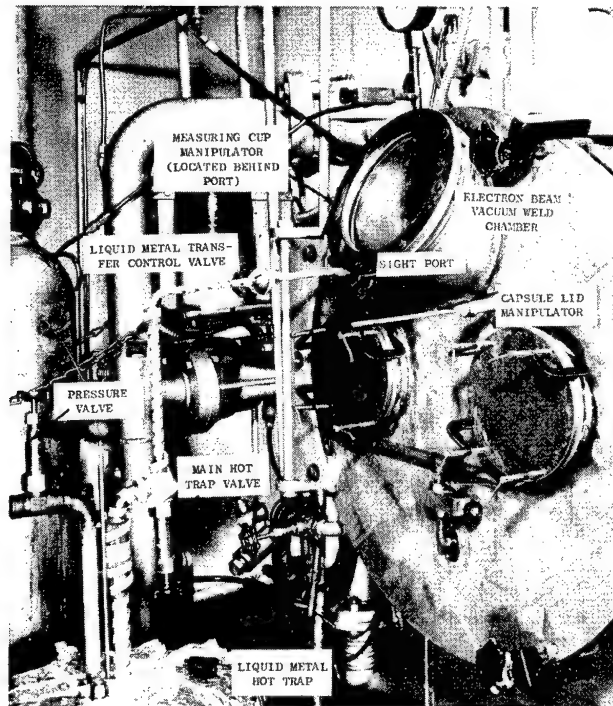
Figure 2. - External view of the apparatus for filling capsules with liquid metal in a vacuum and sealing by electron beam welding.
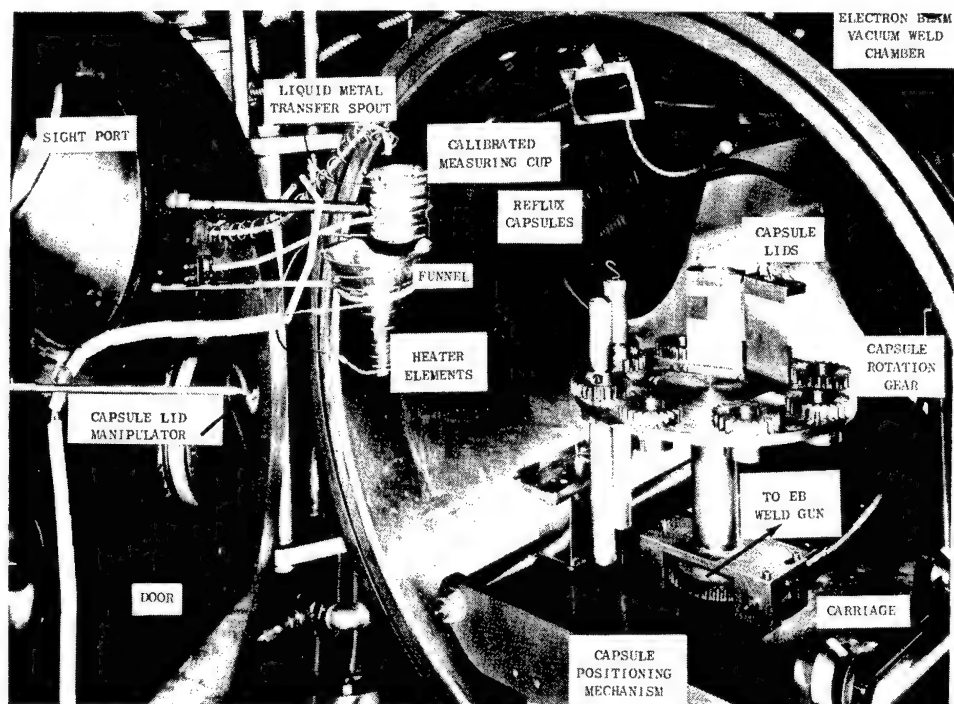
Figure 3. – Internal view of the apparatus for filling capsules with liquid metal in a vacuum and sealing by electron beam welding.
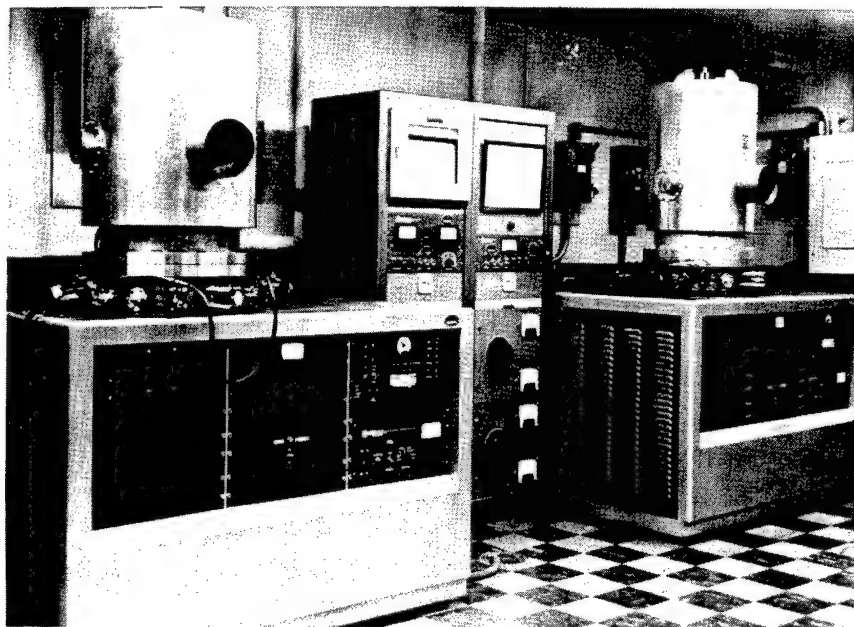

Figure 4. – High vacuum systems (10^{-10} torr range) used in the study of the corrosion behavior of columbium alloys in potassium. Each chamber is 18 inches in diameter and 30 inches high and incorporates a 400 ℓ/sec getter-ion pump and three adsorption pumps.
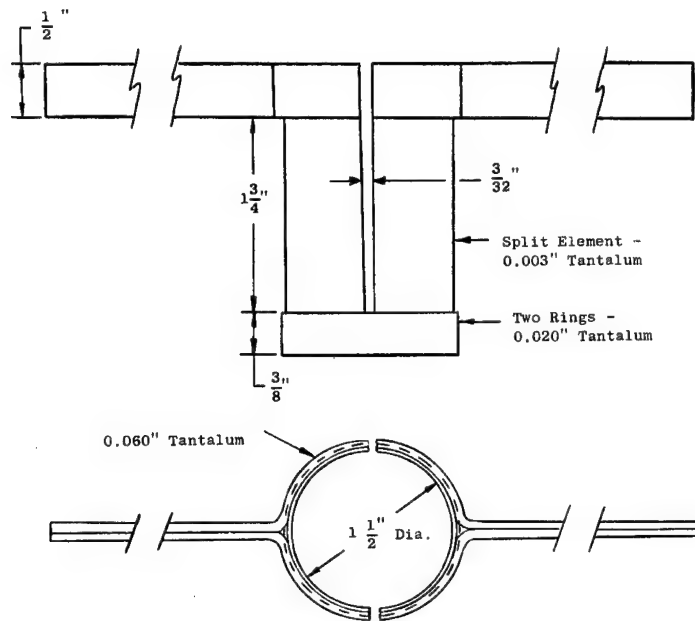
Figure 5. - Tantalum strip heating element used for reflux capsule testing.
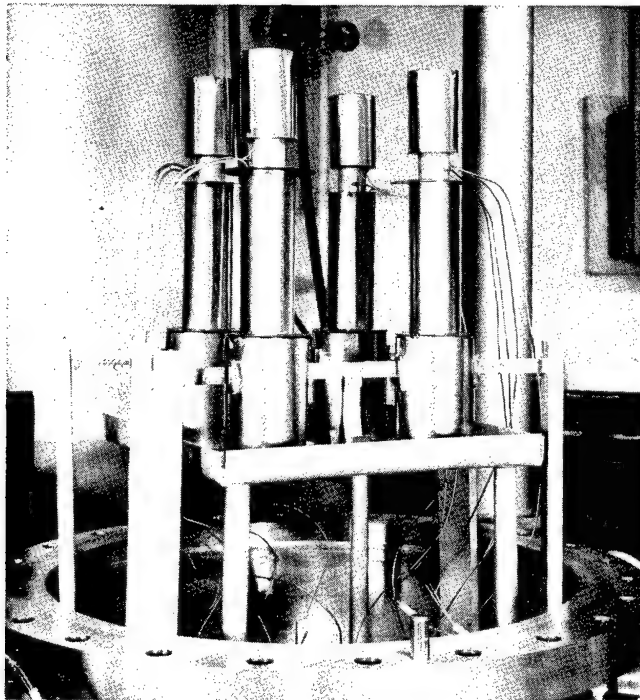
Figure 6. - Tantalum heater and shielding assembly with thermocouples and columbium alloy capsules in position for reflux corrosion testing.

158
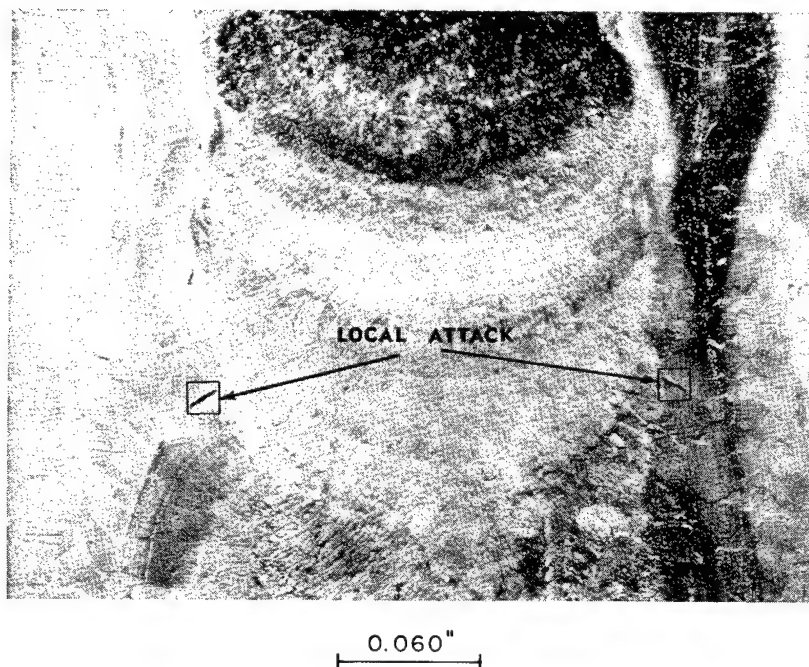
Figure 7. – Localized attack observed on the surface of a Cb-1Zr
weld exposed to liquid potassium for 1000 hours at 2000° F.
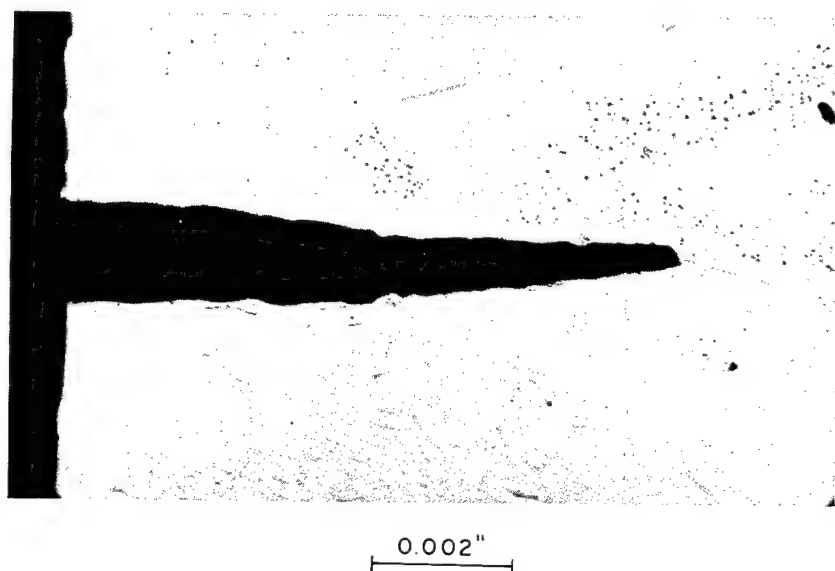
Figure 8. – Intergranular attack observed in the transverse section
of Cb-1Zr capsule weld exposed to liquid potassium for 1000 hours
at 2000° F. Etchant: 60% glycerine, 20% HNO_3, 20% HF.
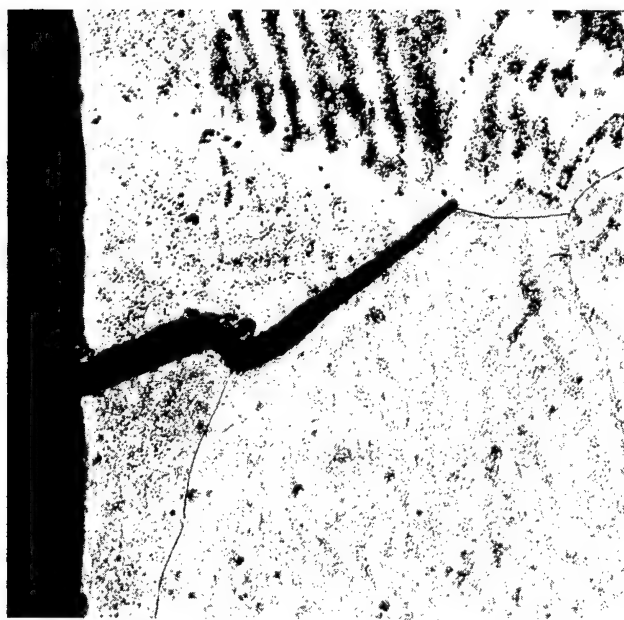
0.010"

Figure 9. – Areas of intergranular attack observed in the transverse section
of Cb-1Zr capsule weld exposed to liquid potassium for 1000 hours at 2000° F.
Etchant: 60% glycerine, 20% HNO$_3$, 20% HF.

Liquid Metal Corrosion Capsule Questionnaire

Questionnaire 1

1. Purpose of Test: To screen possible columbium and tantalum tubing alloys with potassium as a working fluid for advanced space nuclear powerplants.

   Sponsor: NASA.

2. Fluid: K.

3. Type: Two-phase refluxing capsule (fig. 1).

4. Alloys or Materials: Cb-1Zr, B-33, FS-85, AS-55, X-110, Ta-10W, T-111, C-129, S-291, Cb-752, B-66, Cb-5Zr capsules from rod stock, typical chemistry and matching sheet stock for high-vacuum creep program.

5. Test Specimens: Capsule wall and tab inserts from creep stock sheet.

6. Dimensions: $1\frac{3}{4}$ inch by 1/2 inch by 40 mil wall; 1/4 by 1/4 by 0.030 inch tab insert.

7. Controlled Variables: (1) Qualitative: composition (alloys); (2) quantitative: temperature, 1800° - 2200° F; time 1000 - 2000 hours; oxygen content in K, 20 - 200 ppm; oxygen content in alloy as received, +2000 ppm.

8. Purity of Alkali Metal: Cold trapped, hot trapped, followed by vacuum distillation. Oxygen content varied by Granville-Phillips controlled leak valve. Analysis by Hg amalgamation under vacuum.

9. Method of Loading and Sealing Capsules: Vacuum extrusion, hot-wire cut off, and E.B. welding; vacuum $\sim 10^{-5}$ mm Hg (fig. 2).

10. Test Environment: Vac-Ion pumped tanks, tests run in the low 10^{-7} range (fig. 3).

11. Fluid Flow Rate: To be determined.

12. Flow Stability: Constant ΔT, 50°-75°.

13. Method of Heating and Control: Tantalum Cal-Rod heaters with swageable Al_2O_3 insulators and Ta sheath; special terminations. Control-off Pt-Pt-13% Rh check couple at bottom of capsule.

14. Instrumentation: Thermocouple top and bottom of capsule (Pt-Pt-13% Rh). Pressure - vacuum.
    Columbium contamination tabs. Mass spectrometer or oxygen analyzer.
    Bristol multipoint temperature recorders, input electric power.

15. Post-Test Procedure: Drain under butyl alcohol, section longitudinally, photograph, mount for metallography, selected vacuum fusion, microhardness, X-ray diffraction, and E.B. probe.

    Tab will be weighed and other tests run on the capsule where feasible.

16. Method of Measuring Corrosion and Material Change: Metallography, weight change of tabs, microhardness and E.B. probe.

17. Reproducibility of Results: To be determined.

18. Premature Failures: From preliminary tests, approximately one-eighth to one-fourth. Probable failures in weld or thermocouple junction.

19. Manpower Involved - Professional 2
                        Technical   2
                        Analytical   1

20. Summary of Tests to Date: Preliminary.
    Corrosion detected in nongettered alloys (e.g., B-33, Ta-10W); test times to 2000 hours; temperatures 1800° and 2200° F. Oxygen in K at 18 ppm, 90 ppm, and 200 ppm. Alloy as received.

E-2492

162

Questionnaire 2

1. Purpose of Test: To compare the relative corrosiveness of K, Rb, Cs, and Na with high-temperature Fe-, Ni-, and Co-base alloys.

2. Fluid: K, Rb, Cs, and Na.

3. Type: Two-phase reflux capsule.

4. Alloys or Materials: 316, 318, HS-25, Hastelloy X; others later.

5. Test Specimens: Capsule wall; possibly tab inserts.

6. Dimensions: $1\frac{3}{4}$ inch by 1/2 inch by 40 mil; 1/4 by 1/4 inch tab inserts.

7. Controlled Variables: Alloys; temperature, 1400° - 1800° F; fluid; time. Hopefully O_2 in fluid.

8. Purity of Alkali Metal: Same procedure as refractory metal capsule program.

9. Method of Loading and Sealing Capsules: Same procedure as refractory metal capsule program (fig. 2).

10. Test Environment: High-purity argon; positive pressure static system.

11. Fluid Flow Rate: To be determined.

12. Flow Stability: To be determined.

13. Method of Heating and Control: NiCr heater wire wrapped around a magnesium silicate spiral cylinder; sheathed with magnesium silicate. Chromel-Alumel thermocouples to multipoint recorders. Top and bottom of capsule thermocoupled. Control from bottom check couple from manual power setting.

14. Instrumentation: Thermocouples with Bristol Multipoint. Meters to monitor power input and powerstat adjustment. Constant voltage power source.

15. Post-Test Procedure: Comparable to refractory metal program without vacuum fusion.

16. Method of Measuring Corrosion: Same as refractory capsule program.

17. Reproducibility of Results: To be determined.

18. Premature Failures: Unknown.

19. Manpower Involved - Professional 1
                          Technical   1
                          Analytical   1/2

20. Summary of Tests to Date: None; test chambers being constructed.
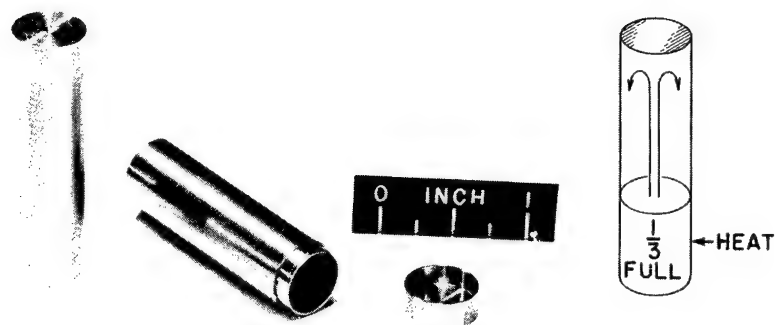
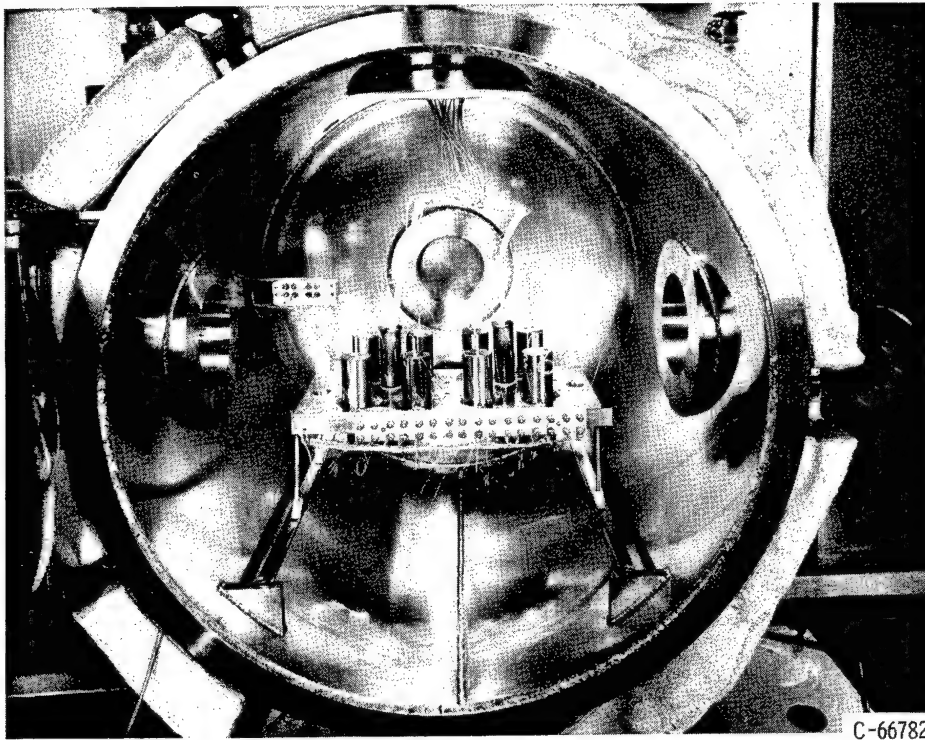CS-22943

Figure 1. - Reflux capsules used in liquid-metal corrosion studies.
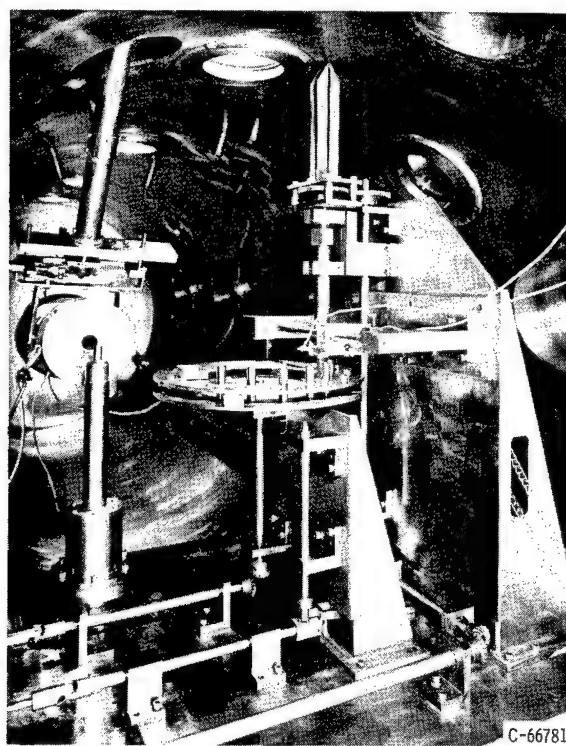
C-66781

Figure 2. - Electron-beam welding capsule facility.

164

Figure 3. – High-vacuum capsule test rig.

AEROJET-GENERAL NUCLEONICS → 177

Liquid-Metal Corrosion Capsule Questionnaire

1. Purpose of Test and Sponsor: USAEC Contract AT(04-3)-368. Techniques were developed for determining the equilibrium concentration of various metals in rubidium and the corrosive effects of rubidium on selected commercial refractory and nonrefractory metal alloys. The equilibrium concentrations of Cb, Zr, Mo, Ti, V, Ta, Fe, Be, Cr, and Ni in rubidium were determined over the temperature range 1000° to 2000° F. The corrosion of Mo-0.5Ti, Cb-1Zr, Haynes-25, alloys and beryllium and vanadium metal by rubidium was determined at various temperatures from 1000° to 2000° F in 1000-hour tests. Equilibrium concentration and corrosion results are reported and evaluated.

2. Fluid: Rubidium

3. Type: Boiling-refluxing, two-phase capsule

4. Alloys or Materials:

   (a) Capsule Cleaning Procedures:
   Capsule tubes, end caps, sample cups, and test materials were rinsed with acetone to remove fine films of grease and fingerprints prior to pickling. Pickling was performed, as shown on Table 1.

   (b) Starting Form and Heat Treatment:
   As shown on Table 2

5. Test Specimens: The test specimens of Cb-1Zr, Mo-0.5Ti, and Be were in the form of 1/2 in. OD tubing. Each specimen was inserted into the tantalum capsule shells, as shown in Figure 1. The vanadium specimens, which were not easily available in tubing form, were tested in the form of strips: 6 by 1/2 by 0.049 in. The position of the vanadium strip in the capsule is the same as the tubular test specimens mentioned above. These tests can be considered bimetallic tests because of the continuous contact of two materials with rubidium; however, due to the good corrosion resistance of tantalum to rubidium at the test temperature, the effect of tantalum on the test materials is expected to be nil.

The Haynes-25 corrosion capsule was made of Haynes-25 tubing. No insert was required. This capsule is shown in Figure 1.

6. Dimensions and Sketch of Capsule: As shown on Figure 1

7. Controlled Variables Studied: Effects of temperature on corrosion were studied for each material for identical lengths of time. The oxide content of rubidium before and after each test was noted but no correlations were attempted between oxide content and the corrosion rate. Test parameters may be found on Table 3.

167

TABLE 1

CLEANING AGENTS FOR CAPSULE MATERIALS

Material	Pickling Agent
Cb-1Zr Vanadium Beryllium Tantalum (tubes, caps, cups) Haynes-25 Rinsed with water and dried in air after pickling.	100 ml HNO_3 100 ml H_2SO_4 50 ml HF 250 ml H_2O
Mo-0.5Ti The parts were rinsed with water and alcohol and dried in air after pickling.	30 ml lactic acid 10 ml HNO_3 2.5 ml HF 37.5 ml H_2O 10 gm $K_3Fe(CN)_6$ 10 gm KOH 100 ml H_2O

After pickling, all surfaces, except the OD of the tantalum containment capsules, were handled with clean forceps. The samples were individually wrapped and placed in plastic bags until ready for capsule loading and welding.

TABLE 2

MATERIALS ANALYSIS AND SOURCE

Material	Composition	Supplier	Condition	Used in Solubility Test For:
Columbium-1% Zirconium	98.75% Cb 1.15% Zr 30 ppm C 94 ppm N 180 ppm O	Wah Chang Corp., Albany, Oregon	Stress-relieved at 1850°F	Cb, Zr, Ta
Molybdenum-0.5% Titanium	99.55% Mo .43% Ti .02% C	Cleveland Tungsten, Inc., Cleveland, Ohio	Tubes machined from crystallized rod. No heat treatment after machining.	Mo, Ti, Ta
Vanadium	99.6% V .01% C .001% H .04% O .04% N	Oremet Metallurgical Corp., Albany, Oregon	Cold-rolled to .050 sheet from bar stock	V, Ta
Beryllium	98.36% Be 1.63% BeO .144% C .165% Fe .088% Al .046% Si .064% Mg .04% Max other impurities	Beryllium Corp., Reading, Penn.	Machined from hot pressed Be block	Be, Fe, Ta

TABLE 2

MATERIALS ANALYSIS AND SOURCE (Continued)

Material	Composition	Supplier	Condition	Used in Solubility Test For:
Haynes-25	49.65% Co 20.42% Cr 15.28% W 10.14% Ni 1.70% Fe 1.39% Mn 0.097%C 0.42% Si 0.02% P 0.015%S	Superior Tube Co., Collegeville, Penn.	Annealed	Co, Cr, W, Ni, Fe, Mn, Ta
Tantalum Capsules and Cups	99.9% Ta .011%O .007%C .004%N .002%H .004%Cb .02% W .011%Fe .01% Ti .01% Si .005%Zr .006%Mo .005%Al	Fansteel Metallur- gical Corp., No. Chicago, Ill.	Annealed	Ta

TABLE 3

CORROSION CAPSULE MATERIALS AND TEST TEMPERATURES

Test Temperature °F	70	1000*	1400*	1700*	2000*
Cb-1Zr	Reference	--	X	X	X
Mo-0.5Ti	Reference	--	X	X	X
Haynes-25 (Co Base)	Reference	--	X	X	--
Be (QMV)	Reference	X	X	--	--
V	Reference	X	X	--	--
Ta (Sample Container)	Reference	X	X	X	X

*All tests run for 1000 hours.

8. Purity of Alkali Metal: Oxygen content only was determined pre and post test. Samples were taken at room temperature, not at the test temperature. Oxygen content of the capsules post test was never over 100 ppm as measured by the mercury amalgamation method. The rubidium was purified before filling the capsule by filtering, gettering with a TiZr alloy at 1100° F, and then fractional distillation. Prepurification content was roughly 111 ppm in contrast to 6-17 ppm after purification.

9. Method of Loading and Sealing Capsules: Capsules were loaded directly from the tank of purified rubidium. After loading under argon gas in an environmental chamber, capsules were transferred to a leak proof bomb. This bomb was then transported to a vendor and inserted into a vacuum chamber. This chamber was evacuated and the capsules were then seal welded by the electron beam process.

10. Test Environment: The environment inside the capsule furnace was argon gas; the purity of the gas was not monitored.

11. Fluid Flow Rate: Not known. ΔT between top and bottom of the capsule as measured on the external surface of the capsule wall can be found in Table 4.

12. Flow Stability: Not known

13. Method of Heating and Control: The heater consisted of a cold wall pressure vessel insulated on the interior with Foam sil. This surrounded a nichrome clam shell heater which in turn surrounded a graphite heat focusing block. Holes were drilled in the heat focusing block to receive the capsules. Furnace temperature was controlled by a null point galvanometer, saturable core-reactor combination. Temperature was controlled automatically between ±5° F.

171

TABLE 4

RECORDED CORROSION CAPSULE TEST TEMPERATURES

Test Temperature ($\pm$ 5°F)	Δ T
1000°F	161°F
1400°F	160°F
1700°F	230°F (this thermocouple became non-functional after the second day)
2000°F	165°F

14. Instrumentation: Control and miscellaneous temperature readout was by Pt/Pt 10% Rh thermocouples.

15. Post-Test Procedure: After the test run the capsules were removed from the furnace and opened in an argon environmental chamber. Test materials were removed, cleaned of excess rubidium and the rubidium from the capsules was analyzed for oxygen. The test specimens were sectioned in three phases for metallographic examination: the top for examination of specimen surfaces exposed to rubidium vapor, the middle for examination of surfaces near the liquid vapor interface, and the bottom for examination of surfaces in the liquid phase. The remaining portions were machined into tensile specimens so that any changes in strength after testing at the various temperatures could be determined.

16. Method of Measuring Corrosion and Material Change: Methods of measuring corrosion and materials changes included macro and metallographic examination, microhardness tests, and tensile tests.

17. Reproducibility of Results: Reproducibility of results does not apply to these tests since duplicate capsules were not run.

18. Number of Premature Failures Due To Causes Other Than Corrosion: A total of 16 capsule tests were run. Of these, four were failures due to heater burnout, cracked welds, and possible impure argon gas external environment.

19. Manpower Involved:

   2357 salary hours

   1948 hourly hours

   $11,759 materials, equipment, and outside production

20. Summary of Results to Date:

A. CORROSION

In general, all alloys tested during this program exhibited adequate resistance to corrosion by rubidium liquid and vapor at test temperatures and times. Within the limits of experimental error no weight or thickness changes were observed. The effects of exposure to test conditions upon the mechanical properties of these materials are difficult to determine since to conduct parallel blank tests at the test temperature in a neutral atmosphere would have exceeded the scope of this program. There was little correlation between oxygen content of the rubidium and corrosion results, except for beryllium at $1400^{\circ}F$. A review of the specific results is as follows:

1. Columbium-1% Zirconium

Columbium-1% zirconium alloy was not corroded by rubidium liquid or vapor in the 1400° to $2000^{\circ}F$ temperature range, nor were corrosion products or mass transfer effects noted; however, there was evidence of selective leaching of the zirconium out of the columbium during the $2000^{\circ}F$ test. Compared to pre-test values, the alloy was considerably softer after the $2000^{\circ}F$ test; this was probably due to annealing effects rather than attack by the rubidium, except in the leached areas along the surface. No mass transfer effects were noted which seems in opposition to the apparent columbium and zirconium solubility results. The alloy is considered conditionally adequate for containing rubidium in this temperature range. Further study of the leaching of zirconium (hardening constituent) is necessary before Cb-1Zr alloy is used under conditions of high stress for long periods of time at $2000^{\circ}F$.

2. Molybdenum-0.5% Titanium

There was no evidence of corrosion products, mass transfer effects, or corrosion of the Mo-0.5Ti alloy by rubidium liquid or vapor in the 1400° to $2000^{\circ}F$ temperature range. There was evidence of selective leaching of the titanium out of the molybdenum during the $2000^{\circ}F$ test, but the analysis techniques were not sensitive enough to quantitatively determine the amount of titanium dissolved out of the alloy. No mass transfer deposits were found. The test temperature had very little effect on the hardness of the alloy. The low ductility of the alloy and the problems encountered in fabricating tensile specimens precluded acquiring tensile data. The Mo-0.5Ti alloy is adequate for containing rubidium at the test conditions. Investigation of the titanium (hardening constituent) leaching is necessary before Mo-0.5Ti alloy is used under conditions of high stress for long times at 2000°F or above.

173

3. Vanadium

There was no indication that the vanadium metal was corroded by rubidium liquid or vapor in the 1000° to 1400^oF temperature range. Except for a slight discoloration at 1400^oF, no corrosion products or mass transfer effects were noted. The solubility results indicated this was to be expected. Some softening of the metal occurred in the tests at 1000° to 1400^oF due to annealing. The ultimate strength after the 1400^oF run was lower than after the 1000^oF run, and lower than that of the as-received material; this is also probably due to annealing rather than to effects of the rubidium environment. Vanadium is considered adequate for containing rubidium at the test conditions.

4. Beryllium

Except for minor surface roughening at 1400^oF, there were no indications of corrosion by rubidium liquid or vapor in the 1000° to 1400^oF temperature range. No corrosion products or mass transfer effects were noted, except for small amounts of black scale on the surface of the samples from the 1400^oF test run. This scale was BeO and is believed to have resulted from reduction of rubidium oxide in the liquid; oxygen content of the rubidium after the 1400^oF run is somewhat lower than the pre-test value. The lack of mass transfer effects was expected on the basis of the solubility results. The corrosion tests had little effect on the hardness of the metal; this is not surprising since the annealing temperature of beryllium is higher than the test temperatures. Tensile data is inconclusive since the material is so brittle that valid results were not obtained. If ductility is not a requirement, beryllium is adequate for containing rubidium at 1000^oF; however, for use in the 1400^oF range, further testing will be necessary to determine the full effects of the scaling tendencies of the metal.

5. Haynes-25

There were no indications of corrosion by the rubidium liquid or vapor in the 1400° to 1700^oF temperature range except for some surface roughening of the liquid phase sample at 1700^oF. No mass transfer or corrosion products were noted in any of the test capsules. The lack of observable mass transfer effects is in opposition to the results of the solubility tests, especially regarding the iron, nickel, cobalt, and chromium results. The alloy increased in hardness during the 1400^oF test due to precipitation hardening, but the hardness anomalies at 1700^oF cannot be explained on the basis of these limited tests. The strength of the alloy increased after the 1400^oF run (precipitation hardening) and decreased after the 1400^oF run (precipitation hardening) and decreased after the 1700^oF test (annealing). Haynes-25 is probably satisfactory for containing rubidium at low or medium stress levels up to 1700^oF. More data from long-time tests and a better understanding of the property changes at 1700^oF are necessary before this alloy could be considered suitable for long-time use.

174

B. SOLUBILITY

The concentration of columbium species in rubidium is less than 14 ppm below 1400°F and in the 14 to 30 ppm range between 1400° and 2000°F. Agreement of duplicate samples and presence of a general upward trend with temperature indicate the results to be relatively valid.

The concentration of zirconium species is between 1 and 10 ppm between 1000° and 1400°F, and rises to between 10 and 100 ppm in the 1400° to 2000°F range. Good agreement of the data was not found in the capsules tested at 1700°F and this data should be held in question. The general upward trend established by the 1400° and 2000°F data appears to be valid.

The concentration of molybdenum species is in the 1 to 10 ppm range between 1400° and 2000°F. A trend cannot be established due to scattering of the data; however, the results are reasonably good considering the low concentrations present.

The concentration of titanium species is in the 1 to 4 ppm range between 1400° and 2000°F. A negative slope in the data occurs at 1700°F, probably due to experimental error. A general upward trend seems to be established by the 1400° and 2000°F data.

No results are included for the solubility studies since it is not within the scope of this conference and since the solubility results are not conclusive.
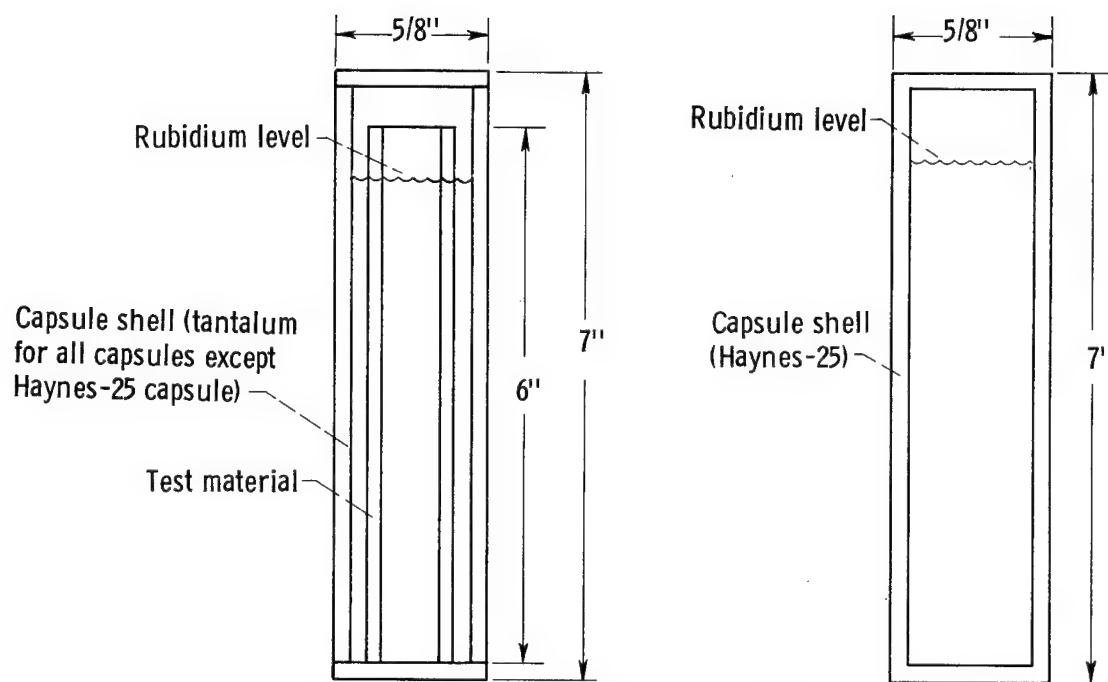
Position of corrosion capsules during testing

Figure 1. - Corrosion capsule design.

JET PROPULSION LABORATORY → 179
Pasadena, California

Liquid-Metal Corrosion Capsule Questionnaire

1. Survey of new Cb and Ta base alloys; Sponser NASA

2. Li, K, Cs, and Rb

3. Tilting and reflux

4. 321 and 410 S.S.
   Cb-1Zr
   Wah Chang C129
   Westinghouse B33 and B66
   Ta-10W
   Union Carbide CB-752
   Westinghouse T-111
   Mo - 1/2 Ti

5. Tabs for both ends to obtain weight change, to be machined
   into tensile specimens and provide metallographic and
   chemical analysis samples.

6. 3/4 in. OD X 10 in. length

7. Effect of Y gettering on mass transfer

8. High purity starting material. Analysis by supplier after test.

9. Melted and poured under high purity atmosphere, sealed by TIG welding.

10. High purity argon monitored by oxygen and moisture monitor.

11. Tilting capsules cycled at 1/min.

12.

13. Recording of thermocouples attached directly to capsule.

14. Thermocouple and atmosphere monitoring.

15. Analysis of liquid metal, weight change, tensile test metallographic
    examination microhardness and analysis of test material.

16. Weight change, metallography, microhardness and liquid metal analysis.

17. Tests just starting

18. None in 6 tests

19. 2 1/2 men full time

20. Material in procurement, stainless steels in test, Cb-1Zr in preparation.

BROOKHAVEN NATIONAL LABORATORY ⟶ 213
Upton (L. I.), New York

Liquid-Metal Corrosion Capsule Questionnaire

1. <u>Purpose of Test</u>: To evaluate the possible use of Na as a coolant and a working fluid for power conversion systems.

<u>Sponsor</u>: A. E. C. Reactor Development Division

2. <u>Fluid</u>: Na

3. <u>Type</u>: Two phase refluxing capsules.

4. <u>Alloys or Materials</u>: Cb-1Zr tubing and other refractory metal alloys in form of tubing and/or drilled rod. The other alloys include X-110, FS-85, X-34, Cb-10Ta-10W, Ta-10W. See Table III for details.

5. <u>Test Specimens</u>: Made from container material.

6. <u>Dimensions</u>: Approximately 6" long x 1/2" inside diameter.

7. <u>Controlled Variables Studied</u>: Variables include temperature (2000-2400°F), oxygen content in Na (as purified to 600 ppm), carbon content, gettering additives (Ba, Mg, Ca, Y) metallic inserts (Ta, Mo, Cb), time (up to 5000 hours).

8. <u>Purity of Alkali Metal</u>: Purified by cold trapping at 250°F for 24 hours and hot trapping with Zr and Ti for 500 hours at 1200°F. Method of analysis not established as yet.

9. Method of Loading and Sealing Capsules: The methods varied for different tests. Methods include loading and sealing in argon dry box, loading under vacuum and sealing in argon dry box, and loading and sealing under vacuum.

10. Test Environment: Vacuum chambers with pressures from 2×10^{-6} to 2×10^{-8} torr.

11. Fluid Flow Rate: Estimated at 2 grams/minute.

12. Flow Stability: Stable according to thermocouples.

13. Method of Heating and Control: Heated by Ta wire wound Alumina furnace cores and instrumented with W/W 26%Re thermocouples.

14. Instrumentation: Temperature control - W/W 26%Re

Vacuum control - Bayard Alpert gages.

15. Post-Test Procedure: Post-test procedure includes metallographic examination for corrosion, x-ray diffraction, mechanical tests, vacuum fusion analysis of container, chemistry of Na, microhardness tests.

16. Method of Measuring Corrosion and Material Change: Metallography.

17. Reproducibility of Results: Not determined.

18. Premature Failures: None due to container failure but several due to heater and instrument failure.

180

19. Manpower Involved: Professional - 1/2 man

Technical - 1 man

Analytical (including metallography) - 1/2 man

20. Summary of Results to Date: No corrosion found in 5000 hours - 2200°F boiling test except for: pure Cb insert, Cb-1Zr wall in 150 ppm oxygen contaminated capsules and Cb-1Zr wall of Ba additive capsule. Maximum penetration on Cb-1Zr capsule has been 0.004". All pertinent details are given in Tables I and II.

Table I

Capsule Tests #1 and 2 - Corrosion Investigation
and Microhardness Tests

Capsule	Material	Additive	Corrosion	Average Microhardness* DPH/200 gm
#15	Cb-1Zr	None	None Detectable	82
#16	Cb-1Zr	75 ppm O	None Detectable	82
#21	Cb-1Zr	150 ppm O	0.003" Max. Depth Transgranular and Intergranular in Liquid Portion	80
#17	Cb-1Zr	300 ppm O	None Detectable	79
#18	Cb-1Zr	500 ppm Mg	Slight Transgranular in Liquid Portion (<0.0005")	81
#20	Cb-1Zr	500 ppm Ba	0.004" Max. Depth Intergranular in Vapor Portion. Possible Transgranular in Liquid Portion	86
#19	Cb-1Zr	(Ta Insert)	Slight Transgranular in Liquid Portion (<0.0005)	–
Insert Ta			None Detectable	–
#22	Cb-1Zr	(Mo Insert)	None Detectable	–
Insert Mo			None Detectable	–
#24	Cb-1Zr	(Cb Insert)	None Detectable	–
Insert Cb			0.006" Max. Depth Intergranular in Vapor Portion	–

Note: *Average Microhardness of Cb-1Zr Tube prior to test was about
192 DPH/200 gm

Table II

Summary of Vacuum Fusion Analyses of Cb-1Zr

Capsule Tests #1 and #2

A. **GENERAL**

Test No.	Capsule No.	Chamber Pressure	Avg. Liquid Temperature	Avg. Vapor Temperature
1	14, 16, 17 18, 20	1×10^{-6} torr	1210°C (2210°F)	1176°C (2150°F)
2	19, 22, 24	5×10^{-6} torr	1210°C (2210°F)	1176°C (2150°F)

B. **STANDARDS**

As Received Material	PPM O	PPM N	PPM H
Cb-1Zr Bar #201 (capsules)	177	34	24
	231	33	24
Cb Bar #192 (Insert)	600	95	9
Ta Bar #190 (Insert)	195	16	9
Mo Bar #191 (Insert)	481	26	10

C. **CAPSULE VAPOR PORTION** (Entire wall sampled)

Capsule No.	PPM Oxygen	PPM Nitrogen
15	520	34
16	664	35
17	676	41
18	673	36
20	888	77
	684 Avg.	45 Avg.
19	922	82
22	938	177
24	835	151
	865 Avg.	137 Avg.

Table II continued

D. __CAPSULE LIQUID-VAPOR INTERFACE__ (Wall sampled in half-sections)

Capsule No.	Half-Section	PPM Oxygen	PPM Nitrogen
15	O.D.	892	26
	I.D.	160	68
		526 Avg.	47 Avg.
17	O.D.	949	8
	I.D.	223	67
		586 Avg.	38 Avg.
24	O.D.	1110	30
	I.D.	515	185
		813 Avg.	108 Avg.

E. __CAPSULE LIQUID PORTION__ (Entire wall sampled)

Capsule No.	PPM Oxygen	PPM Nitrogen
15	832	49
16	827	63
17	863	45
18	943	20
20	907	74
	874 Avg.	50 Avg.
19	1070	108
22	1030	128
24	971	149
	1024 Avg.	128 Avg.

F. __CAPSULE LIQUID PORTION__ (6 mils removed from O.D. - remainder sampled)

Capsule No.	PPM Oxygen	PPM Nitrogen
15	993	83
24	470	41

184

Table II continued

G. <u>INSERTS</u> (Entire wall sampled)

Capsule No.	Insert Material	Portion	PPM O	PPM N	PPM H
19	Ta	Liquid	34	12	41
		Vapor	54	20	42
22	Mo	Liquid	92	17	4
		Vapor	150	57	23
24	Cb	Liquid	49	104	25
		Vapor	75	125	46

E-2492

Table III

Boiling[1] Sodium Reflux Capsule Run #3

Capsule No.	Material	Additive PPM	Remarks
25	Cb-1Zr	None	Note (2)
26	Cb-1Zr	500 Ca	Added as pure Ca
27	Cb-1Zr	500 Mg	Added as pure Mg
28	Cb-1Zr	500 Ba	Added as pure Ba
29	Cb-1Zr	1500 Y[3]	Added as pure Y
30	Cb-1Zr	150 O	Added as pure Na_2O_2
31	Cb-1Zr	600 O	Added as pure Na_2O_2
32	Cb-1Zr	150 C	Added as Spectrographic Carbon
33	Cb-1Zr	600C	Added as Spectrographic Carbon
34	Cb-10Ta-10W	None	Drilled from bar stock
35	Cb-10W-1Zr-.1C	None	Drilled from bar stock
36	Cb-5W-3Zr-.1C	None	Drilled from bar stock

Notes:

1) Operating temperature = 2300°F (1260°C)

2) Sodium was cold trapped and hot trapped before adding to capsules. Additions were made to purified Na.

3) Not soluble

E-2492

186

B. LOOP TESTS

GENERAL ELECTRIC COMPANY
Evandale (Cincinnati), Ohio

Liquid-Metal Corrosion Loop Questionnaire

1. Purpose: To examine the corrosion resistance of AS-55 and a
    columbium, 10%W, 1%Zr alloy in flowing liquid potassium
    and, particularly, to examine the extent of interstitial
    element mass transfer under thermal and compositional
    gradients.

    Sponsor: General Electric Company, Contractor's Independent
    Research and Development Program.

2. Fluid: Potassium liquid.

3. Type: Natural convection.

4. Loop Size: 17 inches high and 7 inches wide from tubing center-
    lines (Figures 10, 11, 12, and 13).

5. Containment Alloys: Seamless tubing (0.887-inch O.D. by 0.068-
    inch wall) of AS-55 and a columbium, 10%W, 1%Zr alloy.
    The latter alloy was specially prepared to have a low
    interstitial element content; 0.0017%C, 0.015%O,
    0.0009%N, and 0.0012%H. The interstitial element con-
    tent of this AS-55 material was 0.067%C, 0.029%O,
    0.024%N, and 0.0012%H. Heat treatments were conducted
    in 10^{-6} torr vacuum environments as follows:
    AS-55: 1 hr at 2800°F + 1 hr at 2400°F; welds:
    1 hr at 2400°F (locally)
    10W-1Zr: 1 hr at 2200°F; welds: 1 hr at 2200°F
    (locally)

    Cleaning procedures included pickling in 20%HF, 20%HNO$_3$,
    60%H$_2$O and degreasing in acetone and ethyl alcohol.
    The loops were assembled by TIG welding, and post-weld
    heat treatments were conducted at the above temperatures
    and as illustrated in Figure 14.

6. Test Conditions: Temperatures - 2000°F (maximum) in the hot zones
    and 1850°F (minimum) in the 7-inch long radiation zones;
    pressure was not measured - 150 psia potassium vapor
    pressure at 2000°F; flow rate - 5 in/sec; operating
    time - 2,000 hrs.

7. Test Specimens: A 6-inch long section of AS-55 tubing was included
    in the hot zone of the columbium, 10%W, 1%Zr loop (Figure 13)
    to determine whether a preferential transfer of interstitial
    elements would result from the differences in the contain-
    ment material compositions. In addition, several TIG welds
    were made in the loop tubing to permit the examination of
    corrosion effects at welded regions (Figures 12 and 13).

189

8. Pretreatment of Loops: None following the cleaning, welding, and
    weld heat treatments described in item 5 above.

9. Method of Filling Loops: Potassium was introduced under an inert
    gas cover, and sealing by electron beam welding was
    conducted in a vacuum of 10^{-5} torr.

10. Start-up Procedure: The loops were slowly heated to approximately
    $1000^{\circ}F$ (hot zone) and then rapidly heated to the test
    temperature conditions, one loop at a time, to minimize
    bumping and to limit the initial vacuum chamber pressures
    to the 10^{-6} torr range.

11. Test Environment: Vacuum - 10^{-6} to 10^{-8} torr at test conditions.
    The vacuum chamber is shown in Figures 4 and 11.
    Pressures were determined from the getter-ion pump
    current and by attached and nude ionization gauges.

12. Instrumentation: Tantalum-clad, Al_2O_3 - insulated, Pt vs. Pt +
    13%Rh thermocouples were attached to the outside of the
    loop by tantalum straps and used to record the tempera-
    ture. Optical pyrometer measurements of the radiation
    zones were used to correct for drift and to adjust the
    tantalum heater voltage.

13. Loop Components: The heater was similar to that shown in Figure 5
    except that the tantalum heating element was 6 inches
    long.

14. Potassium Purity: The potassium was sampled during and after loop
    filling and analyzed with the following results: Oxygen
    - 300 ppm by zirconium gettering in an auxiliary Cb-1Zr
    capsule; 7 to 87 ppm by the amalgamation method. Analyses
    for oxygen were not conducted during or after loop testing.

15. Loop Flow Stability: The loops were unstable at moderate tempera-
    tures during start-up, and bumping with $700^{\circ}F$ temperature
    surges was encountered. At the test temperature condi-
    tions, the loops appeared stable, as indicated by the
    absence of temperature surges (limit of detection approx-
    imately $5^{\circ}F$).

16. Post-Test Procedure: The loops were opened and drained under an
    inert gas cover and then cleaned with a hexane-ethyl
    alcohol solution. Methods of examining for corrosion
    effects include metallographic examination, dimensional
    and hardness measurements, chemical analyses for the
    interstitial element content of sections taken from the
    loop tubing, room temperature and $2000^{\circ}F$ tensile testing,
    and stress-rupture testing of specimens obtained from
    the loop tubing.

17. Major Loop Problems: None.

18. Manpower: Approximately one engineer and one technician with support for design, chemical analyses, and fabrication.

19. Summary of Results: Evaluation of the loops is largely complete, except for the stress-rupture testing. Aside from surface stains that will be mentioned later, there was little evidence of general corrosion or mass transfer which could be observed metallographically or by dimensional changes. Chemical analyses of samples from the AS-55 loop tubing revealed no significant change in carbon, oxygen, nitrogen, or hydrogen content, indicating that the imposed thermal gradient did not result in the transfer of these elements. Analyses of the columbium, 10%W, 1%Zr alloy loop and the AS-55 insert indicated that the carbon, nitrogen, and hydrogen did not undergo significant transfer under the combined thermal and compositional gradients. It was evident, however, that oxygen was gettered by the AS-55 insert but not appreciably by the columbium, 10%W, 1%Zr alloy. In addition to the oxygen in the potassium, oxygen may have been supplied by the columbium, 10%W, 1%Zr alloy; however, this is not readily apparent from the analytical results. Probably, the residual yttrium in the AS-55 (0.4%) makes it the more effective getter, and the stain or thin film (less than 1 mil) on the AS-55 insert (Figure 13) may be a yttrium compound, although it has not yet been identified. The AS-55 from the all AS-55 loop was not stained in this way; this suggests that one of the constituents of the stain may have come from the columbium, 10%W, 1%Zr alloy.

Tensile tests, conducted at room temperature, indicate that the properties of the AS-55 from the AS-55 loop are similar to the initial material. The room temperature tensile strength of the columbium, 10%W, 1%Zr alloy decreased slightly, from 75 ksi to 68 ksi, as a result of the exposure. The 2000°F tensile strength of AS-55 material from both the AS-55 loop and the AS-55 insert in the columbium, 10%W, 1%Zr alloy loop decreased from an initial value of 31 ksi to 24 ksi. Similarly, the 2000°F tensile strength of the columbium 10%W, 1%Zr alloy decreased from 30 ksi to 24 ksi. Tensile elongations were greater than 18% in all the above cases. Metallographic examination of the AS-55 alloy did not reveal any changes in the metallurgical structure, which may have been associated with the decreased tensile strength. Stress-rupture testing is planned to determine if the longer-time, high temperature properties were also altered by the exposure.

191

Weld defects were observed in both the AS-55 and columbium, 10%W, 1%Zr alloy loops at locations where the arc was extinguished upon terminating the weld (Figures 15 and 16). These defects were revealed by radiographic inspection before loop testing. Similar inspection after loop testing provided some slight indication, but not definite proof, that their depth was increased by corrosive attack. It should be noted that these defects are quite different in appearance from the corrosive attack observed in the welded region of a Cb-1Zr reflux capsule*(Figures 7, 8, and 9). Overall, it appears that the presence of the defects in the loop welds and their depth, which has been measured up to approximately 40 mils, are a matter of welding technique and how the weld is terminated. These regions may, of course, exhibit unusual corrosion effects because impurities and alloying constituents may tend to concentrate and segregate at the end of the weld.

In summary, it appears that carbon, oxygen, nitrogen, and hydrogen did not mass transfer as a result of the thermal gradient imposed on the AS-55 loop. In the columbium, 10%W, 1%Zr alloy loop, carbon, nitrogen, and hydrogen did not transfer under the combined thermal and compositional gradients, whereas oxygen was gettered selectively by the AS-55 alloy insert. In these respects, the interstitial elements in the AS-55 alloy, particularly the strengthening carbides, appear stable. The decrease in the 2000°F tensile strength of the AS-55 alloy after loop testing suggests a change in the alloy structure, which was not identified by metallographic examination or confirmed by room temperature tensile tests. Stress-rupture testing of this material must still be conducted; however, such testing of AS-55 material from previously described reflux capsules did not indicate a change in rupture strength. Overall, the strengthening carbides have appeared quite stable during prolonged exposures at 2000°F but this requires further investigation, taking into account the important effects of the prior heat treatment.

---

* See General Electric Company capsule questionnaire, p. 153.
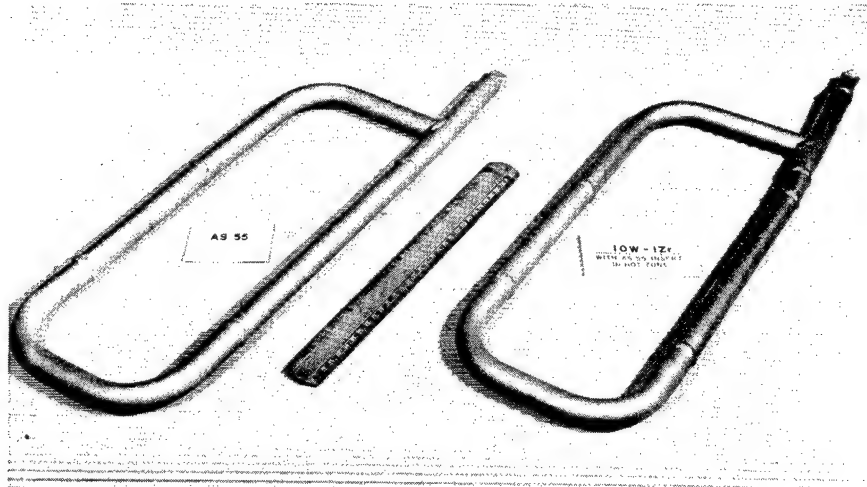
Figure 10. – Columbium alloy natural convection loops filled with 250 grams of potassium. Left: AS-55 alloy (5% W, 1% Zr, 0.06% C, 1% Y added, bal. Cb); Right: 10% W, 1% Zr, bal. Cb with an AS-55 alloy insert.
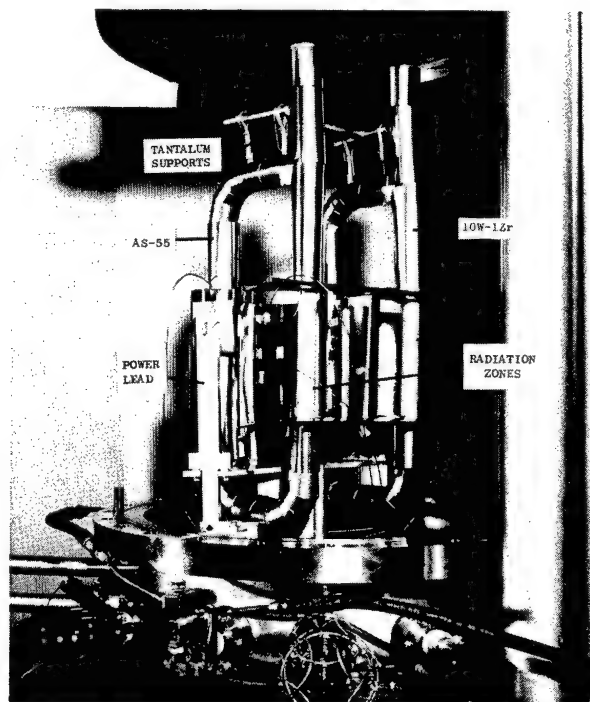
Figure 11. – Two columbium alloy natural convection loops positioned in a high vacuum chamber after testing with liquid potassium for 2000 hours at temperatures of 2000° F in the hot zones and 1850° F in the radiation zones.

193
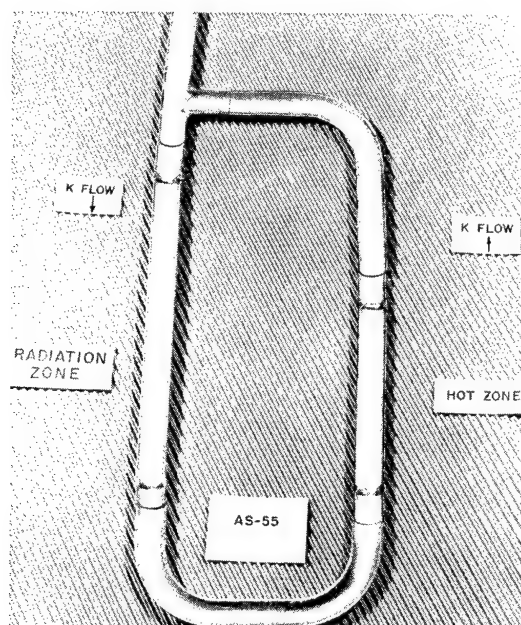
Figure 12. – AS-55 natural convection loop sectioned after testing with liquid potassium for 2000 hours at temperatures of 2000^0 F in the hot zone and 1850^0 F in the radiation zone.

Figure 13. – Columbium, 10% W, 1% Zr alloy natural convection loop, with an AS-55 hot zone insert, sectioned after testing with liquid potassium for 2000 hours at temperatures of 2000^0 F in the hot zone and 1850^0 F in the radiation zone. Note the discoloration of of the AS-55 hot zone insert.

194
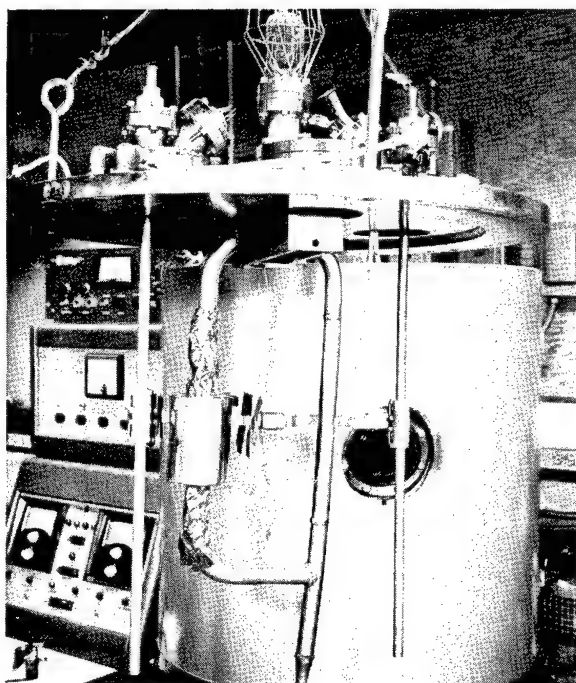
Figure 14. - High vacuum system (10^{-8} torr range) and tantalum strip heater assembly used for heat treating welds in columbium alloy natural convection loops.

0.010"

0.002"

Figure 15. - Cross section of a weld defect area from the hot zone of an AS-55 natural convection loop sectioned after testing with liquid potassium for 2000 hours at temperatures of 2000° F in the hot zone and 1850° F in the radiation zone. Such weld defects sometimes occur at locations where the arc is extinguished, and their size may be increased by corrosive attack. Etchant: 60% glycerine, 20% HNO_3, 20% HF.
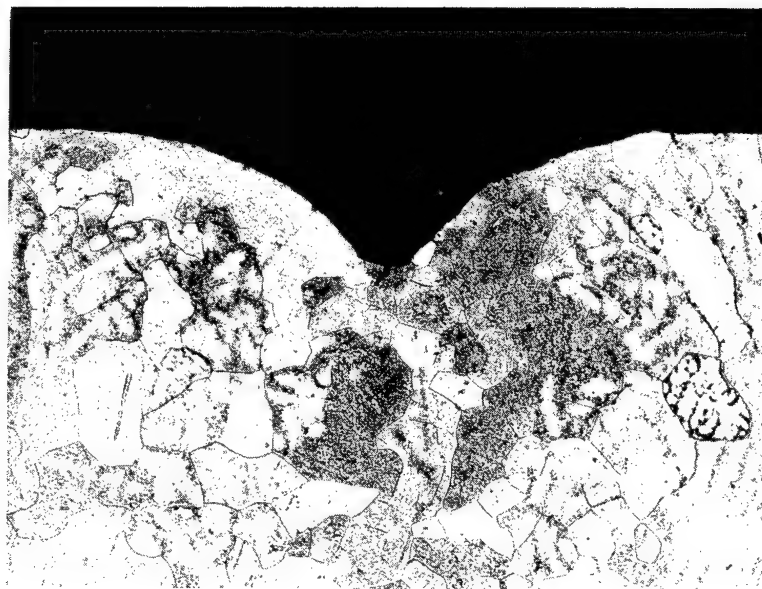
0.010"
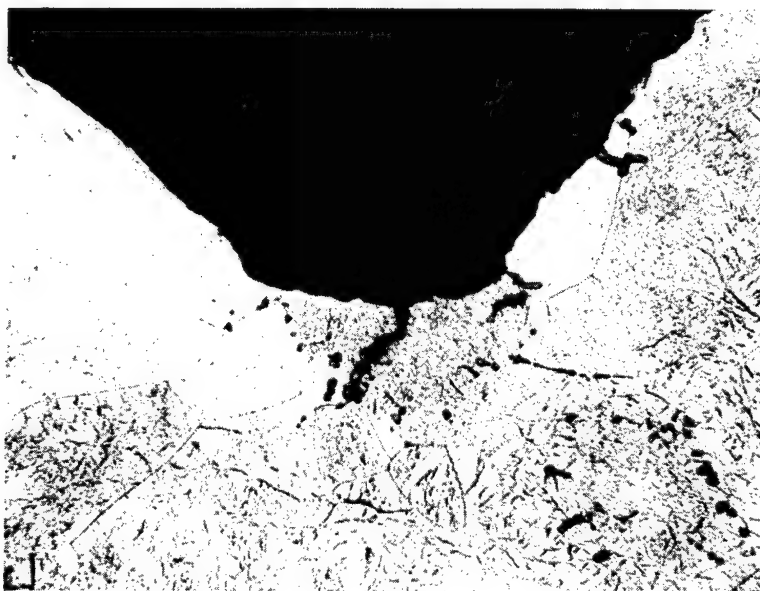
0.002"

Figure 16. – Cross section of a weld defect area from the hot zone of a columbium, 10% W, 1% Zr alloy natural convection loop sectioned after testing with liquid potassium for 2000 hours at temperatures of 2000^0 F in the hot zone and 1850^0 F in the radiation zone. Such weld defects sometimes occur at locations where the arc is extinquished, and their size may be increased by corrosive attack. Etchant: 60% glycerine, 20% HNO_3, 20% HF.

NATIONAL AERONAUTICS AND SPACE ADMINISTRATION
LEWIS RESEARCH CENTER
Cleveland, Ohio

Liquid-Metal Corrosion Loop Questionnaire

1. Purpose of Loop and Sponsor: Corrosion test at advanced space
    power system conditions.

2. Fluid: Potassium.

3. Natural or Forced Convection: Forced convection.

4. Approximate Overall Size of Loop(s): 0.250 inch tubing for all loop
    components except condenser, which will be 0.50 inch tubing. Loop to
    be contained in vacuum bell jar 5 feet O.D. by 11 feet high (fig. 1).

5. Containment Alloys: Monometallic construction from thin-walled tubing
    of advanced refractory metal alloy being produced as result of the
    activity of the joint NASA-DOD-AEC Tubing Panel. The specific alloy
    has not yet been chosen. Majority of material will be 1/4 inch O.D.
    and 1/2 inch O.D. tubing. Some bars stock and rod will be used in .
    fabricating valves, pump, etc.

6. Test conditions: Approximate advanced space power system conditions.

7. Test Specimens: Loop is the containment vessel.

8. Pretreatment of Loop: Determined by choice of containment alloy.
    "Clean room" procedures will be utilized.

9. Method of Filling Loop: Distillation of K directly into loop.

10. Start-up Procedure: Bake-out of vacuum chamber and loop with residual
    gas monitoring to determine end of bake-out period. K will then be
    distilled into loop system.

11. Test Environment: Vacuum 10^{-8} mm Hg monitored with mass spectrometer.

12. Instrumentation: Pt/Pt-Rh thermocouples, strain gage pressure
    transducers, E.M. flowmeter.

13. Loop Components: Helical induction pump. Direct resistance heating
    for preheater and superheater, and radiation heater for boiler. Heat
    rejection from condenser by radiation to vacuum chamber walls through
    radiation controlling shutters.

14. Alkali Metal Sampling or Monitoring Procedure: Initial and final
    sample planned for first loop. Subsequent loops may have sampling taps.

E-2492

15. Loop Flow Stability: Stable Flow. Determination of stable flow is by temperature, pressure, and flow-rate instrumentation.

16. Post-Test Procedure: The loop is cut apart and visually examined. Specific parts are then to be metallographically examined.

17. Major Loop Problems:

18. Manpower: Design - 1 man-year; setup, 1 man-year; operation, 2 man-years; technicians, 1 man-year.

19. Summary of Results to Date: Program is now in the early design stage.
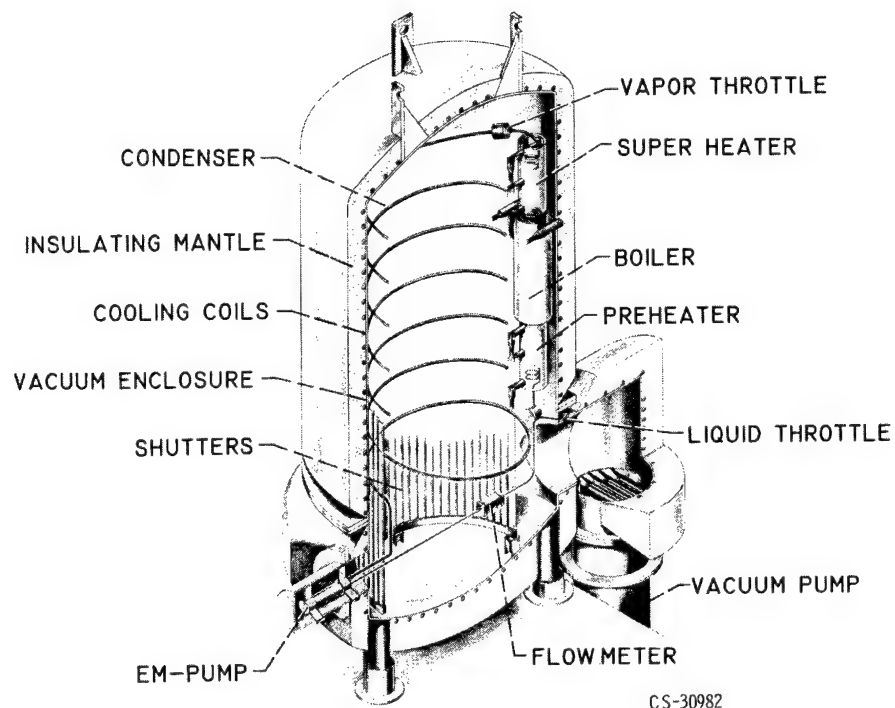
Figure 1. -NASA potassium corrosion loop.

AEROJET-GENERAL NUCLEONICS

Liquid-Metal Corrosion Loop Questionnaire

1. Purpose of Loop and Sponsor: To design, operate, and analyze a pumped corrosion loop simulating some of the characteristics of a boiling rubidium space power conversion system. This work was sponsored under USAEC Contract AT(04-3)-251.

2. Fluid(s): Rubidium.

3. Natural or Forced Convection: Forced convection.

4. Approximate Overall Size of Loop(s): See figure 1.

5. Containment Alloy(s): Cb-1%Zr; 1/2 in. and 1/4 in. O.D. by 0.049 in. wall (plus 316 SS surge tank). Assembly by fusion welding of similar metal joints. The 316 SS/Cb-1Zr joint made with a Swagelok union.

6. Test conditions: The loop operated approximately 330 hours at the following thermal equilibrium conditions:

Measured preheater inlet temperature	520° F
Measured preheater outlet temperature	1500° F
Measured boiler temperature	1790° F
Measured condenser inlet temperature	1770° F
Measured condenser outlet temperature	550° F
Measured rubidium flow rate	0.26 gpm at 520° F
Estimated rubidium flow rate	0.50 gpm
Estimated argon flow rate	1/2 capacity, i.e., 2550 lb/hr
Rubidium operating pressure	175 psia
Measured power to preheater	6.50 kw
Measured power to boiler	8.75 kw
Estimated losses from preheater	~2.00 kw
Estimated losses from boiler	4.00 kw
Approximate rubidium vapor quality	0.09 (9%)
Vapor in boiler by volume	92%

7. Test Specimens: Containment material served as test specimens.

8. Pretreatment of Loop prior to filling: Vacuum outgas the loop interior to less than 1 micron for approximately 24 hours at 130° F.

9. Method of Filling Loop: Transfer of fluid into loop by combination of argon gas pressure on loading tank and vacuum in loop.

10. Startup Procedure: Prior to startup, the loop and all materials within the chamber were heated at approximately 130°F under a vacuum of 5 to 10 microns to outgas any volatile substances in the loop insulation and other components. The chamber was then back filled with high purity argon, with continued heating. Heating of the environmental chamber was accomplished with three finned space heaters. Operation of the blower during the heating period promoted uniform heating of the entire loop and components. The heating of the loop was necessary, prior to loading, to prevent freezing of the rubidium during the loading operation.

11. Test Environment: A portion of the argon environmental gas was continuously passed through a purification train. The train was made up of a 1400°F chip furnace (chips of 50% Ti-50% Zr) for oxygen removal, and a molecular sieve to remove water vapor. The oxygen analyzer (described in paragraph 12) continuously monitored the oxygen content in the chamber, usually below 5 ppm oxygen. The water vapor in the environmental gas could not be detected on a dew point analyzer.

   Two thicknesses of 2 mil zirconium foil (1/2 in. wide) were wrapped around the entire Cb-1Zr surface exposed to the chamber environment. This served as a getter for any minute quantities of contaminants which could not be removed by the gas purification apparatus, but whose presence over a long testing period could be detrimental to the Cb-1Zr surface.

12. Instrumentation:

   Recorder, Temperature: Leeds & Northrup, 0-2200°F range, <±0.3% accuracy full scale; for Chromel-Alumel thermocouples

   Recorder, Flow: Mine Safety Appl., Inc. 0-2.5 Mv range, Model H

   Pressure Recorder & Controller (Loop):   Taylor Instrument Co., 3-300 psi range, to fit and position Hammel-Dahl Series 3000 valve which stabilizes loop pressure

   Temperature Recorder & Controller: (Environmental Chamber)   Honeywell Instrument, 0-1600°F, 115 V 60 cycles, for Chromel-Alumel thermocouple, Model No. 146R16-PSH-148

Temperature & Controller: 0-300°F, Bristol Instrument,
(water in argon to water heat   Model No. OT 504-EW-1A
 exchanger)

Oxygen analyzer: Leeds & Northrup, 0-100 ppm O_2 ±1% full scale
                  precision, ±2% full scale accuracy, Speedomax
                  Type, Response time 5 seconds full scale,
                  Cat. No. 2-930-041-099-6-24-3-34

No limitations on instruments during operating life set by test.

13. Components:

    Pump: Electromagnetic, MSA Type 5-30

    Flowmeter: Electromagnetic, MSA

    Heaters: Electrical potential across the heating section of loop
              yielded an I^2R heating of the containment material

    Boiler: Same as above

    Condenser: A coiled section of the loop was passed through an
              annulus which contained a dynamic argon gas flow. The
              argon gas which was heated in the annulus was cooled
              as it passed through a water heat exchanger.

14. Alkali Metal Sampling or Monitoring Procedure: Only the pre- and
    post-test rubidium were analyzed. The analytical procedures used
    were: (A) Mercury amalgamation method for oxygen content analysis,
    and (B) spectrographic analysis of the rubidium salt for metallics.
    The rubidium salt was prepared by (1) converting the rubidium to
    rubidium methylate by adding anhydrous methyl alcohol; (2) convert-
    ing the rubidium methylate to rubidium hydroxide by reacting with
    water; and (3) converting the rubidium hydroxide to rubidium salt
    by adding acid and drying the precipitate.

15. Loop Flow Stability: Loop flow was stable; criteria for stability
    were constancy of temperature distributions and steadiness of liquid
    flow rate.

16. Post-Test Procedure: The rubidium was drained back into the loading
    tank and the tank removed from the loop. The loop was then physically
    disconnected from all pressure connections made on the environmental
    chamber. The exposed connections were immediately capped with a
    Swagelok cap to prevent reaction of any rubidium which may have con-
    densed in or near the connection joints. The loop was removed to the
    liquid metal decontamination pad, cut into sections and each section
    individually decontaminated with alcohol and water. Areas of interest
    were cut open and examined macro- and microscopically for corrosion
    and/or mass transfer.

17. Major Loop Problems: The environmental atmosphere must be free of oxygen and nitrogen from the air to prevent reaction with the columbium tubing. Lubricants that are exposed to the purified environmental atmosphere and temperature, and which are required for normal operation of components, i.e., blower bearings, mechanical component gears, etc., must be free of carbonaceous or organic impurities. The lubricants must be capable of remaining chemically stable and not outgassing at elevated temperatures or high vacuum. These comments are essential since columbium has a strong affinity for the interstitial elements. The reaction of columbium with minute quantities of interstitials over a long period can produce sufficient corrosion of the columbium to render it structurally useless. During welding it is extremely essential to have a high pure argon atmosphere (<2 ppm O_2, and water vapor below the dew point detection sensitivity). If the interstitials are present in the welding atmosphere (>5 ppm O_2), their reaction with the molten columbium will result in a brittle weld joint which can fracture very easily if joint is subject to any jarring during loop assembly.

18. Manpower:

    6512 salary hours

    4651 hourly hours

    $42,205 material, equipment, and outside production

19. Summary of results to date: The second loop was a Cb-1%Zr alloy loop operated for 455 hours total at 1840°F and a vapor quality of 9%. In the latter loop, the last 335 hours of operation were continuous. Stable boiling at this vapor quality level was achieved without the use of special liquid vapor phase separation devices. Operation of the loop was stable in all phases; however, overheating of the environmental chamber was observed due to insufficient insulation on the loop and resultant high heat losses from the loop heater and boiler. The columbium loop run was terminated by a cracked weld at the entrance to the condenser section in the hot portion of the loop. Negligible corrosion by the rubidium on both loops was observed. Some carbide penetration on the outside of the columbium loop was observed which apparently was caused by carbonaceous impurities in the argon gas. The failure of the weld at the entrance to the condenser was believed to be caused by carbide penetration effects. The protective coating of zirconium foil wrapped around the columbium loop was observed to fulfill its function and to be entirely necessary to insure the long life operation of the columbium loop. However, some alloying of this foil with the columbium occurred at the hottest portions of the loop. Improved and refined existing metallographic techniques were developed for the evaluation of refractory metal corrosion. Results showed corrosion of refractory containment materials by rubidium is not critical in this temperature range. Rather, the critical corrosion occurs from the contaminants in protective and environmental atmospheres.

Figure 1. – Dynamic test loop for liquid rubidium.

BROOKHAVEN NATIONAL LABORATORY

Liquid-Metal Corrosion Loop Questionnaire

Questionnaire 1 - Pumped Loop

1.   Purpose of Loop: To evaluate Cb-1Zr as a possible container material for liquid Na and Na vapor at high velocities in a Rankine cycle system.

Sponsor: A. E. C. Reactor Development Division

2.   Fluid: Na

3.   Forced Convection: Flow achieved by means of a G. E. helical induction pump. Status - under construction.

4.   Approximate Overall Size of Loop: About 8 feet tall and fitting into a 4 foot diameter chamber.

5.   Containment Alloy: Cb-1Zr

6.   Test Conditions: Temperatures - 2000°F boiling
                                       1700°F condensing

                       Flow rates - 20 #/hour.

7.   Test Specimens: Mostly made from container material. Refractory metal alloy specimens in turbine simulator.

8.   Pretreatment of Loop: In general, post weld heat treat at 2200°F for 1 hour.

9.   Method of Filling Loop: Under vacuum into a dump tank. Fill loop under inert gas cover.

10. Start-up Procedure: Undecided.

11. Test Environment: Vacuum chamber at about 1×10^{-8} torr.

12. Instrumentation: W/W 26Re thermocouples, flow meter, and pressure transmitters by Taylor.

13. <u>Brief Description of Components</u>: Flowmeter built by BNL,
Cb-1Zr valves by Hoke, G. E. helical induction pump.

14. <u>Alkali Metal Sampling</u>: None planned to date.

15. <u>Loop Flow Stability</u>: Unknown.

16. <u>Post-Test Procedure</u>: Post-test procedure will include metal-
lographic examination for corrosion, x-ray diffraction, mechanical
tests, vacuum fusion analysis of container, chemistry of Na, micro-
hardness tests.

17. <u>Major Loop Problems</u>: Procurement of good container material
i.e. tubing.

18. <u>Manpower</u>: At present - Professional (Design and Engineers) - 1

                        Technical - 1

                        Analytical (Including Metallography) - 0

19. <u>Summary of Results to Date</u>: Under construction.

Questionnaire 2 - Natural Boiling

1. <u>Purpose of Loops</u>: To evaluate the possible use of Na as a coolant and a working fluid for power conversion systems.

<u>Sponsor</u>: A. E. C. Reactor Development Division

2. <u>Fluid</u>: Na

3. <u>Natural or Forced Convection</u>: Mostly natural convection. One forced circulation loop (discussed in separate questionnaire) and one large natural circulation loop.

4. <u>Approximate Overall Size of Loops</u>: Small natural convection about 8" x 16" rectangular shape. Large natural convection - about 6 feet tall.

5. <u>Containment Alloys</u>: Mostly Cb-1Zr. Others being fabricated are X-110, FS-85 and Ta-10W. Large loop made from Cb-1Zr alloy.

6. <u>Test Conditions</u>: Temperatures - 2000 to 2200°F boiling.

                           Flow rates - 1#/hour to 10#/hour.

                           Operating time - up to 5000 hours.

7. <u>Test Specimens</u>: Mostly made from container material.

8. <u>Pretreatment of Loops</u>: In general, post weld heat treat at 2200°F for 1 hour.

9. <u>Method of Filling Loops</u>: Under vacuum and crimp sealed. Weld after crimp under inert gas cover. Large loop filled via dump tank.

10. <u>Start-up Procedure</u>: Simply apply heat to small loops. Large loop filled under vacuum, raise pressure in dump tank and increase boiler temperature.

11. <u>Test Environment</u>: Vacuum chambers from 1×10^{-6} torr to 1×10^{-8} torr.

12. <u>Instrumentation</u>: W/W-26Re thermocouples for small loops and for large loop. Pressure gage on live ballast dump tank system.

13. <u>Brief Description of Components</u>: For small loops - none. For large loop - low voltage - high current furnace (Ta).

14. <u>Alkali Metal Sampling</u>: None to date.

15. <u>Loop Flow Stability</u>: Small loops stable as indicated by thermocouples. Large loop unstable due to dump tank cold fluid.

16. <u>Post-Test Procedure</u>: Post-test procedure includes metallographic examination for corrosion, x-ray diffraction, mechanical tests, vacuum fusion analysis of container, chemistry of Na, microhardness tests.

17. <u>Major Loop Problems</u>: Procurement of good container material i.e. tubing.

18. <u>Manpower</u>: Professional (Design and Engineers) - 1 1/2 (large loop) and 1/2 (small loops)
Technical - 3 (large loop) and 1 (small loops)
Analytical (Including Metallography) - 1

19. <u>Summary of Results to Date</u>: No corrosion of Cb-1Zr seen after 1000 hours at 2000°F boiling.

Liquid-Metal Corrosion Loop Questionnaire

1. Purpose of Loop and Sponsor: Quantitative comparison of stainless steel corrosion by liquid sodium and potassium, sponsored by UNC.

2. Fluids: Liquid sodium and potassium.

3. Type of Loop: Natural convection.

4. Size of Loop: Small, see attached sketch (run in duplicate).

5. Containment Alloy: Type 316 stainless steel, 1/2 inch IPS schedule 40 pipe, TIG welded joints.

6. Test Conditions: 1575° F maximum, 1100° F minimum, 45 psia, 2 in./sec for sodium, 4 in./sec for potassium, 5000 hours.

7. Test Specimens: Type 316 SS tabs hung at hottest point and removed through top end of loop for weighing at 1000 hour intervals.

8. Pretreatment of Loop: Degreasing by hot detergent, water rinse, acetone rinse and vacuum outgassing.

9. Method of Filling Loop: From bottom, to level of "spark plug" probe temporarily inserted through top end.

10. Startup Procedure: Conventional for natural convection single phase loops.

11. Test Environment: Argon cover gas inside loop, air outside.

12. Instrumentation: Chromel-Alumel thermocouples made from bare 20 gauge wire, and ceramic beads. Maximum temperature measured in a well centered in the stream. This couple was removed and checked at intervals against a secondary standard.

    Cover gas pressure was continuously indicated by a Bourdon gauge.

13. Brief Description of Components: Conventional for natural convection loops. 4 kw Globar heater.

14. Alkali Metal Sampling: Before and after test only.

15. Loop Flow Stability: Stable flow, single phase loops.

16. Post-Test Procedure: Measure tab weights, sample alkali metal in loops, radiograph loops, drain wash and section loops, metallography on loops and tabs.

17. Major Loop Problems: No major problems. One loop sprang a slow potassium leak, first detected by tab weight change measurements. The leak sealed itself and could not be located in post-test examination.

    The sodium used was purified only by aging and filtering. The filling line constituted a small diffusion cold trap during loop operation. The potassium was aged, filtered and gettered with zirconium foil for 100 hours at 1250° F. No purification was provided during loop operation other than the diffusion cold trap.

18. Manpower: Total budget is 1030 man-hours, approximately 1/2 technician, 1/4 engineer, 1/4 chemist. Of the total about a fourth was spent building the two test stands and the potassium purification system.

19. Summary of Results to Date: All work is complete except for oxygen analysis of the potassium samples and some metallography. The corrosion data are summarized in Figure 2. The corrosion rate of stainless steel decreased with time in both sodium and potassium, apparently due to selective leaching of elements from the steel. A ferritic layer formed on the exposed surface in both cases. The corrosion rate was consistently lower in potassium. At 5000 hours the corrosion rate in 1575° F potassium was 20 mg/dm^{2}mo, equivalent to a uniform surface removal rate of 0.12 mils per year. The corresponding rate in sodium was 60 mg/dm^2 mo, or 3 times higher.

    The sodium test was run in duplicate. The two curves differed by a maximum of 13 percent, apparently due to accidental oxygen contamination in one loop at the 2000 hour shutdown. The same two loops, with fresh tabs, were used for the potassium test, but one was shut down by a slow leak at 1000 hours. The 500 hour data points were in excellent agreement. It is believed that the observed difference in sodium and potassium corrosion rates is real and typical for stainless steel thermal convection loops in the absence of any unusual oxygen sources or sinks.
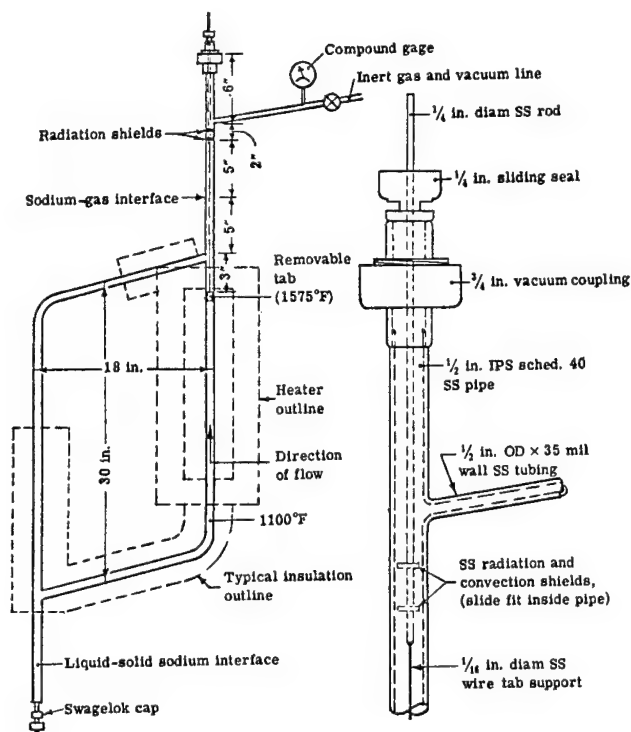
Figure 1. - Thermal convection loop design, showing gas lock details.
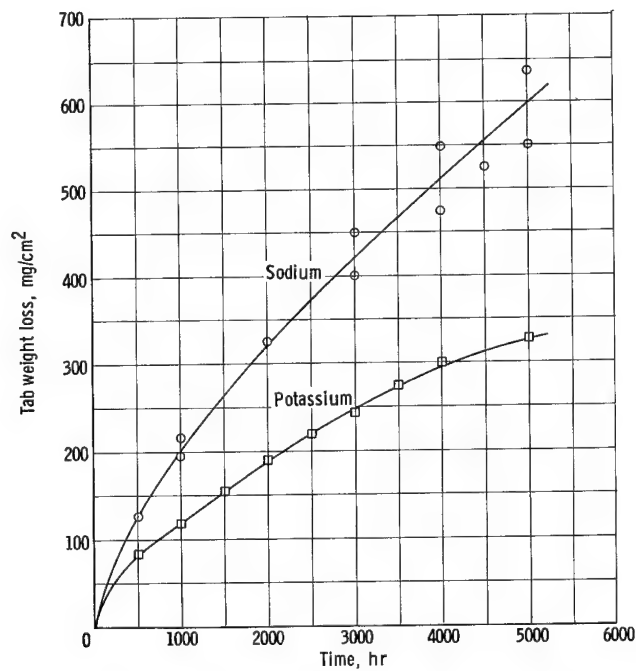
Figure 2. - Sodium-potassium corrosion comparison. Tab weight loss versus time for type 316 SS tabs suspended in sodium and potassium flowing in identical SS thermal convection loops at 1575° F (475° F ΔT).

215

C. MISCELLANEOUS TESTS

Liquid-Metal Corrosion Questionnaire

1. Purpose of Test and Sponsor: Contract for Conduct of Solubilities and Diffusion Studies of Ultra Pure Transition Elements in Ultra Pure Alkali Metals. This program is sponsored by the Lewis Research Center, NASA.

2. Fluid: Potassium (and Lithium)

3. Type: All Liquid.

4. Alloys or Materials: for exposure in liquid potassium; Single crystal Zr, Hf, V, Nb, Ta, Mo, W, Re, and Fe; Metal compounds, NbO, TaO, ZrO_2, ZrC, BeO, VO, "ZrO," and "HfO;" for exposure in liquid Li; Nb and BeO.

5. Test Specimens: Single crystal crucibles.

6. Specimen Dimensions: Nominally a 1/2" D x 2-1/2" long sample material crystal with a nominal 3/8" ID x 2" deep cavity in which the liquid metal is exposed.

7. Controlled Variables: Temperature, 400°, 600°, 800°, 1000°, and 1200°C to ± 1°C if possible; Time: nominal 1-8 hours exposures, but up to 40 hours exposure if required.

8. Purity of Alkali Metal: The goal is to use the purest K and Li that can be produced. Tentative purity goals are set: oxygen, 5 ppm; alkali metals, 5 ppm; C, 2 ppm; total impurities, 100 ppm.

9. Method of Loading and Sealing Capsules: The sample crucibles will be loaded in vacuum with extruded slugs of distilled potassium and sealed with a sample collector within a molybdenum or niobium-alloy test capsule using an electron beam weld seal. (During test, the potassium is contained in the sample crystal; at the end of the test, the test capsule is inverted to pour the potassium into the sample collector.)

10. Test Environment: The test environment for the test capsule will be vacuum at 10^{-5}-10^{-6} Torr level. The test environment for the sample is the interior of the sealed test capsule, which is sized to minimize the amount of vapor volume over the sample. The vacuum will be monitored using an ionization vacuum gauge. In addition, the oxygen content of the atmosphere will be monitored using a liquid alkali metal getter surface and analyzing for oxygen content increase.

11. Fluid Flow Rate: None.

12. Flow Stability: None required.

13. Method of Heating and Control: Radiant heating with thermocouples spot-welded to the test capsule to monitor temperature gradients and to effect control of multi-section heater.

E-2492

14. Instrumentation: Multipoint temperature recorder for sample and furnace monitoring; potentiometer; timers; vacuum gauges.

15. Post-test Procedure: Open test capsule in vacuum, transfer frozen potassium sample in sample collector into glass vial for transfer to laboratory for chemical analysis.

16. Method of Measuring Corrosion and Material Change: Chemical analysis, such as colorimetric techniques and emission spectroscopy.

17. Reproducibility of Results: Program is not yet developing data, but reproducibility within the limits of chemical analytical techniques is the goal.

18. Premature Failures: Experimental phase has not yet begun.

19. Manpower Involved: 12 man-years total over a two-year period.

20. Summary of Results to Date: Test system component specifications have been prepared and have been submitted to vendors for bid. Single crystal suppliers have been canvassed for their ability to produce crystals of the desired purity and size, with several encourgaging responses. Analytical and sample characterization techniques are being critically evaluated.

E-2492

Liquid-Metal Corrosion Questionnaire

I. FATIGUE OF Cb-1Zr SHEET IN POTASSIUM AND LITHIUM

1. **Purpose:** To develop fatigue data for Cb-1Zr sheet during exposure to liquid alkali metals.
   Sponsor: AiResearch Manufacturing Company of Arizona (SPUR Program).

2. **Fluid:** Liquid potassium; liquid lithium.

3. **Type:** Fatigue specimens submerged in liquid during test; saturated vapor (no inert gas) above liquid surface.

4. **Materials:** Cb-1Zr sheet stock, 30 mils thick, surface degreased.

5. **Test Specimens:** Constant-stress cantilever-bending fatigue specimen (Figure I-1), mounted in 316 stainless steel assembly (Figure I-2).

6. **Capsule Configuration:** Pot is 3-1/2-in. ID by 5 in. deep. Liquid depth is approximately 1-1/2-in. (See machine assembly, Figure I-3).

7. **Variables Studied:** Temperature - 800F for potassium; 1600F for lithium. Peak stresses (reversed bending)-to 49,500 psi for specimens tested in potassium; to 30,000 psi for specimens tested in lithium. Runouts - to 10^7 cycles.

8. **Alkali Metal Purity:** Potassium - MSAR special purity potassium, received in glass vials; spot checks by mercury amalgamation showed 75 ppm oxygen. Lithium - Material gettered batch-wise by exposure to 1600F Ti-Zr chips; typical analysis after treatment, $<$ 20 ppm nitrogen (micro-Kjeldahl) and $<$ 150 ppm carbon (Leco conducto-metric); further gettering during test by Ti-Zr foil placed in fatigue-test chamber.

9. **Charging:** Potassium - glass ampoule placed inside sealed sidearm attached to fatigue-test chamber, system evacuated, ampoule shattered by hammer blow on sidearm, potassium melted by external heat, liquid forced by inert gas pressure through stainless filter into fatigue-test chamber. Lithium - individual charging pots loaded and sealed in helium-filled drybox, gettered, connected to evacuated fatigue-test chamber, and lithium transferred by inert gas pressure.

221

10. Test Environment: Static vacuum (1-5 micron, measured by thermo-
    couple gage) in leak-tested fatigue-test chamber.

11. Fluid Flow Rate: No flow.

12. Flow Stability: Not applicable.

13. Heating and Control: Resistance furnace surrounding fatigue-test
    chamber (see Figure I-3). Controller operated by sheathed
    thermocouple immersed in liquid metal.

14. Instrumentation: Conventional thermocouple recording and control
    instrumentation; capacitance-type sensor probe shuts off
    machine and furnace when specimen breaks. Number of
    cycles measured by mechanical counter on drive mechanism.

15. Post-Test Procedure: Apparatus cooled to ∿ 150F above the melting
    point of the liquid metal; liquid metal drained into stor-
    age vessel; fatigue-test chamber opened; specimen pieces
    removed and cleaned in alcohol.

16. Method of Measuring Corrosion: Hardness changes; changes in oxygen,
    hydrogen, nitrogen content of specimens.

17. Reproducibility: No exact duplicate tests were run; scatter in
    S-N data points normal for fatigue results.

18. Premature Failures: About 10 per cent of the tests were invalid for
    one of the following reasons- (1) furnace failure, (2) leak,
    (3) malfunction of failure-sensing cutoff device, (4) dif-
    ficulty in transferring lithium to test chamber.

19. Manpower: One engineer and one technician, about half time, for one
    year.

20. Results: S-N curves were established, as shown in Figure I-4.
    Endurance limits in reversed bending were approximately
    27,000 psi for Cb-1Zr in 800F potassium and 20,000 psi in
    1600F lithium. These are absolute data for bellows design;
    no inert-environment tests were run for comparison. Hard-
    ness and gas-analysis data are summarized in Table I-1.

TABLE I-1. Cb-1Zr Fatigue-Test Samples

Specimen	Exposure Time, hr.	Hardness, VHN(10kg)	Parts Per Million		
			Oxygen	Hydrogen	Nitrogen
As received	0	82.9	367	1.8	100
Specimens Tested in 800F Potassium					
5	20	101.4	456	35	70
7	45	107.6	506	40	45
1	210	113.6	582	154	142
Specimens Tested in 1600F Lithium					
1L	3	106.3	289	4	99
2L	10	87.1	284	1.5	113
6L	95	83.0	280	1.6	125
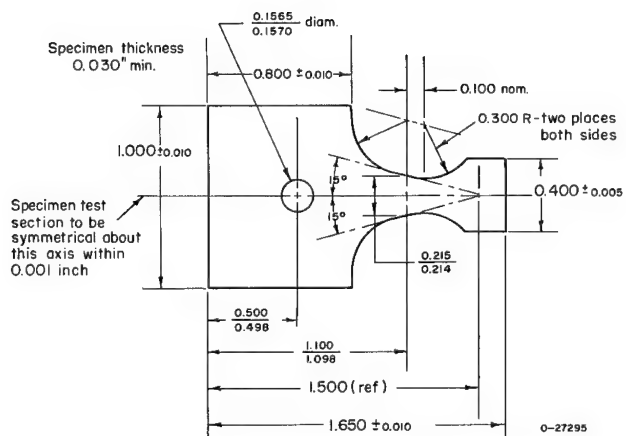
Figure I-1. - Nb-1Zr fatigue specimen.
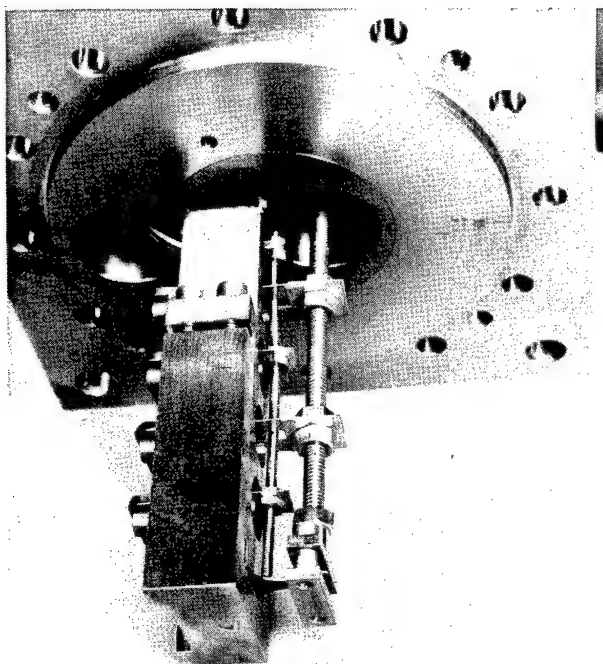
Figure I-2. - Specimen, driving and sensing rods, and flexure plate assembly of cantilever bending fatigue apparatus.
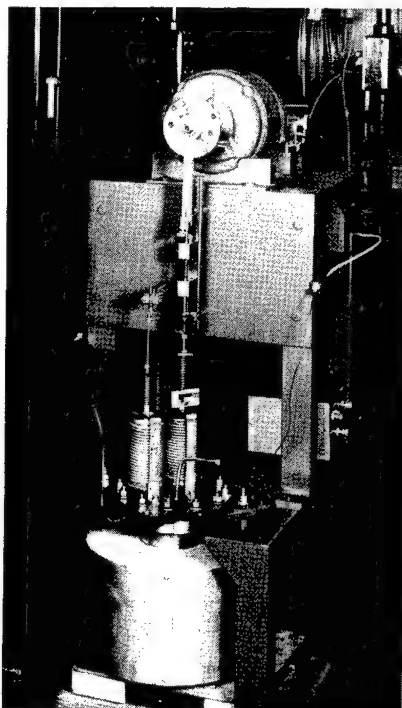
Figure I-3. – Machine for conducting cantilever bending
fatigue tests in liquid metals.
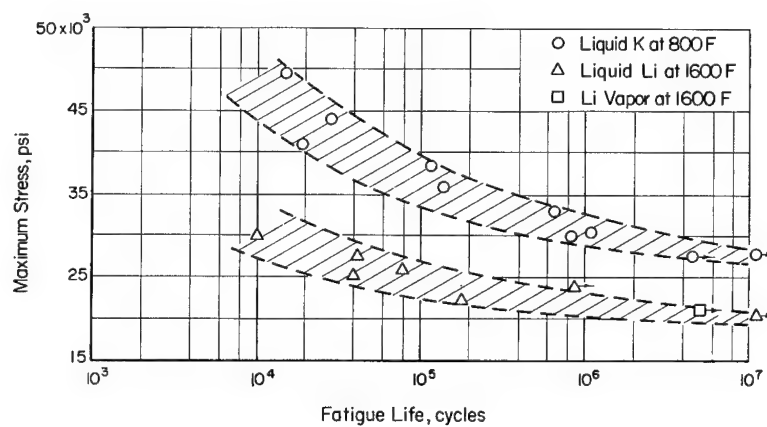
Figure I-4. – Results of reversed-bending fatigue tests on Cb-1Zr in liquid potassium
at 800 F and liquid lithium at 1600 F.

225

II. FATIGUE OF Mo-0.5Ti IN POTASSIUM VAPOR

1. Purpose: To see if exposure to potassium vapor has any influence
    on fatigue behavior of Mo-0.5Ti.
    Sponsor: AiResearch Manufacturing Company of Arizona (SPUR Program).

2. Fluid: Potassium.

3. Type: Inside surfaces of hollow specimens exposed to saturated
    vapor.

4. Materials: Arc-vacuum-cast, hot-rolled, ground, 3/4-in.-diam bar
    stock, stress-relieved 1 hr. at 1800F.

5. Test Specimens: Cylindrical, threaded-end axial-load fatigue
    specimens, hollow with welded end plugs (Figure II-1).

6. Capsule Configuration: Vacuum chamber is 2-in. I.D. Inconel tube,
    with Mo-0.5Ti specimen grips sealed through stainless
    steel bellows, as shown in Figure II-2. A few drops of
    potassium inside the specimen cause the specimen cavity
    to be filled with saturated potassium vapor at the test
    temperature.

7. Variables Studied: Temperature - 1500 and 2000F; load ratio
    (alternating stress: mean stress) - 0.95; peak stress
    range - 31,500 psi to 100,000 psi; runouts - to 10^8 cycles.

8. Alkali Metal Purity: MSAR special purity potassium. A single glass
    vial supplied potassium for all tests; no oxygen analysis
    made on this particular sample; other samples from same
    MSAR batch, handled in the same manner, showed 75 ppm
    oxygen by mercury amalgamation.

9. Charging: Potassium taken by hypodermic needle from heated (200F)
    glass vial and inserted in specimen cavity inside helium-
    filled drybox; end caps Heliarc welded in place.

10. Test Environment: Specimen internal - saturated potassium vapor
    plus helium; specimen external - dynamic vacuum to 5
    microns or less.

11. Fluid Flow Rate: No flow.

12. Flow Stability: Not applicable.

13. Heating and Control: Resistance furnace surrounding vacuum chamber; thermocouples wired to tantalum-foil-wrapped specimens used for temperature measurement and control.

14. Instrumentation: Conventional thermocouple recording and control instrumentation; number of cycles, specimen strain, and failure cutoff device are part of the Ivy Dynamic Creep Machine instrumentation (Figure II-3).

15. Post-Test Procedure: Apparatus cooled down and specimen removed in air and cleaned with alcohol.

16. Method of Measuring Corrosion: Hardness changes; metallography; endurance limit comparison with results on specimens with no potassium present.

17. Reproducibility: Very few duplicate tests run; scatter in S-N data points only slightly greater than usual for fatigue results.

18. Premature Failures: Three tests out of 28 were stopped early for various reasons: (1) vacuum leak, (2) failure of a part in the specimen grip assembly, (3) furnace burnout.

19. Manpower: One engineer and one technician about half time for a year.

20. Results: Summarized in Figure II-4; exposure of Mo-0.5Ti to both 1500 and 2000F potassium vapor appears to reduce the endurance limit by a significant amount.
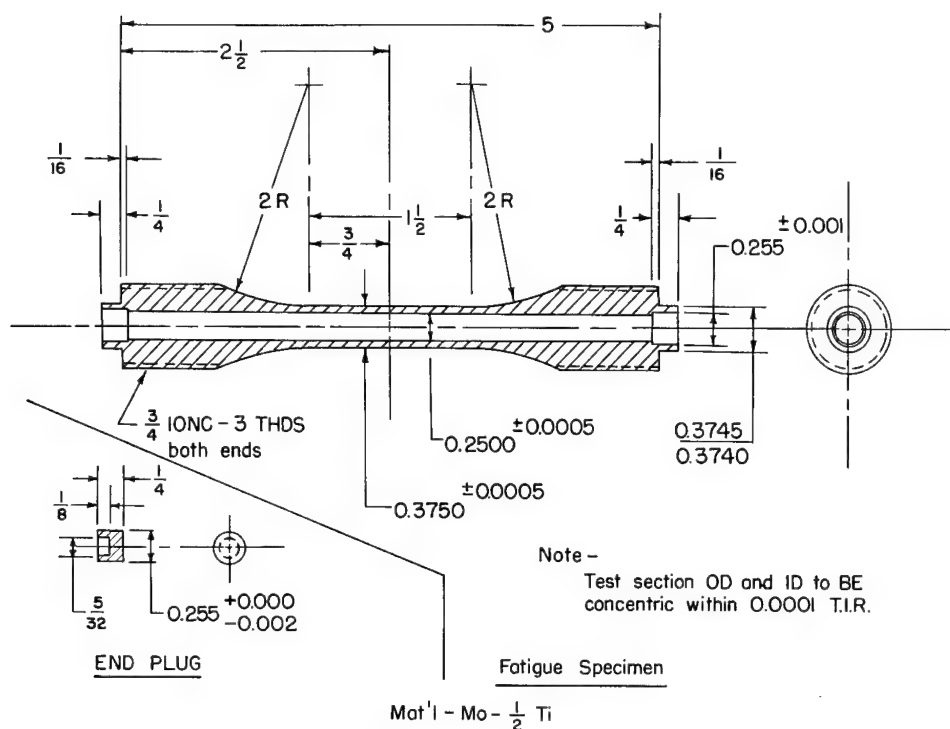
Figure II-1. - Dynamic creep specimen for modified Ivy machine.

$\frac{3}{4}$ IONC - 3 THDS both ends

END PLUG

Note –

Test section OD and ID to BE concentric within 0.0001 T.I.R.

Fatigue Specimen

Mat'l – Mo – $\frac{1}{2}$ Ti
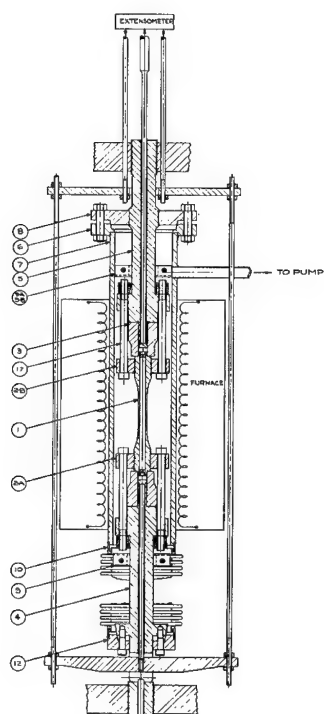
Figure II-2. - Furnace, vacuum chamber, and specimen holder assembly for Mo-0.5 Ti fatigue tests.

228
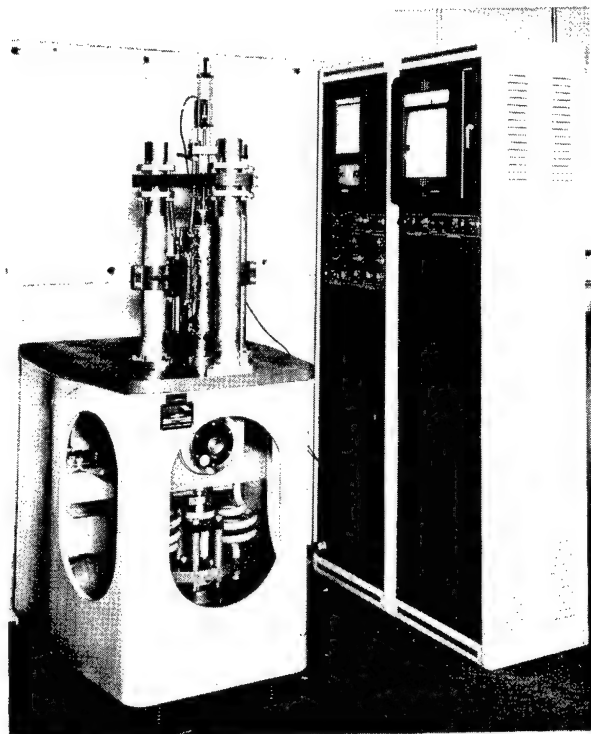
Figure 11-3. – Ivy dynamic creep machine.
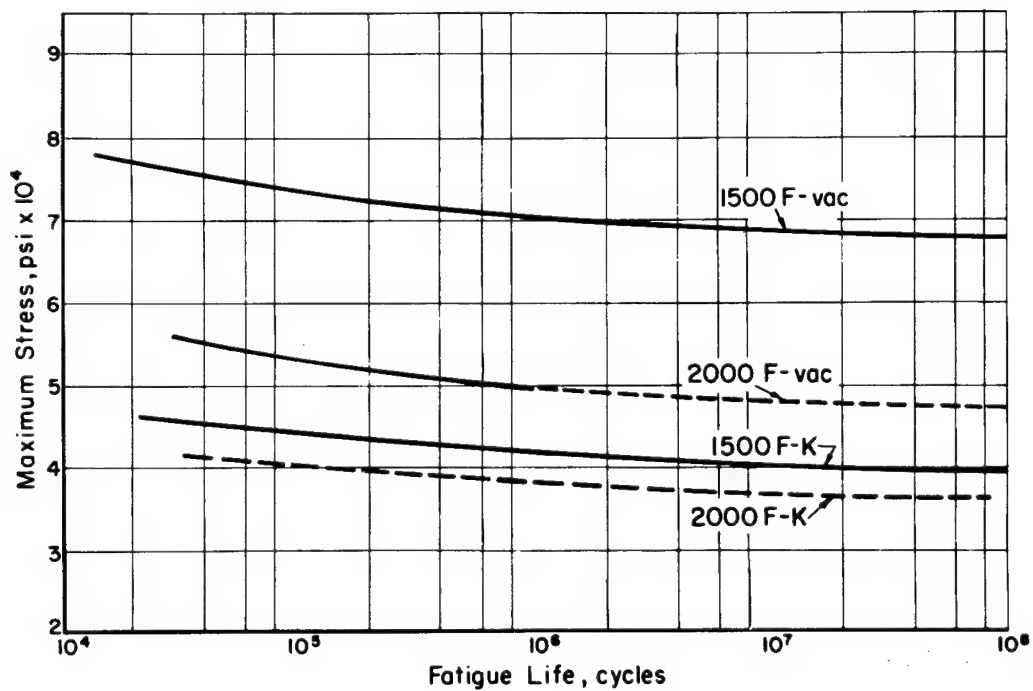
Figure 11-4. – Results of axial load fatigue tests on Mo-0.5 Ti in helium-vacuum atmosphere, or potassium-vacuum atmosphere at 1500 F and 2000 F.

229

III. STRESS-RUPTURE OF Mo-0.5Ti IN POTASSIUM VAPOR

1. Purpose: To see if the stress rupture behavior of Mo-0.5Ti is any different in a potassium vapor environment than in a vacuum at the same temperatures.

   Sponsor: AiResearch Manufacturing Company of Arizona (SPUR Program).

2. Fluid: Potassium.

3. Type: Inside surfaces of hollow creep specimens exposed to potassium vapor.

4. Materials: Arc-vacuum-cast, hot-rolled, ground, 3/4-in.-diam bar stock, stress-relieved 1 hr at 1800F.

5. Test Specimens: Cylindrical, threaded-end creep specimens, hollow with welded end plugs (Figure III-1).

6. Capsule Configuration: Tests conducted in conventional vacuum-creep apparatus. The specimen itself is the capsule. A few drops of potassium sealed inside the specimen cause the cavity to be filled with saturated potassium vapor at the test temperature.

7. Variables Studied: Temperature - 1800 and 2000F; stress levels - 25,000 to 60,000 psi; time - to 1000 hr.

8. Alkali Metal Purity: MSAR special purity potassium; a single glass vial supplied potassium for all tests; no oxygen analysis made on this particular sample; other samples from same MSAR batch, handled in the same manner, showed 75 ppm oxygen by mercury amalgamation.

9. Charging: Potassium transferred by hypodermic needle from heated glass vial to specimen cavity inside helium-filled dry-box; end caps Heliarc welded in place.

10. Test Environment: Specimen internal - saturated potassium vapor plus helium; specimen external - dynamic vacuum to 5 microns or less.

11. Fluid Flow Rate: No flow.

12. Flow Stability: Not applicable.

E-2492

13. Heating and Control: Resistance furnace, with 5 independent windings, surrounding vacuum chamber; thermocouples wired to tantalum-foil wrapped specimens used for temperature measurement and control.

14. Instrumentation: Conventional thermocouple recording and control instruments; specimen strains measured optically by platinum-strip extensometers attached to specimens.

15. Post-Test Procedure: Apparatus cooled down and specimen removed in air and cleaned with alcohol.

16. Method of Measuring Corrosion: creep curve comparisons between tests with and without potassium present; metallography.

17. Reproducibility: Creep curves from the few duplicate tests show good agreement. Results from tests under other conditions are consistent.

18. Premature Failures: Two of ten experiments yielded dubious data because they were restarted after furnace burnouts.

19. Manpower: One engineer and one technician about half time for a year.

20. Results: Potassium vapor appears to have no influence on the creep properties of Mo-0.5Ti. Design curves (Figure III-2) were the same for specimens exposed to potassium vapor and those tested in vacuum.

Gage section

O.D. = 0.500 ± .0005
I.D. = 0.375 ± .0005
surfaces to be concentric
within 0.0001 tir

$\frac{3}{4}$ – 10 thd
both ends

8 to 10 mil deep 90°
groove both ends, $\frac{1}{16}$
from shoulder at
gage section

$\frac{1}{8}$ $\frac{5}{16}$ 1   2 $\frac{5}{8}$ 0.52   0.400 ± .001 $\frac{3}{4}$

$5\frac{1}{4}$

Specimen

Notes:
All dimensions in inches

0.400 $\pm^{.000}_{.002}$

$\frac{3}{8}$ $\frac{5}{16}$

End Plugs
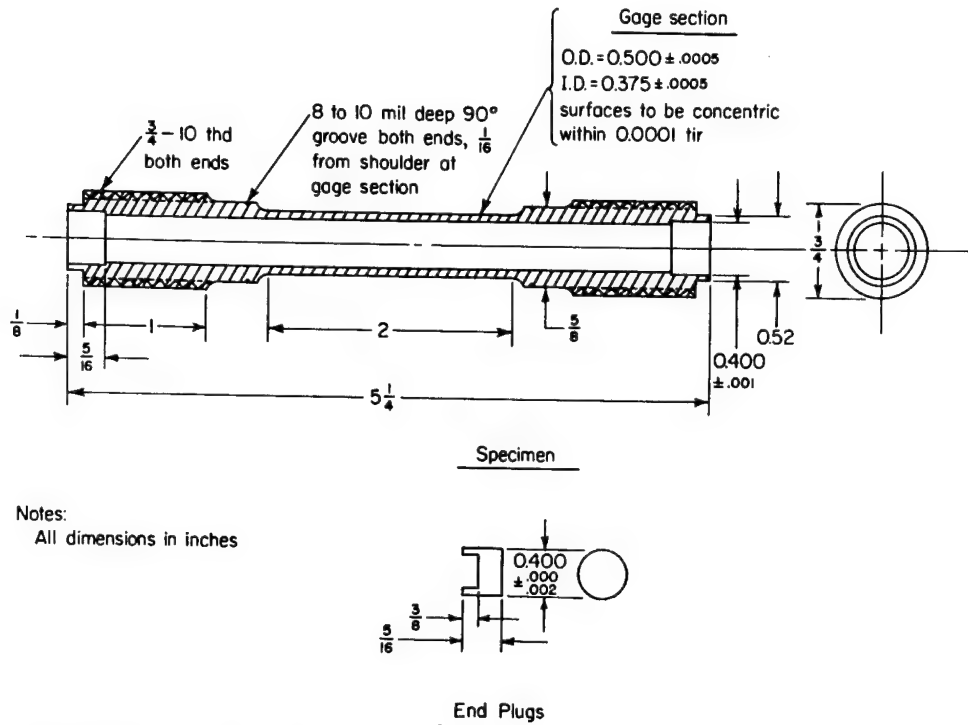
Figure III-1. – Hollow specimen for 1800 and 2000 F creep-rupture tests on Mo-0.5 Ti.

Rupture 1800 F
2.0% 1800 F
0.5% 1800 F
1.0% 1800 F
Rupture 2000 F
2.0% 2000 F
1.0% 2000 F
0.5% 2000 F

Stress, 1000 psi

Time to Reach Indicated Deformation or Rupture, hr
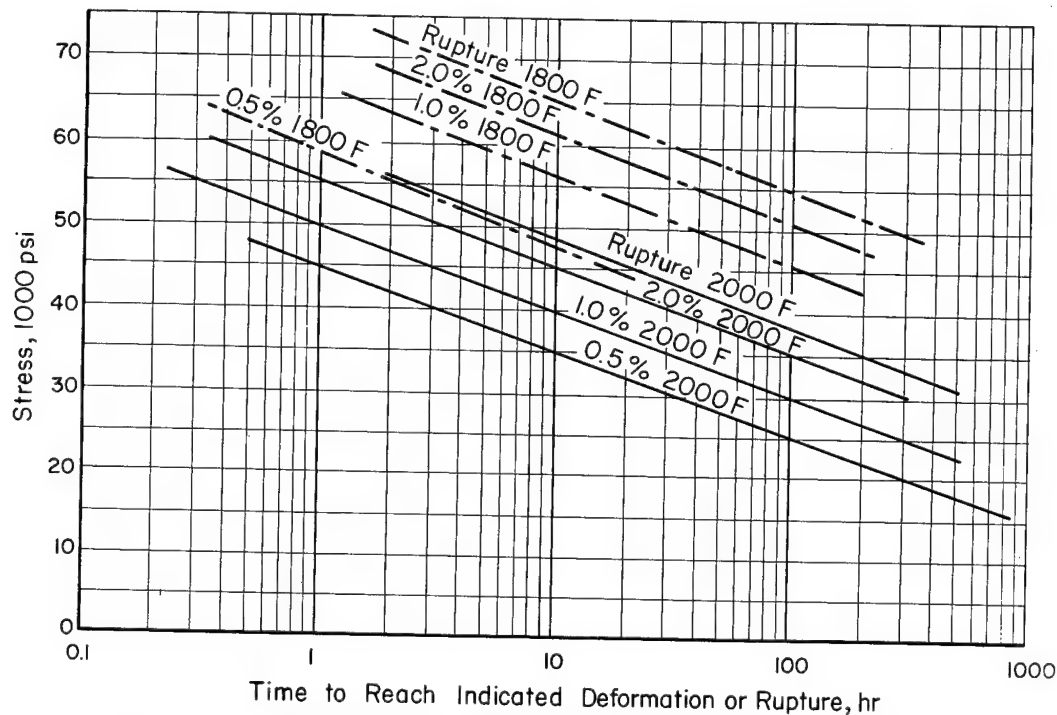
Figure III-2. – Design curves for stress-relieved Mo-0.5 Ti alloy in potassium vapor or vacuum.

IV. STRESS-RUPTURE OF SAE-4340 STEEL IN POTASSIUM VAPOR

1. **Purpose:** To see if the stress-rupture behavior of SAE-4340 steel is any different in a potassium vapor environment than it is in air at the same temperatures.
   Sponsor: AiResearch Manufacturing Company of Arizona (SPUR Program).

2. **Fluid:** Potassium.

3. **Type:** Saturated vapor.

4. **Materials:** Specimens machined from rolled bar stock which had been normalized 1 hr at 1750F and tempered 1 hr at 1100F to a hardness of 33RC.

5. **Test Specimens:** Cylindrical, button-head creep specimens with ground, 2/16-in.-diam gage section.

6. **Capsule Configuration:** Tests conducted in a Hastelloy X pot, with a Mo-0.5Ti pull rod sealed through stainless steel bellows. A small pool of potassium in the bottom caused the pot to be filled with saturated vapor at the test temperature (See Fig IV-1).

7. **Variables Studied:** Temperature - 800 and 1000F; stress - 24,500 to 85,000 psi; time - to 1000 hr.

8. **Alkali Metal Purity:** MSAR special-purity potassium received in sealed glass vials; spot checks by mercury amalgamation showed 75 ppm oxygen.

9. **Charging:** Glass ampoule placed inside sealed sidearm attached to creep-test chamber, system evacuated, ampoule shattered by hammer blow on sidearm, potassium melted by external heat, liquid forced by inert gas pressure through stainless filter into creep-test chamber. Chamber evacuated and sea led off before starting creep test.

10. **Test Environment:** Static vacuum (1 to 5 micron) in creep chamber at start of test; specimen surrounded by saturated potassium vapor during test.

11. **Fluid Flow Rate:** Since the top of the test chamber was cooler than the rest, there was some refluxing; rate not measured.

12. Flow Stability: Satisfactory, as indicated by constancy of intra-
                     capsule temperatures.

13. Heating and Control: Mo-wound resistance furnace, located in
                     inert-gas-filled annulus around creep-test chamber, con-
                     trolled from sheathed thermocouples in contact with creep-
                     specimen surface.

14. Instrumentation: Conventional furnace temperature recording and
                     control instruments; specimen strains measured by external
                     dial gages.

15. Post-Test Procedure: Apparatus cooled down; flange weld ground
                     off; potassium reacted with alcohol; specimen pieces
                     removed, cleaned, and measured.

16. Method of Measuring Corrosion: By effect of exposure on creep
                     behavior; limited hardness measurements and metallography.

17. Reproducibility: Normal scatter for creep-rupture data.

18. Premature Failures: Several abortions traced to nonuniform axial
                     temperature distributions; situation corrected by separate-
                     ly controlled buffer furnace at top, and subsequent tests
                     were satisfactory.

19. Manpower: One engineer and one technician, about half time, for
                     one year.

20. Results: Potassium vapor at 800 and 1000F appears to have no
                     effect on the creep-rupture characteristics of SAE 4340
                     steel. This is illustrated by typical creep-rupture
                     curves, Figure IV-2.
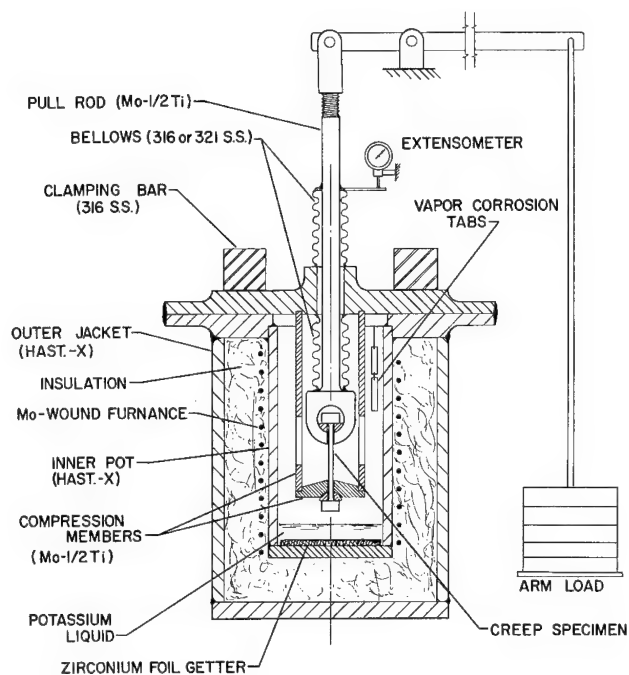
Figure IV-1. – Schematic arrangement of apparatus for studying effect of potassium vapor on creep.
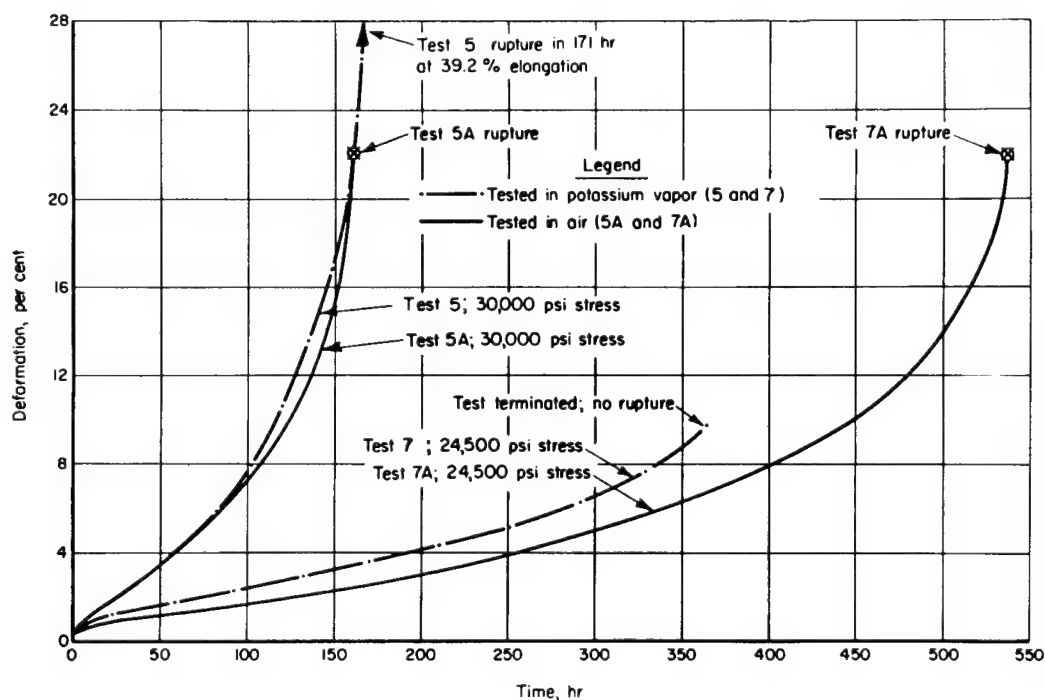
Figure IV-2. – Typical creep curves for SAE-4340 steel at 1000 F, with and without potassium vapor environment.

235

V. REFRACTORY METALS FOR THERMIONIC CONVERTERS

1. Purpose: To find materials most suitable for contact with liquid lithium to 3000F and cesium vapor to 3400F.
   Sponsor: USAF - Research and Technology Division

2. Fluid: Cesium and lithium.

3. Type: Cesium - saturated vapor
   Lithium - liquid

4. Materials: W, W-0.95Cb, W-15Mo, W-25Re, Ta-12W, TZM, B-66, and T-111. Starting form is rod, procured from commercial sources.

5. Test Specimens: Specimens are 3/8-in.-OD cans, machined from solid bar. Sealed inside each can is a snug fitting fuel pellet (UO_2, UC, or UN).

6. Capsule Configuration: Test specimen is sealed inside a 5/8-in-ID can made of Mo-0.5Ti, with either cesium vapor or lithium liquid in the annulus between the specimen and the outer shell (Figure V-1).

7. Variables to be Studied: Time - 100 and 1000 hr; temperatures for cesium - 2500, 2800, 3100, 3400F; temperatures for lithium - 2500, 2800, 3000F; fuel pellet composition - UO_2, UC, UN.

8. Alkali Metal Purity: Lithium - gettered with zirconium-titanium alloy chips, 4 hr at 1600F; arc-emission spectrography for structural-metal impurities, yielding 5 ppm Fe, 10 ppm Cr, 10 ppm Cu, 100 ppm Ti, 500 ppm Zr, 120 ppm C. Cesium - used as received from Dow Chemical; Vendor's analysis showed 11 ppm O_2; major metallic impurities were 35 ppm Rb, 18 ppm Ca, 18 ppm Li.

9. Charging: Lithium - transferred manually from gettering capsule to test capsule inside helium-filled drybox with < 7.5 ppm O_2 in drybox atmosphere at start of transfer; test capsule sealed by Heliarc welding and leak checked. Cesium - transferred by hypodermic syringe from glass shipping vial to test capsule inside helium-filled drybox; test capsule sealed by Heliarc welding and leak checked.

10. Test Environment: Vacuum $9x10^{-6}$ to $3.5x10^{-6}$ torr maintained in furnace chamber during entire test.

11. Fluid Flow Rate: Isothermal capsules, no flow.

12. Flow Stability: Not applicable.

13. Heating and Control: Resistance - heated tantalum sheet vacuum furnaces; no measured temperature gradients; temperature held to $\pm$ 25F at 2500F.

14. Instrumentation: Optical pyrometer used for temperature measurements.

15. Post-Test Procedure: Furnace cooled down; capsules transferred to helium-filled drybox; specimens removed, weighed, examined visually, examined metallographically.

16. Method of Measuring Corrosion: By appearance, weight change, metallography, micro-hardness.

17. Reproducibility: Gross changes were reproducible; Quantitatively weight-change reproducibility was variable. Metallography results completely consistent.

18. Premature Failures: A few capsules failed because of weld leaks; some suffered gross distortion from internal pressure.

19. Manpower: Equivalent of 2 engineers and 3 technicians for a year.

20. Results: 100-hr capsule tests run as of 10/1/63

Capsule	2500F		2800F		3100F	
	Cs	Li	Cs	Li	Cs	Li
W	8	8	6	0	1	0
W-25Re	6	6	6	0	0	0
Ta-12W	6	6	6	0	6	0
TZM	6	8	6	0	5	0

W - No evidence of attack
W-25Re - No evidence of attack
Ta-12W - Consistently attacked at both fuel and alkali-metal interfaces.
        Cs and Li at 2500F, about 2 mils penetration;
        Cs at 2800F, about 8 mils gross attack, light precipitate
                    throughout
        Cs at 3100F, about 20 mils gross attack, heavy precipitate
                    throughout.
   TZM - Cs and Li at 2500F, essentially no attack
        Cs at 2800F, slight surface roughening; some weight loss.
        Cs at 3100F, large grain growth near Cs-exposed surface.
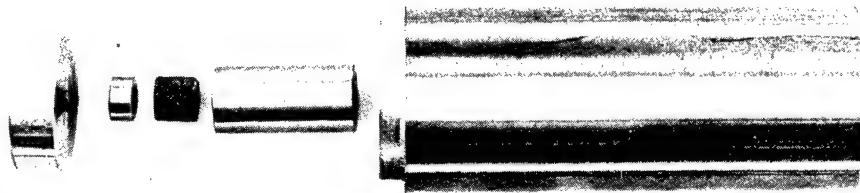
1X

a. Complete Can Prior to Loading

Components from left to right are
Mo-1/2Ti lid, fuel-element lid (TZM),
fuel slug (UC), fuel-element can (TZM),
and outer can of Mo-1/2Ti.
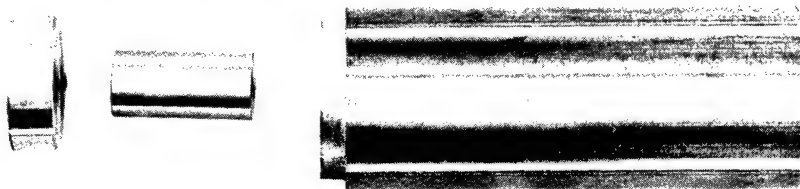
1X

b. View Showing Fuel Element Assembled
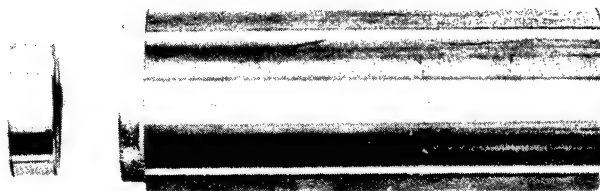
1X

c. View Showing Element in Place;
2 or 3 Elements per Can

1X

d. Assembly Prior to Welding and
Loading of Cesium or Lithium

Figure V-1. - Exploded view of corrosion and compatibility assembly at various stages of loading.

239

VI. MATERIALS FOR POTASSIUM SEALS

1. **Purpose:** Effect of Potassium Exposure on Potentially Useful Materials
   for Rubbing Members of Rotating Seals.
   Sponsor: ASD (Part of a large seal-development program).

2. **Fluid:** Potassium.

3. **Type:** Liquid and Vapor.

4. **Materials:** Materials selection is one of the objectives of this
   program. Criteria include the ability to form a replenish-
   able lubricating film upon exposure to potassium.

5. **Test Specimens:** Powders and slugs of composite materials are being
   examined for film-formation behavior via chemical-reaction
   (DTA) screening experiments. To date, only a few exploratory
   runs have been made. Corrosion-screening experiments are
   planned for a later stage. Some of the specimens at this
   time will be in the form of tensile and impact bars for
   post-exposure mechanical-property determinations.

6. **Capsule Configuration:** The DTA experiments utilize type 316 stain-
   less steel capsules with O.D.=5/8 in., I.D.=1/2 in.,
   length = 3 in. See Figure VI-1. The container design for
   later experiments has not been firmed up.

7. **Variables Studied:** For the DTA experiments – materials, temperature
   to 1400F and heating rates of 5F/min to 60F/min. For
   later corrosion experiments, materials, temperature to
   1400F, liquid vs vapor, and time to 1000 hr.

8. **Alkali Metal Purity:** Potassium purity, particularly oxygen content,
   is of special interest because of its possible role in the
   film-replenishing mechanisms. Starting material is MSAR
   high-purity (< 50 ppm O_2), low-sodium (< 50 ppm) potassium.
   The handling technique now under investigation is as
   follows. As-received potassium is gettered at Battelle in
   a recirculating loop system (1200F, one week).

9. **Charging:** After gettering, a solid-potassium-filled leg of the loop
   is removed and fitted into an extruding device mounted on
   a helium-filled drybox. Solid slugs of potassium are
   extruded into the drybox and inserted into the test
   capsules, the latter are closed by heliarc welding.

10. Test Environment: DTA capsules are being run in air.

11. Fluid Flow Rate: No flow - static.

12. Flow Stability: Not applicable.

13. Heating and Control: Two potassium-filled capsules, one with a material of interest and one without, are mounted in a heavy copper block, surrounded by a resistance-wound furnace. Each capsule contains a sheathed thermocouple sealed through the bottom and immersed in the liquid metal.

14. Instrumentation: One KVA furnace, X-Y plotter for recording reaction capsule temperature and differential temperature, recorder for control of capsule temperature, and furnace control.

15. Post-Test Procedure: Dry-box recovery of capsule and contents.

16. Method of Measuring Corrosion: If an interesting DTA reaction occurs and if the specimen of test material has retained its integrity, X-ray or electron-diffraction analyses of specimen surfaces will be made to identify films.

17. Reproducibility: Good reproducibility of reaction temperatures has been obtained in the few DTA experiments run to date.

18. Premature Failures: None to date.

19. Manpower: For DTA's: part-time engineer and technician for about 6 mo. For the planned corrosion series: part-time engineer and technician for about 9 mo.

20. Results: Initial DTA data indicate that the Mo-O-K and W-O-K systems behave as predicted thermodynamically (measured compound-formation temperatures and identified compounds). Continuing with other systems.
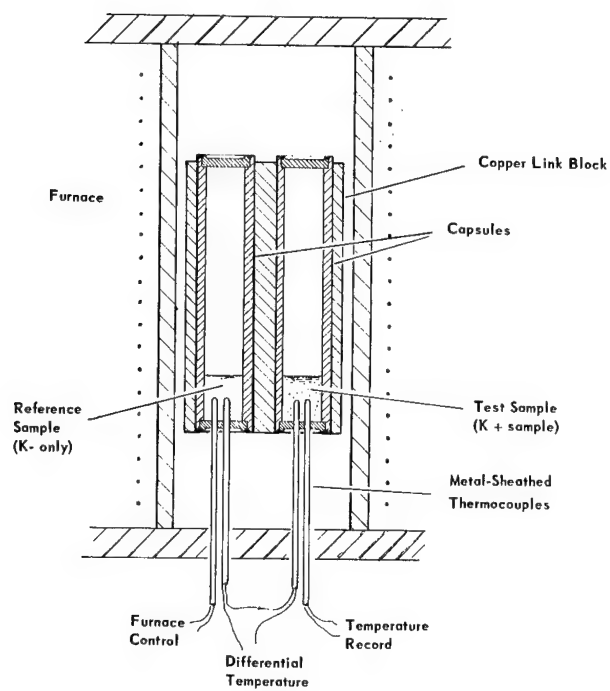
Figure VI-1. – Differential thermal analysis experiment set-up.

Liquid-Metal Corrosion Questionnaire

1. Purpose of Test and Sponsor: Determine compatibility of metallic materials with cesium for ion engine applications for NASA-Lewis.

2. Fluid: Cesium.

3. Type: Both liquid and vapor.

4. Alloys: Not heat-treated. Cleaned by vapor degreasing and pickling. The materials that were evaluated were

   (1) Timken Sicromo $2\frac{1}{2}$ bar

   (2) 347 Stainless steel sheet

   (3) 316 ELC stainless steel sheet

   (4) Sensitized 302 stainless steel sheet

   (5) Inconel sheet

   (6) Haynes 25 sheet

   (7) Titanium - 6 Al - 4V alloy sheet

   (8) Copper (OFHC) sheet

   (9) Nicrobraze cast

   (10) Tungsten sheet

   (11) Molybdenum bar

   (12) Tantalum sheet

   (13) Brazed joints of 347 stainless to molybdenum using copper as the brazing alloy

   (14) Brazed joints of 347 stainless to molybdenum using Nicrobraze LM as the brazing alloy

   (15) 50 Ti - 50 Zr alloy turnings

5. Test specimens: Tensile specimens for room temperature and 400° C exposure, wire filaments for 980° and 1370° C exposures.

6. Dimensions: 1/2 inch O.D. by 6 inch length with ends crimped and welded for tensile specimens, 3/4 inch O.D. glass tubes for filament specimens.

7. Controlled Variables studied and Range of Variables:

The exposures used were:

    (1) 50 hr at 400° C in cesium liquid.

    (2) 50 hr at 400° C in cesium vapor.

    (3) 500 hr at 400° C in cesium liquid.

    (4) 500 hr at 400° C in cesium vapor.

    (5) 50 hr at 980° C in cesium vapor for tungsten, tantalum, and molybdenum.

    (6) 500 hr at 980° C in cesium vapor for tungsten, tantalum, and molybdenum.

    (7) 500 hr at 1370° C in cesium vapor for tungsten, tantalum, and molybdenum.

    (8) 4000 hr at 35° C in cesium liquid.

All tests were static exposures.

8. Purity of Alkali Metal: Oxygen, 300 ppm; carbon, not reported. No further purification beyond vendor's processing.

9. Method of Loading and Sealing Capsules:

Tensile specimens - Loaded in inert atmosphere dry box, metal capsules crimped close, sealed with tape while transported to welding area, inserted in special fixture which maintained helium atmosphere over capsule, cesium frozen by immersion of bottom of capsule in liquid nitrogen, tape removed, and crimped end TIG welded.

Filament specimens - Loaded in inert atmosphere, sealed off with rubber tube, removed from dry box, evacuated to 10^{-4} torr, and tubulation fused closed.

10. Test Environment: Tensile specimen capsules - held in sealed aging vessel with helium circulating through vessel while held at temperature. Filament specimen capsules - held in oven maintained at 265° C with filaments resistance heated to desired temperature.

11. Fluid Flow Rate: --

12. Flow Stability: --

13. Method of Heating and Control: Tensile specimen capsules - resistance heated, furnace controlled by pyrometer with no temperature gradient. Filament specimens - resistance heated oven with pyrometer control with no temperature gradient; filament temperature measured by optical pyrometer and temperature adjusted by Variac control.

244

14. Instrumentation: Tensile specimen capsules - Minneapolis Honeywell Electronic Controller. Filament specimens - Pyrometer Instrument Co. Pyro Optical Thermometer.

15. Post-Test Procedure: Cool capsules and transfer to dry box for unloading.

16. Method of Measuring Corrosion and Material Change: Weight change, metallographic examination, visual examination, mechanical testing, and spectrographic analysis of cesium.

17. Reproducibility of Results: Undetermined.

18. Number of premature failures due to causes other than corrosion: Six failures due to capsule failure either in weld or base metal.

19. Manpower Involved: Two professionals, two technicians.

20. Summary of Results to Date:

Of the materials tested, only tantalum exposed at 400° C was found to be completely unsatisfactory. Tantalum tubes exposed to this environment cracked and tantalum contents as high as 10,000 PPM were found in the exposed cesium. For this same exposure, tungsten was the second most severely attacked material based on weight loss. Its rate of attack in liquid cesium was 4.5×10^{-3} cm/yr. The rate of attack on all other materials in either vapor or liquid was quite negligible with the highest rate being 7×10^{-5} cm/yr. No significant difference between the vapor and liquid exposures was noted. In the long term storage tests at 35° C for 4000 hr the highest rate of attack was 4×10^{-5} cm.

The predominant pattern of the austenitic stainless steels exposed to either liquid or vapor at 400° C was weight gain. Metallographic evidence was obtained showing that a film 0.0002 in. thick was formed on the stainless steels exposed to either vapor or liquid atmospheres. The formation of this film (or diffusion coating) was attributed to the reaction of the cesium oxide with the stainless steel, i.e., the cesium oxide was reduced by the stainless steel to form chromium oxide or a complex oxide on the stainless steel. The fact that this phenomenon occurred in both liquid and vapor zones indicates that a source for oxygen exists in both zones.

There was no grain boundary attack of the sensitized 302 stainless steel and its performance was as good as the stabilized 347 grade and the 316 low carbon stainless steel.

The low alloy steel (Sicromo $2\frac{1}{2}$) was decarburized to a depth of 0.002 in. in 500 hr exposures at 400° C.

245

Except for the elements titanium, boron, and tantalum, no significant solubility was detected in the exposed cesium. A slight increase of iron and chromium was usually found in the cesium. Even with these elements, it is quite probable that their existence in the cesium is in the form of their oxides rather than in their elemental state. For example, from the relative free energies of formation of the oxides of cesium and titanium it is expected that titanium would reduce cesium oxide to form an oxide of titanium. The titanium specimens lost weight as contrasted to the stainless steel specimens which gained weight. It is believed that the oxidation reaction occurs with both materials, but in the case of the titanium, the oxidation product is not adherent and is sloughed off into the solution.

Although certain of the refractory metals were attacked at 400° C, no attack was observed at the 980° and 1370° C exposures. This apparent anomaly is explained by the variation in exposure procedures. In the lower temperature tests, the entire capsule containing the specimen was heated to 400° C. In the higher temperature tests, the specimens were filaments which were resistance heated in a cesium vapor that was generated at a temperature of 265° C. At this temperature, little cesium monoxide is decomposed so that the result is that the cesium vapor surrounding the test specimen should be quite pure and relatively free of oxygen. Evidence that cesium vapor generated at higher temperatures is more aggressive to refractory metals was found in an ion engine examined after operation. In this engine, the cesium vapor was generated at a temperature of 400° C and passed through a molybdenum tube heated to a temperature of approximately 1000° C. The molybdenum was severely attacked. The mechanism for the reaction that occurred appears to be decomposition of cesium monoxide, to produce an oxygen - containing vapor and oxidation of the molybdenum followed by sublimation of the molybdenum oxide.

This study has indicated the importance of oxygen in the corrosion behavior of cesium. While the oxygen content does not place severe restrictions on the choice of materials for service at 400° C, there are indications that cesium containing oxygen can be quite aggressive to refractory metals operating at temperatures of 1000° C.

MSA RESEARCH CORPORATION
Callery, Pennsylvania

Liquid-Metal Corrosion Questionnaire

1. Purpose of Loop and Sponsor

Sponsor: AEC, Chicago Office

Purpose: Two liquid metal loops are used in the physical properties research program which was initiated for the purpose of determining the effects of reactor grade sodium, and normally anticipated contaminants, upon Type 316 stainless steel and 2-1/4 CR-1 Mo steel. For comparison, the physical properties of these same materials were to be determined in air and helium. The test temperatures selected were 1200 F for the austenitic and 1100 F for the ferritic. The contaminants to be intentionally introduced into the sodium after the reactor grade sodium tests were completed would be oxygen, carbon and nitrogen. The types of tests selected for revealing any possible effects of the environments upon the materials were tensile, creep, stress-to-rupture, and fatigue.

2. Fluid

Reactor grade sodium

3. Natural or Forced Convection

Forced convection

4. Approximate Overall Size of Loops

15 ft wide × 30 ft long × 10 ft high
Schematic sketch is attached

5. Containment of Alloys

316 ss
Majority of piping is 1/2 in. Sch 40
Loops assembled by both metal arc and T.I.G. welding processes

6. Test Conditions

Temperature: 1200 F and 1100 F
Pressure: 1 psig
Flow Rate: 1/2 gpm through test specimen units and 5 gpm
            in main system
Operating Time: Approximately 12,000 hours

7. Test Specimens

Type: No. 5

Specimens were placed in test units designed such that after preheating a flow rate of 1/2 gpm was established through the unit at either 1100 or 1200 F. The test specimens were then subjected to a creep, creep to rupture or fatigue test. Following the test, the unit was drained, cooled and the test specimen removed.

8. Pretreatment of Loop Prior to Filling

System piping and components were degreased and washed with commercial solvents and detergents prior to assembly only. After assembly the system was preheated, evacuated and filled.

9. Method of Filling Loop

Loop preheated to 350 F and then evacuated to 1 mm. System charged by forcing sodium from the sump tank into the system. Helium cover gas pressure on the sump tank served as the driving force. Vacuum on system during charging was replaced with 1 psig of helium during operation.

10. Start-up Procedure

Circulation was initiated first in the bypass system. Test specimens were installed in test units as scheduled and circulation initiated through test units by opening isolation valve off the bypass system.

11. Test Environment

Reactor grade sodium under helium cover gas. The oxygen level was measured by a plugging indicator and controlled at 30 ppm by cold trapping.

12. Instrumentation

Pressure - standard commercial Bourdon tube gages for cover gas - no liquid metal.

Temperature - standard commercial temperature recorders and controllers with thermocouples.

Flow - magnetic flowmeters with millivolt indicators.

Specimen Elongation - standard dial gages.

Liquid Level - MSAR indicating hand probe (accuracy ± 1/4 in.)

13. Description of Components

Pumps - Standard MSAR Style V electromagnetic pump.

Heaters - Twelve 1000 watt tubular heaters welded in a flat tube sheet which in turn is welded in to an 8 in. Sch 40 pipe.

OCI System - A standard oxide control and indicating system is in parallel with the main system. This system includes a standard air cooled finned cold trap, a plugging indicator valve, economizer and flowmeter.

Valves - 1/2 in. Type 316 ss Powell bellows sealed valves.

Stress Machines - Arcweld Model K with a 6000 pound capacity.

14. Description of Alkali Metal Sampling or Monitoring Procedure

The oxygen content of the systems was monitored by plugging indicator valves at a frequency of at least once a week. Prior to this the reliability of the plugging indicators was established by comparing plugging runs against sodium samples removed from instream sampling and expansion tanks. Samples were also taken and analyzed at least once a week for carbon and metals in solution.

15. Loop Flow Stability

Loop flow was maintained manually by use of the EM pump and magnetic flowmeter. Flow was considered stable as detectable on standard commercial millivolt indicators.

16. Post-Test Procedure

Test units drained, cooled under helium cover gas, specimens removed and washed in alcohol and water, photographed and measured and held in dessicator until ready for metallographic examination. These examinations included the following:

> Physical measurements
> Weights
> Hardness
> Photography
> Microprobe analyses (selected specimens)
> Photomicrographs
> Chemical analyses

17. Major Loop Problems

Failure of bellows sealed valves has been a continuous problem throughout the test. Many valves have failed after two to three operations. The manufacturer has modified the bellows for these valves and as failures occur, these new bellows are being installed in the valves. It is too early to say if the new bellows will eliminate the failures. There are approximately 30 valves per system of which perhaps half have failed during the first year of operation.

18. Manpower

Design - Approximately 6000 engineering hours.

Operation (per month) - Four operators, one technician and 1/2 engineer.

Analyses (per month) - One engineer, one metallurgist, one chemist and two technicians.

19. Summary of Results to Date

Type 316 stainless steel, 1200 F

1. The creep rates in helium and sodium are higher than in air.

2. The number of cycles to failure in fatigue is extended by helium followed by sodium as compared to air. However, at low strains all three environments may show equal life.

3. All other physical properties showed little effect.

For 2-1/4 CR-1 Mo Steel, 1100 F

1. The tensile strength was lower in helium than in air.

2. The stress-rupture strength in sodium was slightly lower than for helium or air.

3. Pre-exposing the specimens for 4000 hrs (in sodium) lowered the stress rupture strength.

4. The creep rate in sodium is higher than in air.

5. The creep rate in helium is lower than air at high stresses and higher in air at low stress.

6. The number of cycles to failure in fatigue is extended by both helium and sodium.
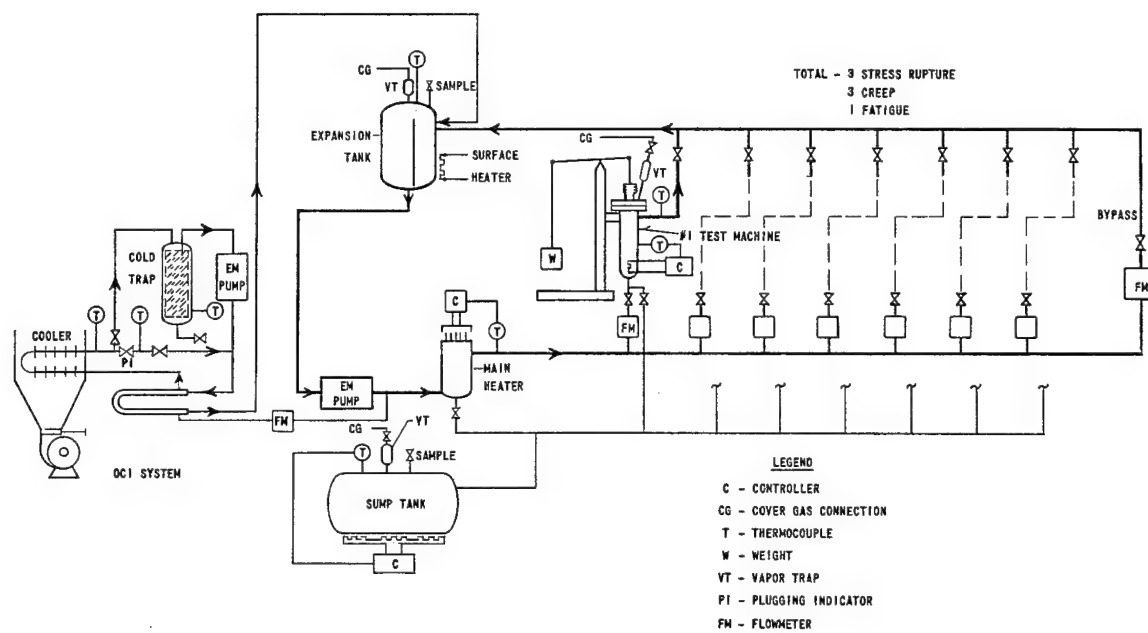
Figure 1. – Flow sheet of physical properties test loop.

III. PROBLEMS RELATED TO COMPATIBILITY TESTING

Louis Rosenblum, Chairman
NASA Lewis Research Center
Cleveland, Ohio

A. HEAT TRANSFER AND FLUID FLOW

Paul A. Lottes
Argonne National Laboratory
Chicago, Illinois

H. W. Hoffman
Oak Ridge National Laboratory
Oak Ridge, Tennessee

BOILING STABILITY

Paul A. Lottes⌋ ⌈Argonne National laboratory →
273

Many of you are probably wondering what connection there is between corrosion testing and boiling stability. As we will see shortly, the problem of boiling stability arises in any apparatus that produces vapor by boiling a liquid. If boiling instability shows up in a particular system, there will be flow oscillations, pressure surges, and temperature excursions and, generally speaking, the system will not be in steady-state operation. Further, instruments adequate to measure flow under steady-flow conditions will not indicate the true test conditions.

In liquid metal corrosion tests, flow instability would upset temperature and concentration gradients, thus affecting mass transfer, disturb impurity accumulations at liquid-vapor interfaces, affect the entrainment of liquid droplets in vapor region, and change the location of sensitive corrosion sites in the system. Thus in order to determine corrosion rates and mechanisms, you must ensure steady-state flow. That means preventing boiling or condensing flow instabilities.

The general method of attacking the problem of instability is to avoid rather than to solve it. In order to avoid it, we must first have some basic understanding of the cause. Most of the information or experience with instability which will be described has been obtained with boiling water systems. As shall be seen, however, the test fluid is unimportant. We are primarily interested in the physical properties of the fluid, such as latent heat of vaporization, change in specific volume due to vaporization, and specific heat.

In order to understand our stability problem we should first discuss some relations that describe a boiling fluid flow system. I might add at this point that although a mathematical model for two-phase flow systems does not exist yet, we can describe the process well enough to understand the steps required to avoid instability.

Vapor quality or flow rate ratio x may be related to the heat input Q and the flow rate W by

$$x = \frac{Q}{W_t h_{fg}} - \frac{c_p(T_{sat} - T_{in})}{h_{fg}} \tag{1}$$

where the second term on the right side of the equation is a measure of the quantity of heat required to raise the liquid up to the boiling point; and from a mass balance

$$\frac{V_g}{V_f} = \left(\frac{x}{1 - x}\right)\left(\frac{1 - \alpha}{\alpha}\right)\left(\frac{v_g}{v_f}\right) \tag{2}$$

257

which relates the velocity ratio of vapor and liquid V_g/V_f to the weight flow ratio $x/(1 - x)$, the flow area ratio $(1 - \alpha)/\alpha$, where α is the fraction of flow area occupied by the vapor, and the specific volume ratio v_g/v_f. It should be noted that x is the flow rate ratio, that is, the number of pounds per unit time of vapor flowing for each pound per unit time of mixture. The flow rate ratio has the same value as the "thermo-dynamic quality" when the velocity ratio is unity.

The average density, weighted by flow area, of the mixture ρ for any flow passage cross section is defined by

$$\overline{\rho} = \rho_f(1 - \alpha) + \rho_g\alpha \tag{3}$$

From a simple pressure balance on a vertical heated pipe that carries a boiling fluid within it, we get

$$\Delta P_t = \Delta P_f + \Delta P_a + \Delta P_h \tag{4}$$

The three terms on the right are friction pressure drop, momentum pressure drop, and hydrostatic head. The first term will be discussed later; it is strictly a pressure loss term. The second term is not a loss, but rather a change in pressure due to the acceleration of the mixture as boiling takes place along the channel. In theory at least, a part of this pressure change may be recovered at the end of the heated channel as the mixture expands into a larger area. Usually, however, most of the pressure change is not recoverable. The third term is simply a measure of the weight of the mixture contained within the pipe. For a horizontal pipe, of course, this term would be zero.

The momentum pressure change is described by

$$\Delta P_a = r \, \frac{G^2}{g_c} \tag{5}$$

where

$$r = v_f\left[\frac{(1 - x)^2}{1 - \alpha} + \frac{x^2}{\alpha}\left(\frac{v_g}{v_f}\right) - 1\right] \tag{5a}$$

The term r is called an acceleration multiplier. This equation was developed by Martinelli and Nelson in a pioneer paper on boiling (Trans. ASME, 1948, p. 695). The first term inside the bracket is a measure of the liquid momentum leaving; the second term, the vapor momentum leaving; and the third term, the fluid momentum entering.

The hydrostatic head is defined as

$$\Delta P_h = \int_0^l \rho \, dl = \int_0^{x_0} \rho \, dx \qquad (6)$$

At this point, we should stop and consider fluids that have a very large change in specific volume due to vaporization. Under these conditions, equation (2) tells us that very small values of x will yield large values of α. In other words, in a flowing system with homogeneous flow ($V_g = V_f$), a small vaporization rate x will give rise to a large volume change. Suppose, for example, that we are using a fluid whose liquid to vapor density ratio is 100. Further imagine the liquid and vapor velocities to be equal ($V_g = V_f$). Then for a value of $x = 0.01$ or 1 percent vaporization, the flow area for the liquid ($1 - \alpha$) will be reduced to 0.5 or 50 percent of its original value.

Now with an appreciation of the significance of equations (1) to (5), we are in a position to look at some old data and examine the behavior of two-phase flow systems. Some early data taken from a natural circulation boiling loop are shown in fig. 1. The inlet velocity is correlated as a function of steam void and is independent of pressure in the loop up to moderate pressure levels. This indicates that the steady-state behavior of the system is controlled by the amount of vapor present by volume. The amount of vapor is a measure of the volumetric vapor flow, which is controlled by the forces or pressure drops resulting from this flow. In other words, when the volume fractions were identical, the system behaved in the same manner, independent of pressure.

A sample of two-phase flow friction data is shown in fig. 2. The ratio of boiling friction pressure drop to nonboiling friction pressure drop at the same flow rate $\bar{R}$ is correlated as a function of the exit steam volume fraction and is also independent of system pressure. Incidentally, these data turned out to have too high a value because of a pressure loss near the boiler exit caused by a constriction in the flow passage from a faulty weld. The results, however, still indicate the lack of a pressure effect.

Values of the acceleration multiplier r calculated from eq. (5a) are shown as functions of the exit steam volume fraction for various slip ratios and pressures in figs. 3(a) and (b), respectively. The acceleration multiplier increases greatly with an increase in steam volume fraction but is almost independent of the slip ratio. This means that the acceleration pressure drop is large because of the change in momentum of the liquid which is to be expected.

In fig. 3(b), the effect of pressure on the acceleration multiplier is shown to be not too important for values of exit steam volume fraction less than 0.8, because most of the momentum is tied up in the liquid.

Measured and calculated (eq. (3)) values of mean density ratio, defined as the weight of the mixture in the boiling channel divided by the weight of an equal volume of water, versus exit steam volume fraction are shown in figs. 4(a) and (b). Again, it may be seen that pressure effects below 1000 psia are negligible. Even at pressures of 2000 psia, there is little effect. The reason is, of course, that the vapor density is small until the vapor pressure reaches high enough values; at 2000 psia the vapor is about 14 percent as dense as the liquid. The critical pressure (3206 psia) line is horizontal since the vapor and liquid densities are equal at the critical pressure.

Let us now look at a forced circulation system with flow of a boiling liquid through a uniformly heated pipe or channel. The pressure drop curves for such a system are shown in fig. 5. The right-hand curve that goes through point 3 is the frictional pressure drop curve for all liquid flowing through the channel. The left-hand curve is the frictional pressure drop curve for all vapor flowing through the channel.

Imagine that we are operating at point 3 in fig. 5. If the flow is reduced while the power input is held constant, we will soon arrive at a condition where boiling will start at the channel exit. Any further reduction in flow will cause more steam to be produced. The increasing steam rate causes increased momentum pressure changes and higher friction factors. The decreasing flow tends to offset some of these effects, but the net change in pressure may either increase or decrease as shown. Experimental verification of this behavior, in a single tube with a diameter of 1/4 inch and a length of 2 feet, is given in fig. 6.

In 1938, Ledinegg analyzed this peculiar looking curve. He made certain simplifying assumptions in the system, such as equal vapor and liquid velocities, constant friction factor, density equal to homogeneous density, etc., and wrote the equation of the multivalued pressure drop curve shown in figs. 5 and 6. The details can be found in the "Reactor Engineering Handbook," RH-2, Vol. 3 (Engineering) or in "Progress in Nuclear Energy, Series IV, Technology, Engineering and Safety," Pergamon Press (1961). On page 17 of the latter text, a detailed derivation is given. Ledinegg found that when he differentiated the pressure drop to get the inflection point, the conditions necessary for a zero slope at the inflection could be written in terms of channel geometry and fluid pressure. In other words, for a given system, it is sufficient to know only the length to diameter ratio L/D, the friction factor, and the pressure. The results of Ledinegg's analysis for water are shown in fig. 7. A similar set of curves could be generated for any other fluid. Assume, for example, that our system operates at 100 psia with an fL/D ratio of 10. The curve tells us that we will get a multivalued pressure drop curve if the inlet subcooling is greater than about 24 Btu per pound. In other words for water, under these conditions, if the inlet temperature is less than the boiling point temperature by 25° F, we have a good chance for boiling instability.

The reason for the instability is the fact that there is more than one value of flow for a given value of pressure drop. In a parallel flow device

260

with many heated channels connecting two plenums, the flow rate in any one of these channels is set by the pressure drop between the plenums. This means that the value of ΔP_t in fig. 5 is the control variable. If the ΔP_t drops lower than the minimum point of curve 1-2-B-3, the flow will stop and come out of both ends. This is the condition that we want to avoid. The result of this condition is violent flow oscillation, or chugging, and if the power is high enough the element may go into film boiling and physically melt during these flow oscillations. If the power is low enough, the system may just continue to chug. The characteristics of such a system are shown in fig. 8. The upper curve does not intersect the horizontal line representing the "available" pressure drop. Since the upper line always exceeds this available pressure, steady-state flow is impossible and the flow would pulsate. This is the kind of action seen in a common coffee percolator.

Figure 9 shows how the flow and temperatures within a system can oscillate for a vertical natural circulation boiler. This was taken from a report by Wissler, Isbin, and Amundson (AIChE Journal 2, 157 (1957)). It was felt that a multivalued flow relation such as shown in fig. 5 was the cause of the flow oscillations in many of our boiling loops. We discovered much to our amazement that this was not always the case. Results for a natural circulation boiling loop are shown in fig. 10. The curves were measured after we put a pump in the system. None of the curves are multi-valued. Yet the system did go unstable. The cause of instability in this type of system is recognized today as being related to the momentum of the liquid in the entire flow loop. There are many publications in the heat-transfer literature covering this problem.

An example of flow oscillations picked up by fast response instrumentation is shown in fig. 11. Some of the high-frequency pulses turned out to be due to mechanical vibrations of the pressure transducer. (This latter fact is an example of the ever present need to know exactly what an instrument is measuring.) In this case, since we did not care what frequencies were involved, but rather what power caused the system to start oscillating, we continued to use the transducer as a "flow oscillation detector."

Natural circulation flow oscillations can cause misinterpretation of experimental data. An example of misleading instrument readings due to flow oscillations can be given by examining the case of a simple natural circulation flow loop shown in fig. 12(a). Pressure drop characteristics shown in fig. 12(b) for the heated annular section were measured by pumping the fluid through the annulus. The horizontal line represents the pressure drop available and is equal to the hydrostatic head in the downcomer leg of the loop less any small friction losses external to the heater. The point of intersection of the measured curve with the horizontal line is the point where the pressures are balanced around the closed loop and is by definition the operating point at the given value of power.

By plotting these operating points as flow rate versus power as shown in fig. 12(c), we have a so-called predicted flow characteristic curve. The measured flow rates agree with the predicted flow rates only for powers

less than 8 kilowatts per liter. Flow rates were indirectly measured by a heat balance method. The temperature decrease in the recirculating liquid was measured with a thermopile. This decrease was due to heat losses and the injection of cold make-up water. As long as the flow was steady (for powers less than 8 kw/liter as shown by the recording of an electromagnetic flow meter - see fig. 12(d)), the measured values were probably correct. During flow oscillations, however, the time average flow as indicated from a heat balance did not agree with the true flow.

A good description of the stability problem and the use of orifices to prevent flow oscillations is given in Professor Bonilla's text book, "Nuclear Engineering." I would refer you to this text for an extensive treatment of the problem. The effect of an inlet orifice can be inferred from fig. 9. It is possible to provide an orifice such that the sum of the orifice pressure drop and the multivalued pressure drop from the channel will yield a single-valued curve. For this condition, only one flow would be possible for a given value of pressure drop and the flow would therefore be steady. The practice of making sure that the flow is steady by providing an orifice at the inlet to the boiling channel is called "orificing."

Before concluding, I should mention that condensing a vapor causes many of the same problems as boiling a liquid. If the ratio of steam volume to total volume in a system is small, then sudden changes in condensing rate can cause large pressure changes. We have found in our systems that pressure control is difficult when condensing at system pressure, but control is adequate when steam is throttled out of the system, condensed externally and added back to the system in the liquid state. Typical pressures recorded with these systems were 600 psia plus or minus 15 psi for the former case and 600 psia plus or minus 1/4 psi for the latter.

In summary, there are two types of boiling instability. The first type is related to a multivalued pressure drop characteristic of a parallel flow system. The second type is tied up in momentum changes, etc., in a closed loop of flowing liquid and vapor.

The first type can be avoided in some cases by orificing. The second type can be avoided by providing a pump rather than using natural circulation - and including orificing as a safety measure.

In order to provide steady flow in a boiling system, the ideal design would use a high head pump, an inlet orifice, plenty of vapor volume in the system, and no compressible vapor or gas spaces between the pump and the heated channel.
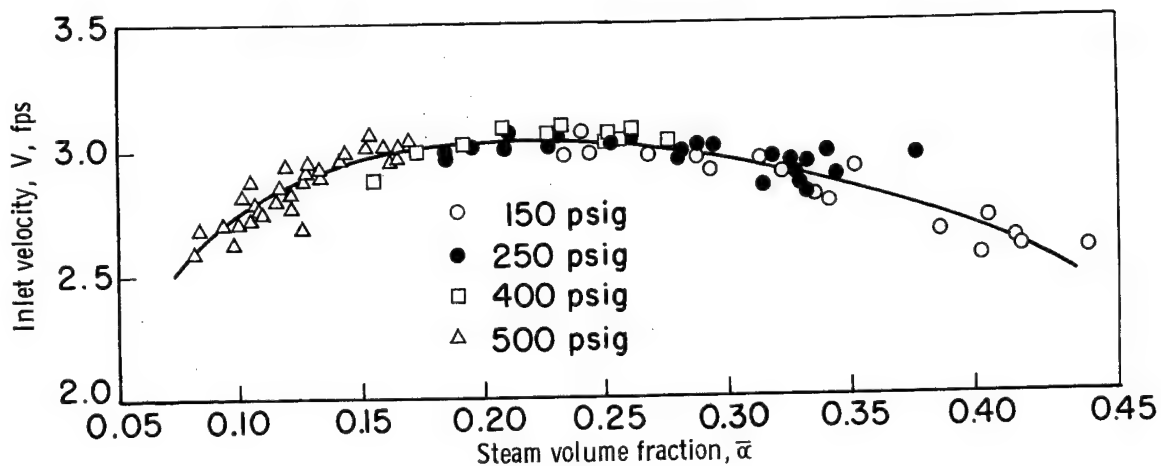
Figure 1. - Effect of steam volume fraction on inlet velocity.
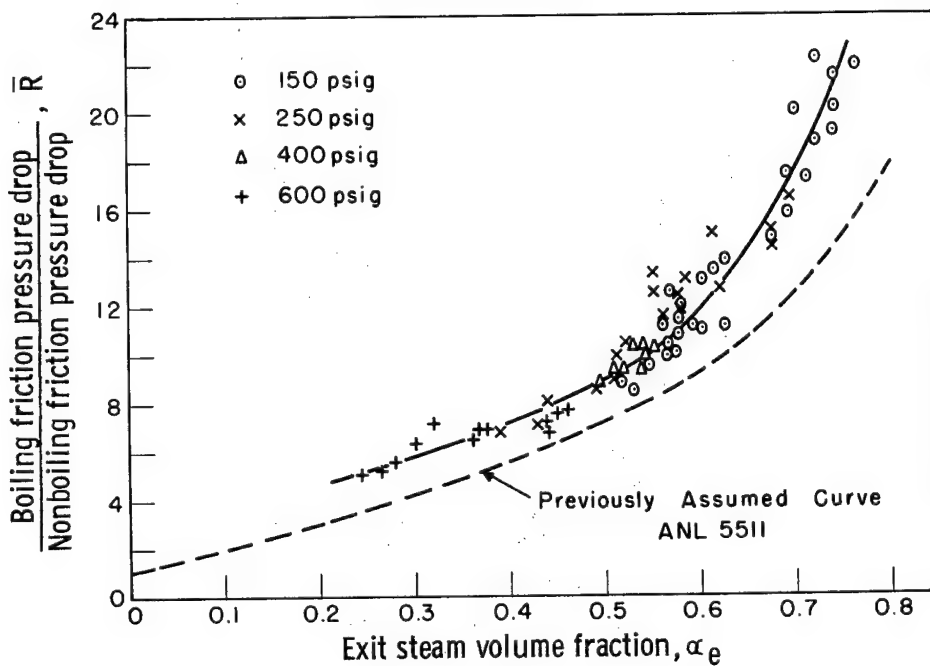
Figure 2. - Effect of steam volume fraction on friction
pressure drop.

(a) With variation in slip ratio.

(b) With variation in pressure.
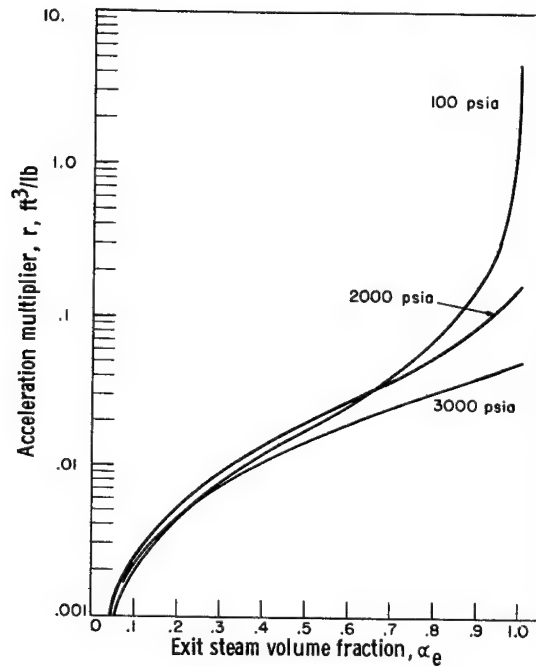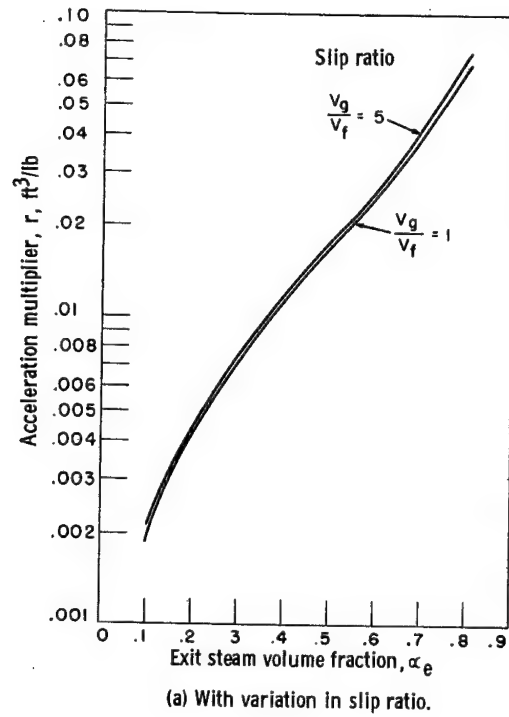
Figure 3. – Effect of steam volume fraction on
acceleration multiplier.
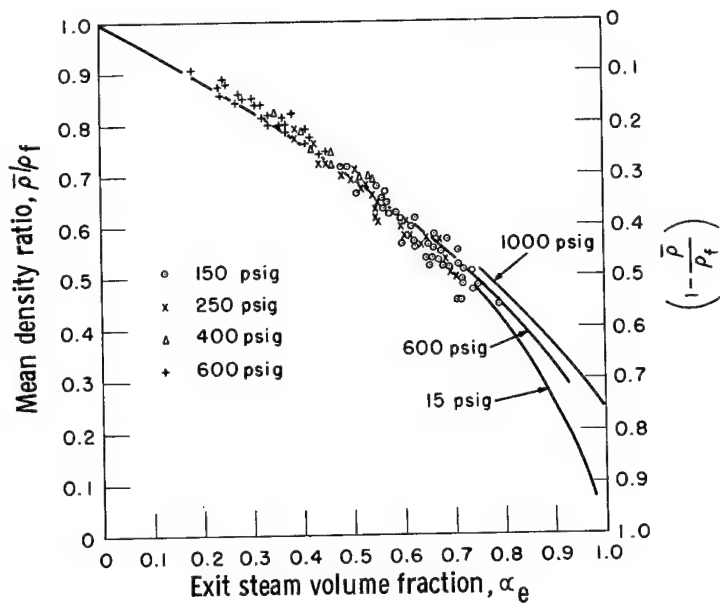
(a) For values measured over a pressure
range from 150 to 600 psig.
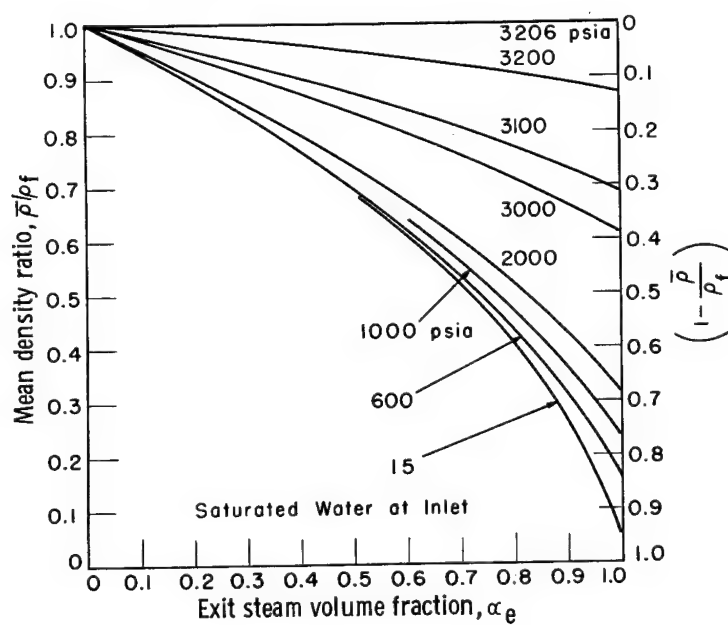
(b) For values calculated over a pressure
range from 15 to 3206 psia.

Figure 4. – Effect of steam volume fraction on
mean density ratio.
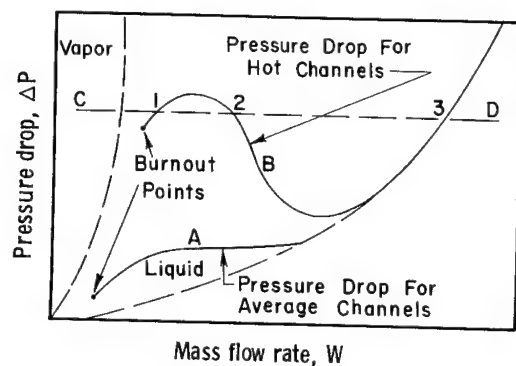
Figure 5. – Pressure drop map for two phase flow burnout conditions in parallel channels.
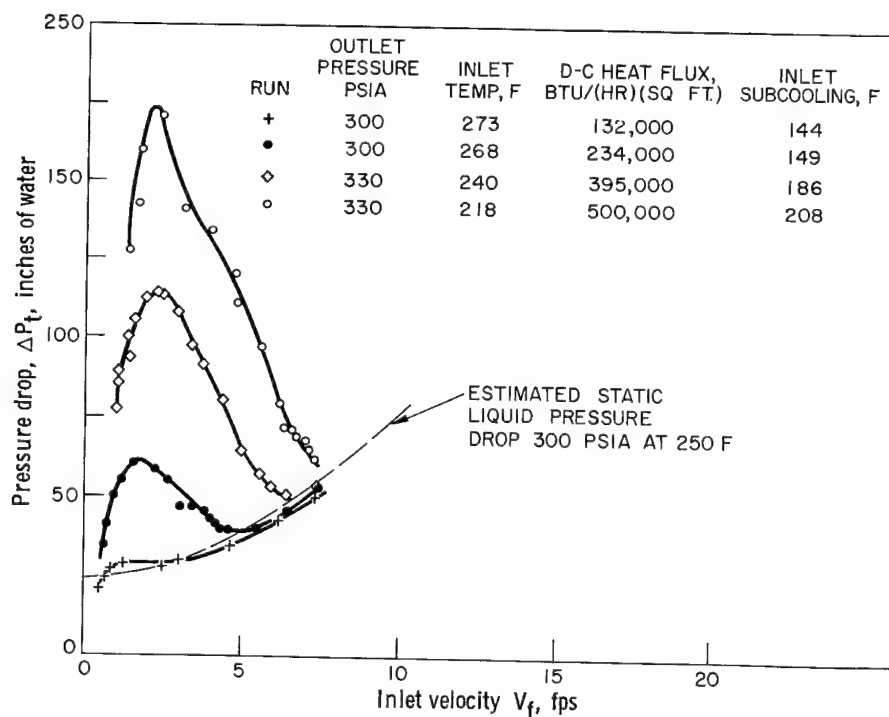
Figure 6. – Effect of inlet velocity on pressure drop for various heat fluxes for two phase flow in a single tube.

266
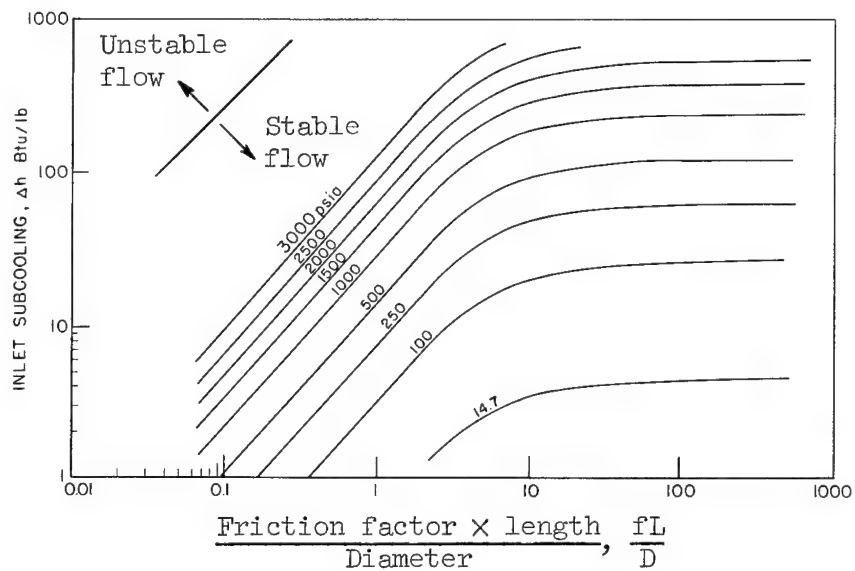
Figure 7. – Two-phase flow stability criteria for water.
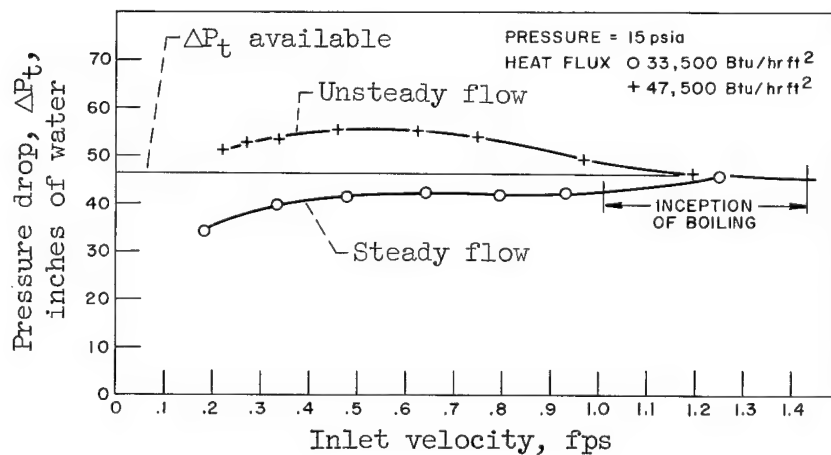
Figure 8. – Hypothetical representation of stability criteria.
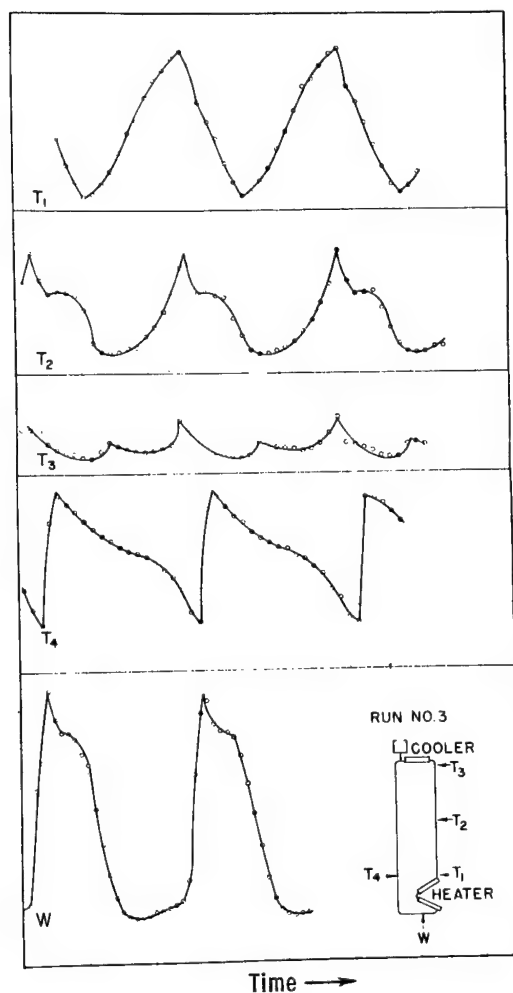
Figure 9. - Representative temperature and flow oscillations in vertical natural circulation boiler.
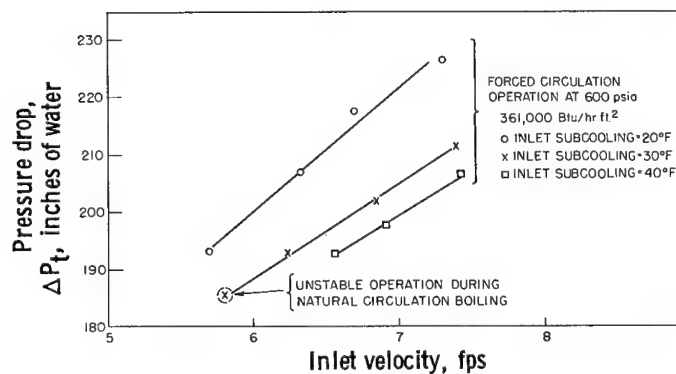
Figure 10. - Effect of inlet subcooling on pressure-drop-flow curves for natural circulation loop.

268

STABLE

TRANSITION

|← 1 MINUTE →|

UNSTABLE

Time
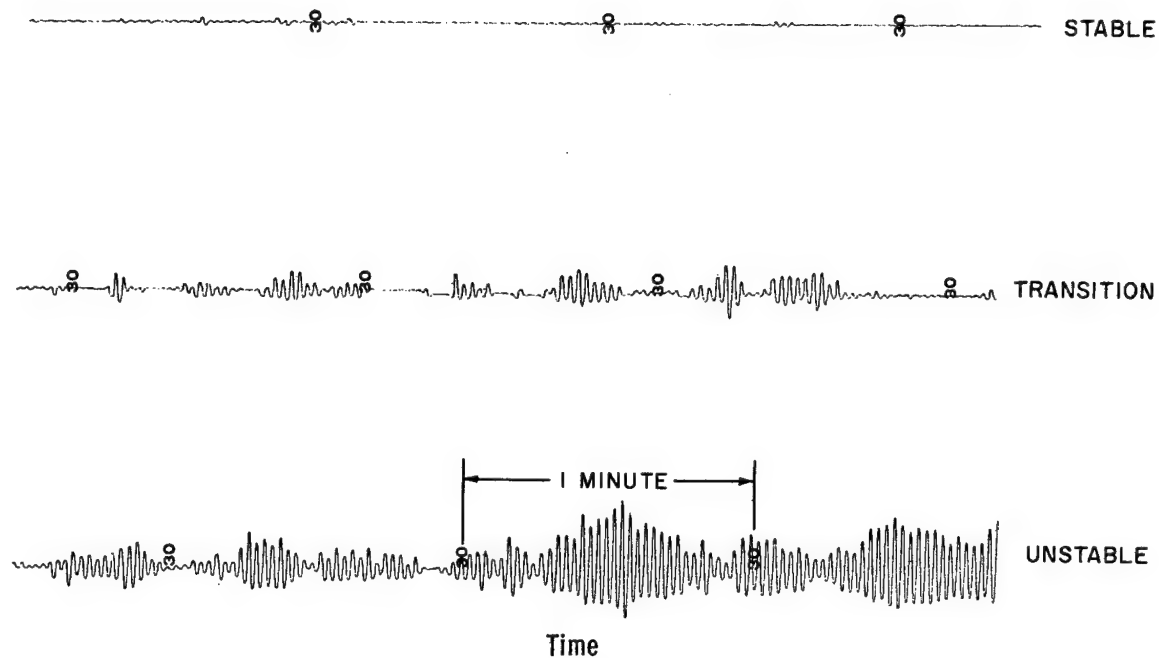
Figure 11. – Representative flow oscillations indicated by fast response pressure transducer in a natural circulation loop.

WATER LEVEL

CALROD
0.496 IN OD

GLASS
TUBE

DOWNCOMER
1 IN. OD

36 IN.
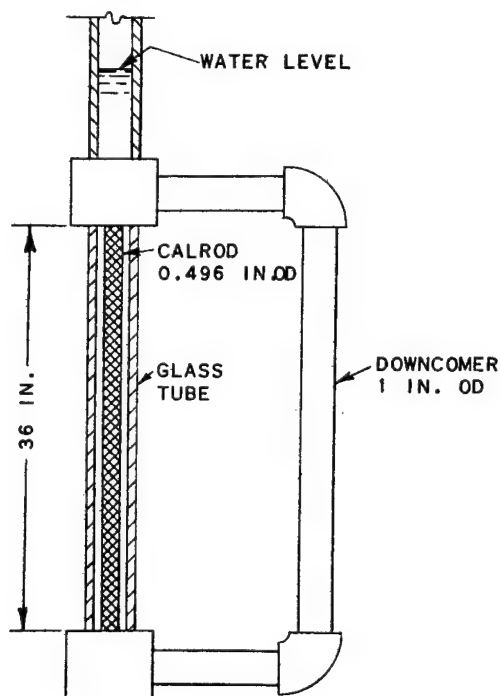
(a) Schematic diagram of natural circulation loop.

Figure 12. – Effect of flow instability on data interpretation.
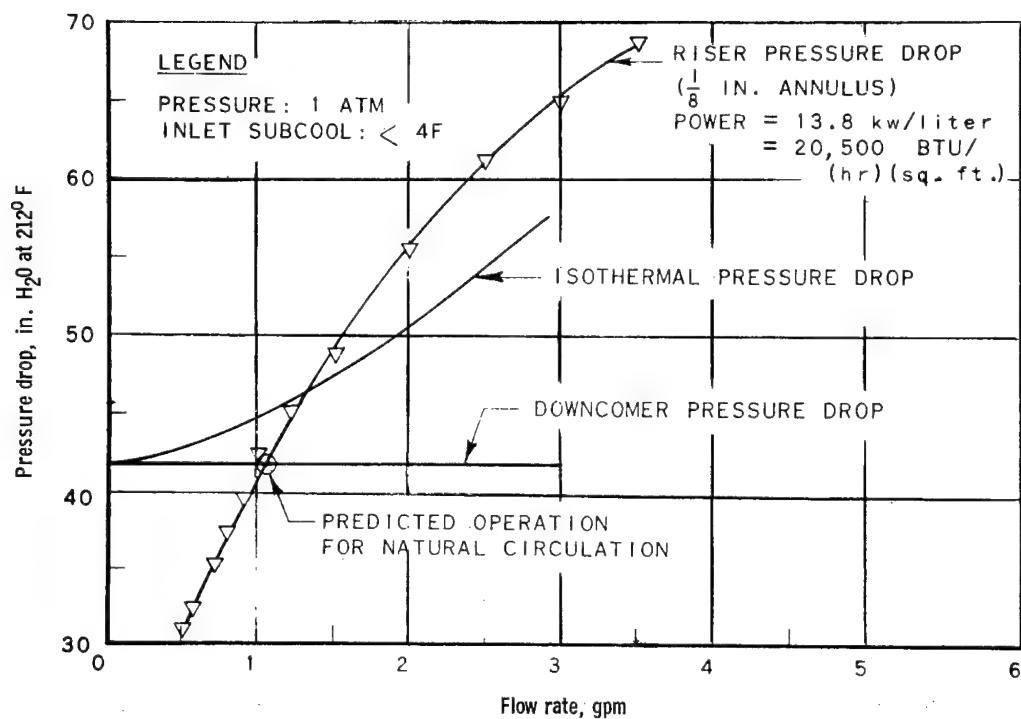
(b) Loop pressure drop characteristics.
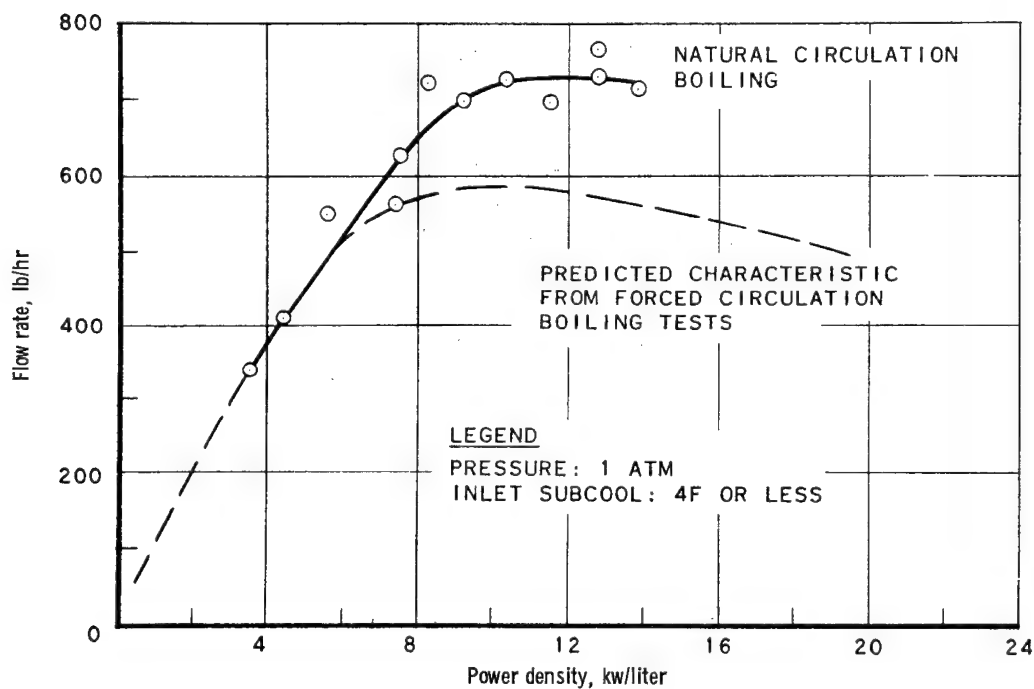
(c) Comparison of measured and predicted flow characteristics.

Figure 12. – Continued. Effect of flow instability on data interpretation.
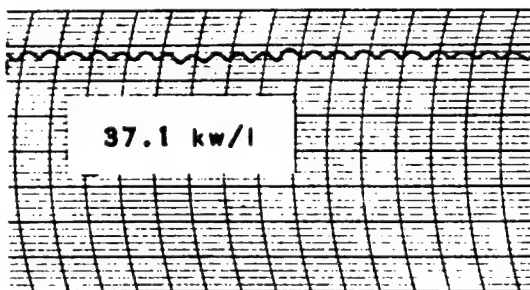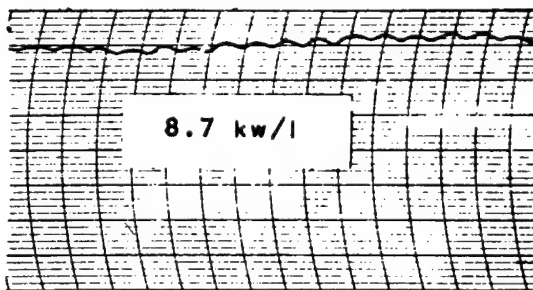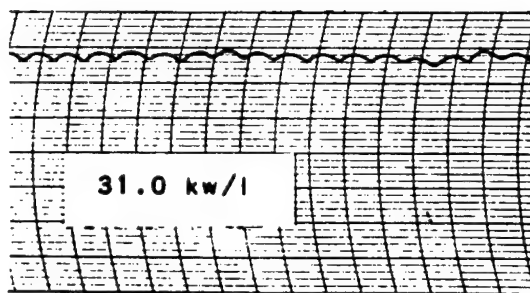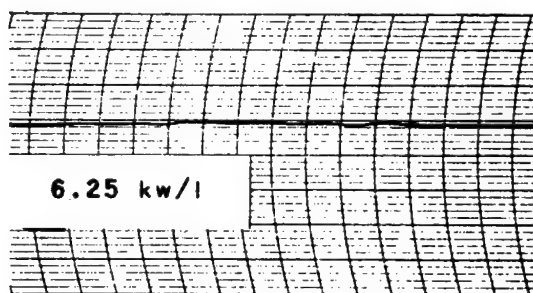
(d) Electromagnetic flow meter traces.

Figure 12. – Concluded. Effect of flow instability on data interpretation.

HYDRODYNAMIC AND THERMAL INFLUENCES IN

CORROSION STUDIES

H. W. Hoffman   [Oak Ridge National laboratory] →305

INTRODUCTION

The transfer of heat or mass between a flowing fluid and a bounding surface depends intimately on the hydrodynamic situation existing for the specific geometry of concern. In general, the equations describing the motion of the fluid with simultaneous transport of heat and/or mass are mathematically intractable without linearizing assumptions. For certain cases, as for example where the flow is laminar — i.e., a fluid element follows a predictable path without distortion (curvilinear motion) and the primary force acting on the fluid is dissipative (viscosity) — analytic solutions to the transport problem are possible. Even here, however, for what appears to be the relatively simple case of heat transfer with laminar flow around the leading half of a circular cylinder, there are many approaches and many answers. Spalding and Pun,[1] in a recent summary, report 15 methods for predicting the distribution of the heat-transfer coefficient in this situation and find wide differences in the coefficients predicted. If the flow is turbulent — wherein the fluid element is subject to random velocity fluctuations in all directions and inertial forces are significant — difficulties in analytic solution are even more severe and resort is made, in the most promising approach, to a statistical characterization of the motions and interactions of fluid elements.

Since this complexity exists for flow even in the simplest situation of a straight duct of circular, uniform cross section, it becomes the function of the experimenter to provide both the engineering data needed for technological advance and the fundamental data useful to the theoretician. By his work, the experimenter in no way deprecates the efforts of the formidable talent which continues to attack the theoretical problem. However, the researcher in heat transfer, or in corrosion, must have more than a casual knowledge of the flow situation which exists before he even makes his measurements. For example, the experimenter looking to the determination of coefficients of mass or heat transfer has long spent what may seem to be a disproportionate time on the design of the entrance region to his test channel and on the elimination of other extraneous upstream disturbances. In contrast, the corrosion engineer has generally been unaware of such problems and, as a consequence, has often found himself at a loss to

explain his results.

Rather than attempting to point out explicitly the many difficulties which may arise in corrosion experiments due to the neglect of the hydrodynamic aspects of the design, this paper attempts to high light some of the problems through a description of a number of studies within the experience of the author. In all cases, flow was either through circular pipes or along flat surfaces; the fluids — uranyl sulfate solutions, molten salts, and liquid metals — which are ofttimes termed exotic, are normal in their flow characteristics.

SINGLE-PHASE, STEADY FLOW

During the years in which the homogeneous reactor concept was under development at the Oak Ridge National Laboratory, a significant portion of the total effort was directed to the study of the corrosive effects of uranyl sulfate solutions on containment materials, principal among these being type 347 stainless steel.[2] The experimental program was well-conceived and comprehensive; included among the test variables were temperature, oxygen concentration, uranyl sulfate and sulfuric acid concentrations, corrosion inhibitors, flow rate, exposure time, and, though not initially recognized as such, test-section geometry. With this number of variables, extracting valid conclusions during the progress of the program was difficult, particularly in the initial stages of experimentation. To be able to obtain pertinent results for use in directing future studies was obviously of economic importance for a research effort as grand as this. Accordingly, a number of test-section geometries were conceived and used. Since our concern in this paper is with hydrodynamic influences, the discussion following will consider primarily only that variable without any intent to minimize the importance of other effects.

The experimental apparatus assembled for these studies is shown schematically in Fig. 1. A uranyl sulfate solution was circulated through a number of parallel channels containing the corrosion test specimens by a canned-motor centrifugal pump. The pressurizer served several functions, the principal one being to provide the loop overpressure; this was accomplished by control of the fluid temperature in the pressurizer. The

multiple-passage loop allowed the simultaneous exposure of several sets of test specimens at different flow conditions. Flanged construction facilitated the insertion and removal of the test samples which were positioned within a split-channel holder as shown in the photograph of Fig. 2 and in more detail in Fig. 3. Two holders could be located in series in each test channel. There is some disadvantage to this loop design in that (1) the concentration of corrosion products in solution increased with length of exposure (i.e., one of the initial conditions was variable), and (2) the entrance condition [both as to flow and corrosion-product concentration] for the second of two holders in a channel was ill-defined.

Two types of specimens were used in these studies: a cylindrical pin, and a small flat plate termed a coupon. With the first of these, the pins were mounted "in-line" in the direction of flow with a 1-in. spacing between pins. While a variety of materials could thus be exposed at a uniform bulk fluid velocity, the hydrodynamic environment in which the pins existed was complicated by the wakes arising from the pins themselves. In the second geometry, the coupons were mounted so as to form a septum down the center of a duct of rectangular cross section, thus defining two parallel flow channels. This arrangement yielded a better flow situation even though some uncertainty remained due to the secondary flows generated in the corners of the channels. Since the flow passages were of low aspect ratio (height of specimen to gap width), it was possible that the influence of these secondary flows extended over a significant portion of the coupon surface. The effect of fluid velocity was investigated by tapering the flow channel in the flat plate holder such that the velocity increased uniformily along the passage length. With this scheme, it was possible to obtain velocities in a single experimental exposure which ranged from about 7 ft/sec at the inlet to as high as 80 ft/sec at the outlet. Again, however, a further extraneous hydrodynamic factor was introduced in that with a convergent geometry there results, not only a reduced turbulence level in the flow, but also an increased shear.

In looking for velocity effects, attention was centered on the tapered-channel system, since this arrangement yielded the greatest return in data as a function of time. Since it was known that at temperatures above 225°C

a heavy scale formed on the surface which provided essentially complete protection against further corrosion, the data were examined in regard to the effect of the surface shear stress on the formation and/or removal of this film. It was postulated that in the initial period of exposure the corrosion rate would be high and uniform over the entire surface. As the corrosion-product film developed, the corrosion rate would then decrease and, in the absence of hydrodynamic effects, remain uniform over all the coupons. However, if shear at the fluid-film interface did remove the protective coating in whole or part, some velocity would be observed above which the corrosion rate increases to a limiting value equal to the initial corrosion rate. This transition velocity would depend on the strength of the bond between the film and the metal substrate.

A typical set of data obtained under nearly identical experimental conditions is shown in Fig. 4, where the average corrosion rate per coupon side is given as a function of the square of the average bulk velocity at each coupon.* The corrosion rate was calculated from the weight loss of the coupons after any remaining corrosion-product film had been stripped from the surface. As seen, these results suggest a very significant effect of surface shear consistent with the hypothesis described above. Thus, for short exposures (Run A-41), the corrosion rate was high and fairly uniform. Some discrepancies exist, as in the break in the curve between the fifth and sixth coupon and in the low corrosion rate for the first coupon. Discussion of these points remains speculative and will not be considered further in this paper. As the length of exposure increased (50 through 1000 hr), the corrosion rate decreased progressively and became essentially independent of velocity at velocities below about 30 ft/sec. Above 40 ft/sec, for all exposure times, the corrosion rate increased abruptly and was

---

* The shear stress at the wall can be written as $\tau_o = K \bar{u}^2$, where K is a function of the Reynolds modulus and the fluid density. While the velocity varies with distance along the channel, the Reynolds modulus is essentially invariant; and K, in an isothermal system, is constant. Since the corrosion rate data are derived from the total weight loss of each coupon, it is convenient to define an average bulk velocity, $\bar{u}_a$, to which the coupon was exposed. This velocity was taken as the arithmetic mean of the calculated velocities at the leading and trailing edges of each coupon and was used in place of the local bulk velocity, $\bar{u}$, in calculating the shear stress. Thus, in Fig. 4, $\bar{u}_a^2$, rather than τ_o, is plotted as the abscissa.

effectively equal to the rate at initial exposure. The data shown here, along with results from other similar experiments, led to the concept of a "critical velocity" with important effect on the design of aqueous homogeneous reactors.

Visual observation of the coupons at the conclusion of a run gave further evidence to the stated hypothesis as to surface shear effects in dynamic corrosion. An example is shown in Fig. 5. It was found that coupons at the outlet end had little or no film on them; in the illustration, corrosion proceeded to the point of total loss of metal. Upstream the film thickness increased progressively to a maximum near the inlet. While not present in the data of Fig. 4, the initial coupon often showed a higher rate of corrosion than was found for succeeding coupons. In this region, an entrance condition existed with the associated high shear at the fluid-solid interface. Again, a verification of the effect of shear is indicated.

It is interesting to note that in absolute magnitude the shear force is low; e.g., at a velocity of 55 ft/sec, τ_o is calculated to be of the order of only 0.04 psi. Fluid shear at the wall thus appears to act on a microscopic scale, removing solid corrosion products as they form. It is possible, of course, that a protective film formed at below critical velocities could be removed when the velocity exceeded the critical value; the rate of such removal would probably be low. Experiments along these lines were not specifically performed.

A further experiment utilizing a circular duct was devised to establish the extension of the flat-plate results to another geometry, as well as to define more clearly entrance region influences. This geometry was in better agreement with normal reactor piping and avoided the problems of edge effects and turbulence-level reduction. The velocity was, of course, constant along the length of the specimen; and it was necessary to obtain data at several different velocities.

The experimental apparatus utilized in these studies is as described above with the exception that the specimen holder was of circular cross section. The specimens themselves were 1-in. long sections of type 347 stainless steel tubing with 0.15-in.-ID and 0.025-in.-wall thickness; these

were mounted in-line in the holder to form a "continuous" tube. Again, the corrosion rate was established by the weight loss of the individual sections.

Data were obtained for exposure times of 10, 50, 100, and 200 hr at velocities of 10, 30, and 50 ft/sec; experimental conditions were identical with those for the flat plate studies. The results are presented graph-ically in Fig. 6. Since entrance conditions prevailed, the corrosion rate plotted is the far-downstream, asymptotic value. In general, the data show the same characteristics as observed in the coupon experiments with two notable exceptions: (1) the corrosion rate in the tubular specimens appears to be approximately a factor of two higher than with the coupons, and (2) the critical velocity seems to be in the range of 55 to 65 ft/sec rather than the 30 to 40 ft/sec found with the coupons. The experimental program was discontinued before either of these two discrepancies could be resolved. One can speculate that there are hydrodynamic origins for both of these factors deriving perhaps from the difference in the Reynolds modulus, and hence in the boundary-layer thickness and in the turbulence level, at the same velocity in the two geometries. Lacking additional data, it was not possible to pursue these particular results further.

Some further results of interest can be obtained by considering the axial variation in the corrosion rate for a typical run. This is done in Fig. 7 in which the mg/hr[*] of metal loss from the inside tube surface is plotted as a function of the distance from the channel entrance for an exposure of 100 hr with a fluid velocity of 50 ft/sec. It is noted that the corrosion rate is very high at the entrance and then falls off to an asymptotic value of about 0.55 mg/hr at the end of the test channel. This pattern is typical of that observed in the entrance region — defined as the region of boundary-layer development — for the transfer of heat, mass, or momentum. At the inlet, where the boundary layer is of "zero" thick-ness, the resistance to transfer is low; and the transfer rate is high. As the boundary thickens, the resistance increases; and the transfer rate

---

[*]The ordinate, mg/hr, can be converted to mils/yr through multiplica-tion by the constant 129.9.

correspondingly decreases. The distance required for the full development of the boundary layer is not a simple function of the flow parameters when turbulent flow exists; in normal practice, the entrance length required to attain a fully developed velocity profile is taken to be greater than 60 tube diameters. On the other hand, Deissler[3] has found theoretically that the friction factor (which may be related through analogy[4] to the heat-transfer and mass-transfer coefficients) is fully developed at values of L/d of as little as 10. The results of the experiment shown in Fig. 7 are at least consistent with this range.

A second phenomena of interest is also noted in Fig. 7. Ignoring for the moment the lines drawn through the data points, it would appear that considerable scatter exists in the data presented. However, in the light of the discussion above on entrance-region phenomena, a reasonable explanation of this "scatter" can be advanced in terms of boundary-layer interruption due to mismatching of the individual sections comprising the tube. At each step in the wall, a perturbation is introduced which results in the break-up and reinitiation of the boundary-layer flow. Thus, the corrosion rate in the section downstream of the interruption will be somewhat greater than that anticipated if the surface were even with the preceding section. This is indicated by the dashed lines in Fig. 7. Since the diameter mismatch is probably small for these specimens, the effect is damped fairly quickly; in some runs, interruption of the boundary flow was sufficient to return the corrosion rate to essentially the inlet value. Where the geometry change is a slight step enlargement in the tube diameter, the eddy created in the wake of the upstream section will also contribute to a higher corrosion rate for the downstream section.

SINGLE-PHASE FLOW WITH THERMAL OSCILLATIONS

With the addition of heat transfer, the study of corrosion is further complicated. Again, rather than a general discussion of the problem, two specific though related experiments will be described; in both of these investigations, the heat transfer was oscillatory in nature.

Thermal oscillations at an interface can derive directly from the flow of a coolant adjacent to a heated wall; i.e., turbulent eddies at

bulk-fluid temperatures, which are known to penetrate possibly as deeply as the laminar sublayer, can cause rapid fluctuations in the local rate of heat transfer. In combination with this, there may exist gross flow instabilities which originate in the geometry as with divergent channels or in the heat-transfer mechanism itself as with boiling. When, for some fluid-fuel reactors, there also occurs an adverse temperature profile (i.e., the highest temperature occurs where the mean velocity is lowest), the temperature fluctuation at the wall can assume a significant magnitude.

The two experiments discussed below were both intended to investigate the influence of temperature oscillations at the fluid-wall interface on the wall material itself; this is to be distinguished from studies in which the "bulk" wall temperature is cycled. The thermal fluctuations were generated by different means, and the wall thickness was found to have a significant effect on the results. In both cases, a fused fluoride salt mixture $NaF-ZrF_4-UF_4$ (56-39-5 mole %) with a melting temperature of 986°F was the heat carrier and Inconel was the wall material.

In one of these studies, Keyes and Krakoviak[5] devised a thermal pulse generator (shown in Fig. 8) which utilized two reciprocating pistions driven in phase opposition to provide approximately sinusoidal gas-pressure oscillations to a pair of chambers holding the working fluid at two temperature levels. Thus, alternate slugs of "hot" and "cold" liquid were injected into a common line leading to the test section. In operation, since one pulse chamber emptied while the other filled, constant flow was maintained in the test section. Frequencies in the range of 0.1 to 10 cps were possible. The fluid leaving the test section, as shown in Fig. 9, was again divided with one stream being pumped to a forced-convection air cooler wherein it was cooled to 1150°F and the other stream being pumped to an electrically resistance heated section which raised the temperature to 1650°F. At 0.1 cps, fluid temperature amplitudes in excess of ±250°F were generated; the amplitude decreased at higher frequencies.

Typical test sections are shown in Fig. 10; wall thicknesses were chosen to give just perceptible temperature fluctuations on the outside wall. The left-hand section (1.375-in. OD) was used in the low-frequency experiments where the depth of penetration of the thermal oscillations was

relatively great; that on the right had two thinner wall sections (0.779- and 0.667-in. OD) for the higher frequency runs.

Data were obtained for frequencies of 0.1, 0.4, and 1.0 cps at exposures ranging from 23 to 612 hr (total cycles of 9×10^3 to 2.2×10^6); typical results are given in Figs. 11 through 14. With the thick tubes (0.445-in.-wall thickness) at a frequency of 0.1 cps, it was found that severe cracking occurred which at times extended as much as halfway through the wall. The photomicrograph in Fig. 11 shows one such intergranular crack which was 208 mils in depth after an exposure of 200 hr (72,000 cycles) at ±156°F. An indication of the extent of this cracking is given in Fig. 12 which shows a plane cut tangent to the inside surface of a tube after being subjected to a surface temperature fluctuation of ±104°F for 135 hr at 0.4 cps. At these same conditions, the exposure time was also a factor. In the left-hand portion of Fig. 13, it is observed that after 194,000 cycles cracking extended to 0.072 in., while the photomicrograph on the right shows that there existed only incipient cracking after 33,000 cycles. As the stress level at the inside wall was reduced (by decreasing the amplitude of the temperature fluctuation or by thinning the wall at the same amplitude), a substantial increase in the number of cycles required to effect cracking was necessary. This is illustrated in Fig. 14 for a run at 1 cps with a temperature oscillation of ±46°F; the total number of cycles of exposure was slightly in excess of 2.2×10^6. The test section was machined to give wall thicknesses of 0.147, 0.091, and 0.060 in. at the same inside diameter. For the thick-walled region (upper left), there occurred some light cracking and moderate to heavy intergranular attack and void formation to a depth of 12 mils. The corrosive attack appears to be related to the thermal stress variations in that a marked decrease in the depth of attack is noted for the intermediate and thin-walled sections without change in fluid velocity or mean temperature. This result is of particular interest since it suggests that the application of a relatively small thermal-stress fluctuation, if applied over a sufficiently long period, can influence the extent of corrosive attack. It was also found that the severity of cracking increased greatly in entrance and transition regions and in the vicinity of welds; this is noted in the upper right photo.

In the second experiment, the salt was passed through a thin-walled tube located between the two reservoirs. Flow was effected by alternately pressurizing the reservoirs with an inert gas. The test section is pictured in Fig. 15; the Inconel tube was of 0.25-in. OD × 0.035-in.-wall thickness and 12 in. long. Four inches of the tube could be heated by passage of an electric current through the tube wall; temperature oscillations were induced in the flowing salt by cycling the power to this heater. The remaining 8 in. of the tube comprised the test region and was unheated. During the first half of the flow cycle, the unheated portion of the tube was subjected to a cyclic temperature variation by the fluid passing downstream from the heater; for the second part of the cycle, in which the fluid was returned to the first reservoir, the test section was exposed to the uniform mixed-mean temperature of the fluid. Data was accumulated at frequencies of 0.01 and 0.4 cps.

A result, typical of those obtained in these studies, is shown in the photomicrographs of Fig. 16. In the heater, the interface temperature, as calculated from outside tube surface measurements, was 1730 ± 125°F; in the test section, 1600 ± 19°F. The total exposure was 66 hr at 0.4 cps; the total number of cycles imposed on the test-section surface was 48,000. Significant intergranular attack and subsurface void formation was observed; in particular, intermittantly spaced long intergranular stringers of voids were noted which penetrated well below the depth of the general uniform attack. Cracking was not found in any run.

Since corrosion in molten salt-Inconel systems is a function of the metal surface temperature, it is to be expected that the general corrosive attack in the second system would significantly exceed that in the first. Thus, as shown in Fig. 16 for Test ETH-B, subsurface void formation existed to a depth of 4 mils after 66 hr; while in Run 10 (Fig. 14) for the "hot-cold" slug system, attack was predominantly intergranular and then to a depth of only 2 to 4 mils in the thinner sections after an order of magnitude longer exposure (612 hr). At the same time, in contrast to results obtained at a uniform surface temperature, there appeared local regions of enhanced corrosion as well as some deeply penetrating intergranular attack. These occurrences are believed to be evidences of stress effects, even

though in the higher temperature system the thinner wall and lower amplitude of the temperature fluctuation resulted in decreased stresses.

Thus, the results obtained in a study of the compatability of a molten salt with Inconel indicate that local thermal oscillations at the fluid-metal interface can seriously affect both the general corrosion rate and the mechanical integrity of the system. It was found that the corrosion rate was increased above that obtained in a steady-state system even for temperature cycles as low as 0.01 cps (one complete cycle every 1.2 min). These experiments show further that the damage incurred may be related to the total number of thermal cycles felt by the surface with the cycles to failure (defined, for example, as crack initiation) increasing with decreasing temperature-fluctuation amplitudes. The situation is further complicated by a dependency on wall thickness.

For most situations of practical interest, the temperature fluctuations are not, of course, artificially generated but derive from the interaction between the thermal and hydrodynamic fields. As stated above, the hydrodynamic part is embedded in the nature of the turbulent flow itself, although it may be accentuated by geometric factors. Thus, the thermal cycling problem exists to some extent in any system operating above environmental temperatures where specific precautions have not been taken to assure isothermal conditions. When the phenomenon is rooted only in the turbulent structure of the flow, it is to be expected that the fluctuations in surface temperature will be local and randomly distributed in time over the surface. Based then on the results of the studies described, it is believed that damage will still occur but that the time scale will be extended. On the other hand, where the hydrodynamic source derives from regions of separated flow, wakes, etc., the effects should accord more closely with the results described. Thermally, the situation is aggravated when, as in high-performance systems, a large film temperature drop exists so that the incoming eddy is at a temperature substantially different from that of the wall. In this respect, both the relative thermal diffusivities and conductivities of wall and coolant are also important.[*] Where the

---

[*] An asymptotic solution, for an eddy contacting the wall at negligible thermal resistance and zero temperature yields $\Delta T/T_0 = A/1+A$, for $A = k'/k \sqrt{\alpha/\alpha'}$, where "prime" refers to fluid and "unprime", the wall material. Δt is the fluctuation amplitude, T_0, the initial wall temperature, k, the thermal conductivity, and α, the thermal diffusivity.

diffusivity of the fluid is much less than that of the wall (as with a gaseous coolant in contact with stainless steel), the equilibrium wall temperature will remain close to the initial wall temperature; when the situation is reversed (as with a liquid-metal coolant), the wall will transiently assume a temperature close to that of the coolant eddy. Thus, it is reasonable to expect the fluctuations to be greater with a liquid metal even though the wall-fluid temperature difference is much smaller. For example, using the asymptotic solution, for potassium in contact with 347 stainless steel at 1400°F, $\Delta T/T_o = 0.27$, for a molten salt in contact with Inconel at 1200°F, $\Delta T/T_o = 0.25$, and for helium in contact with 347 stainless steel at 1000°F, $\Delta T/T_o = 0.01$.

TWO-PHASE FLOW

The final portion of this paper considers some aspects of systems in which liquid potassium was circulated under boiling conditions. In contrast to the work described in previous sections, the experiment to be discussed was concerned with the heat transfer and flow characteristics of the system rather than with corrosion. However, keeping in mind the surface thermal cycling phenomenon, the results relating to the oscillatory nature of the system under some conditions and to the wall superheat requirements may be of interest.

This study was intended primarily to establish the magnitude of the critical (or burnout) heat flux for potassium in forced convection through a vertical, circular tube when the liquid entered the boiler at saturation conditions. The experimental system assembled for this experiment is shown schematically in Fig. 17. Liquid potassium was circulated by an electro-dynamic pump through the boiler to a liquid-vapor separator. A restriction at the boiler inlet provided the pressure drop necessary to decouple the boiler from the pumping system. The flow rates of the liquid and of the vapor after condensation were determined both volumetrically in calibrated hold tanks and dynamically by electromagnetic flow meters; the boiler exit quality was based on these measurements. A finned coil cooled by an air blast served as the condenser. Oxygen was kept at a low concentration by the continuous bypass circulation of a small stream of liquid potassium through a heated titanium sponge trap.

Two boilers have been used; these will be referred to as the low-flux boiler capable of operation at heat fluxes of the order of 40,000 Btu/hr·ft², and the high-flux boiler in which fluxes up to 500,000 Btu/hr·ft² could be achieved. The former (shown in Fig. 18) was a 6-ft long, 1-in.-OD (0.87-in.-ID) type 347 stainless steel tube radiantly heated by a set of six 3-in.-ID X 12-in.-long clamshell heaters. It was instrumented with six 8-mil-diam Pt-Pt 10% Rh thermocouples welded to the outside surface of the tube at the approximate axial mid-point of each heater and with thermowells and pressure taps for determining the fluid conditions at the entrance and exit. At the inlet, the boiler tube was welded to a 0.245-in.-ID section; and at the outlet end, to a 0.625-in.-ID line.

In attaining the critical heat flux, the boiler was maintained at a constant heat flux level while the flow rate was progressively reduced. A typical set of outside tube-wall temperature traces for a series of runs approaching burnout is shown in Fig. 19; thermocouples 5 and 6 were located near the exit of the boiler. Each section of the curves gives approximately one minute of the temperature trace; the frequency of the oscillation is thus of the order of 0.15 to 0.35 cps. At the higher flow rates, the amplitude of the temperature ripple was ±1°F; as the flow rate was decreased, the total magnitude of the fluctuation above the fluid mean progressively increased, reaching 30 to 50°F near "burnout". The burnout point was defined by the automatic interruption of the boiler power when the wall temperature in any oscillation exceeded 1750°F. In some earlier runs without this cutoff, temperature excursions of as much as 350°F above the mean were noted.

Of more interest, perhaps, from the point of view of this paper was the observation that during some phases of operation with the low-flux boiler there existed a condition of stable tube-wall temperature oscillation of very high amplitude; associated with this were extreme fluctuations in both flow and pressure. A typical temperature trace obtained during one such oscillatory situation is shown by the upper curve in Fig. 20. In comparison, the lower curve gives the trace for a stable condition at approximately the same inlet mass flow and net exit quality (in excess of 60%). The frequency of the temperature oscillations was of the order of 0.05 to 0.10 cps; amplitudes of ±150 to ±200°F were common. While there

was evidence that this condition could continue over long periods of time, it was generally terminated after about 10 min to avoid excessive damage to the boiler. Not unsurprisingly, the critical heat flux values obtained were reduced by about 40% below those obtained with stable flow. As indicated in Fig. 20, the rate of temperature rise during these cycles was determined to be about 17°F/sec. Interpretation of this pattern will be deferred until later in this paper.

The cause of this instability remains somewhat uncertain and may relate in part to the restriction at the boiler exit. It was found, however, that a reasonable correlation could be made with the amount of inlet subcooling; this is indicated in Fig. 21. When the inlet subcooling was held to less than about 40°F, stable performance was obtained; this result is consistent with analytic descriptions of closed-loop systems in which the preheater is hydrodynamically coupled to the boiler.

The high-flux boiler is shown in the cut-away schematic of Fig. 22. This was a 44-in. long, 0.325-in.-ID (0.028-in.-wall thickness) type 347 stainless steel tube brazed within a segmented copper sleeve of 5-in. outside diameter. The twenty-one, 2-in.-thick copper disks comprising this sleeve were separated by 0.119-in. gaps to minimize axial heat flow. Each disk was heated externally by an individually controlled clamshell heater; the converging geometry of the heat-flow path results in high heat fluxes at the fluid-metal interface for reasonable heater temperatures. The radial temperature gradient in each copper block was measured with three logarithmically spaced 0.040-in.-OD sheathed Chromel-Alumel thermocouples. These thermocouple readings were extrapolated to give the temperature at the boiling surface and, in combination with the copper conductivity, the heat flux through each copper segment.

In this system, it was found that stable operation was possible only when vapor existed at the boiler inlet; for all-liquid inlet conditions, a rapidly amplifying thermal oscillation was observed. The required quality at the inlet was generally obtained by allowing some liquid to flash to vapor at the upstream restriction. It is estimated that the inlet quality was less than 0.5%.

The presence of vapor at the inlet leads to an interesting conjecture as to the mechanism of heat transfer in these systems. The liquid-vapor density ratio for saturated potassium at 1550°F is 675; neglecting slip, this corresponds to a void fraction of about 0.80 at the inlet. For this condition, the data of Radovcich and Moissis[6] for the flow of air-water mixtures in vertical tubes predicts an annular flow condition. The liquid would therefore be present as a thin layer on the wall; the thickness of this film has been estimated to be 0.040 in. in a 0.87-in.-ID tube at an inlet flow of 100 lb/hr. For a Δt of 375°F (justified below in regard to superheat required for bubble nucleation), conduction through the film could sustain a flux of 2×10^6 Btu/hr·ft^2, well above the values attainable in these experiments. This suggests that in these studies the heat was transferred by conduction through a thin liquid film followed by evaporation at an inner liquid-vapor interface. Alternatively, Goldmann et al.[7] have proposed that hydrodynamic forces and the high mass-transfer (evaporation) rates required are sufficient to strip the film completely from the wall and create a mist or fog flow. Diffusion of the liquid droplets along the radial velocity gradient and evaporation at the wall then would account for the heat transfer. From a corrosion point of view, if one is concerned with mechanism, the difference in these two interpretations is spectacular in that in the first instance the wall is in contact with a flowing liquid; while in the second, the wall is scrubbed primarily by a vapor flow.

Since the temperature at the fluid-metal interface is of importance in corrosion, it is worthwhile to consider briefly the problem of bubble nucleation in a liquid metal. By combining the condition for dynamic equilibrium of a spherical vapor bubble in a liquid pool with the Clausius-Clapyron relation, it is found that

$$T_v - T_{sat} \cong \frac{2\,R\,T_{sat}^2\,\sigma}{h_{fg}\,P_\ell\,r} \quad , \tag{1}$$

where T_v is the absolute temperature of vapor within the bubble; T_{sat}, the absolute temperature of the saturated liquid at pressure, P_ℓ; R, the gas constant; h_{fg}, the latent heat of vaporization of the liquid; σ, the interfacial tension between liquid and vapor at bubble surface; and r, the

bubble radius. This equation, which predicts the approximate liquid super-
heat required at equilibrium for a bubble of radius, r, has been found to
be adequate for water and a number of organic fluids. If the superheat
required for bubble nucleation with the liquid alkali metals is then cal-
culated by direct comparison with water using Eq. (1), the values given in
Table 1 result.[8] Note that the bubble radius is eliminated as a variable

Table 1. Estimated Liquid Superheats with
Alkali Liquid Metals at 1 Atm

Fluid	Calculated Superheat Based on Water at		Measured Superheat, °F
	30°F	90°F	
Na	258	774	—
K	125	375	342
Rb	101	303	135
Cs	67	201	—

by this process. The first column gives values based on a superheat of
30°F for water and indicates, for potassium for example, a superheat of
125°F. The 30°F value for water derives from measurements on a natural
surface (such as a pipe wall) having a normal distribution of boiling
sites (cavities). From Eq. (1), it is seen that as the surface tempera-
ture rises above the saturation temperature, bubbles will form first in
the cavities of largest radius. As these sites are used up, the wall
temperature will continue to rise and smaller and smaller cavities will
be brought into action. Presumably these cavities are not completely wet
by the fluid; i.e., the fluid does not completely displace trapped or
adsorbed gases. On the other hand, liquid alkali metals wet most solid
metals easily (definitely at the boiling temperature); and it is to be
expected then that the boiling site distribution will be drastically
skewed, predominating in very small cavities, or perhaps even completely
eliminating all sites. Further, the liquid metals used are generally of
very high purity and are in contact with clean, smooth surfaces in the
absence of inert gases. The superheat required to initiate bubble forma-
tion with a liquid metal should thus significantly exceed that required

with water. Data obtained with distilled, deaerated water in contact with clean, very smooth surfaces show just this effect, with superheats of 90°F and higher being observed. The second column in Table 1 shows the superheats anticipated based on a 90°F value for water. The final column gives some experimental information obtained at ORNL with boiling in reflux capsules and in natural- and forced-circulation loops; these results are consistent with the predictions.

The requirement of high liquid superheat for bubble initiation in a liquid metal can also be used in developing a possible explanation for the quasi-stable fluctuating boiling described previously. For a flowing liquid metal, the high thermal conductivity results in a nearly flat radial temperature distribution for the condition of heat transfer at the wall. For example, when the wall temperature reaches 375°F (the condition for bubble nucleation), the centerline temperature in a 1-in. tube will be about 340°F. Once the bubble forms, the entire energy of superheat becomes available for bubble growth and, due to the high thermal diffusivity (for K, α is about 335 times the diffusivity for H_2O), is released in a matter of microseconds as a sudden explosion of liquid into vapor. The energy of superheat in a unit volume of potassium under these conditions is sufficient to produce a vapor quality in excess of 7 wt %. There then results a momentary high-pressure surge, aggravated by the constricted exit in the low-flux boiler, with an attendant decrease in flow. This cycle will repeat itself at a frequency which depends on the heat flux and the thermal gradient in the bubble-producing cavity.

Two further factors should be mentioned in regard to the stable boiling condition. If annular flow exists, then burnout occurs when there is no longer sufficient liquid present to cool the wall. This situation (termed dry-wall or liquid deficient) does not correspond to a unique position on the tube; i.e., because of hydrodynamic forces, the "liquid—no liquid" position will wash back and forth in a random fashion over a region of the tube wall. Accelerated corrosion observed in this area can perhaps be explained in terms of the thermal cycling phenomenon. If fog flow exists, a cyclic cooling condition again occurs as the result of the liquid droplets which impinge on the wall and evaporate.

289

The results for the critical heat flux with potassium are shown in Fig. 23 as a function of the inlet-liquid mass flow. The data at $L/D = 83$ were obtained in the low-flux boiler; the dashed line indicates the unstable flow situation. An interesting feature of these data is the excellent correlation found with the results of Lowdermilk, Lanzo, and Siegel[9] for the saturation boiling of water in a vertical tube. While potassium boiling differs markedly from water boiling on a microscale, the gross phenomena, at least in regard to burnout, appear similar.

<p style="text-align:center">RECAPITULATION</p>

It has been the intent of this paper to consider the influence of heat transfer and fluid mechanics on dynamic corrosion. Rather than a general enumeration of the many areas of interrelationship between heat, mass, and momentum transfer, this discussion has attempted to illuminate some aspects of the problem through a description of specific experiments drawn from the personal experience of the author. This has included comments on the role of surface shear and boundary-layer flow and development with uranyl sulfate solutions, on the effects of surface temperature oscillations on the mechanical integrity and corrosion resistance of an alloy metal wall in a molten salt environment, and finally on flow and temperature phenomena which could affect corrosion in a boiling alkali metal system.

Because of this approach, there have been omitted many other areas in which both the thermal and hydrodynamic characteristics of the system modify the corrosion. Among the interesting factors not considered are the influence of thermal gradients on gross mass transfer, the development and perpetuation of local concentration cells, mass transfer through the buffer and laminar layers adjacent to a wall, the specific application of classical laminar-flow analyses in the prediction of corrosion in certain well-defined systems, etc. It is hoped, however, that this paper will give to the corrosion experimenter, and perhaps also to the reactor designer, a better feel for the importance of considering corrosion in dynamic systems as a part of the general transport problem.

E-2492

REFERENCES

1. D. B. Spalding and W. M. Pun, "A Review of Methods-for Predicting Heat-Transfer Coefficients for Laminar Uniform Property Boundary Layer Flows," Int. J. Heat-Mass Transfer, 5: 239–249 (1962).

2. Fluid Fuel Reactors, edited by J. A. Lane, H. G. MacPherson, and F. Maslon, pp. 198-210, 219-226, Addison-Wesley Publishing Company, Reading Massachussets, 1958.

3. R. G. Deissler, "Turbulent Heat Transfer and Friction in the Entrance Regions of Smooth Passages," Trans. ASME, 77: 1221–1233 (1955).

4. C. O. Bennett and J. E. Myers, Momentum, Heat, and Mass Transfer, pp. 65-66, 320-332, 486-489, McGraw-Hill, New York, 1962.

5. J. J. Keyes, Jr., and A. I. Krakoviak, "High-Frequency Surface Thermal Fatigue Cycling of Inconel at 1405°F," NSE, 9: 462–474 (1961).

6. N. A. Radovcich and R. Moissis, "The Transition from Two-Phase Bubble Flow to Slug Flow," MIT Report No. 7-7673-22, Department of Mechanical Engineering, Massachusetts Insittite of Technology, June 1962.

7. K. Goldmann, H. Firstenberg, and C. Lombardi, "Burnout in Turbulent Flow — A Droplet Diffusion Model," Trans. ASME, Journal of Heat Transfer, 83: 158–162 (1961).

8. A. I. Krakoviak, "Notes on the Liquid-Metal Boiling Phenomenon," USAEC Report ORNL-TM-618, Oak Ridge National Laboratory, 1963.

9. W. H. Lowdermilk, C. D. Lanzo, and B. L. Siegel, "Investigation of Boiling Burnout and Flow Stability for Water Flowing in Tubes," Nat. Adv. Comm. Aero. Report TN-4382, September 1958.

E-2492
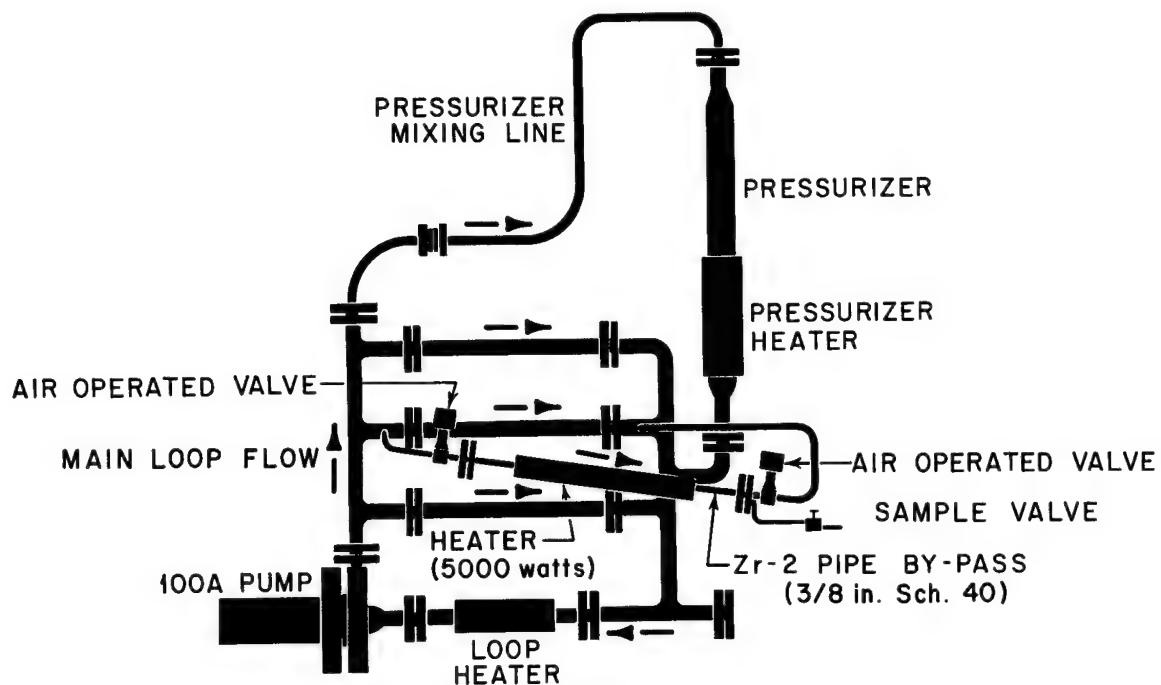
Figure 1. – Schematic of typical loop for study of corrosion with uranyl sulfate solutions.
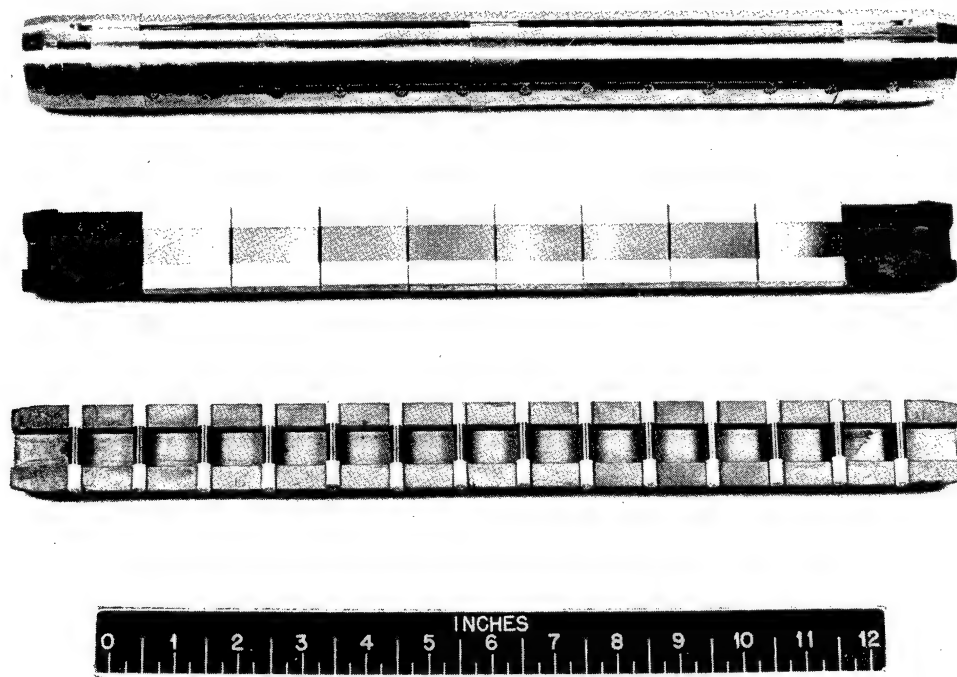
Figure 2. – Specimen holders used in uranyl sulfate corrosion studies. Upper assembly, closed holder; central assembly, with flat-plate specimens; lower assembly, with round pin specimens.
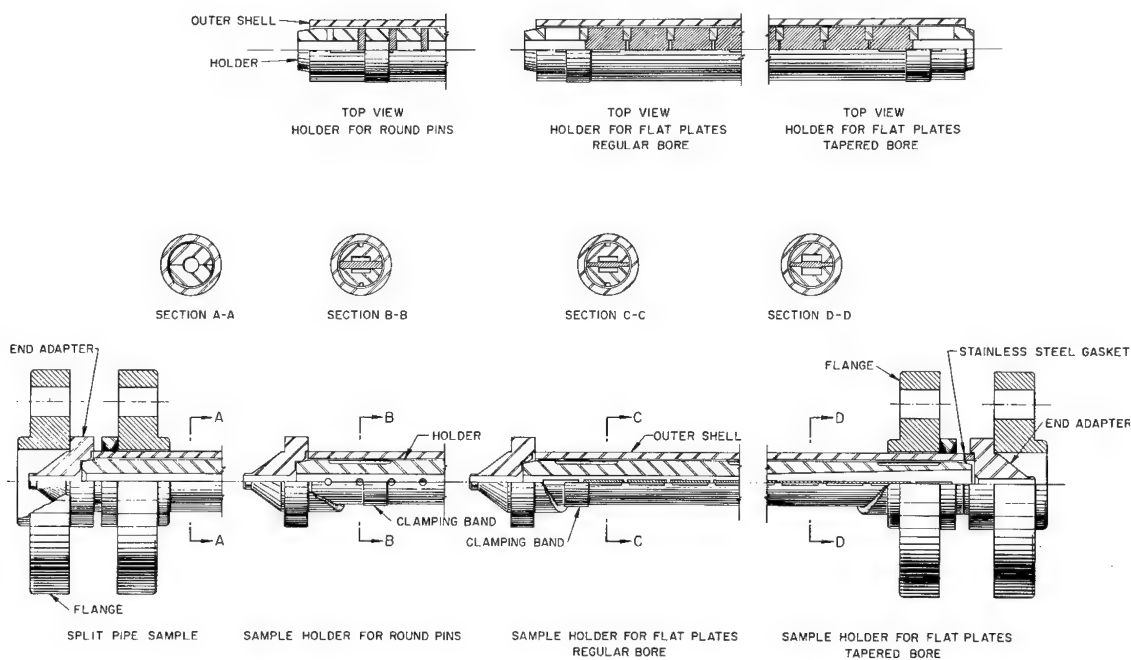
Figure 3. – Details of uranyl sulfate corrosion specimen holders.

$$\tau_0 \sim \overline{u_a}^2$$
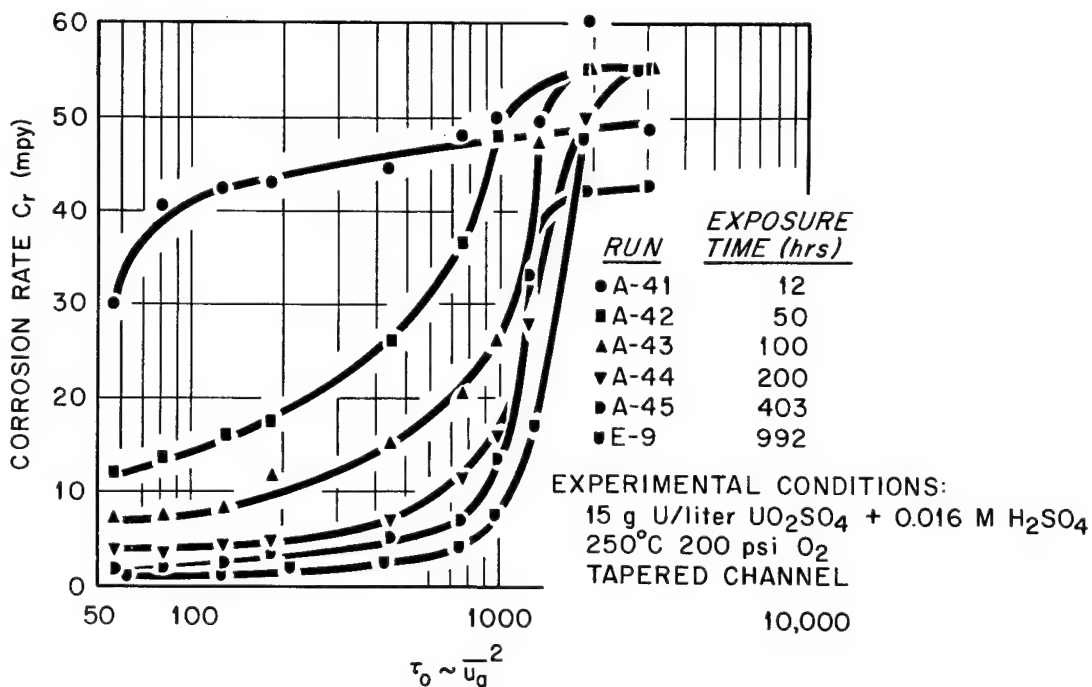
Figure 4. – Effect of shear at fluid-solid interface on corrosion of flat-plate specimens in uranyl sulfate solutions.

TYPE 347 SS COUPONS

FLOW (fps)   10   11   14   17   23   36   41   47   55   68   83

RUN A-100
1.3 m UO$_2$SO$_4$ + 1.3 m Li$_2$SO$_4$ @ 300°C FOR 1000 HRS.
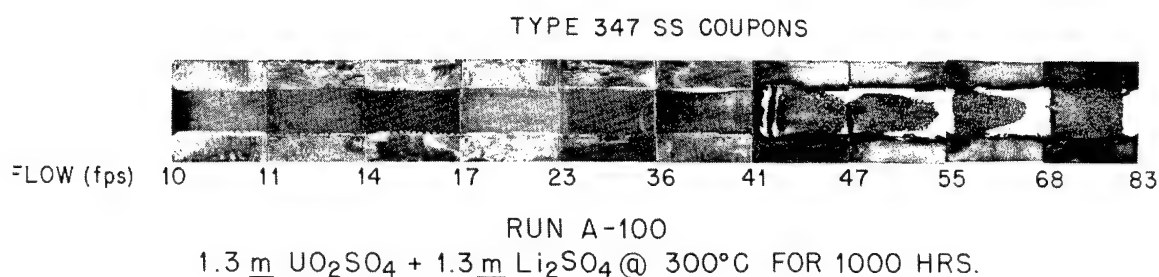
Figure 5. - Visual evidence of shear effects on corrosion of flat-plate specimens in uranyl sulfate solutions.
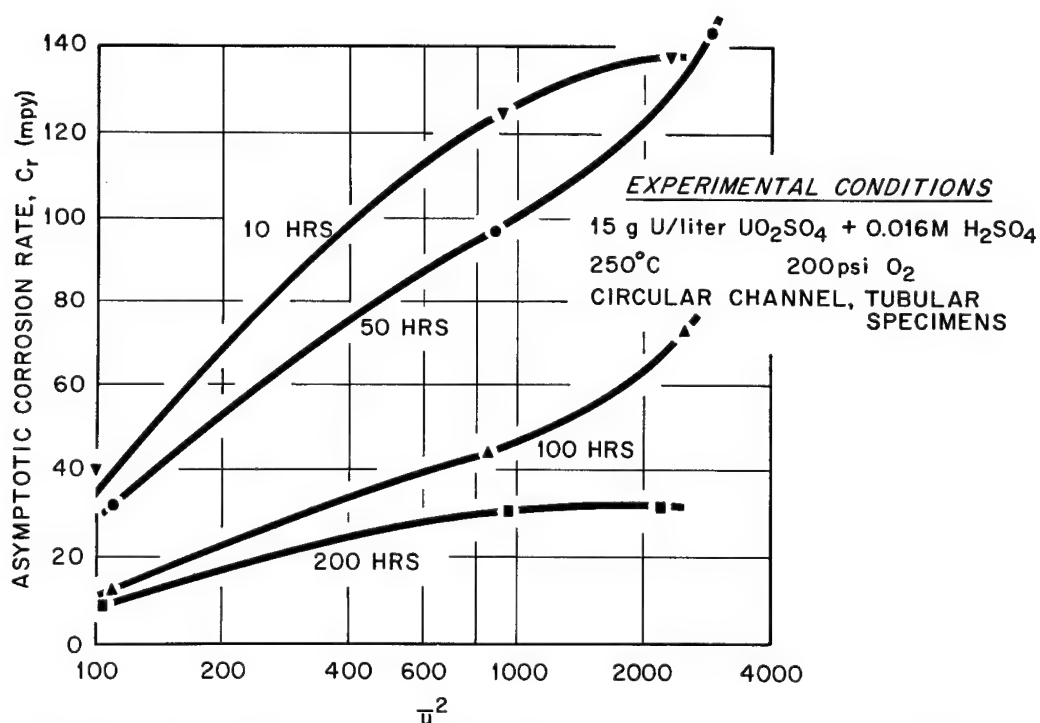
Figure 6. - Influence of shear on corrosion at the inside surface of tubular specimens exposed to flowing uranyl sulfate solutions.

294
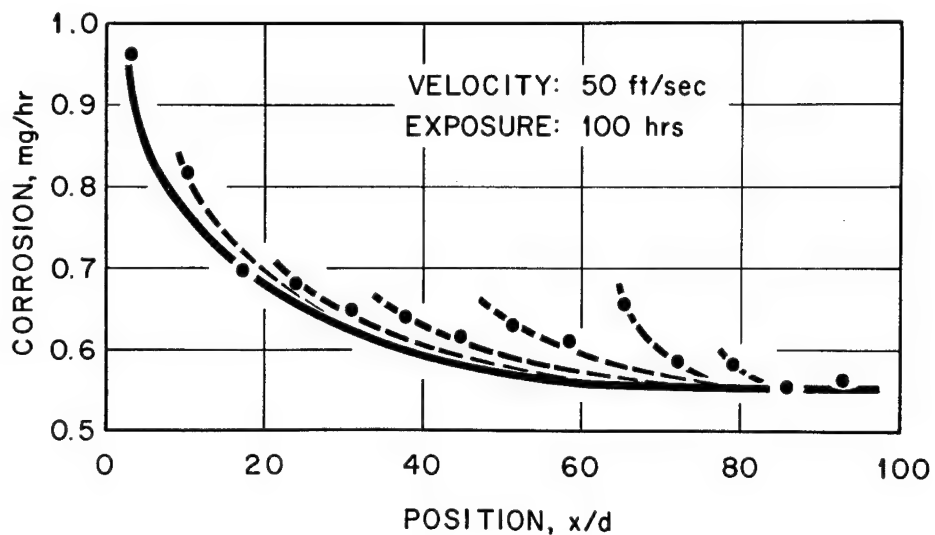
Figure 7. – Corrosion of tubular specimens in uranyl sulfate solutions as a function of distance from the channel inlet.
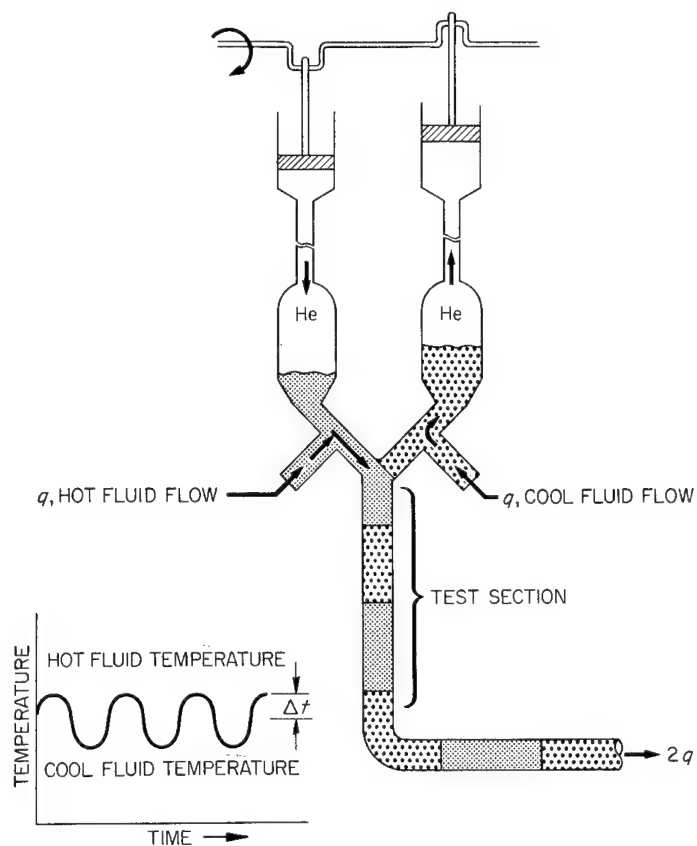
Figure 8. – Schematic diagram of thermal pulse generator.
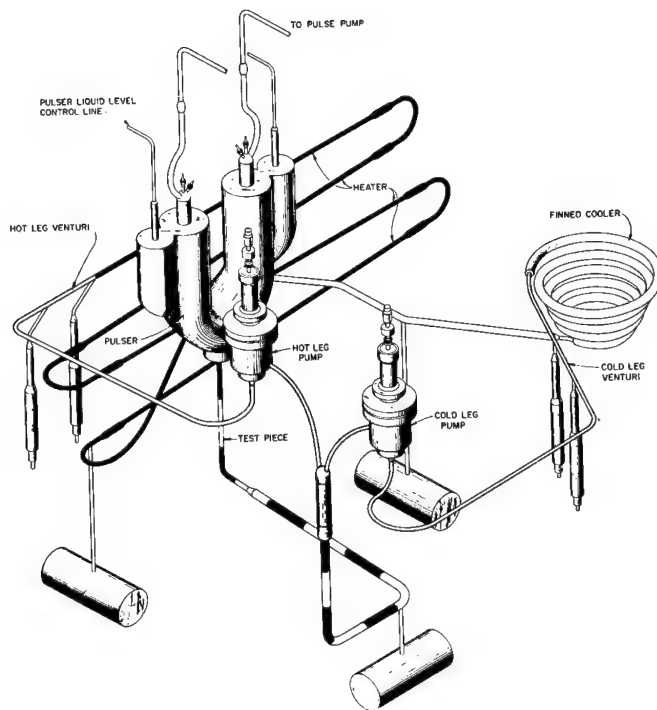
Figure 9. – Flow diagram of thermal cycling test loop with pulse generator.
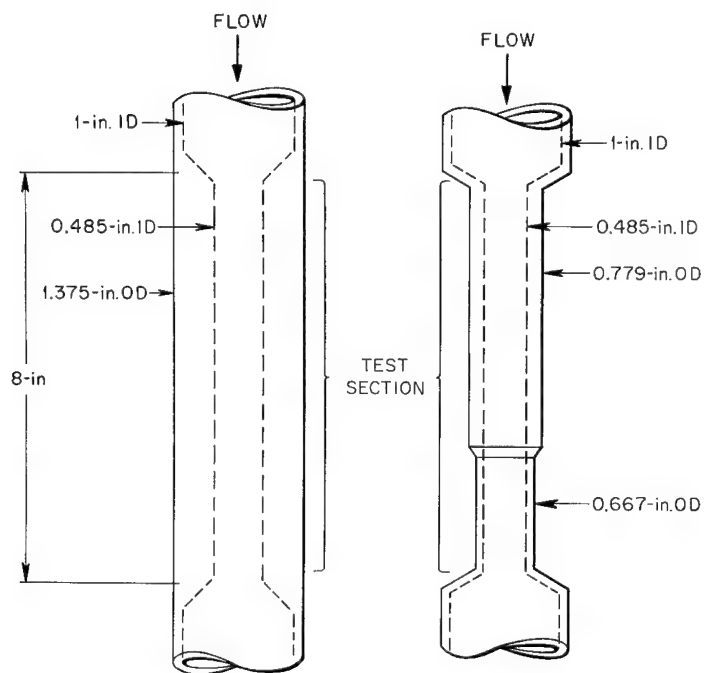
Figure 10. – Typical test sections used in thermal cycling studies with pulse generator loop.
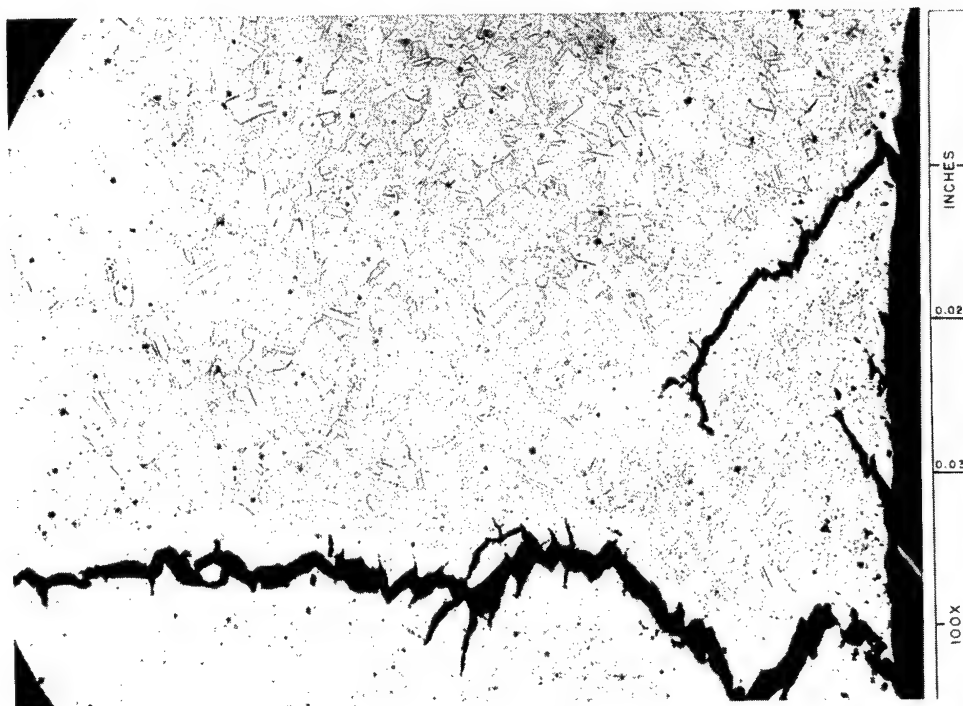
Figure 11. - Effect of thermal fatigue cycling at 0.1 cps on thick-walled Inconel tube in a fused-salt environment.

FLOW
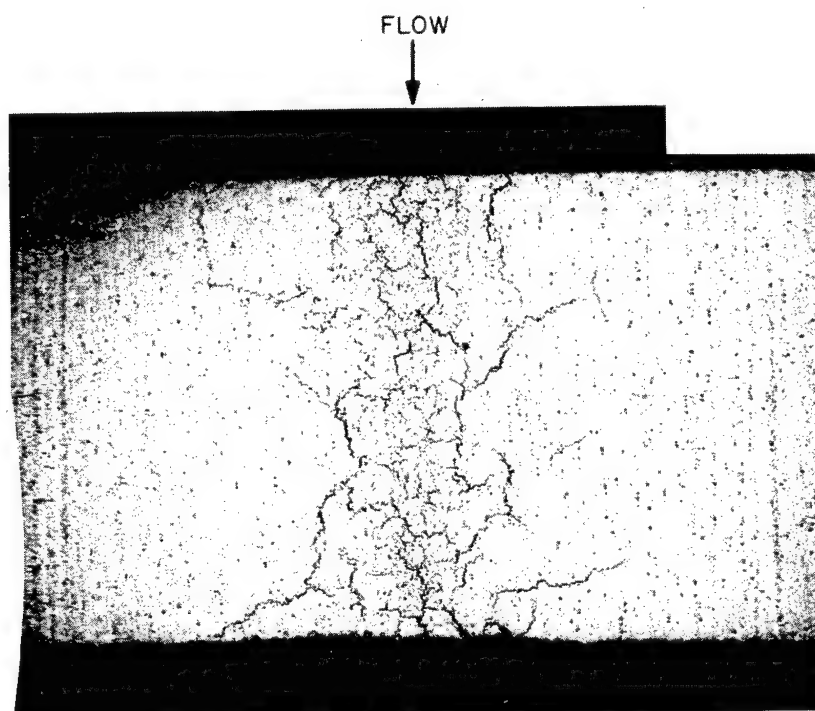
igure 12. - View of plane cut tangent to inside surface of Inconel test section showing orientation of thermal fatigue cracks after exposure at 0.4 cps in a fused-salt environment.

RUN 1: 194,000 CYCLES   RUN 2: 33,000 CYCLES

ETCHANT: MODIFIED AQUA REGIA, 50X
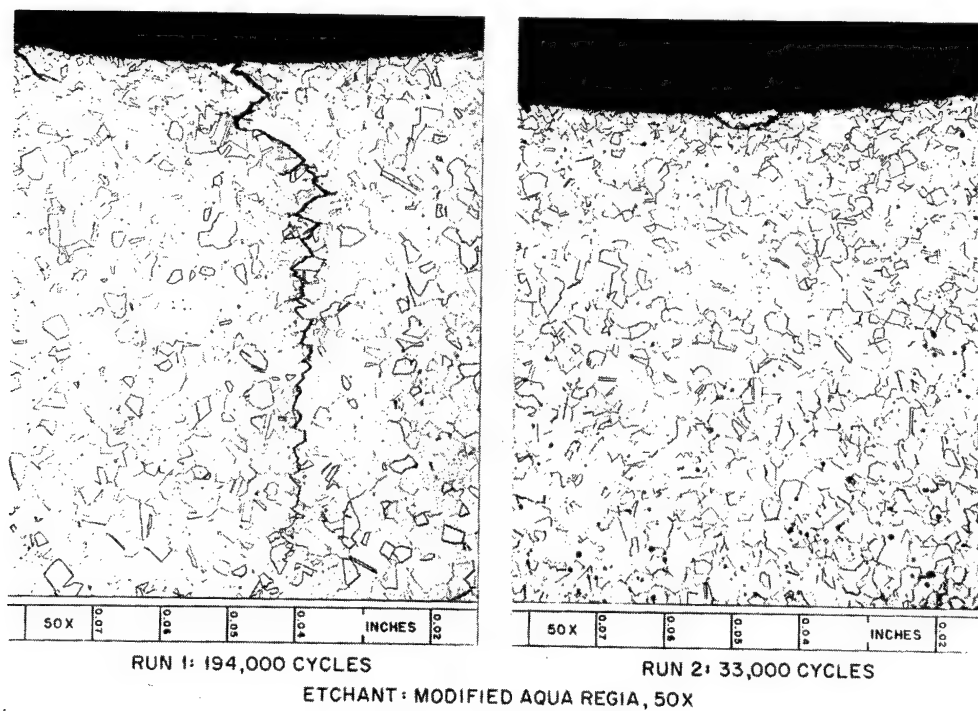
Figure 13. - Effect of exposure time on thermal fatigue cracking of an Inconel tube at 0.4 cps in a fused-salt environment. Left photomicrograph - 194,000 cycles exposure; right photomicrograph - 33,000 cycles exposure.

0.147-in. WALL, σ = 12,800 psi   TRANSITION FROM 0.147-in WALL TO 0.090-in. WALL

0.090-in. WALL, σ = 11,200 psi   0.060-in. WALL, σ = 7500 psi
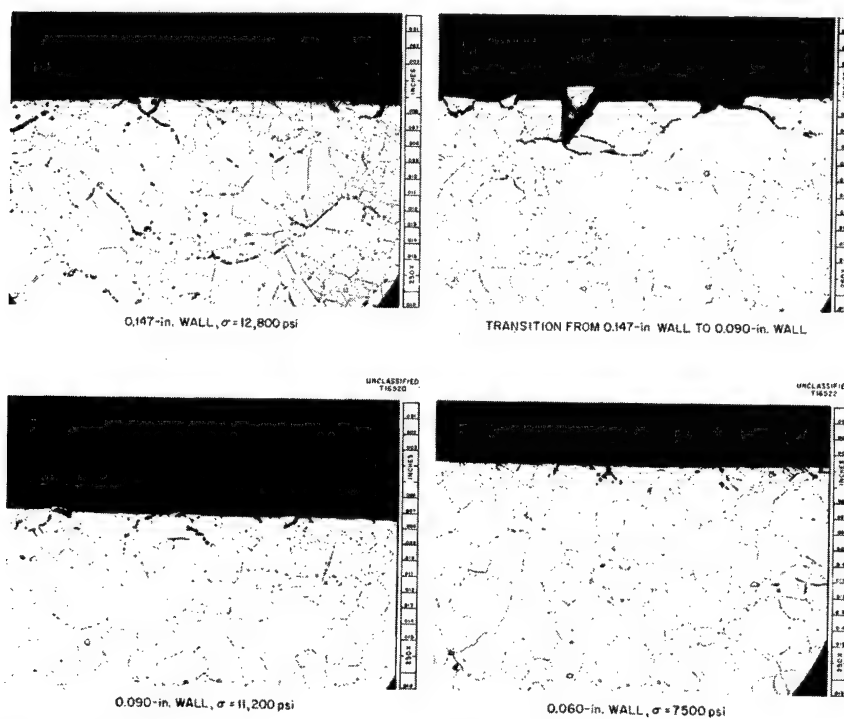
Figure 14. - Effect of test section wall thickness and transition on thermal fatigue cracking and corrosion of Inconel at 1.0 cps in a fused-salt environment.

298
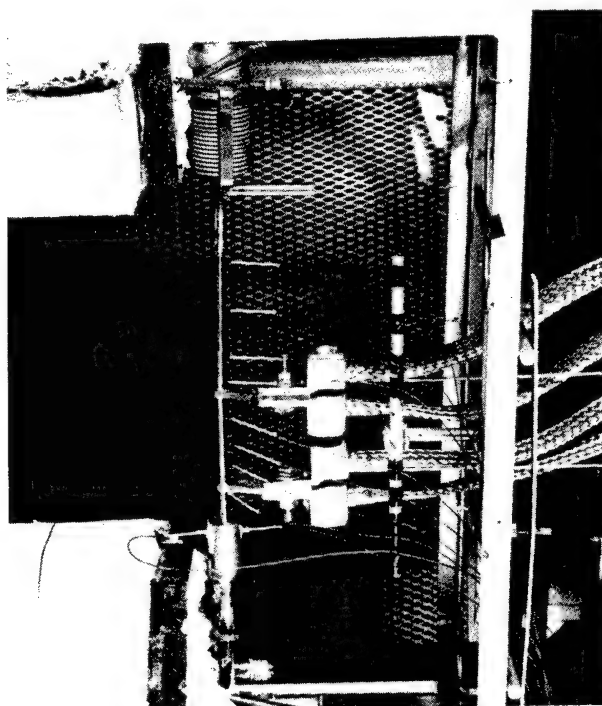
Figure 15. – Test section for thermal cycling system using pulsed-power to heater for generation of surface thermal oscillations.
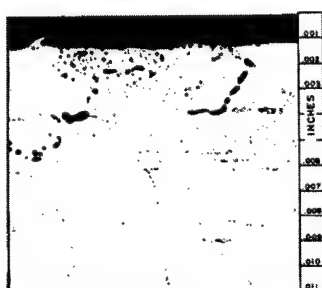
HEATER   TEST SECTION

:RFACE TEMPERATURE: 1730 ± 125°F   INTERFACE TEMPERATURE: 1600 ± 19°F

DURATION: 66 HRS. - SALT NO. 30 IN INCONEL

Figure 16. – Effect of thermal cycling at fluid-metal interface on corrosion of thin-walled Inconel tube in pulsed-power system at 0.4 cps with fused-salt environment.

299
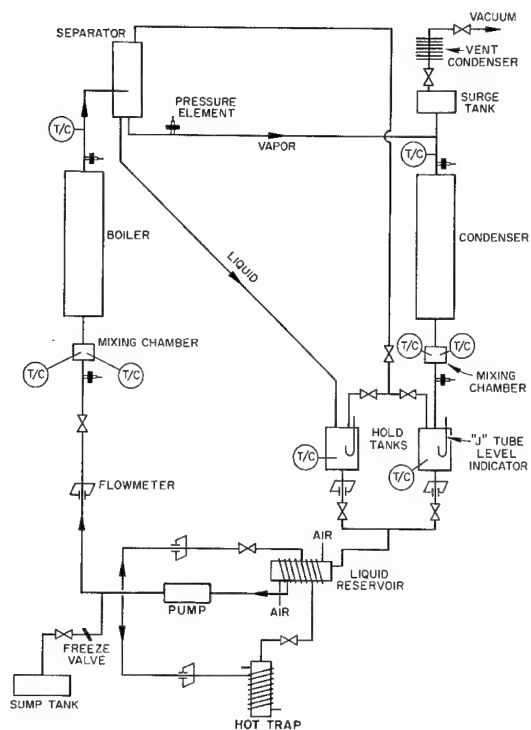
Figure 17. – Schematic diagram of forced-circulation loop for study of boiling heat transfer with liquid potassium.
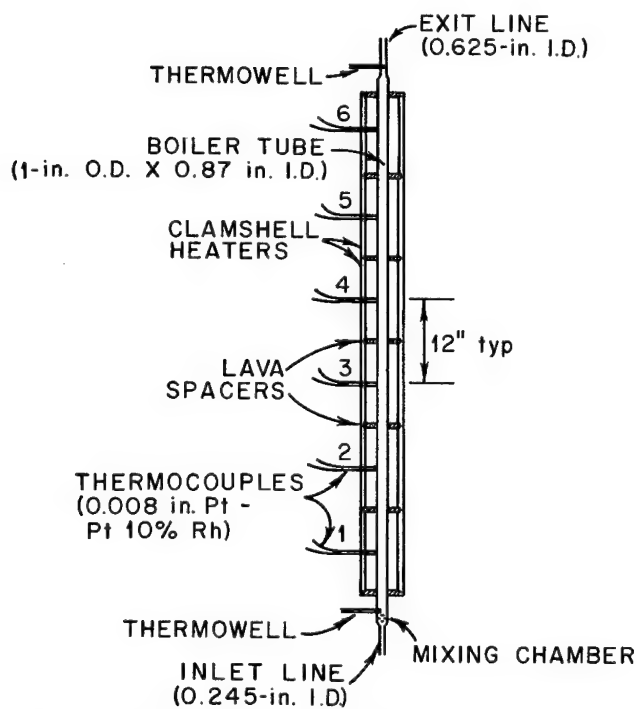
Figure 18. – Low-flux boiler used in forced-circulation potassium boiling studies.

FLOW RATE
lb/hr   152   86   63   54

QUALITY
(%)   34   61   81   92   BURNOUT

6

5

TIME ⟶
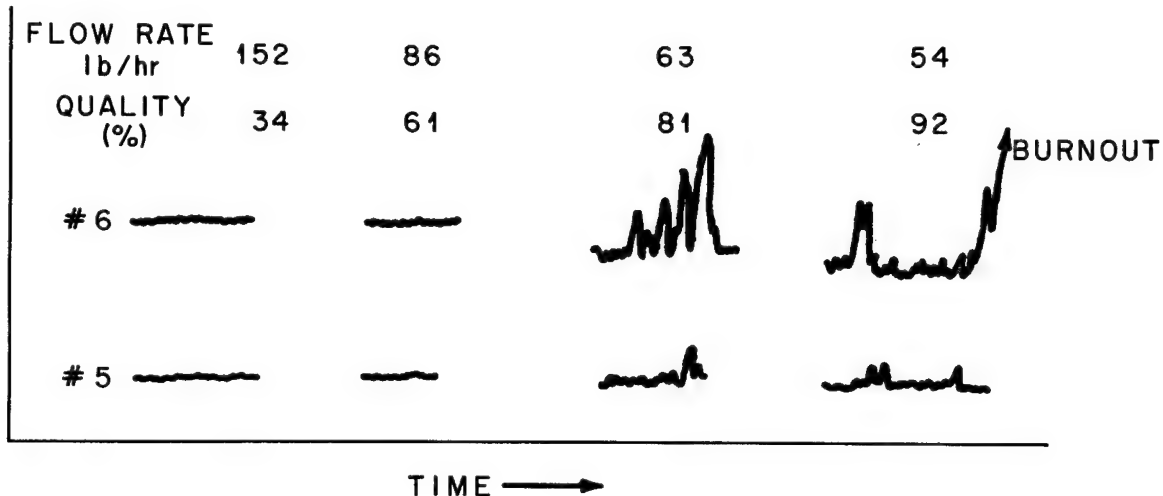
Figure 19. - Typical sequence of tube-wall temperatures during approach
to the critical heat flux in the low-flux boiler.

$\frac{\Delta T}{\Delta \tau}$ = -104 °F/sec

$\frac{\Delta T}{\Delta \tau}$ = 17.4 °F/sec
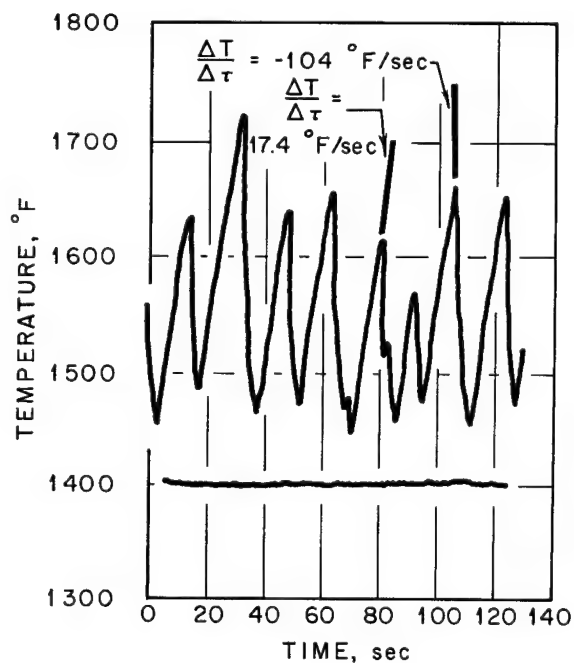
Figure 20. - Tube-wall temperature patterns illustrating
differences during quasi-stable (top) and stable (bottom)
boiling in the low-flux boiler.

301
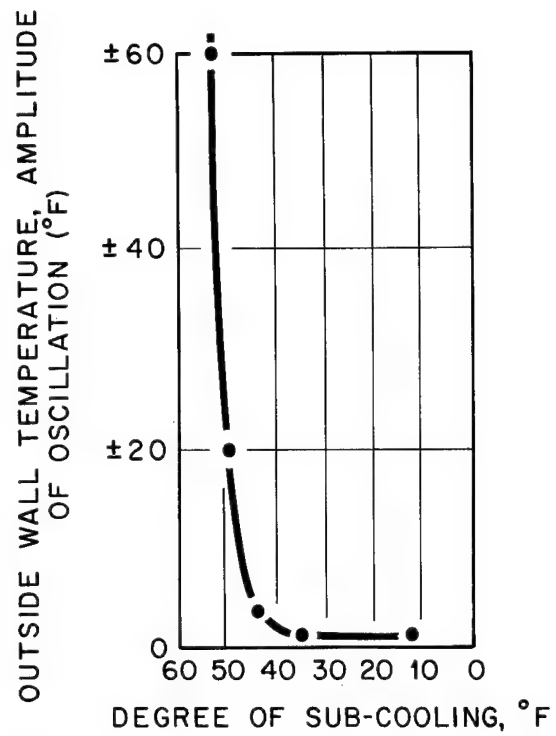
Figure 21. - Stability curve showing influence of inlet subcooling on amplitude of wall temperature oscillation in the low-flux boiler.
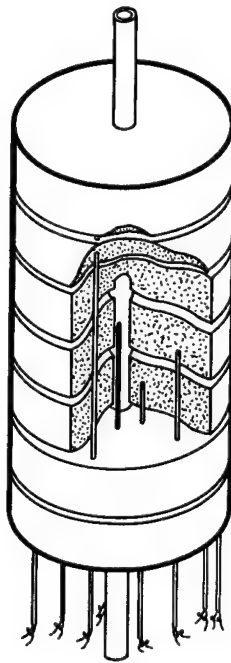
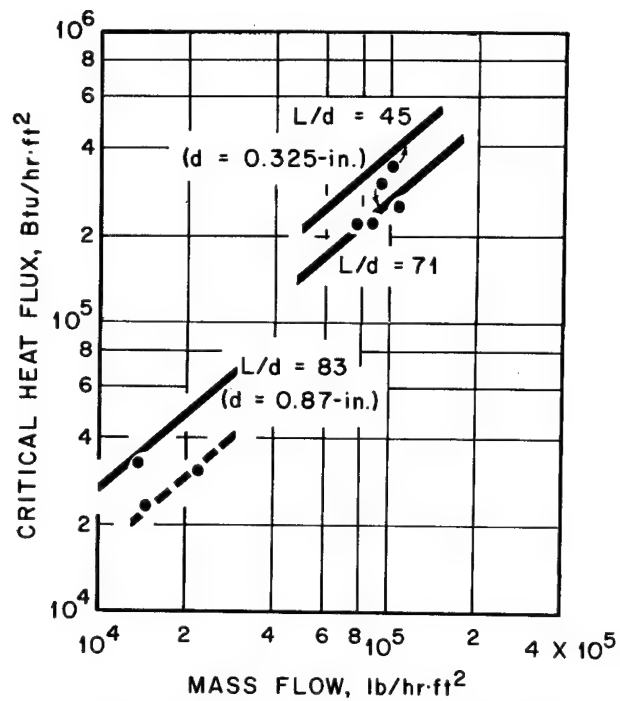Figure 22. - High-flux boiler for forced-circulation potassium boiling studies.

Figure 23. - Critical heat flux data obtained in forced-circulation potassium boiling studies.

B. ENVIRONMENT →307

Charles A. Barrett
NASA Lewis Research Center
Cleveland, Ohio

M. F. Parkman
Argonne National Laboratory
Chicago, Illinois

OXYGEN "PUMPING EFFICIENCY" OF REFRACTORY METALS

Charles A. Barrett and Louis Rosenblum $\rfloor$ $\overline{NASA\ Lewis\ Research\ Center}$ $\longrightarrow 313$

Several years ago, at the start of our space power system materials program, we became concerned with the effect of contamination of columbium at elevated temperatures in vacuum environments. Since most testing of space power systems would be performed on the ground rather than in space, a definition of environmental requirements was needed.

It seemed clear that contamination of columbium by impurities in the environment involves two processes: (1) contaminants impinging and sticking to an exposed metal surface, and (2) diffusion of contaminants from the metal surface to the interior. Either one of these two processes could be rate controlling, depending on the partial pressure of impurity molecules, the temperature of the metal, and the concentration present in the metal of the particular impurity.[1] If, for example, the diffusion rate of oxygen (the most detrimental contaminant) into columbium is greater than the product of oxygen flux to the surface and the fraction of oxygen molecules sticking to the surface, no detectable surface columbium oxide layer should form. Conversely, when diffusion is rate controlling, a surface oxide layer should form and grow. Therefore, in this case, the weight gain of oxygen, essentially as surface oxide, should be proportional to the square root of the exposure time (ref. 1).

From calculations made with the diffusion rates of oxygen in columbium at 1000° C (refs. 2 and 3), it can be shown that at oxygen partial pressures greater than 10^{-5} torr the influx of oxygen molecules to the surface is the rate-controlling process, even when the fraction of oxygen molecules sticking to the surface is 1. When oxygen flux to the surface is the rate-controlling process, this flux can be equated directly to the amount of oxygen picked up by the columbium. A relation between oxygen pick-up and pressure is given in the Langmuir equation

$$F_L = 0.0583\ P\epsilon\left(\frac{M}{T}\right)^{1/2} \tag{1}$$

where

F_L oxygen pick-up of species, $g/(cm^2)(sec)$

P partial pressure of species, torr

M molecular weight of species

---

[1] A third rate-controlling process can also be postulated to explain certain experimentally observed phenomena, namely, surface coverage control. Over the range of experimental conditions covered herein, this process is not believed to be significant. In the interests of simplification, discussion of this process will be deferred to future papers.

T   absolute temperature, $^{\circ}K$

ϵ sticking probability, or pumping efficiency,[2] of metal

From the Langmuir equation and the assumption of the equivalence of oxygen flux and weight gain rate of the metal $\dot{w}$, it follows that $\dot{w}$ is directly proportional to P and also that weight gain w will increase linearly with time.

If the pumping efficiency ϵ can be determined, the oxygen weight gain of the columbium can be readily calculated for various temperatures and partial pressures of oxygen. From Inouye's work (ref. 4) on the low-pressure oxidation of columbium (down to 3×10^{-5} torr), values of $\epsilon \approx 0.05$ in the temperature range of 1000° to 1200° C and oxygen partial pressure about 10^{-5} torr can be derived.

The upper operating temperature of an advanced power system may be about 1100° C with a projected system life of 10,000 hours. Arbitrarily setting an oxygen contamination pick-up limit of 2000 ppm for a 50-mil columbium wall and using a value of $\epsilon = 0.05$, we can calculate that the environment for a 10,000-hour test at 1100° C should have a partial pressure of oxygen no greater than 1×10^{-7} torr.

In view of these estimates, it seemed important to establish the validity of the contamination process, which predicts

(1) When diffusion of oxygen in columbium is rate determining, surface oxide formation occurs, $w \propto t^{1/2}$, and $\dot{w}$ is independent of P.

(2) When oxygen flux is rate determining, no surface oxide forms, $w \propto t$, and $\dot{w} \propto P$.

Also it would be desirable to determine experimentally the pumping efficiency over a range of pressures and temperatures for a typical columbium alloy such as Cb-1Zr that might be considered for use in an advanced space power system.

In 1961 the Lewis Research Center, jointly with the General Electric Engineering Laboratory, Schenectady, New York, initiated an experimental program to determine the impurity weight gain of Cb-1Zr specimens exposed at 980° and 1100° C to impurity partial pressures from 10^{-5} to 10^{-7} torr as a function of time. The GE Engineering Laboratory exposed the specimens in their high-vacuum facility. The Lewis Center analyzed the specimens chemically and metallurgically before and after exposure and reduced and analyzed the data.

---

[2]Pumping efficiency is the preferred term to use here rather than sticking probability since we are concerned with steady-state conditions rather than equilibrium conditions.

Continuous (i.e., instantaneous) contamination rates were obtained by means of a unique technique devised by the GE Laboratory. With this technique, weight changes in the order of 10^{-9} gram per second (expected in exposures at 10^{-7} torr) could be measured. Gravimetric methods, long used by experimenters to measure weight changes, are limited to detecting changes in the order of 10^{-6} gram per second.

A photograph and a schematic drawing of the test setup used by the GE Engineering Laboratory are shown in figures 1(a) and (b), respectively. The gas species of interest is continuously passed into the system through a controlled leak at the same time as two "pumps" - a diffusion pump and the columbium alloy specimen - are working to remove it from the system. Measuring the difference in pressure between two stations separated by a length of tube of known conductance allows calculation of the pumping rate (i.e., weight gain rate) of the specimen for any set pressure and temperature condition in the sample chamber:

$$\text{Pumping rate} = \Delta P \times \text{Tube conductance} = \dot{w} \qquad (2)$$

All the tests reported here were run for 236 hours. The total weight gain as determined by integrating the instantaneous weight-gain rates (eq. (2)) over the time of the test and the weight gain determined from the difference in weight of the specimen before and after exposure as well as the weight gain determined by fusion analysis of the exposed sample were all in good agreement.

The log of oxygen weight gain is plotted against the log of time for three partial pressures of oxygen in figure 2, and the log of oxygen contamination rate against the log of oxygen partial pressure is shown in figure 3. The slopes of all the curves are approximately 1, that is, $w \propto t$ and $\dot{w} \propto P$.

No surface oxide layer was detected on specimens exposed at pressures less than 10^{-5} torr. On specimens run at 980° C and 2.5×10^{-5} torr, a thin discontinuous patch of black oxide, identified by X-ray diffraction as mainly CbO_2, was noted on the surface. Under the conditions of the test a crossover in the rate-controlling process of contamination from flux control to diffusion rate control probably occurred at some late time in the test. Additional credence can be given this conclusion by comparing the calculated time required to reach oxygen saturation at the surface of the specimen (for a flux passing through the surface and diffusing inward and equal to that calculated from the Langmuir equation) with the actual test time. The calculated time to reach oxygen saturation at the surface is 200 hours compared with the actual test exposure time of 236 hours.

The pumping efficiency ϵ of Cb-1Zr for oxygen, as calculated from the contamination-rate data presented herein, has a value of 0.02 to 0.03 over the pressure range 10^{-7} to 10^{-5} torr and the temperatures range from 1100° to 980° C. Plainly, it is now possible to determine maximum total oxygen contamination pick-up of Cb-1Zr used in experiments run at advanced power system temperatures in vacuum by means of the Langmuir equation

309

together with the experimental value for ϵ. With use of the experimental value of ϵ, plots can be made, as in figure 2. The intersection of the horizontal line - representing in figure 2 a 2000 ppm oxygen contamination level for a 0.05-inch thickness of Cb-1Zr - and a weight-gain curve gives the time required to reach the given contamination level. For example, as shown in figure 2, a partial oxygen pressure of 5.5×10^{-7} torr will allow operation up to 5500 hours before the 2000 ppm oxygen contamination level is exceeded.

REFERENCES

1. Kubaschewski, O., and Hopkins, B. E.: Oxidation of Metals and Alloys. Butterworths Scientific Publications, London, 1953.

2. Crank, J.: Mathematics of Diffusion. Oxford University Press, 1956.

3. Powers, R. W., and Doyle, Margaret V.: Diffusion of Interstitial Solutes in the Group V Transition Metals. J. Appl. Phys., vol. 30, no. 4, Apr. 1959, pp. 514-524.

4. Inouye, H.: The Oxidation of Columbium at Low Oxygen Pressures. Columbium Metallurgy. Interscience Publishers, 1961.

E-2492
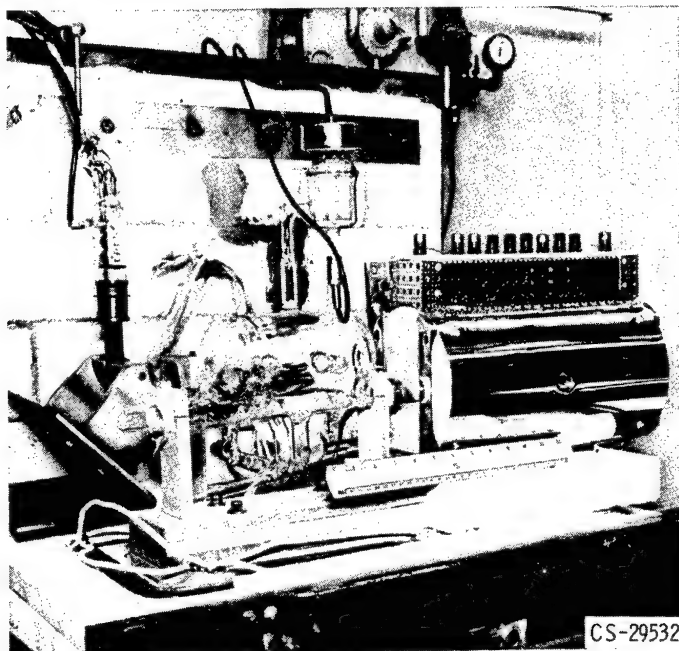
(a) Overall view.
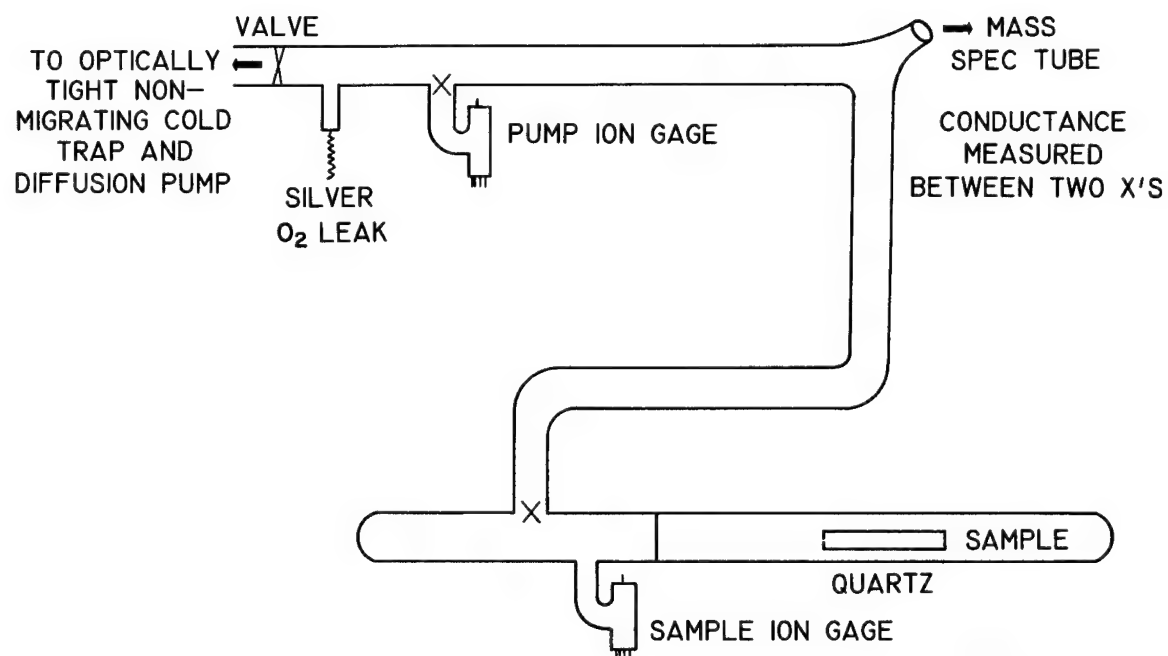
(b) Schematic diagram of system.

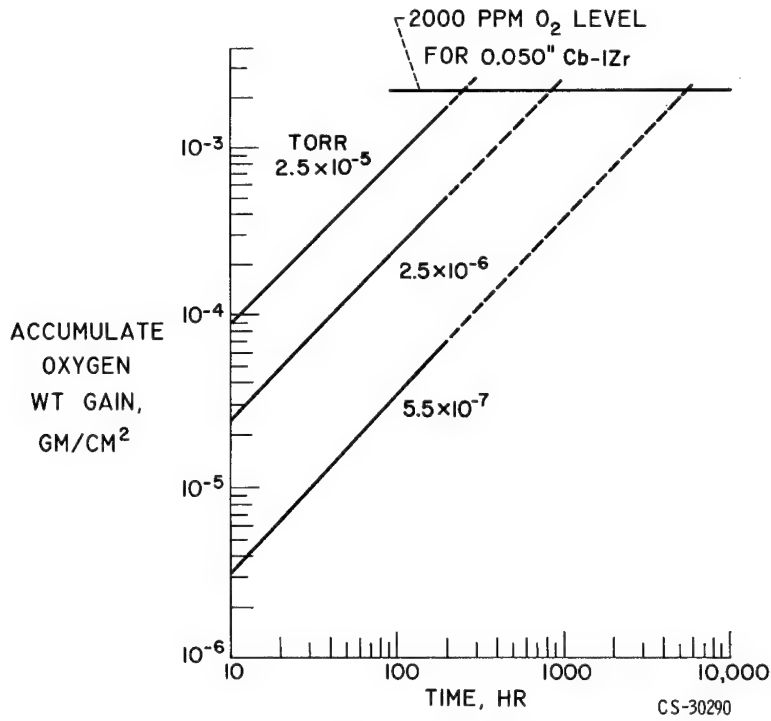Figure 1. - High-temperature controlled contamination rig.

311

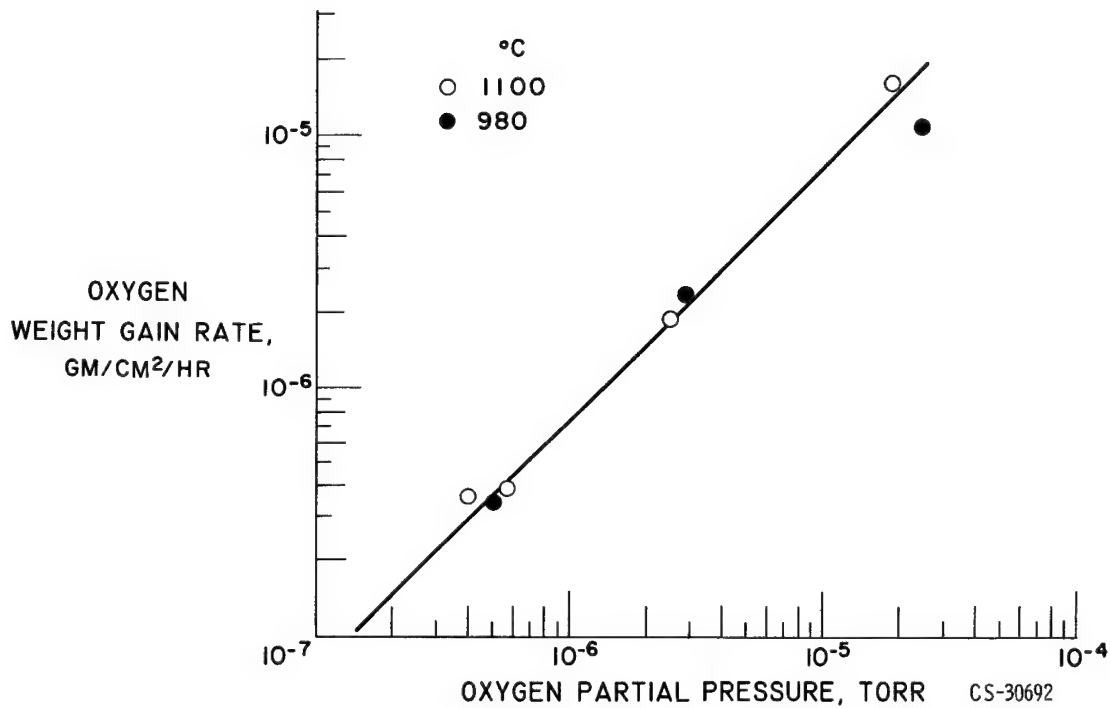Figure 2. – Oxidation of Cb-1Zr alloy at low oxygen pressures at 980° and 1100° C.

Figure 3. – Cb-1Zr contamination rate as a function of oxygen pressure.

E-2492

312

PURIFICATION OF ARGON FOR GLOVE BOXES

AND ENVIRONMENTAL CHAMBERS

M. F. Parkman   Argonne National Laboratory

Argon is used as a cover gas for alkali metals or hot refractory metals in several applications. These include: environmental chambers for loops, glove boxes for alkali metal sampling, analysis, welding refractory metals, and for furnaces for heating refractory metal capsules. Two major problems are establishing and achieving maximum desired contaminant levels. In the absence of data on the first problem, we approach the second problem by using gas with the lowest obtainable impurity level. Thus, gas purifiers and procedures are in use based on the best available qualitative knowledge. Results of a number of tests to determine what purity of gas is being obtained in existing systems will be outlined in this paper.

The efficiency of Ti-50 atomic % Zr in removing oxygen from argon was studied. A galvanic cell, similar to that of Baker, et al.,[1] was constructed to measure the oxygen concentration of the argon.

A schematic diagram of the test system is shown in Figure 1. High purity argon, containing 4 ppm oxygen (as determined during the investigation) was used as the test gas. Oxygen was introduced into the argon through a needle valve from a bottle of compressed air. The piping arrangement allowed either the feed or the product from the furnace to be analyzed.

A 1-in. diameter Vycor tube was used to contain the Ti-Zr turnings.[2] Bed lengths of 1, 3, and 6 inches were used with varying temperatures and gas velocities.

The cell was calibrated against an electrochemical cell that generates known amounts of oxygen. The calibration curve is shown in Figure 2. The

sensitivity is shown to be about 4.4 microamps/ppm. Accuracy in readings is low below 2 ppm because of the uncertain shape of the calibration curve.

A 45-hour run was made with 1.5 l/min flow rate, 1500°F bed temperature, 3-in. bed length, 0.8 void fraction, and 60 ppm oxygen feed concentration. Outlet concentration was < 1 ppm during the period. About 0.45 gm of oxygen was absorbed during the run, nearly all of it in the top 1/4-in. of the bed. The chips in this layer were completely consumed. Visual evidence of oxygen reaction occurred for about 1 in. along the bed. The remainder of the chips turned a golden color, typical of nitrides. Apparently, the oxygen reaction is very rapid, with a nonadherent scale formed. No nitrogen analysis was made so the only evidence of nitrogen reaction was color. On this basis, the nitrogen reaction was incomplete.

The flow velocity of argon containing 60 ppm oxygen was varied from 0 to 2.6 ft/sec through a 6-in. bed at 1200°F. Outlet concentration remained below 1 ppm oxygen. At 1300°F, the same result was obtained with a 1-in. bed.

The above tests indicate that the efficiency and utilization of Ti-50% Zr turnings is high when used to remove oxygen from air contaminated argon.

The performance of two types of gas purifiers were measured. A CEC Moisture Monitor was used in addition to the oxygen analyzer. Purifiers consisting of a molecular sieve trap followed by a Ti-50% Zr hot trap produced argon containing < 1 ppm oxygen and about 2 ppm water. A NaK bubbler produced argon containing 2.5 ppm oxygen and about 1.7 ppm water. Because of the long period of time for an equilibrium to form between moisture in a gas stream and on the walls, the moisture content may have been even lower.

The performance of a 26-ft^3 vacuum glove box containing 4 - 9-in., 20 mil neoprene gloves and capable of being pumped to 1×10^{-5} torr when not in use

was measured. Argon containing about 4 ppm oxygen and 8 ppm water was used to fill the dry box. Immediately on filling the glove box after one to two days under high vacuum, the gas analyzed 4 ppm oxygen and 40 ppm water. Apparently the time under vacuum was not sufficient to remove water absorbed by the gloves. During 3 hours of bare-handed use with 2 gloves after the above measurement, the moisture content of the argon was observed to rise at the rate of 50 ppm/glove-hour. Oxygen content remained the same. The moisture pickup rate could be significantly reduced by wearing surgeon's gloves during operation. The need for continuous repurification of the glove box atmosphere was thus demonstrated if the box were to be used for more than a short time.

A book has recently been published[3] summarizing argon purification practice. The most recent bibliography we know of is listed as Reference 4.

References:
1. W. J. Baker, J. F. Combs, T. L. Zinn, A. W. Wotring, and R. F. Wall, "The Galvanic Cell Oxygen Analyzer," Ind. Eng. Chem. 51, 1959.

2. Supplied by Oregon Metallurgical Corporation, Albany, Oregon, average size: 0.20 x 0.25 x .03 inches.

3. P. A. F. White and S. E. Smith, Inert Atmosphere, Butterworths, London, 1962.

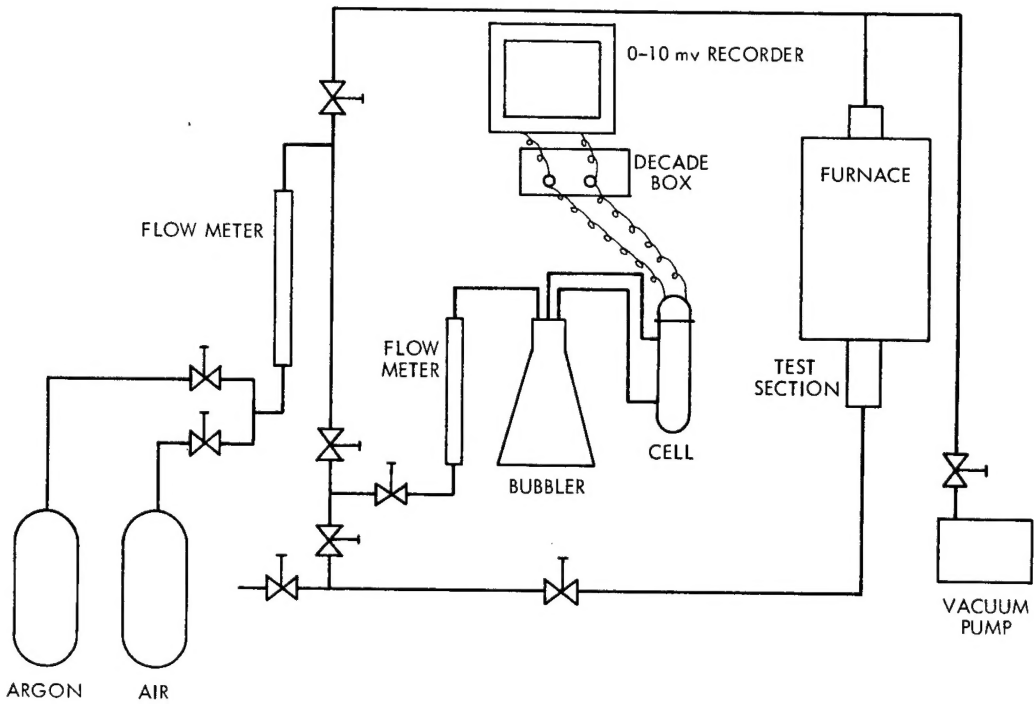4. E. A. Cernak, AEC Rept. CNLM-1802-2, Purification of Argon, Helium, and Xenon, September 1959.

Figure 1. – Schematic diagram of system for studying gettering properties of titanium – 50 percent zirconium alloy turnings.
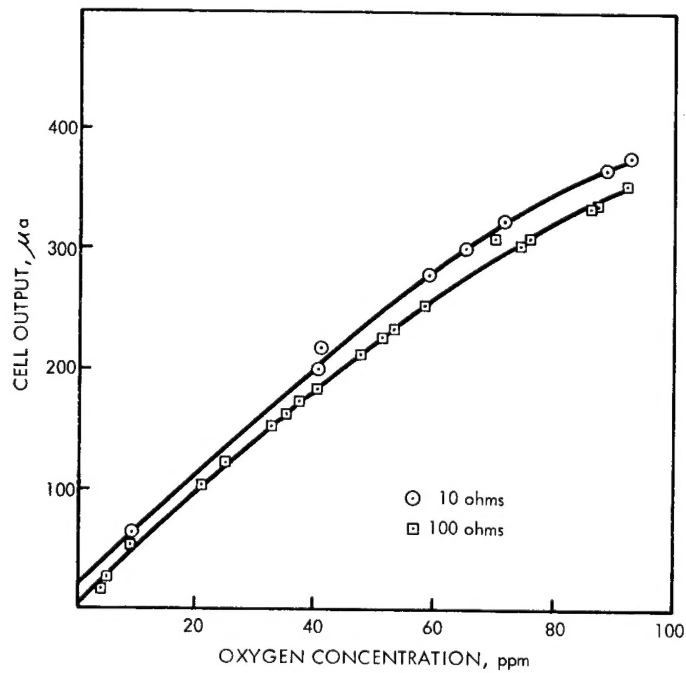

Figure 2. – Calibration curve for oxygen analyzer using 10 ohm and 100 ohm load resistors.

NASA SCIENTIFIC AND TECHNICAL PUBLICATIONS

TECHNICAL REPORTS: Scientific and technical information considered
important, complete, and a lasting contribution to existing knowledge.

TECHNICAL NOTES: Information less broad in scope but nevertheless
of importance as a contribution to existing knowledge.

TECHNICAL MEMORANDUMS: Information receiving limited distri-
bution because of preliminary data, security classification, or other reasons.

CONTRACTOR REPORTS: Technical information generated in con-
nection with a NASA contract or grant and released under NASA auspices.

TECHNICAL TRANSLATIONS: Information published in a foreign
language considered to merit NASA distribution in English.

TECHNICAL REPRINTS: Information derived from NASA activities
and initially published in the form of journal articles or meeting papers.

SPECIAL PUBLICATIONS: Information derived from or of value to
NASA activities but not necessarily reporting the results of individual
NASA-programmed scientific efforts. Publications include conference
proceedings, monographs, data compilations, handbooks, sourcebooks,
and special bibliographies.

Details on the availability of these publications may be obtained from:

SCIENTIFIC AND TECHNICAL INFORMATION DIVISION

NATIONAL AERONAUTICS AND SPACE ADMINISTRATION

Washington, D.C. 20546